ABSTRACT

KENNEDY, KAREN ALYCE. Characterization of Phase Equilibrium Associated with Heterogeneous Polymerizations in Supercritical Carbon Dioxide. (Under the direction of Dr. George W. Roberts and Dr. Joseph M. DeSimone)

This thesis details research to understand the phase equilibrium associated with heterogeneous polymerizations in supercritical carbon dioxide ($scCO_2$), particularly the polymerization of vinylidene fluoride (VF2) in $scCO_2$. Knowledge of the equilibrium between the supercritical fluid and polymer phases may be applied to understanding the mechanisms involved in heterogeneous polymerizations in $scCO_2$. Several experimental systems were developed and/or utilized for measuring the phase equilibrium. These included a system for measuring the swelling of solid polymer particles in the presence of $scCO_2$, a system for measuring the mass sorption and diffusion of supercritical fluids into the polymer phase, and a system for measuring the partitioning of reactant species between the polymer and supercritical fluid phases. The sorption and swelling of poly(vinylidene fluoride) (PVDF) was measured at conditions similar to those of the polymerizations. The Sanchez-Lacombe equation of state was applied to modeling the binary and ternary phase equilibria for the VF2-CO_2-PVDF system. Carbon dioxide exhibits a favorable interaction with PVDF that is enhanced at increasing fluid densities. Additionally, the monomer exhibits a favorable interaction with PVDF that improves the mass sorption into the polymer phase and expands the tunability of the fluid to change the polymer properties. The impact of the phase equilibrium on the precipitation polymerization of vinylidene fluoride in $scCO_2$ is discussed. The bimodal molecular weight

distribution of PVDF synthesized in CO_2 could be due, in part, to the sorption of VF2 into the polymer phase and the plasticization of the polymer to facilitate propagation of the polymer chains to high molecular weights within the polymer particles. This dissertation provides a foundation for understanding the impact of the phase equilibrium on heterogeneous polymerizations in supercritical carbon dioxide. It provides techniques for identifying and improving conditions for polymerizations in supercritical carbon dioxide and optimizing CO_2-based processes of a heterogeneous nature.

CHARACTERIZATION OF PHASE EQUILIBRIUM ASSOCIATED WITH HETEROGENEOUS POLYMERIZATIONS IN SUPERCRITICAL CARBON DIOXIDE

by

KAREN ALYCE KENNEDY

A dissertation submitted to the Graduate Faculty of
North Carolina State University
in partial fulfillment of the
requirements for the Degree of
Doctor of Philosophy

CHEMICAL ENGINEERING

Raleigh

2003

APPROVED BY:

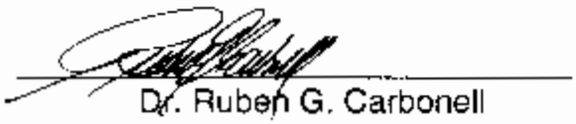

Dr. Ruben G. Carbonell

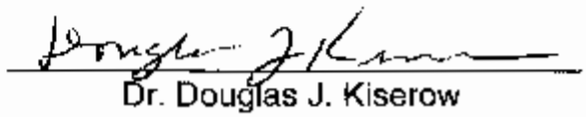

Dr. Douglas J. Kiserow

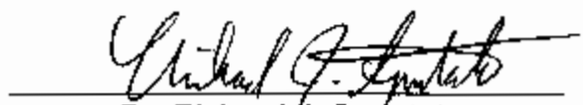

Dr. Richard J. Spontak

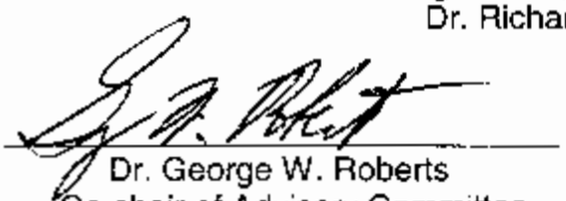

Dr. George W. Roberts
Co-chair of Advisory Committee

Dr. Joseph M. DeSimone
Co-chair of Advisory Committee

This dissertation is dedicated to my grandparents,

Sylvia, Ernest, Willie, Erma, and Raymond,

for the legacy that started with you and your continued love and guidance which is a never ending source of inspiration to me.

BIOGRAPHY

Karen A. Kennedy began graduate studies in the chemical engineering program at North Carolina State University in Raleigh, North Carolina in the fall of 1997. Her research focused on understanding the thermodynamics associated with polymerizing fluorinated monomers in supercritical carbon dioxide under the advisement of Professors George Roberts and Joseph DeSimone. Her work involved the development of equipment and models for measuring the sorption of carbon dioxide and other small molecules into polymers. This work was part of a larger effort in the Kenan CO_2 Center and the NSF Science and Technology Center for Environmentally Responsible Solvents and Processes (CERSP) to access the feasibility of using carbon dioxide as an environmentally friendly alternative to solvents and water currently being used in industry.

Karen served as chair of the continuous polymerization group (CPG) meeting, which fostered collaboration between members conducting similar research. Karen mentored several undergraduates in projects related to her research. In 2002, Karen was recognized by CERSP for her research and K-12 education activities with a fellowship to attend a course on global sustainability in Braunwald, Switzerland.

Karen was born in New Orleans, Louisiana. Karen left home at the age 15 to finish her junior and senior years of high school at a residential public high school, the Louisiana School for Math, Science, and the Arts, in Natchitoches, Louisiana. While there, Karen majored in math and science and minored in piano. It was during this time that Karen decided to pursue a research career in chemical engineering.

Following graduation from high school, Karen enrolled at the Georgia Institute of Technology in Atlanta, Georgia. During her tenure at Georgia Tech, Karen co-oped with Air Products and Chemicals, Inc., where she worked in manufacturing, research, and product safety. Karen worked with Professor Agaram Abhiraman at Georgia Tech to study structure-property relationships of newly developed polymers for NASA.

Besides her graduate research, Karen was involved in numerous activities outside the research lab. In 1999, she served as a recruiting captain for incoming graduate students to the department. She served on panels and gave presentations to undergraduates considering graduate school. She also gave a presentation at a national convention to high school students considering college. Karen's activities also included being a workshop presenter with the Science House, an active member and former programs chair of the National Society of Black Engineers Research Triangle Park Alumni Association, and an active member and former director of the orchestra at Martin Street Baptist Church.

Following graduation, Karen will enter the Career Development Program at Air Products and Chemicals, Inc. in Allentown, PA as a senior research engineer.

ACKNOWLEDGEMENTS

There are many who have contributed in small and large ways to the completion of this dissertation and to whom I give special thanks for what they have given and what I have learned from them.

I thank ***my Lord and Savior*** for his grace and mercy that has blessed me since before I was born. Psalm 138 reminds me of all that the Lord does for me. Glory be thy name.

To ***my grandparents***, I thank you for the example you have shown. You provided me with inspiration and instruction for how I live my life.

To ***my parents, Alice and Feltus, my brothers, Bryan and Allan, and their families***, I thank you for always being there for me, for taking the time whenever I needed you. I love you all very much.

To ***my "sister" cousins, JoNell and Kendra***, thank you for your friendship. With every season in life, our sisterhood grows stronger and I thank God for having you in my life.

To ***my church family at Martin Street Baptist Church***, I thank you for being my family when none was nearby. I will always remember the special times and special people at the church. You gave me friendship, support, and guidance. My relationship with God has grown stronger from the love and instruction I received at Martin Street.

To ***my friends in NSBE***, I thank you for the opportunity for leadership, personal and professional growth, and friendship. We had some really great times and made our mark on the Triangle in professionalism and service to the community.

To ***my research lab***, I thank you for useful discussions and the interaction we shared on a daily basis. My abilities as a researcher and professional have grown from working with all of you.

To ***my dissertation committee***, I thank you for taking the time to serve on this important committee and for your useful suggestions that added to the culmination of this work.

To ***my advisors***, I thank you for your guidance and advice throughout this dissertation process. Your extensive knowledge and resources equipped me for success in my research and prepared me for my future as a researcher in industry.

And finally to all my family and friends, near and far, who gave me friendship, prayers, and support. I love you and I thank you for being in my life.

TABLE OF CONTENTS

List of Tables

Page

Appendix B Characterization data

Appendix C Modeling results

List of Figures

Page

Chapter 1

Introduction

Solvent-based systems are prevalent in industry. However, during the last few decades, regulations and concerns from the general public have spurred an interest by industry to reduce or eliminate the use of solvents in their processes. “Green chemistry” has become an important concept and approach for minimizing solvent use. Green chemistry [1] is “the design, development, and implementation of chemical processes and products to reduce or eliminate substances hazardous to human health and the environment”. One area of research in green chemistry is the use of liquid and supercritical carbon dioxide ($scCO_2$) as a solvent, reaction medium and processing aid. Commercial processes that have benefited from the use of CO_2 include dry cleaning, heterogeneous catalyzed reactions, and polymerizations.

Extensive research has been conducted to replace both aqueous and organic media used in polymerization reactions with supercritical carbon dioxide. For example, supercritical carbon dioxide has been studied as an alternative to water in the polymerization of methyl methacrylate and acrylic acid. Supercritical carbon dioxide has also been successful in replacing chloroflourocarbons (CFCs) in the production of specialty copolymers of tetrafluoroethylene (TFE). Supercritical carbon dioxide has the potential to replace some of these solvents, in some cases with the added benefit of improved polymer properties. In fact, Dupont has begun sale of TFE-based polymers made in CO_2 that have improved properties [2].

The use of supercritical carbon dioxide as a polymerization medium has several benefits. First, $scCO_2$ can be used over a wide range of temperatures because the supercritical state exists at ambient conditions. Second, the solvent properties are tunable by adjusting the temperature or pressure. Third, CO_2 is an inert medium in many reactions. That is, there is no chain transfer to CO_2. Supercritical carbon dioxide is environmentally benign, inexpensive, and readily available. It can eliminate the use of hazardous organics and reduce the amount of wastewater generated in polymerization processes. Finally, the polymer formed in $scCO_2$ is free of moisture. This translates into significant energy savings because there is no need to dry the polymer.

Supercritical carbon dioxide has found particular promise in the polymerization of fluoromonomers. Fluoropolymers are generally produced by an emulsion or suspension process with water, or with the use of CFCs that are harmful to the environment. Hydrochlorofluorocarbons and hydrofluorocarbons have been considered as alternatives to CFCs, but a negative environmental impact still exists. Supercritical carbon dioxide is the only known alternative that is environmentally benign and doesn't generate the wastes associated with aqueous polymerizations. Additionally, numerous fluoropolymers are produced using perfluorooctanyl sulfonate (PFOS) surfactants that are biopersistant and nonbiodegradable. There is a desire to discontinue use of these surfactants, but suitable alternatives have yet to be identified. The use of CO_2 as a polymerization medium will eliminate the need for these potentially hazardous surfactants.

Among the research of heterogeneous polymerizations in $scCO_2$, there has been very little attempt to understand the extent to which the reaction proceeds in the solid and fluid phases that are present in the reactor. Consequently, there has been very little characterization of the effect of mass transport and equilibrium between species in the polymer and $scCO_2$ phases. Relatively few studies have been conducted to measure the polymer swelling and sorption, and to model this behavior. Finally, the effect of partitioning on the polymerization kinetics and polymer properties has not been explored.

The main objective of this work was to gain a better understanding of the phase equilibrium associated with heterogeneous polymerizations in $scCO_2$, particularly the polymerization of vinylidene fluoride in $scCO_2$. Chapter 2 is a review of polymerization of fluoroolefins in CO_2. The polymerization of vinylidene fluoride in CO_2 produces interesting polymer properties, which will be explained in the context of the phase equilibrium in this work. In Chapter 3, experimental and modeling approaches to studying phase equilibrium will be reviewed. Chapter 4 presents results of the sorption and swelling of poly(vinylidene fluoride) in CO_2, including modeling of this phase equilibria. Chapter 5 details work to study a three component system of carbon dioxide, poly(vinylidene fluoride) and vinylidene fluoride monomer. The impact of the presence of monomer on the sorption of CO_2 into the polymer is discussed. Additionally, the partitioning of the monomer between the polymer and supercritical phases is studied by two methods. Finally, the three component phase equilibria are modeled using an equation of state.

The main issues that this dissertation attempts to answer are:

1) What effect do the polymerization conditions in CO_2 have on the phase equilibria?
2) Can these phase equilibria be predicted using equation of state models?
3) What are the implications of phase equilibrium on the locus of polymerization, polymerization kinetics, and polymer properties in heterogeneous polymerizations in scCO_2?

1.1 References

1. Poliakoff, M., Fitzpatrick, J.M., Farren, T.R., and Anastas, P.T., *Green chemistry: Science and politics of change.* Science, 2002. **297**: p. 807-810.
2. *DuPont introduces fluoropolymers made with supercritical CO_2 technology*, www.dupont.com/corp/news/products_today.html, Press Release: March 22, 2002.

Chapter 2

Review

Heterogeneous polymerization of fluoroolefins in supercritical carbon dioxide

Kennedy, K.A., Roberts, G.W., and DeSimone, J.M., Heterogeneous polymerization of fluoroolefins in supercritical carbon dioxide, submitted to *Advances in Polymer Science (Polymer Particles)*. Springer: New York.

2.1 Introduction

The first application of supercritical fluids (SCFs) to the polymer industry occurred in the 1930s, with the development of a free-radical bulk polymerization of supercritical ethylene to produce low-density polyethylene (LDPE) [1, 2]. LDPE is synthesized by a high-pressure process, at 180-300°C and 1000-3000 bar, in which the polymer is soluble in supercritical ethylene monomer [3]. However, inert SCFs have only recently been exploited in a wide range of polymer applications. Research with supercritical carbon dioxide ($scCO_2$) has outpaced research with other SCFs because carbon dioxide is inexpensive, has a critical point (Table 2.1) at conditions lower than that of most other SCFs (increasing the range of tunability), and is environmentally benign. Supercritical carbon dioxide has found particular application as a polymerization medium because of its inertness to free radicals [4], i.e. no chain transfer to CO_2, and because of high initiator efficiencies that exist in CO_2. DuPont has built a commercial scale facility for the production of tetrafluoroethylene-based polymers, including Teflon® FEP (a copolymer of tetrafluoroethylene and hexafluoropropylene), in carbon dioxide [5]. Significant research [6-8] has been reported for studying the use of $scCO_2$ as a polymerization medium. This review will focus on recent developments to polymerize fluoroolefins, such as tetrafluoroethylene, by heterogeneous polymerization in $scCO_2$. The particular challenges and rewards associated with polymerizing fluoroolefins in CO_2 will be discussed.

Table 2.1
Critical temperature and pressure of substances useful as supercritical fluids [9]

	Critical Temperature T_c (°C)	Critical Pressure P_c (bar)
Carbon Dioxide (CO_2)	31.1	73.8
Water (H_2O)	374.4	221.2
Ethane (C_2H_6)	32.4	48.8
Propane (C_3H_8)	96.8	42.5
Ammonia (NH_3)	132.4	113.5
Nitrous Oxide (N_2O)	36.6	72.4
Fluoroform (CHF_3)	26.3	48.6

2.2 Conventional Polymerization of Fluoroolefins

The major commercial fluoropolymers are made by homopolymerization of tetrafluoroethylene (TFE), chlorotrifluoroethylene (CTFE), vinylidene fluoride (VF2), and vinyl fluoride (VF), or by co-polymerization of these monomers with hexafluoropropylene (HFP), perfluoro(propyl vinyl ether) (PPVE), perfluoro(methyl vinyl ether) (PMVE), or ethylene. The polymers are formed by free-radical polymerization in water or fluorinated solvents.

Currently, there is concern about the use of ammonium perfluorooctanoate (APFO), also known as “C8”, which is necessary for the manufacture of fluorinated plastics and elastomers in water. C8 is a perfluorinated anionic surfactant used as a dispersing agent in the polymerization and copolymerization of many fluoropolymers, including poly(tetrafluoroethylene) (PTFE), poly(vinylidene fluoride) (PVDF), poly(tetrafluoroethylene-co-hexafluoropropylene) (FEP), poly(tetrafluoroethylene-co-perfluoro(propyl vinyl ether)) (PFA), and poly(tetrafluoroethylene-co-perfluoro(methyl vinyl ether)) [10]. It is necessary to use a perfluorinated anionic surfactant for two

important reasons. First, fluorinated anionic surfactants have the right interfacial properties to disperse such hydrophobic particles like fluoropolymers in water. Second, fluorinated carbon-centered radicals are extremely electrophilic and will react (chain transfer) with any hydrocarbon-based species in solution, including the surfactant. Hence, the surfactant chosen needs to be hydrogen free.

Earlier this year, the Environmental Protection Agency (EPA) released a preliminary risk assessment of C8 and other fluorochemicals [10]. Although the EPA refers to C8 as a persistent organic pollutant, there have been no reported adverse health affects in humans. However, because of these potential environmental and health problems, 3M, who was the leading manufacturer of C8, exited the C8 business [11]. DuPont and other members of the Fluoropolymers Manufacturers Group (FMG) have conducted research during the last 30 years to identify alternatives to C8 for economic reasons and because C8 persists in the body. However, no viable, alternative dispersing agent has been identified. Carbon dioxide is the only known alternative to eliminate the need for C8 in the manufacturing process.

Polymers made from TFE and VF2 dominate the fluoropolymer market. Existing methods for making these polymers will be reviewed in the following sections.

2.2.1 Tetrafluoroethylene

Poly(tetrafluoroethylene) is a fluorinated analog of polyethylene with chains that arrange into a helical twisting conformation in which the carbon backbone is

shielded by fluorine atoms. This results in a polymer with superior chemical resistance. Additionally, PTFE has great thermal stability and a very low coefficient of friction. This makes PTFE a unique polymer for application as an anti-stick coating and for use with aggressive chemicals. U.S. consumption of PTFE was 39.7 million pounds in 2001 – the greatest of any fluoropolymer [12]. PTFE is sold as a granular resin, fine powder, or aqueous dispersion for use in a variety of applications, including coatings, chemical processing equipment, and wire insulation.

PTFE is made by either suspension or dispersion polymerization in water, depending on the particle size required. Both processes are run at 70-120°C and 1-6 MPa using a water-soluble initiator, such as ammonium persulfate [13]. In the dispersion polymerization, a dispersing agent, such as ammonium perfluorooctanoate (C8) and mild agitation are used to produce a stable dispersion of fine PTFE particles of average particle size 0.2 μm. Hydrocarbon wax can be added to prevent coagulation of the particles. Because the amount of dispersing agent is typically less than the critical micelle concentration (CMC), the polymerization is not a true emulsion polymerization. However, the polymerization does possess characteristics of an emulsion polymerization. After the polymerization is complete, the particles may be precipitated to form a fine powder or the dispersion may be concentrated for direct use as a coating. Fine powder PTFE is commonly mixed with a lubricant such as kerosene to perform paste extrusion of tubing and wire insulation.

In suspension polymerization, little or no dispersing agent and vigorous agitation is used to produce a coagulated granular resin with particles 1-2 mm in size. The particles are dried and ground to varying particle sizes for molding or ram extrusion into precision parts.

Conventional wisdom suggests that PTFE homopolymer cannot be melt-processed to form molded parts due to its extremely high molecular weight and high melt viscosity. Grades of PTFE, known as micropowders, with low molecular weight and low melt viscosity are typically used as additives in coatings and thermoplastics [14]. However, these grades cannot be melt-processed due to their brittleness. Tervoort et al. [15] recently reported that PTFE with medium viscosities (melt flow rate 0.2 - 2.6 g / 10 min) and bimodal molecular weight distributions can be melt processed. PTFE grades with high and low viscosity are blended in a twin-screw extruder to form a blend exhibiting a pseudobimodal molecular weight distribution. The blend retains the mechanical strength of the high viscosity material, but the presence of the low viscosity material enables melt-processing of the material into a variety of parts and also suggests the possible recycling of PTFE.

2.2.2 Vinylidene Fluoride

Poly(vinylidene fluoride) is a semi-crystalline polymer that is produced commercially by a free-radical emulsion or suspension polymerization of vinylidene fluoride ($CH_2=CF_2$) in water [16-18]. PVDF exhibits a unique combination of mechanical and electrical properties due to the alternating spatial arrangement of CH_2 and CF_2 groups along the polymer backbone. PVDF is the second largest

consumed fluoropolymer, after PTFE [12], due to its (1) high mechanical and impact strength, (2) resistance to environmental stress, (3) ease of melt-processability, and (4) low cost relative to other fluoropolymers. PVDF is used in architectural coatings (~40%), semiconductor manufacture and chemical processing (~40%), and wire and cable insulation (~20%) [19]. A small, but increasing amount of PVDF is used as electrodes in lithium batteries [12, 20].

Polymerization of vinylidene fluoride by emulsion or suspension polymerization in water is conducted at conditions between 10 to 130°C and 10 to 200 bar. In the emulsion polymerization, either water-soluble peroxides or monomer-soluble peroxy or organic peroxides are used as initiators [17]. Fluorinated surfactants, such as ammonium perfluorooctanoate, are used as dispersing agents. Chain transfer agents, such as acetone, chloroform, or trichlorofluoromethane, may be used to control the molecular weight [13]. The resulting latex of dispersed particles is coagulated, washed, and spray dried to form a fine powder. The powder consists of spherical agglomerates 0.2 to 0.5 μm in diameter.

The suspension polymerization is conducted using monomer-soluble peroxy initiators. Water-soluble polymers, such as poly(vinyl alcohol), are typically used as suspending agents to reduce the coalescence of the polymer particles [17]. A slurry of polymer particles 30 to 100 μm in diameter is formed during the polymerization. The particles are washed and dried before further processing.

The effect of polymerization conditions on the polymer morphology in PVDF has been studied [16, 21]. Regioisomer defects in the form of reversed head-to-tail addition are common in the polymerization of vinyl monomers [22]. These defects affect the crystallinity and final properties of the polymer. The fraction of defects in PVDF ranges from 3.5 to 6 mol%, increasing with reaction temperature [22]. The α-phase crystal is the most common crystal observed in PVDF. However, an increase in defects leads to a greater amount of β-phase crystals in the polymer [16, 23], which gives PVDF its piezoelectric properties. An increase in the amount of β crystals formed was observed for different initiating systems [23]. Additionally, enhancement of the β crystals in PVDF is done by applying tensile forces or mechanical stretching to the polymer [24]. The γ and δ crystal phases may be generated from the α-phase by heat or electric field, respectively. The γ-phase crystal has also been formed by crystallization under high pressure [25].

Commercial PVDF is sold in powder form or may be compression molded into pellets. Depending on the polymerization conditions, differing properties of PVDF may be produced. PVDF exhibiting a multimodal molecular weight distribution has been reported for improved melt flow characteristics [26] and use in lithium batteries [24]. Dohany [26] reports the formation of a distinct bimodal molecular weight distribution that is strongly dependent on the addition of the initiator to the reaction. The initiator is continuously fed to the reaction until about 50% of the total monomer feed is added to the reactor. At that point, the addition of the initiator is stopped and the remaining monomer is continuously fed to the reactor. The high molecular

weight peak measured by gel permeation chromatography is more than 30% of the overall molecular weight distribution. The high molecular weight portion allows processing of the polymer at high shear rates for improved productivity. The use of these polymers in lithium batteries is largely the result of their relatively high defect structure, which promotes ionic conductivity in the electrochemical cell [24].

2.2.3 Copolymers

PVDF and PTFE have wide application in industry due to their strength, chemical and wear resistance, and dielectric properties. However, VF2 and TFE may be reacted with comonomers such as hexafluoropropylene (HFP) and vinyl ethers to modify the properties of the polymer. For example, copolymerizing VF2 with HFP improves the flexibility of the polymer without compromising the electrical properties. Thus, VF2-HFP copolymers find more application in cable insulation than VF2 homopolymer. Copolymers of TFE with perfluoroalkyl vinyl ethers have properties very similar to the TFE homopolymer except that the copolymer may be processed by injection molding because of its lower melt viscosity. Copolymers of TFE and VF2 can also be made to form fluorinated elastomers and perfluorinated elastomers when cure site monomers are used. Important examples of such elastomers include terpolymers of VF2, TFE, and either HFP or PMVE along with a cure site monomer such as bromotetrafluorobutene [19].

Copolymers are produced by aqueous copolymerization of the monomers in a manner similar to the homopolymerizations. Nonaqueous polymerizations of TFE with PPVE may be conducted in water or in fluorinated solvents at lower

temperatures (30-60°C) using a soluble organic initiator such as perfluoropropionyl peroxide. The molecular weight is controlled by addition of chain transfer agents such as methanol in nonaqeuous polymerizations or hydrogen in aqueous polymerizations.

2.3 Supercritical Carbon Dioxide as a Polymerization Medium

2.3.1 Properties of Supercritical Carbon Dioxide

Supercritical fluids possess characteristics that make them interesting for use as polymerization media. A supercritical fluid exists at temperatures and pressures above its critical values. In the supercritical state, the fluid exhibits physical and transport properties intermediate between the gaseous and liquid state. This is illustrated in Table 2.2. SCFs have liquid-like densities, but gas-like diffusivities. These intermediate properties can provide advantages over liquid-based processes. In particular, the higher diffusivities of SCFs reduce mass transfer limitations in diffusion-controlled processes. Additionally, lower energy is required for processing the supercritical fluid because its viscosity is lower than that of most liquids, and because the need to vaporize large quantities of liquid is avoided.

Table 2.2
Comparison of typical SCF, liquid, and gas properties [27]

	Liquid	SCF	Gas
Density (g/cm^3)	1	0.1 – 0.5	10^{-3}
Viscosity (Pa s)	10^{-3}	10^{-4} – 10^{-5}	10^{-5}
Diffusivity (cm^2/s)	10^{-5}	10^{-3}	10^{-1}

SCFs have a tunable density that may offer further advantages in reaction and processing applications. This tunability is illustrated in Figure 2.1 for carbon dioxide. Near the critical point, even small changes in the temperature or pressure of carbon dioxide dramatically affect its density. Similarly, the viscosity, dielectric constant, and diffusivity are also tunable parameters, which allows specific control of systems involving supercritical fluids.

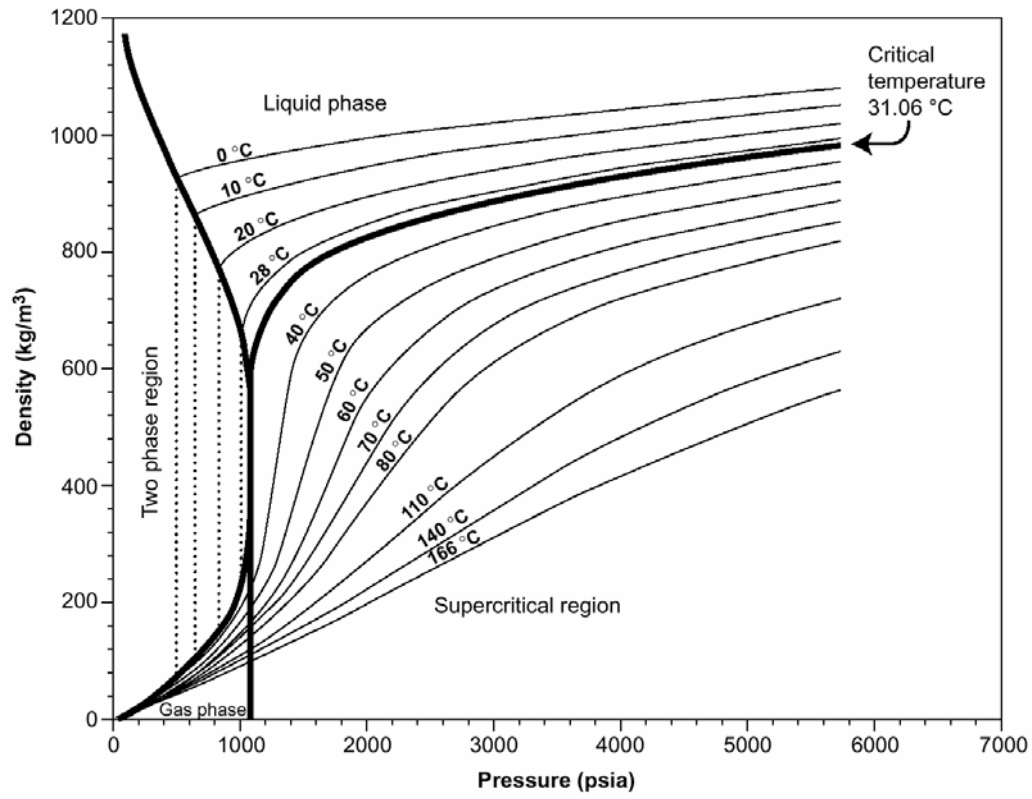

Figure 2.1 Density versus pressure isotherms for carbon dioxide [28]

Carbon dioxide is inexpensive and widely available. The main source of carbon dioxide is from chemical manufacturing. For example, it is a major byproduct

in the production of ammonia, ethanol, and hydrogen. Finally, carbon dioxide is non-toxic, nonflammable, and easily recycled.

2.3.2 Advantages of Using Supercritical Carbon Dioxide

Supercritical carbon dioxide is a very good solvent for small molecules, but a poor solvent for most high molecular weight polymers at mild conditions ($T<100^{\circ}C$, $P<350$ bar). Amorphous fluoropolymers and silicones are the only polymers known to be soluble in CO_2 at mild conditions [6]. This difference in solubilities is an advantage for CO_2-based polymerizations, as it can be used to reduce the energy requirements necessary to separate and purify a polymer after synthesis. Consider, for example, a batch precipitation polymerization in CO_2. Initially, the reactor contains a homogeneous solution of monomer and initiator (and perhaps a chain transfer agent) in CO_2. As the polymerization proceeds, the polymer precipitates to form a separate phase. When the polymerization is complete, the polymer is separated from the reaction mixture by a conventional fluid/solid separation process, e.g., sedimentation, filtration, centrifugation, etc. The fluid phase contains unreacted monomer and initiator, which can be recycled. When the polymer is depressurized, the CO_2 escapes, leaving a dry polymer. This contrasts with water-based processes in which the polymer must be dried to remove water. The drying step can be quite energy intensive. Additionally, CO_2 can remove residual monomer from the polymer by supercritical fluid extraction. Significant energy savings may be realized in a CO_2-based polymerization.

Other advantages of CO_2-based polymerizations are there is no chain transfer to solvent and the production of unstable end groups can be dramatically reduced. Guan et al. [4] studied the decomposition of 2,2'-azobis(isobutyronitrile) (AIBN) in $scCO_2$. It was found that initiator efficiencies greater than 80% were possible due to the low viscosity of CO_2 and negligible solvent cage effects. Additionally, analysis of the decomposition products showed that there was no chain transfer to CO_2.

Reactive end groups, such as acyl fluoride and carboxylic acid end groups, are commonly formed in the aqueous polymerization of fluoroolefins, especially the copolymerization of TFE with HFP and PPVE [13]. These unstable end groups may decompose during melt processing of the polymer and cause defects in the final application. Generally, finishing steps are required after the polymerization to remove these end groups by hydrolysis or fluorination. Using CO_2 as a polymerization medium eliminates the need for these finishing steps and additional control of the polymerization is achieved with the absence of chain transfer to solvent.

The feasibility of using $scCO_2$ in polymerizations has been demonstrated by the commercial production of Teflon® in CO_2 [29] using methods developed by DeSimone and Romack [30-35]. Polymerization in carbon dioxide does not require the use of C8, which has received negative publicity for being persistent in the blood. DuPont has built a $40 million development facility for the production of Teflon® FEP using CO_2-based technologies [5]. Poly(vinylidene fluoride) (PVDF) is another fluoropolymer that may be manufactured in supercritical carbon dioxide. DeSimone

and co-workers [36, 37] reported the first continuous polymerization of vinylidene fluoride in $scCO_2$. Subsequently, Solvay Corporation patented a process for making poly(vinylidene fluoride) in $scCO_2$ [38]. As researchers continue to better understand CO_2-based polymer applications, and as industry continues to look for more economical and environmentally sound alternatives to existing processes, the use of supercritical carbon dioxide in commercial polymer reactions and processing will increase.

2.4 Precipitation Polymerization in Supercritical Carbon Dioxide

2.4.1 Introduction

The first reported polymerization of fluoroolefins in carbon dioxide was by Fukui and coworkers [39, 40]. Tetrafluoroethylene, chlorotrifluoroethylene, and other fluoroolefins were polymerized in the presence of CO_2 using ionizing radiation [39, 40] and free-radical initiators [40]. DeSimone and coworkers reported the homogeneous telomerization of tetrafluoroethylene [41] and vinylidene fluoride [42] in CO_2 using AIBN as an initiator. The kinetics of AIBN decomposition in CO_2 is well understood [4]. However, peroxide initiators are preferred over azo initiators for producing stable endgroups in fluoroolefins [43]. The peroxy initiators bis(perfluoro-2-N-propoxypropionyl) peroxide (BPPP) and diethyl peroxydicarbonate (DEPDC) have had the greatest application in the heterogeneous polymerization of fluoroolefins in CO_2.

DeSimone and coworkers have studied the decomposition kinetics of BPPP [44] and DEPDC [45] in CO_2. The decomposition of DEPDC was studied [45] by a

technique in which the decomposition rate constant, k_D, and the initiator efficiency, f, were determined from a single set of experiments using a continuous stirred tank reactor (CSTR). It was found that the decomposition was first order and that the rate constant was independent of the pressure. The activation energy of the decomposition rate constant in CO_2 was consistent with those in other solvents. It was concluded that the nature of the solvent did not affect the decomposition kinetics. The decomposition kinetics of BPPP [44] in CO_2 and fluorinated solvents was measured using FTIR. Based on results from the effect of viscosity on the observed decomposition rate constant, it was concluded that the decomposition mechanism was a single-bond homolysis. Additionally, it was concluded that the decomposition rate constant in CO_2 and in fluorinated solvents should be similar. The studies of BPPP and DEPDC decomposition in CO_2 sets the stage for better understanding the overall kinetics of polymerizations in CO_2. The next section contains a discussion of recent research to polymerize fluoroolefins in CO_2 using BPPP, DEPDC, and ionizing radiation.

2.4.2 Polymerization of Tetrafluoroethylene

Several alternative polymerization media have been proposed for reducing the amount of unstable end groups in poly(tetrafluoroethylene). These include chlorofluorocarbons, which are detrimental to the environment, perfluorocarbons, hydrofluorocarbons, and perfluoroalkyl sulfide acids, which are all expensive. Supercritical carbon dioxide has been identified as a viable alternative to aqueous and fluorocarbon reaction media [31]. Furthermore, mixing tetrafluoroethylene with

carbon dioxide increases the safety of handling the monomer [46]. Pure tetrafluoroethylene (TFE) is susceptible to autopolymerization and may be explosive without proper handling. Storing and shipping TFE in a mixture with CO_2 makes handling safer.

The polymerization of TFE in CO_2 [31-35, 41, 47] has been studied extensively. Polymerizations were typically run at 35°C using BPPP as an initiator. This particular initiator was selected to produce stable end groups in the polymer made in CO_2. The selection of initiators for polymerization of fluoromonomers in CO_2 that would produce stable end groups had not been reported previously. The reaction produced up to a 100% yield and a 160,000 g/mol molecular weight polymer. This work set the stage for commercialization of a CO_2-based process for making TFE-based polymers by DuPont [5]. DuPont has begun the sale of melt-processible polymers having enhanced performance capabilities [29] that were polymerized in a CO_2-based process.

2.4.3 Polymerization of Vinylidene Fluoride

The current means for commercial production of poly(vinylidene fluoride) generates large amounts of wastewater due to water-based suspension or emulsion polymerization. Additionally, large amounts of energy are required to remove the water from the polymer before downstream processing. The use of $scCO_2$ as a polymerization medium for vinylidene fluoride has been previously demonstrated in batch polymerizations [42, 48]. A CO_2-based system has the advantage of eliminating wastewater generation during the polymerization. Because the polymer

is readily separated from CO_2, significant energy savings may be realized. Recently, Charpentier et al. have developed a system for polymerizing vinyl monomers, including vinylidene fluoride, in $scCO_2$ using a continuous stirred tank reactor [36]. The technical viability of continuously polymerizing vinylidene fluoride in $scCO_2$ was demonstrated with this system. Furthermore, Solvay Corporation has recently patented a system for continuous polymerization of vinylidene fluoride and other halogenated monomers in $scCO_2$ [38].

The first demonstration of vinylidene fluoride polymerization in $scCO_2$ was the homogeneous telomerization of vinylidene fluoride with perfluorobutyl iodide and AIBN [42]. Several batch studies [48, 49] then were conducted to identify appropriate initiators for CO_2-based synthesis of high molecular weight PVDF. Kipp [48] used several different peroxy and azo initiators and found that the azo initiators, AIBN and 2,2'-azobis(2,4-dimethyl-methoxypentanitrile), were ineffective in producing significant amounts of PVDF. Amongst the peroxy initiators studied, Kipp found that BPPP was very effective as an initiator for vinylidene fluoride. Number-average molecular weights (M_n) upwards of 24,000 g/mol and conversions up to 85% were reported. Brothers [49] found that dimethyl(2,2'-azobisisobutyrate) was better than other azo initiators, such as AIBN, for initiating polymerization of vinylidene fluoride in CO_2. Brothers reported reaction yields of 22.8%, compared to only 2.6% for an AIBN-initiated system.

Galia and coworkers [50] used γ-radiation to initiate polymerization of VF2 in CO_2. Reactions were run at 20-40°C at pressures less than 25 MPa. Number-

average molecular weights as high as 607,000 g/mol were observed in polymerizations with initial monomer concentrations ranging from 3.4 to 4.7 mol/L. The polydispersity ranged from 2.5 to 8.8. Conversions were 20-42%. At the highest monomer concentration studied (6.2 mol/L), a conversion of 73% was observed. Galia concluded from rheological measurements of the polymers that increasing the monomer concentration increased the degree of branching and crosslinking in the polymer. The effect of temperature and system density on the kinetics and polymer properties was also studied. There was no observable impact of the system density on the kinetics or polymer properties. However, the polymer properties were very sensitive to the reaction temperature.

Recently, Charpentier et al. [36] demonstrated the synthesis of PVDF by a continuous precipitation polymerization in $scCO_2$, using diethyl peroxydicarbonate (DEPDC) as an initiator. Low molecular weight polymers (M_n < 20,000 g/mol) were reported in this first work. However, subsequent research has yielded PVDF with number-average molecular weights upwards of 79,000 g/mol [51, 52]. PVDF made in the continuous CO_2-based system had molecular weights comparable to commercial polymers, but also exhibited unique properties not observed in PVDF made by conventional processes.

2.4.3.1 Continuous Polymerization

In a typical continuous polymerization [36, 51-54], vinylidene fluoride (VF2), carbon dioxide, and initiator are continuously fed to a continuous stirred tank reactor (CSTR). The initiator is dissolved in Freon-113 and the ratio of initiator to monomer

was typically less than 0.01g/g. This initial reaction mixture is homogeneous over the full range of monomer concentrations evaluated (up to 6 M or 50 wt% VF2 in CO_2). As the reaction proceeds, the polymer precipitates from the fluid phase to form a solid polymer phase. The effluent exiting the reactor consists of polymer particles suspended in a fluid mixture of carbon dioxide, unreacted monomer, and unreacted initiator. The effluent is passed through a heat exchanger to quench the reaction. The polymer is collected in one of three filters, depending on whether the reactor is running at unsteady state or steady state. Finally, after the polymer is separated, the effluent is vented into a hood. Conceivably, the effluent may be recycled back to the reactor. A schematic of the polymerization system is shown in Figure 2.2. Typical conversions in the reactor are 7-25%. A range of reaction conditions was studied at 30-80°C, 130-280 bar, and average residence times of 12-50 minutes.

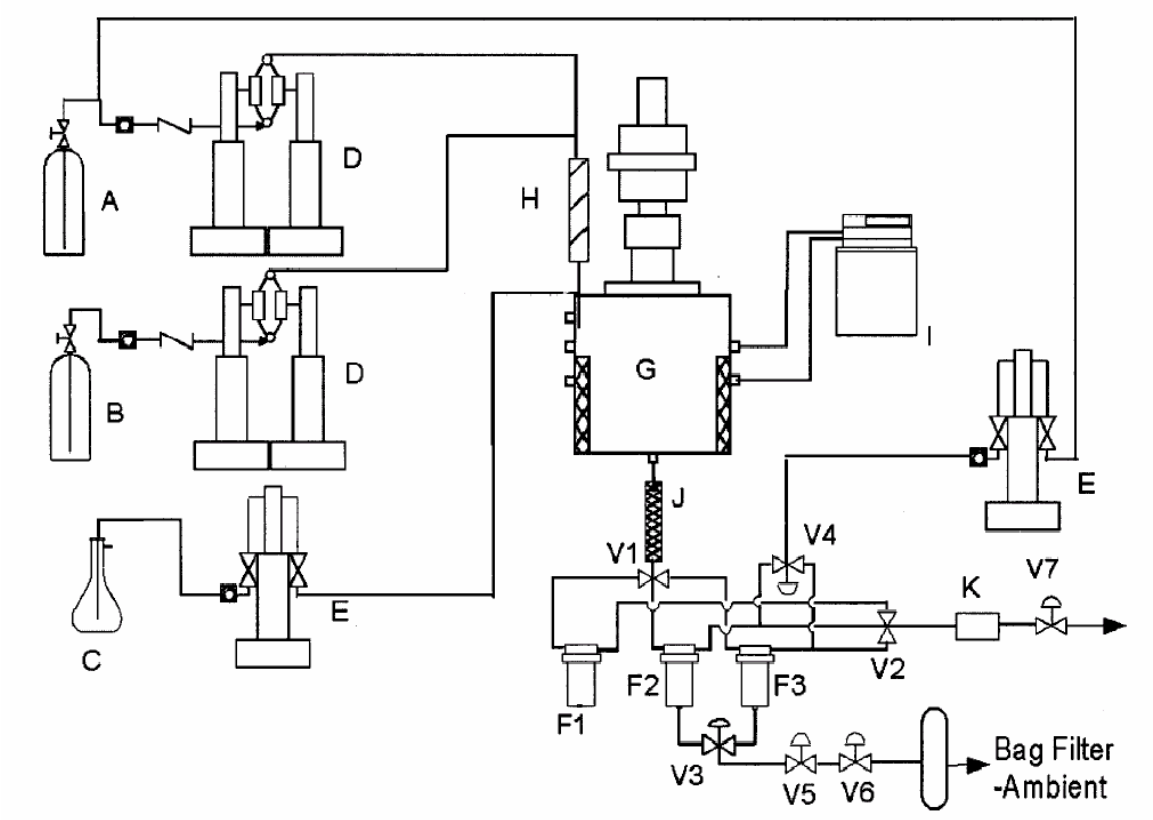

Figure 2.2 Continuous polymerization apparatus: A, CO_2 cylinder; B, monomer; C, initiator solution; D, continuous syringe pumps; E, syringe pumps; F1, steady-state filter; G, thermostated autoclave; H, static mixer; I, chiller/heater unit; J, effluent cooler; K, gas chromatograph; V1, V2, four-way valves; V3, V4, three-way valves; V5, V6, two-way valves; V7, heated control valve [51]

A kinetic model based on homogeneous polymerization was developed to describe the polymerization in CO_2 [51, 54]. A model based on the reaction scheme in Figure 2.3 adequately described the polymerization rates and the polydispersity of the polymer. Monomer inhibition was incorporated into the model to account for the observed deviation from first-order kinetics. However, imperfect mixing of the higher viscosity medium is an alternative explanation. It was concluded that termination was by combination, for three reasons. First, there was no existing literature to

support termination by disproportionation for PVDF. Second, the polydispersity was approximately 1.5 at low monomer concentrations. Third, NMR studies showed no evidence of unsaturation.

$$I \xrightarrow{k_D} 2fR^{\bullet} \qquad \text{(Initiator decomposition)}$$

$$R^{\bullet} + M \xrightarrow{k_M} P_1^{\bullet} \qquad \text{(Chain initiation)}$$

$$P_n^{\bullet} + M \xrightarrow{k_p} P_{n+1}^{\bullet} \qquad \text{(Propagation)}$$

$$P_n^{\bullet} + P_m^{\bullet} \xrightarrow{k_{tc}} P_{n+m} \qquad \text{(Termination by combination)}$$

$$P_n^{\bullet} + M \xrightarrow{k_Q} P_n + M^{*} \qquad \text{(Inhibition)}$$

$$P_n^{\bullet} + P_m \xrightarrow{mk_{tp}} P_m^{\bullet} + P_n \qquad \text{(Chain transfer to polymer)}$$

Figure 2.3 Kinetic scheme to model the continuous polymerization of vinylidene fluoride in supercritical carbon dioxide [51]

Chain transfer to polymer was proposed to account for the broadening of the molecular weight distribution at high monomer concentrations. However, as discussed in the next section, the model failed to predict the bimodal character that is unique to PVDF polymerized in $scCO_2$ at high monomer concentrations.

2.4.3.1.1 Polymer Properties

A comparison was made between the properties of PVDF synthesized in CO_2 and a commercial PVDF sample. The polymers synthesized in CO_2 had molecular weights similar to the commercial polymer and the melt flow indices (MFIs) were

similar [54]. For PVDF synthesized in CO_2 having a weight-average molecular weight of 150,000 g/mol, the MFI was 2.6 g/10 min. The MFI for a commercial sample with a weight-average molecular weight greater than 195,000 was 1.4 g/10 min.

Unique PVDF properties have been observed from polymerization in supercritical carbon dioxide [38, 51-53, 55] at certain conditions. The polymer synthesized in supercritical carbon dioxide exhibits a bimodal molecular weight distribution (MWD), as illustrated in Figure 2.4 [52]. At molar VF2 feed concentrations less than about 1.9 M, the polymer has a unimodal distribution, at the conditions of Figure 2.4. As the monomer concentration is increased, the distribution becomes broader and bimodal. Changes in temperature, pressure, and residence time also have an effect on the MWD [51, 52]. In Figure 2.4, τ is the average residence time, i.e., the reactor volume divided by the inlet volumetric flow rate.

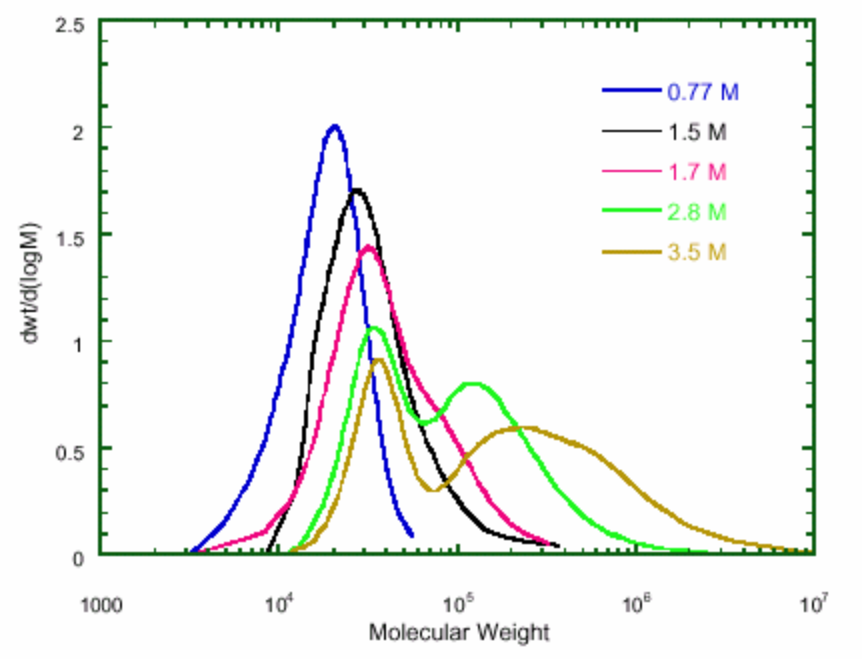

Figure 2.4 Effect of inlet monomer concentration on molecular weight distribution. Polymerization conditions are 75°C, 4000 psig, τ = 20-22 min, $[I]_o$ = 2.8 - 3.3 mmol/L [52]

Several hypotheses were investigated to explain the bimodal character of the polymer. These include: (1) imperfect mixing, (2) long chain branching, and (3) heterogeneous polymerization. A heterogeneous polymerization is characterized by polymerization in both the fluid and precipitated polymer phases, so that the phase equilibrium is an important element of kinetics and polymer properties. It was stated that neither imperfect mixing nor a homogeneous polymerization with long chain branching due to chain transfer to polymer could explain the bimodal nature of the CO_2-polymerized PVDF [51, 52]. However, it was recently demonstrated that a combination of chain branching and heterogeneous polymerization could produce the bimodal MWDs observed experimentally [56]. The impact of phase equilibrium

on the polymerization of vinylidene fluoride in supercritical carbon dioxide will be addressed in this dissertation.

2.4.4 Synthesis of Copolymers

Copolymerizations of TFE [31, 47, 57-61] and VF2 [57, 58, 61, 62] in $scCO_2$ have been reported. Romack and coworkers [47, 60] did early work to perform precipitation polymerizations of TFE with HFP and TFE with perfluoropropyl vinyl ether (PPVE) at 35°C and moderate pressures (<133 bar). A chain transfer agent, methanol, was necessary to limit the molecular weight to a range of commercial interest. Hydrogen chloride and hydrogen bromide have also been reported as effective chain transfer agents for these polymerizations in CO_2 [58]. Romack and coworkers concluded that the significantly higher molecular weights produced in CO_2 were due to the fact that chain transfer and β-scission reactions occurred to a lesser extent in $scCO_2$, especially at the lower temperatures used. These undesirable reactions are commonplace in the copolymerization of TFE/PPVE conducted at elevated temperatures in conventional solvents. The limited β-scission reactions were attributed to the enhanced diffusion of TFE into the polymer phase to improve the rates of radical cross-propagation with TFE. It was demonstrated that conducting the polymerization in CO_2 improved the effectiveness of the propagation reaction over that of the chain transfer reactions to produce high molecular weight polymers.

The research group of Shoichet [57, 59] also has demonstrated that using CO_2 as a polymerization medium can improve the effectiveness of the propagation

reaction over chain transfer reactions in fluoroolefin synthesis. Shoichet's group polymerized vinyl acetate with fluoroolefins in CO_2 with [59] and without [57] surfactants. The copolymers formed in CO_2 were linear, compared to the highly branched copolymers formed by aqueous polymerization. They concluded that because radical hydrogen abstraction from vinyl acetate was significantly reduced in CO_2, branching of the polymer was practically eliminated.

There has been research on new, novel fluoroolefin-based copolymers that benefit from synthesis in $scCO_2$. In 2000, Wheland and Brothers [61] described novel copolymers of fluoroolefins with maleic anhydride (MAN) and maleic acid (MAC) for use as coatings and as adhesives or compatibilizing agents for fluoropolymers. Currently, maleic anhydride must be grafted onto existing fluoropolymers to achieve the desired properties. Maleic acid does not readily copolymerize with fluoroolefins in the presence of water. Thus, polymerization of MAN or MAC with fluoroolefins in CO_2 provides a means by which to synthesize the desired fluoropolymer directly. In the area of microchip manufacture, there is an interest in using 157 nm photoresists to create smaller and smaller features in the circuitry. Zannoni and DeSimone [62] have copolymerized fluoroolefins with norbornene and a norbornene analog for use as 157 nm photoresists. Ultimately, these photoresists may be synthesized, processed and developed entirely in CO_2, with dramatically reduced solvent use and revolutionizing the manufacture of microchips.

2.5 Conclusions

Supercritical carbon dioxide shows promise as a polymerization medium for synthesis of fluoroplastics and fluoroelastomers. CO_2 offers the benefit of an environmentally friendly process that reduces the amount of waste generated and energy for processing polymers. Additionally, polymerization kinetics and polymer properties may be enhanced by polymerization in CO_2. DuPont has already commercialized a process for making fluoropolymers in CO_2. Use of CO_2 as a polymerization medium for certain grades of fluoropolymers eliminates the need for C8, which has received a lot of controversy in recent years. It remains to be seen whether many of the current grades of fluoropolymers can be synthesized in carbon dioxide. For PTFE, to date only granular forms of PTFE have been achieved. It would be of importance to synthesize fine powders of PTFE and other fluoropolymers in CO_2 to eliminate the C8 problem. As researchers continue to better understand CO_2-based polymer applications and as industry continues to look for more economically and environmentally sound alternatives to existing processes, supercritical carbon dioxide should become a technology of choice for new and improved commercial polymerization processes.

2.6 References

1. Swallow, J.C., *The history of polythene*, in *Polythene: The Technology and Uses of Ethylene Polymers*, A. Renfrew and P. Morgan, Editors. 1960, Interscience Publishers Inc.: New York. p. 1-10.

2. Kirby, C.F. and McHugh, M.A., *Phase behavior of polymers in supercritical fluid solvents.* Chemical Reviews, 1999. **99**(2): p. 565-602.

3. Folie, B. and Radosz, M., *Phase equilibria in high-pressure polyethylene technology.* Industrial and Engineering Chemistry Research, 1995. **34**(5): p. 1501-1516.

4. Guan, Z., Combes, J.R., Menceloglu, Y.Z., and DeSimone, J.M., *Homogeneous free radical polymerizations in supercritical carbon dioxide: 2. Thermal decomposition of 2,2'-azobis(isobutyronitrile).* Macromolecules, 1993. **26**(11): p. 2663-2669.

5. McCoy, M., *DuPont, UNC partnership yields Teflon investment.* Chemical and Engineering News, 1999. **77**(17): p. 10.

6. Canelas, D.A. and DeSimone, J.M., *Polymerizations in liquid and supercritical carbon dioxide*, in *Advances in Polymer Science*. 1997, Springer: New York. p. 103-140.

7. Cooper, A.I., *Polymer synthesis and processing using supercritical carbon dioxide.* Journal of Materials Chemistry, 2000. **10**(2): p. 207-234.

8. Kendall, J.L., Canelas, D.A., Young, J.L., and DeSimone, J.M., *Polymerizations in supercritical carbon dioxide.* Chemical Reviews, 1999. **99**(2): p. 543-563.

9. Manivannan, G. and Sawan, S.P., *The supercritical state*, in *Supercritical Fluid Cleaning: Fundamentals, Technology and Applications*, J. McHardy and S.P. Sawan, Editors. 1998, Noyes Publications: Westwood, NJ. p. 1-21.

10. *Perfluorooctanoic Acid (PFOA) and Fluorinated Telomers*, www.epa.gov/opptintr/pfoa/, Federal Register: April 14, 2003.

11. Lee, J., *Chemical might pose health risk to younger women and girls* in *New York Times*, New York, March 29, 2003

12. Ring, K.-L., Kalin, T., and Kishi, A., *Fluoropolymers*, in *Chemical Economics Handbook*. 2002, SRI International: Menlo Park, California.

13. Feiring, A.E., *Fluoroplastics*, in *Organofluorine Chemistry: Principles and Commercial Applications*, R.E. Banks, B.E. Smart, and J.C. Tatlow, Editors. 1994, Plenum Press: New York. p. 339-372.

14. Gangal, S.V., *Polytetrafluoroethylene, homopolymer of tetrafluoroethylene*, in *Encyclopedia of Polymer Science and Engineering*, H.F. Mark, N.M. Bikales, C.G. Overberger, and G. Menges, Editors. 1985, Wiley: New York. p. 577-600.

15. Tervoort, T., Visjager, J., Graf, B., and Smith, P., *Melt-processable poly(tetrafluoroethylene).* Macromolecules, 2000. **33**(17): p. 6460-6465.

16. Lovinger, A.J., *Poly(vinylidene fluoride)*, in *Developments in Crystalline Polymers*, D.C. Bassett, Editor. 1982, Applied Science Publishers: London. p. 195-273.

17. Dohany, J.E., *Poly(vinylidene fluoride)*, in *Kirk-Othmer Encyclopedia of Chemical Technology*, J.I. Kroschwitz, Editor. 1994, John Wiley & Sons, Inc.: New York. p. 694-712.

18. Seiler, D.A., *PVDF in the Chemical Process Industry*, in *Modern Fluoropolymers: High Performance Polymers for Diverse Applications*, J. Scheirs, Editor. 1997, John Wiley & Sons: Chichester. p. 487-506.

19. Scheirs, J., *Fluoropolymers: Technology, Markets, and Trends*. Rapra Industry Analysis Report Series. 2001, Shawbury: Rapra Technology Limited. 128.

20. *Kynar PVDF for Lithium Batteries*, www.atofinachemicals.com/kynarglobal/kynar-literature.cfm, Internet brochure: 2003.

21. Kochervinskii, V.V., Danilyuk, T.Y., and Madorskaya, L.Y., *Effect of polymerization conditions on morphology and molecular mobility in poly(vinyl fluoride).* Polymer Science U.S.S.R., 1986. **28**(3): p. 690-699.

22. Dohany, J.E. and Humphrey, J.S., *Vinylidene fluoride polymers*, in *Encyclopedia of polymer science and engineering*, H.F. Mark and J.I. Kroschwitz, Editors. 1985, Wiley: New York. p. 532-548.

23. Jo, S.M., Lee, W.S., Oh, H.J., Park, S., Ahn, B.S., and Park, K.Y., *A study on polymerization of PVDF based fluoropolymers with high performance for battery (I).* Polymer (Korea), 1999. **23**(6): p. 800-808.

24. Wille, R.A. and Burchill, M.T., *Copolymers of vinylidene fluoride and hexafluoropropylene having reduced extractable content and improved solution clarity*, WO Patent 9838687 (to Elf Atochem North America, Inc.), 1998.

25. Doll, W.W. and Lando, J.B., *The polymorphism of poly(vinylidene fluoride). II. The effect of hydrostatic pressure.* Journal of macromolecular science. Physics, 1968. **2**(2): p. 219-233.

26. Dohany, J.E., *Vinylidene fluoride polymer having improved melt flow properties*, US Patent 4076929 (to Pennwalt Corporation), 1978.

27. Savage, P.E., Gopalan, S., Mizan, T.I., Martino, C.J., and Brock, E.E., *Reactions at supercritical conditions: Applications and fundamentals.* AIChE Journal, 1995. **41**(7): p. 1723-1778.

28. DeSimone, J.M., *Practical Approaches to Green Solvents.* Science, 2002. **297**: p. 799-803.

29. *DuPont introduces fluoropolymers made with supercritical CO_2 technology*, www.dupont.com/corp/news/products_today.html, Press Release: March 22, 2002.

30. DeSimone, J.M., *Method of making fluoropolymers*, US Patent 5496901 (to University of North Carolina), 1996.

31. DeSimone, J.M. and Romack, T., *Nonaqueous polymerization of fluoromonomers*, US Patent 5618894 (to University of North Carolina at Chapel Hill), 1997.

32. DeSimone, J.M. and Romack, T., *Nonaqueous polymerization of fluoromonomers*, US Patent 5674957 (to University of North Carolina at Chapel Hill), 1997.

33. DeSimone, J.M. and Romack, T., *Nonaqueous polymerization of fluoromonomers*, US Patent 5981673 (to University of North Carolina at Chapel Hill), 1999.

34. DeSimone, J.M. and Romack, T., *Nonaqueous polymerization of fluoromonomers*, US Patent 5939501 (to University of North Carolina at Chapel Hill), 1999.

35. DeSimone, J.M. and Romack, T., *Nonaqueous polymerization of fluoromonomers*, US Patent 5939502 (to University of North Carolina at Chapel Hill), 1999.

36. Charpentier, P.A., Kennedy, K.A., DeSimone, J.M., and Roberts, G.W., *Continuous polymerizations in supercritical carbon dioxide: Chain-growth precipitation polymerizations.* Macromolecules, 1999. **32**: p. 5973-5975.

37. DeSimone, J.M., Charpentier, P.A., and Roberts, G.W., *Continuous process for making polymers in carbon dioxide*, WO Patent 0134667 (to University of North Carolina), 2001.

38. Blaude, J.-M., Chauvier, J.-M., Martin, R., and Bienfait, C., *Method for preparing halogenated polymers and resulting halogenated polymers*, WO Patent 02055567 (to Solvay), 2002.

39. Fukui, K., Kagiya, T., and Yokota, H., *Fluorocarbon resins*, JP Patent 45003390 (to Sumitomo Chemical Co., Ltd.), 1970.

40. Fukui, K., Kagiai, T., and Yokota, H., *Fluorine-containing polymers*, JP Patent 46011031 (to Sumitomo Chemical Co., Ltd.), 1971.

41. Romack, T.J., Combes, J.R., and DeSimone, J.M., *Free-radical telomerization of tetrafluoroethylene in supercritical carbon dioxide.* Macromolecules, 1995. **28**(5): p. 1724-1726.

42. Combes, J.R., Guan, Z., and DeSimone, J.M., *Homogeneous free-radical polymerizations in carbon dioxide. 3. Telomerization of 1,1-difluoroethylene in supercritical carbon dioxide.* Macromolecules, 1994. **27**(3): p. 865-867.

43. Hintzer, K. and Lohr, G., *Melt processable tetrafluoroethylene-perfluoropropylvinyl ether copolymers (PFA)*, in *Modern Fluoropolymers: High Performance Polymers for Diverse Applications*, J. Scheirs, Editor. 1997, John Wiley & Sons: Chichester. p. 223-238.

44. Bunyard, W.C., Kadla, J.F., and DeSimone, J.M., *Viscosity effects on the thermal decomposition of bis(perfluoro-2-N-propoxypropionyl) peroxide in dense carbon dioxide and fluorinated solvents.* Journal of the American Chemical Society, 2001. **123**(30): p. 7199-7206.

45. Charpentier, P.A., DeSimone, J.M., and Roberts, G.W., *Decomposition of polymerisation initiators in supercritical CO_2: a novel approach to reaction kinetics using a CSTR.* Chemical Engineering Science, 2000. **55**(22): p. 5341-5349.

46. Bramer, D.J.V., Shiflett, M.B., and Yokozeki, A., *Safe handling of tetrafluoroethylene*, US Patent 5345013 (to E. I. du Pont de Nemours and Company), 1994.

47. Romack, T.J., *Polymerization of fluoroolefins in liquid and supercritical carbon dioxide (free radical)*. PhD Thesis, Department of Chemistry, University of North Carolina at Chapel Hill, 1997.

48. Kipp, B.E., *The synthesis of fluoropolymers in carbon dioxide and carbon dioxide/aqueous systems*. PhD Thesis, Department of Chemistry, University of North Carolina at Chapel Hill, 1997.

49. Brothers, P.D., *Polymerization of fluoromonomers in carbon dioxide*, US Patent 6103844 (to E. I. du Pont de Nemours and Company), 2000.

50. Galia, A., Caputo, G., Spadaro, G., and Filardo, G., *γ-Radiation-initiated polymerization of vinylidene fluoride in dense carbon dioxide.* Industrial and Engineering Chemistry Research, 2002. **41**(24): p. 5934-5940.

51. Saraf, M.K., Gerard, S., Wojcinski.II, L.M., Charpentier, P.A., DeSimone, J.M., and Roberts, G.W., *Continuous precipitation polymerization of vinylidene fluoride in supercritical carbon dioxide: formation of polymers with bimodal molecular weight distributions.* Macromolecules, 2002. **35**(21): p. 7976-7985.

52. Saraf, M.K., *Polymerization of vinylidene fluoride in supercritical carbon dioxide: Molecular weight distribution*. Masters Thesis, Department of Chemical Engineering, North Carolina State University, 2001.

53. DeSimone, J.M., Charpentier, P.A., and Roberts, G.W., *Multimodal fluoropolymers and methods of making the same*, WO Patent 0190206 (to University of North Carolina), 2001.

54. Charpentier, P.A., DeSimone, J.M., and Roberts, G.W., *Continuous precipitation polymerization of vinylidene fluoride in supercritical carbon dioxide: Modeling the rate of polymerization.* Industrial and Engineering Chemistry Research, 2000. **39**(12): p. 4588-4596.

55. Saraf, M.K., Wojcinski, L.M., Kennedy, K.A., Gerard, S., Charpentier, P.A., DeSimone, J.M., and Roberts, G.W., *Continuous precipitation polymerization of vinylidene fluoride in supercritical carbon dioxide: Molecular weight distribution.* Macromolecular Symposia, 2002. **182**(1): p. 119-129.

56. Saraf, M.K., Personal communication, 2002.

57. Baradie, B. and Shoichet, M.S., *Synthesis of fluorocarbon-vinyl acetate copolymers in supercritical carbon dioxide: Insight into bulk properties.* Macromolecules, 2002. **35**(9): p. 3569-3575.

58. Farnham, W.B. and Wheland, R.C., *Chain transfer agents in fluoroolefin polymerization*, WO Patent 0146275 (to E.I. DuPont de Nemours and Company), 2001.

59. Lousenberg, R.D. and Shoichet, M.S., *Synthesis of linear poly(tetrafluoroethylene-co-vinyl acetate) in carbon dioxide.* Macromolecules, 2000. **33**(5): p. 1682-1685.

60. Romack, T.J., DeSimone, J.M., and Treat, T.A., *Synthesis of tetrafluoroethylene-based nonaqueous fluoropolymers in supercritical carbon dioxide.* Macromolecules, 1995. **28**(24): p. 8429-8431.

61. Wheland, R.C. and Brothers, P.D., *Copolymers of maleic anhydride or acid and fluorinated olefins*, US Patent 6107423 (to E.I. du Pont de Nemours and Company), 2000.

62. Zannoni, L.A. and DeSimone, J.M., *Synthesis, characterization and properties of copolymers prepared in dense carbon dioxide towards the development of a 157 nm photoresist.* Polymeric Materials: Science & Engineering, 2002. **87**: p. 197-198.

Chapter 3

Review

Phase equilibrium between polymers and supercritical fluids

Supercritical carbon dioxide has been researched and applied in a variety of applications that involve polymers. These include microelectronics [1], foams [2], textile dying [2] and polymerizations in CO_2 [3]. An important aspect to all of these heterogeneous processes is the role of phase equilibrium. This involves the equilibrium between the polymer, CO_2, and other species present in the system. The degree to which CO_2 sorbs into the polymer phase can greatly impact the resultant processing conditions and polymer properties. For example, when spin coating photoresists with liquid CO_2, it is important to know the degree to which the polymer is soluble in CO_2 in order to form uniform coatings. In the heterogeneous polymerization of many monomer systems, the monomer is soluble in CO_2 whereas the polymer is insoluble in CO_2. However, CO_2 may plasticize the polymer, causing it to swell. Additionally, other species present in the system may partition between the polymer-rich and CO_2-rich fluid phases. This phase equilibrium will impact the reaction kinetics, polymer properties, and downstream processing of the polymer. These issues are not unique to supercritical fluids (SCFs). For example, Schubert and coworkers [4] studied microemulsions of styrene and hexyl methacrylate in formamide and found that a difference in the phase equilibrium of the monomer with the reaction medium greatly impacted the conversions and polydispersity of the

polymer. However, due to the significant compressibility of SCFs, small changes in temperature and pressure can have a much more significant impact in SCF-based processes than processes when the solvent is a conventional, essentially incompressible, liquid. Thus, studying the phase equilibrium in polymer and $scCO_2$ systems is necessary for fully understanding and exploiting the commercial potential of using $scCO_2$ with polymers.

This chapter will review the major approaches to understanding the phase equilibrium associated with polymers in supercritical carbon dioxide, including several experimental techniques and modeling approaches based on the Sanchez-Lacombe equation of state. Finally, existing studies of the phase equilibrium of poly(vinylidene fluoride) (PVDF) in CO_2 will be discussed.

3.1 Experimental Studies of Phase Equilibrium between Polymer and $scCO_2$ Phases

For several decades, researchers have been interested in understanding the advantages of using $scCO_2$ in polymer applications. The phase equilibrium, which considers how the polymer and supercritical fluid interact at equilibrium, allows researchers to study the major variables involved with optimizing the use of $scCO_2$. Several important techniques have emerged for studying the phase equilibria associated with polymers in CO_2. Those techniques can be divided into two categories: those used to study two component polymer-CO_2 systems, and those for the study of multi-component systems involving one or more polymers, CO_2, and one or more additional small molecules. Study of two component systems includes polymer swelling and sorption in the presence of CO_2 and the solubility of polymers

in CO_2. The multi-component systems involve similar phenomena, in addition to the partitioning of small molecules between the polymer and $scCO_2$ phases. The major methods for studying these phenomena will be discussed in the following section.

3.1.1 Polymer Solubility

The solubility of polymers in CO_2 is measured primarily by a static method. A representative apparatus is shown in Figure 3.1. A known weight of polymer is added to the variable-volume view cell. The system is heated to the desired temperature before adding a known amount of CO_2. The pressure is increased with the piston until a one-phase system is visually observed. The pressure is then slowly decreased until the system loses its transparency, or until two fluid phases are observed. This represents the cloud point for the system.

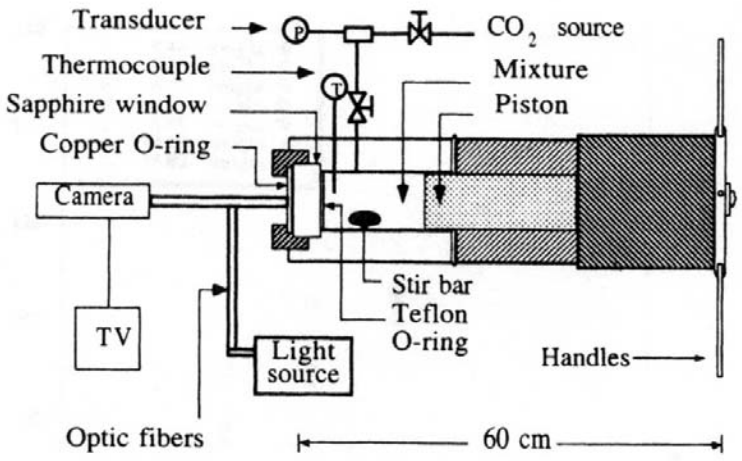

Figure 3.1 Apparatus for measuring solubility of polymers in carbon dioxide [5]

Cloud point curves for PVDF and a copolymer of vinylidene fluoride and hexafluoropropylene in CO_2 are shown in Figure 3.2. Conditions above the cloud point curve represent a one-phase region. Below the cloud point curve, two or more phases exist. PVDF required much greater temperatures and pressures than the copolymer in order for it to be soluble in CO_2. The melting point for this PVDF polymer in CO_2 is 130 °C. At temperatures below 130 °C, PVDF becomes a solid, such that separate solid and fluid phases exist in the region to the left of the cloud point curve.

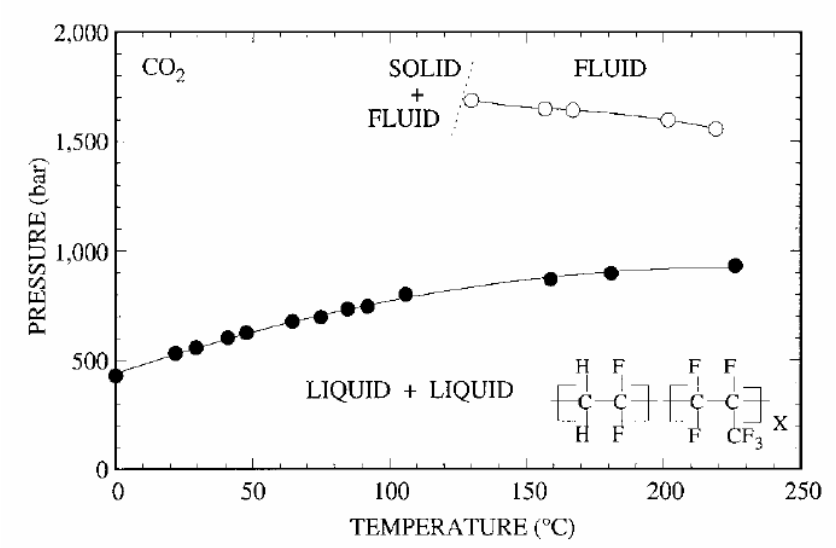

Figure 3.2 Cloud point curve for semicrystalline poly(vinylidene fluoride) (○, M_w = 269,000, x = 0) and amorphous poly(vinylidene fluoride-co-hexafluoropropylene) (●, M_w = 85,000, x = 22 mol%) in CO_2. Polymer compositions are 5 wt% [6]

Polymer solubility in CO_2 is dominated by the strength of the polymer-polymer interaction [7]. The strength of the polymer-CO_2 interaction has a secondary effect. O'Neill and coworkers [7] found that the polymer surface tension was a good

indicator of the polymer-polymer interaction. The strength of the interaction increased with the surface tension. The surface tension of several polymers and their corresponding solubility in CO_2 at 35 °C and 206.8 bar (3000 psi) is summarized in Table 3.1. The polymers with lower surface tension have weaker polymer-polymer interactions and are increasingly more soluble in CO_2.

Table 3.1
Surface tensions and solubilities in CO_2 for various homopolymers [7]

Polymer	Surface Tension (mN/m), 20 °C	Solubility, wt% (MW) @ 206.8 bar, 35 °C
Poly(1,1-dihydrodecafluorooctyl acrylate)	10	>>10 (1,000,000 g/mol)
Poly(1,1-dihydroheptafluorobutyl acrylate)	15	>>10 (1,000,000 g/mol)
Poly(dimethylsiloxane) (PDMS)	20	4 (13,000 g/mol)
Poly(tetrafluoroethylene) (PTFE)	23.9	Insoluble (high MW)
Poly(vinylidene fluoride) (PVDF)	33.2	Insoluble (500,000 g/mol)
Poly(vinyl acetate) (PVAc)	36.5	
Polystyrene	39.3	Insoluble (1700 g/mol)
Poly(methyl methacrylate) (PMMA)	41.1	Insoluble (3,000 g/mol)

3.1.2 Polymer Swelling

Several techniques have been employed for measuring the swelling of polymers in the presence of $scCO_2$. In recent years, ultrasonic transducers [8], neutron reflectivity [9], and linear variable differential transformers (LVDT) [10] have been used to measure polymer swelling in the presence of $scCO_2$. However, the most common method for measuring the swelling of polymers in $scCO_2$ is by visually observing the change in length of a polymer film [11-18]. Some of the first work done to measure the swelling of polymers in CO_2 was done at the University of Texas at Austin [13] and the University of Delaware [17]. These studies were conducted at pressures less than 10 MPa (1450 psi). More recently, the swelling of

polymer films in $scCO_2$ has been measured at pressures up to 30 MPa (4351 psi) [11].

The results of swelling polystyrene and poly(ethylene terephthalate) (PET) by CO_2 is shown in Figure 3.3. This work [11] demonstrates that polymers may be swollen by $scCO_2$ to increase their free volume. The percent volume change of the polymer film, $\left(\Delta V/V_o\right)\cdot 100\%$, was calculated by the equation,

$$\Delta V/V_o = \left(L/L_o\right)^3 - 1$$

where L_o is the initial dimensional length of the film and L is the length at equilibrium. This assumes that the polymer will swell isotropically. Isotropic swelling is applicable for films that are homogeneous, free of strain, and unoriented [18]. As shown in Figure 3.3, the swelling of crystalline PET was significantly less than the swelling of polystyrene. The crystalline regions largely impact the limited swelling of PET. Indeed, semicrystalline polymers are known to be intrinsically solvent resistant, including when the solvent is a supercritical fluid. The swelling of both polymers was greater at the lower temperature (308.15 K). The swelling increases almost linearly for polystyrene at pressures less than 10 MPa. At higher pressure, the swelling levels off to a constant value. This is due to a dominating hydrostatic pressure effect that restricts the polymer from swelling. In fact, Wang et al [19] demonstrated the dominating hydrostatic effect over plasticization at elevated pressures in polystyrene exposed to CO_2. The T_g of polystyrene in different CO2 environments was calculated using the WLF equation and creep compliance experiments. Initially, as the CO_2 pressure was increased, the T_g dropped

dramatically and reached a minimum around 20 MPa. The drop in T_g signified a plasticization of the polymer by carbon dioxide. With further increases in the pressure, the T_g began to increase as the hydrostatic pressure effect became more prominent.

The mass sorption of CO_2 into polymers has been calculated using swelling results [11]. However, specific techniques have been developed for measuring polymer sorption. This will be discussed in the next section.

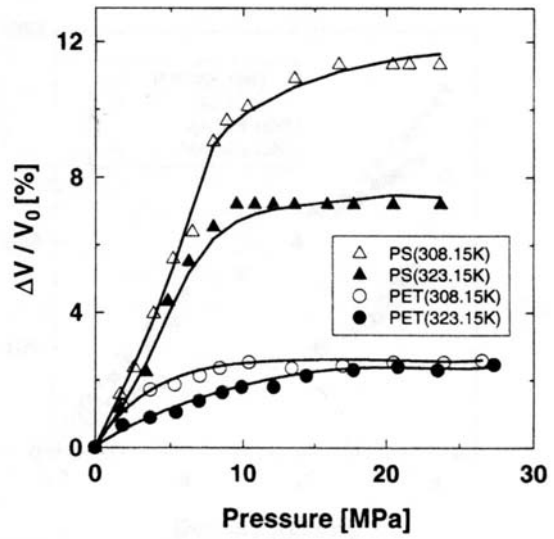

Figure 3.3 Swelling of polystyrene (PS) and poly(ethylene terephthalate) (PET) in CO_2. Lines represent prediction from combined Flory equation and Peng-Robinson equation of state [11]

3.1.3 Polymer Sorption

The sorption of supercritical carbon dioxide into polymers has been measured by a variety of techniques. The earliest studies of polymer sorption were conducted using a quartz spring [11, 17, 18]. In recent years, the quartz crystal microbalance

(QCM) [20, 21], vibrating rod [8], and magnetic suspension balance [22, 23] have been used to measure polymer sorption in the presence of supercritical carbon dioxide.

The quartz spring technique has been widely used due to its simple operation and relatively low cost. In this approach, the polymer is suspended from a quartz spring in a CO_2 atmosphere. As the polymer sorbs fluid, the spring is displaced. The change in mass of the polymer is calculated by

$$\Delta m = k(x-x_o) + \rho_g(V_p + V_t)$$

where k is the spring constant, x is the spring extension at equilibrium, x_o is the spring extension in the absence of CO_2, ρ_g is the density of CO_2, V_p is the volume of swollen polymer (determined from swelling experiments), and V_t is the volume of the sample pan and spring. The second term on the right hand side accounts for the buoyancy of CO_2. Figure 3.4 shows the results for sorption of CO_2 into polystyrene measured using a quartz spring. At low pressures, the sorption increases linearly with the pressure. As the temperature decreases, the sorption increases. The temperature and pressure effects correlate with an increase in the CO_2 density.

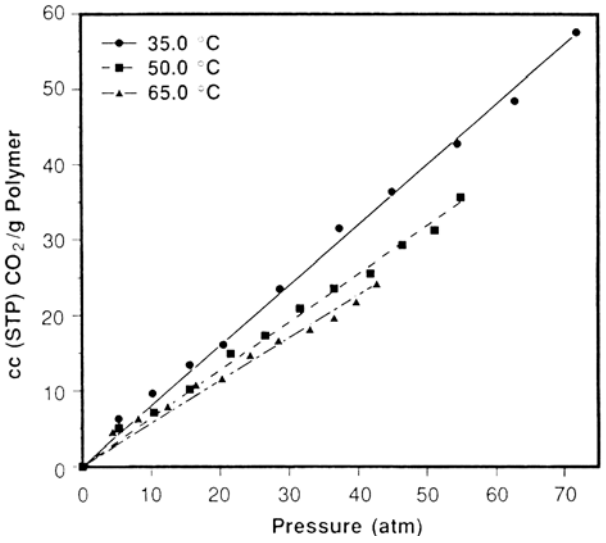

Figure 3.4 Sorption of CO_2 into polystyrene measured using a quartz spring [17]

The quartz crystal microbalance has been used to measure the sorption of polymers by CO_2 at pressures up to 172 bar (2500 psig) [20, 21]. In this technique, a quartz crystal is coated with the polymer. The polymer-coated quartz crystal is attached to electrodes that generate an alternating electric field in the crystal. This causes the crystal to vibrate at its resonant frequency. The change in mass of the polymer is measured by monitoring the change in frequency. This behavior is described by the Sauerbrey equation,

$$\Delta f = -C\Delta m$$

where Δf is the change in frequency, Δm is the corresponding change in mass, and C is a constant which is a function of the quartz crystal properties. The change in mass can be measured with a sensitivity of ± 1 ng. The two major assumptions for application of the Sauerbrey equation are that the coated film is thin and rigid. Lucklum and coworkers [24] determined how the structure of the polymer affects the

accuracy of the Sauerbrey equation. They found that the Sauerbrey equation is accurate for glassy polymers applied as thin films and rubbery polymers applied as very thin films. Figure 3.5 shows that for polystyrene, a glassy polymer, the QCM method produced results similar to those obtained by the quartz spring method.

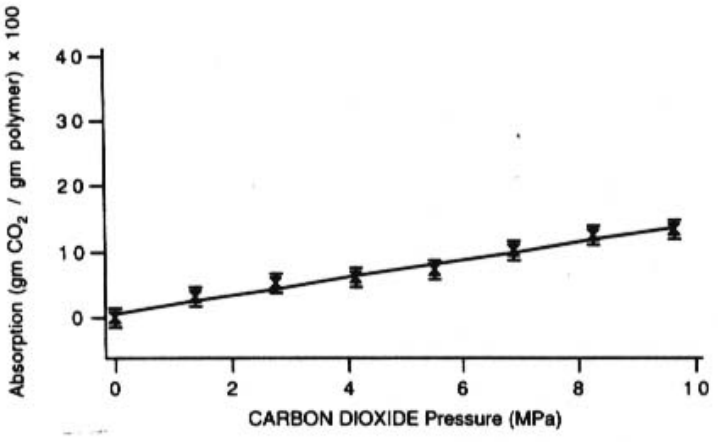

Figure 3.5 Sorption of CO_2 in polystyrene at 40 °C. Points represent data obtained by quartz crystal microbalance. Line represents data obtained by quartz spring at 35 °C [20]

Just as the QCM technique is based on correlating the change in mass with the change in frequency of the coated crystal, the vibrating rod technique correlates the change in mass with the change in the period of vibration of a beam with a rectangular polymer rod suspended on it. The beam is caused to vibrate by an electromagnetic coil. The period of vibration is a function of the ratio of the mass of the polymer rod to the mass of the beam. As gas is sorbed into the polymer, the ratio changes. The period of vibration changes as well. Briscoe and coworkers [8] used this technique to measure the sorption of $scCO_2$ into poly(vinylidene fluoride)

(PVDF). Their results are shown in Figure 3.6. At pressures lower than 18 MPa, the mass sorption is greater at the lower temperature (42 °C). This result is consistent with the general observation that the solubility of CO_2 in the polymer decreases at higher temperatures. At the higher pressures, the sorption at 80 °C is greater. The higher pressures restrict the dimensional change of the polymer, but the higher temperature (80 °C) allows the polymer to have greater mobility than at the lower temperature (42 °C).

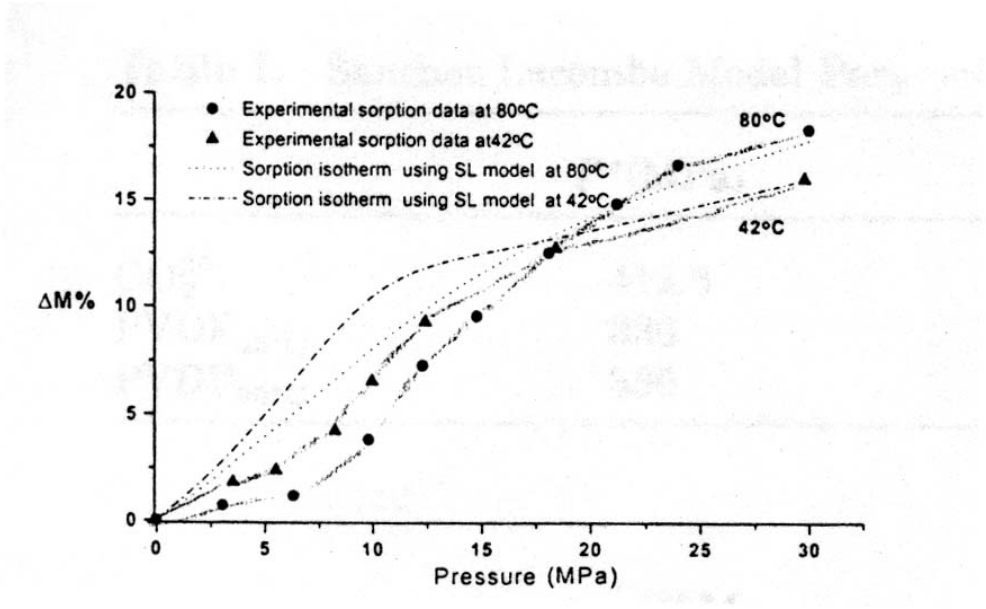

Figure 3.6 Sorption of CO_2 into poly(vinylidene fluoride) at 42 °C and 80 °C. Lines represent prediction based on Sanchez-Lacombe model [8]

Most recently, the magnetic suspension balance has been used as a precise technique for measuring the sorption of $scCO_2$ into polymers [22, 23, 25]. The polymer sample is suspended from a magnetic coupling that measures the change in mass of the sample exposed to a gas environment. This technique allows

measurement of the mass change in increments as low as 0.01 mg. Additionally, the balance may be equipped with the means to measure the density of the sorbing fluid to accurately account for the buoyancy in the system. Figure 3.7 shows that the sorption of CO_2 into polystyrene was consistent from measurement using the magnetic suspension balance and by a pressure decay method.

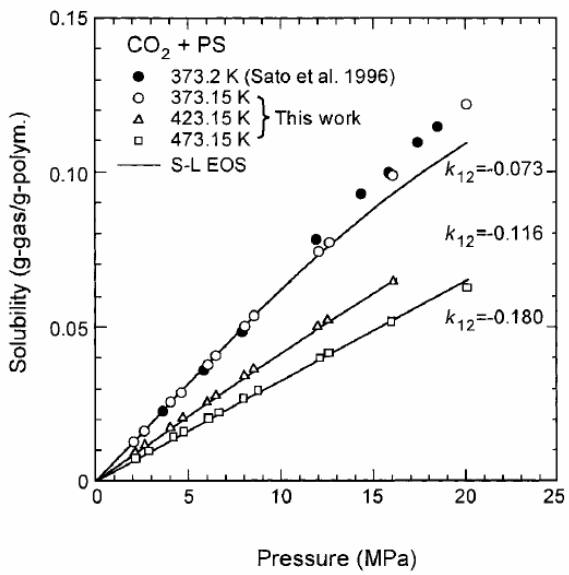

Figure 3.7 Sorption of CO_2 into polystyrene. White data points were obtained using magnetic suspension balance. Black data points were obtained using a pressure decay method. Lines represent prediction based on Sanchez-Lacombe model ($k_{12} = 1-\zeta$, the binary interaction parameter). Reprinted from Sato et al [25]

The magnetic suspension balance has also been used to detect retrograde vitrification [23] in polymer-CO_2 systems. Retrograde vitrification occurs when a polymer goes from a rubbery to a glassy state with an increase in temperature. This phenomenon has been predicted using lattice fluid theory [26]. The retrograde glass transition is commonly measured using creep compliance measurements [27].

Using the magnetic suspension balance, the diffusion coefficients of CO_2 in PMMA were measured over a range of temperatures and pressures [23]. A sharp increase in the diffusion coefficient with pressure indicated the presence of a glass transition pressure. By plotting the glass transition pressures with the corresponding temperatures, the retrograde glass transition behavior is observed (Figure 3.8). At a single pressure, as the temperature is increased, the polymer may go from a rubbery to a glassy to a rubbery state.

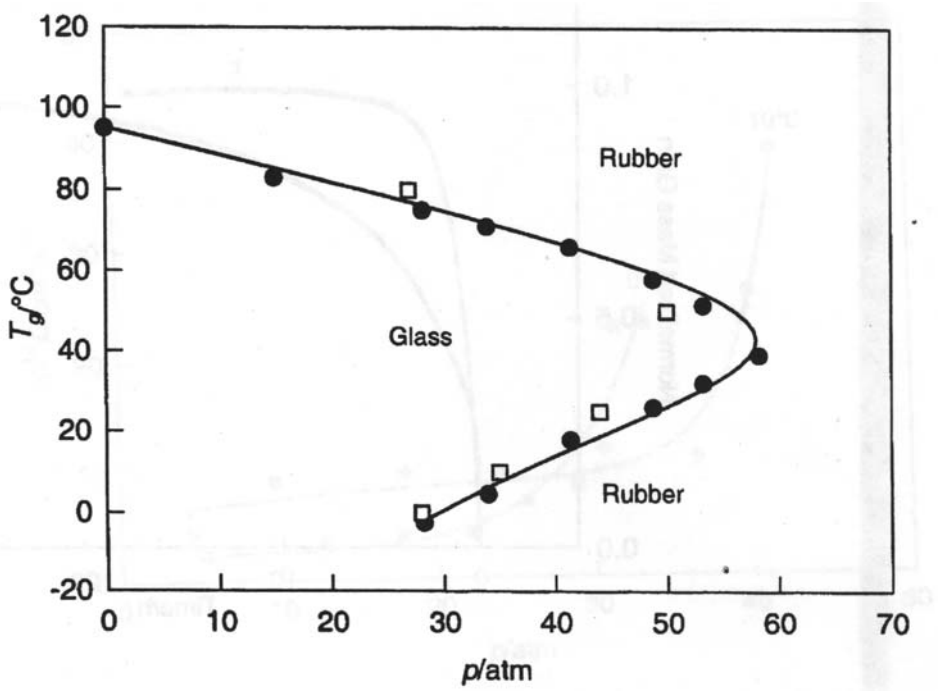

Figure 3.8 Tg of PMMA in the presence of CO_2 as a function of pressure measured using a magnetic suspension balance (□) and with a temperature scanning high-pressure calorimetric technique (●). Reprinted from [23]

Researchers have used spectroscopy as a tool to predict the degree to which CO_2 would be soluble in a polymer. Kazarian and coworkers [28] found that a measure of the width of the v_2 band for CO_2 by infrared spectroscopy could be used

to estimate the solubility of CO_2 in polymers. An example of the change in the v_2 bending mode of CO_2 impregnated in a polymer is illustrated in Figure 3.9. The authors impregnated various polymers with CO_2 and noted the change in the v_2 band for CO_2. Their results are summarized in Table 3.2. If a specific interaction existed between the polymer and CO_2, the v_2 band was split. As illustrated in Table 3.2, the increase in CO_2 solubility correlated with an increased average width of the v_2 band for CO_2.

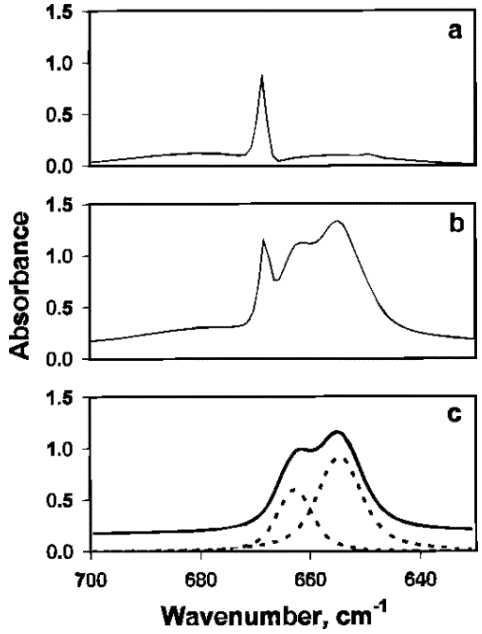

Figure 3.9 IR absorption spectra of CO_2 in the v_2 bending mode region: (a) gaseous sample, (b) PMMA film impregnated with CO_2 immediately after decompression, and (c) film after removal of gaseous CO_2 [28]

Table 3.2
Solubilities and half-width of adsorption band of ν_2 mode of CO_2 in polymers [28]

Polymer	$\Delta\nu_{1/2}$*, cm^{-1}	CO_2 Solubility, wt% @ 14 bar, 25 °C
Poly(vinyl acetate)	16	5.7
Poly(ethyl methacrylate) (PEMA)	15	4.6
Poly(methyl methacrylate) (PMMA)	15	4.2
Polystyrene	11.5	3.1
Polyethylene	5.5	0.8

* $\Delta\nu_{1/2}$ = full width at half-maximum of the ν_2 absorption band

3.1.4 Partitioning between Polymer and $scCO_2$ Phases

Most research on phase equilibrium in $scCO_2$ has focused on the sorption and swelling of polymers. Relatively little has been done to measure the partitioning behavior of solutes between polymer and $scCO_2$ phases. The partition coefficient is defined as the ratio between the concentration of solute (i) in the polymer phase (II) to that in the $scCO_2$ phase (I),

$$K_c = \frac{C_i^{II}}{C_i^{I}}$$

The partition coefficients for several solutes in $scCO_2$ and poly(dimethylsiloxane) (PDMS) have been determined using inverse supercritical fluid chromatography [29] and FTIR [16, 30]. These techniques measured partition coefficients at very low concentrations. The results demonstrate the impact of the tunable properties of CO_2 on partition coefficients. This is illustrated in Figure 3.10. The partition coefficient for methanol in PDMS decreases with increasing CO_2 density at constant temperature. Two reasons have been proposed for this behavior. First, as the CO_2 density increases, the solvating power of CO_2 increases. More solute can dissolve

in the fluid phase at higher CO_2 densities. Second, as the density increases, the polymer is increasingly swollen with CO_2, weakening the attraction of the solute to the polymer.

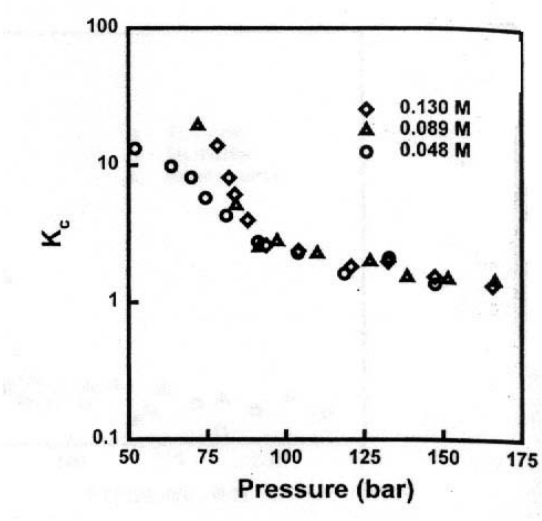

Figure 3.10 Partition coefficient of methanol between poly(dimethylsiloxane) and CO_2 at different concentrations of methanol in the fluid phase. T=41.5 °C [16]

Although the methods used to study partitioning in PDMS were at low solute concentrations, there have been studies of partitioning at concentrations similar to monomer concentrations in CO_2-based polymerizations. For example, the partitioning of styrene between $scCO_2$ and polystyrene has been studied [31, 32] to assess the devolatilization of polystyrene with CO_2. Initially, polystyrene pellets were saturated with styrene in a petri dish and then subjected to a vacuum oven to obtain pellets containing 1 wt% styrene. These pellets were then placed in an extraction cell and CO_2 was added to the desired pressure. At equilibrium, the CO_2 with extracted styrene was passed through a series of U-tubes to collect the styrene in the fluid phase. A wet-flow meter measured the amount of CO_2 in the sample. The

main results these works are shown in Figures 3.11 & 3.12. In this case, the partition (or distribution) coefficient is defined as the ratio of the mass fraction of styrene in the fluid to that in the polymer. The distribution coefficient and residual monomer in the polymer phase were insensitive to changes in temperature and pressure. The lines in Figure 3.12 are calculations of the distribution coefficient over an extended range of conditions using the Sanchez-Lacombe equation of state. The model calculations matched the experimental results reasonably well. In general, the model predicts that as the pressure is increased, the distribution coefficient will increase until it reaches a limiting value of approximately 0.1 at pressures greater than 20 MPa (2900 psi). At low pressures, the distribution coefficient will increase with increasing temperature. However, when the pressure is increased above the critical point, the correlation with temperature is reversed.

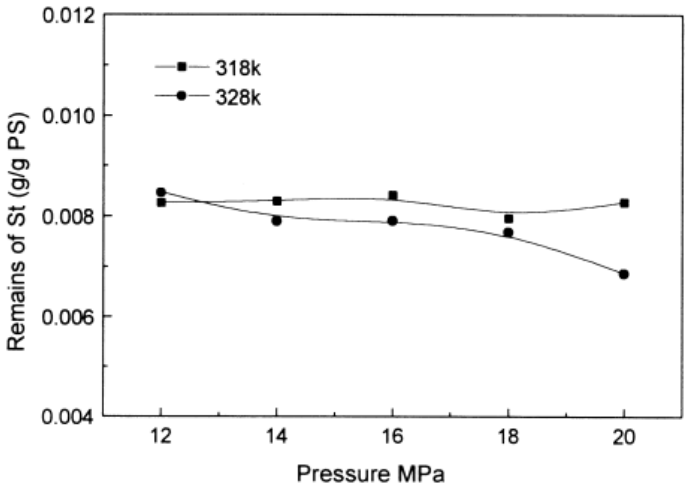

Figure 3.11 Residual styrene in polystyrene as a function of T and P for a styrene/CO_2/polystyrene ternary system. Polystyrene initially contained 1 wt% styrene. Reprinted from Wu et al [32]

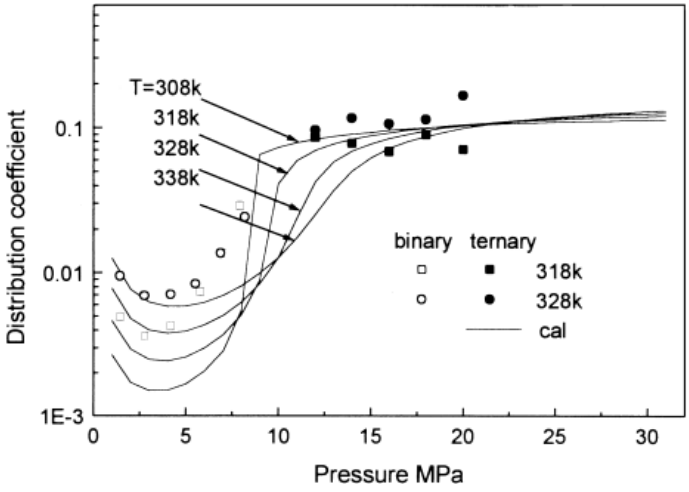

Figure 3.12 Distribution coefficients of styrene between the supercritical phase and the dense phase for a styrene/CO_2/polystyrene ternary system. Binary data are for a styrene/CO_2 system. Reprinted from Wu et al [32]

Von Schnitzler and Eggers [22] measured the partitioning of dyes between poly(ethylene terphthalate) (PET) and scCO_2 using a magnetic suspension balance. A given concentration of dye in CO_2 was circulated around the polymer while monitoring its change in mass with time. As shown in Table 3.3, they were able to calculate the mass sorption of dye and diffusion coefficients for the dye by coupling the change in mass with the change in concentration of the dye in the fluid phase as measured with a VIS photometer.

Table 3.3
Mass sorption and calculated diffusion coefficients of two disperse dyes in a CO_2-PET system at 120°C and 300 bar [22]

Dye	Sorption in PET (g_{dye}/g_{PET})	Solubility in CO_2 (g_{dye}/g_{CO2})	D_{dye} in PET (m^2/s)
C.I. disperse red 324	7.00×10^{-3}	7.69×10^{-6}	1.07×10^{-13}
C.I. disperse orange 149	6.80×10^{-3}	1.30×10^{-4}	1.93×10^{-11}

3.2 Thermodynamic Modeling of Phase Equilibrium between Polymer and $scCO_2$ Phases

Thermodynamic modeling is a convenient approach to studying the phase equilibrium. Models that predict the phase equilibria serve to generalize experimental results, and allow the impact of changes to the system parameters to be studied. For a variety of polymer applications, including polymer foams, polymer impregnation, and polymer purification, different scenarios can be explored with equilibrium models without the need for extensive experimentation. When experimentation is necessary, specific experimental regions and systems can be targeted based on the predictions of the model.

Various approaches to modeling SCF-polymer systems are available. Cubic equations of state (EOS) and lattice models have been successful in predicting the phase behavior of complex, multiphase, supercritical fluid systems [33]. The thermodynamic properties of a pure component are modeled by an equation of state, which relates the pressure, volume, and temperature of the fluid at equilibrium. When modeling the thermodynamic properties of mixtures, mixing rules are applied to account for binary interactions between species in the mixture. By fitting the model to binary system data using adjustable binary interaction parameters, the model prediction is optimized.

The Peng-Robinson (P-R) equation of state [34] is frequently used for modeling the solubility of small molecules in supercritical fluids [35]. The equation is of the form

$$P = \frac{RT}{v-b} - \frac{a(T)}{v(v+b)+b(v-b)}$$

where P is the pressure, T is the temperature, R is the gas constant, v is the molar volume, and a and b are attraction and repulsive parameters. The P-R EOS provides an excellent fit to experimental data for solute-CO_2 systems, as demonstrated in Figure 3.13. However, the P-R EOS cannot be readily applied to polymer-solvent systems because the standard means for determining the pure component parameters, a and b, are based on the critical properties and vapor pressure, which do not exist for polymers. There has been some work to assume values for the vapor pressure of polymers in order to apply the P-R equation of state. However, the model parameters lack physical significance and can only be applied in very limited ranges [36].

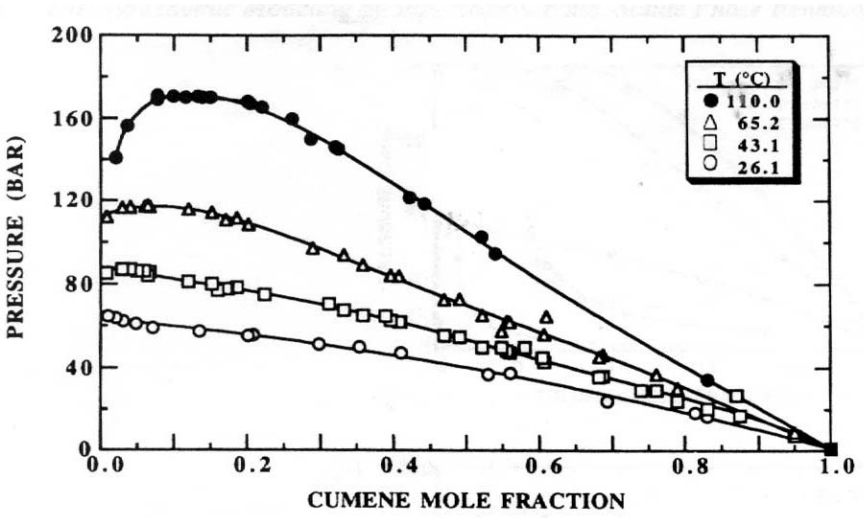

Figure 3.13 Solubility of cumene in CO_2. Lines represent prediction by Peng-Robinson equation of state [35]

Excellent reviews of equations of state for polymer-solvent [36, 37] and specifically polymer-SCF systems [38] exist in the literature. The prevailing models for describing phase equilibrium in polymer-SCF systems are the statistical associating fluid theory (SAFT) and Sanchez-Lacombe (S-L) equations of state. The S-L equation of state (EOS) is a lattice-fluid model in which the polymer segments and solvent molecules are placed on a lattice that includes vacant sites to account for the compressibility of the system. The molecules interact according to a mean field intermolecular potential. SAFT [39] is a relatively new EOS that is based on perturbation theory. Molecules are represented as covalently bonded chains of segments that may form associative complexes. The perturbation is given in terms of the residual molar Helmholtz energy. The residual Helmholtz energy consists of three contributions to the total intermolecular potential: the hard-sphere repulsion of individual segments, the connectivity of the segments in the main chain, and the energy of specific interactions between segments in the same chain or with other molecules.

The SAFT and S-L models provide reasonable representations of the phase equilibrium in polymer-SCF systems. In fact, the models have been shown to produce similar results for some polymer-solvent systems [40]. However, the SAFT equation is better suited for systems in which components may cross-associate or self-associate [38]. Additionally, the SAFT model is more predictive than the S-L model due to its accounting of the molecular shape of molecules and their association in a single equation. However, the predictive capabilities of the SAFT

model for phase equilibria calculations are limited due to the need to use cloud-point data to determine the pure component polymer parameters. Despite the fact that the S-L model is not as predictive as the SAFT model, it has been overwhelmingly applied to understanding phase equilibrium in polymer-scCO$_2$ systems. The following section discusses the governing equations associated with the S-L equation of state and its application for phase equilibria in polymer-scCO$_2$ systems.

3.2.1 Sanchez-Lacombe Equation of State

Of all the equations of state used to model phase equilibria in polymer/SCF systems, the Sanchez-Lacombe equation of state has found the greatest application. This is due, in part, to its mathematical simplicity. More complicated models, such as the Panayiotou-Vera [41] and SAFT equations of state, have been applied. However, these models do not greatly improve upon the model description of the phase equilibria.

The S-L model [42, 43] is based on a lattice theory in which the lattice contains occupied and unoccupied sites, with the site volumes being based on the components. The total number of lattice sites in a single component system, N_r, is given by

$$N_r = N_o + rN \tag{3.1}$$

where N_o is the total number of vacant sites, r is the number of lattice sites occupied by an r-mer and N is the total number of r-mers. The close-packed volume of a single mer, v*, is the volume of a single lattice site. The close-packed molecular volume is rv*. The total volume of the system is

$$V = (N_o + rN)v^* \tag{3.2}$$

The molecular volume is related to the molecular weight, M, according to

$$rv^* = \frac{M}{\rho^*} \tag{3.3}$$

where ρ^* is the close-packed mass density. The reduced density $\tilde{\rho}$ is defined as the fraction of occupied lattice sites, f, which is

$$f = \tilde{\rho} = \frac{\rho}{\rho^*} = \frac{rN}{N_o + rN} = \frac{v^*}{v} = \frac{1}{\tilde{v}} \tag{3.4}$$

where ρ is the density, v=V/rN is the volume per segment, and $\tilde{v}$ is the reduced volume. The fraction of vacant sites, f_o, is

$$f_o = \frac{N_o}{N_o + rN} = 1 - \tilde{\rho} \tag{3.5}$$

The energy of the lattice is based only on nearest-neighbor interactions. The total number of pair interactions is $(z/2)(N_o+rN)$, where z is the coordination number. Assuming random mixing of vacancies and mers, the probability of two sites being occupied by mers is f^2. The interaction energy associated with vacancy-vacancy and vacancy-mer interactions is zero. The mer-mer interaction energy is given by ε. The mean intermolecular energy of the lattice is

$$E = -\varepsilon\left(\frac{z}{2}(N_o + rN)\right)f^2 = -\varepsilon^* N_r \tilde{\rho}^2 = -rN\varepsilon^* \tilde{\rho} \tag{3.6}$$

$$\varepsilon^* = \frac{z\varepsilon}{2} \tag{3.7}$$

where ε^* is the total interaction energy per mer.

According to statistical mechanics, the Gibbs free energy G is related to the configurational partition function Z in the pressure ensemble by

$$G = -kT \ln Z(T,P) \tag{3.8}$$

$$Z(T,P) = \sum_{V} \sum_{E} \Omega(E,V,N) \exp\left[-\frac{E + PV}{kT} \right] \tag{3.9}$$

where k is the Boltzman's constant and $\Omega(E,V,N)$ is the number of configurations available to a system of N molecules having configurational energy E and volume V. The temperature T and pressure P is assumed to be constant in this case. The number of configurations is approximated by the lattice containing N r-mers and N_o vacant sites,

$$\Omega \cong \left(\frac{1}{f_o} \right)^{N_o} \left(\frac{\omega}{f} \right)^{N} \tag{3.10}$$

where ω is the number of configurations available to a r-mer in the close-packed state. This assumes that the coordination number z of the lattice is large and that all of the configurations for the N r-mers and N_o vacant sites are energetically equivalent. Since E and Ω are only functions of the number of vacant sites, the double sum over E and V in the partition function can be replaced by a single sum over N_o, such that

$$Z(T,P) = \sum_{N_o} \Omega \exp\left[-\frac{E + PV}{kT} \right] \tag{3.11}$$

Again using statistical mechanics, the partition function is approximated by its largest term. The Gibbs free energy is then

$$G = E + PV - kT \ln \Omega \tag{3.12}$$

and the reduced free energy is

$$\tilde{G} = \frac{G}{rN\varepsilon^*} \tag{3.13}$$

Minimization of the free energy,

$$\left.\frac{\partial \tilde{G}}{\partial \tilde{v}}\right|_{\tilde{T},\tilde{P}} = 0 \tag{3.14}$$

yields the equation of state for pure components and mixtures [44]

$$\tilde{\rho}^2 + \tilde{P} + \tilde{T}\left[\ln(1-\tilde{\rho}) + (1-\frac{1}{r})\tilde{\rho}\right] = 0 \tag{3.15}$$

where $\tilde{T} = T/T^*$ is the reduced temperature and $\tilde{P} = P/P^*$ is the reduced pressure. T* and P* are the characteristic temperature and pressure, respectively. The characteristic parameters are related to one another according to the following relationships:

$$T^* = \frac{\varepsilon^*}{R} \qquad P^* = \frac{\varepsilon^*}{v^*} \qquad \rho^* = \frac{M}{rv^*} \tag{3.16}$$

The characteristic parameters for pure components may be determined from any thermodynamic property. However, the parameters for small molecules are most commonly determined from vapor pressure data, which is generally readily available. For polymers, PVT data is used to fit the three parameters. If good PVT data is not available, the polymer characteristic parameters may be estimated from the density, the thermal expansion coefficient α, and the isothermal compressibility β of the polymer at a single temperature and atmospheric pressure. That temperature

must be above the glass transition or melting temperature. The following equations [45] permit calculation of the characteristic parameters.

$$T\alpha = \frac{1}{\frac{\tilde{T}}{1-\tilde{\rho}} - 2} \tag{3.17}$$

$$P^* = \frac{T\alpha}{\tilde{\rho}^2 \beta} \tag{3.18}$$

These equations are valid in the limit $r \to \infty$ and at atmospheric pressure ($\tilde{P} \cong 0$). At these conditions, the equation of state reduces to

$$\tilde{\rho}^2 + \tilde{T}\left[\ln(1-\tilde{\rho}) + \tilde{\rho}\right] = 0 \tag{3.19}$$

For a given value of $\tilde{T}$, $\tilde{\rho}$ is calculated from Equation 3.19 and then $T\alpha$ is determined from Equation 3.17. Plots of $\tilde{T}$ versus $T\alpha$ and $\tilde{\rho}$ versus $T\alpha$ are constructed from incremented values of $\tilde{T}$. The characteristic parameters T* and ρ^* can then be determined from the plots by using experimental data for $T\alpha$. Finally P* is calculated from Equation 3.18.

The critical properties for the lattice fluid are a unique function of the r-mer size. The reduced critical properties are given by

$$\tilde{\rho}_c = \frac{1}{1+r^{1/2}} \tag{3.20}$$

$$\tilde{T}_c = 2r\tilde{\rho}_c^2 \tag{3.21}$$

$$\tilde{P}_c = \tilde{T}_c\left[\ln\left(1+r^{-1/2}\right) + \frac{\left(1/2 - r^{1/2}\right)}{r}\right] \tag{3.22}$$

Selected literature values for the pure component parameters of CO_2 and poly(vinylidene fluoride) are given in Table 3.4. The parameters for CO_2 vary widely in the literature. This is due to the fact that different thermodynamic properties were used to obtain the parameters. However, all of the parameters produce similar results for the density of CO_2 over a range of conditions (Section 4.2.1.1). Similarly, for poly(vinylidene fluoride), the parameters (sets 3 & 4) determined based on polymer PVT data are very different from the parameters (sets 1 & 2) determined from values of α, β, and ρ for the polymer.

Table 3.4
Sanchez-Lacombe EOS characteristic parameters for carbon dioxide and poly(vinylidene fluoride) (PVDF) from the literature

	Mn (g/mol)	P* (bar)	T* (K)	ρ* (g/ml)	r	Source
Carbon Dioxide	44.01	5737	309	1.504	6.54	[46]
		4643	328	1.426	5.25	[41]
		4126	316	1.369	5.11	[47]
		6510	283	1.62	7.6	[48]
		5670	305	1510	6.6	[49]
		7101	280	1.6177	8.4	[50]
PVDF	111,000	3300	800	1.92		[8],42°C
	111,000	3300	900	1.92		[8],80°C
	88,000	4450	698	1.7187		[51], 200-250°C
	420,000	4508	694	1.7229		[52], 178-248°C

In the Sanchez-Lacombe model, the properties of mixtures are based on three combining rules: 1) the molecular volume of each component is conserved, 2) the total number of pair interactions in the close-packed mixture is equal to the sum of the pair interactions of the components in their close-packed pure states, and 3)

the characteristic pressures are pairwise additive in the mixture. The characteristic parameters P*, T*, ρ* and r for a binary mixture are given by

$$\mathbf{P}^* = \phi_1 \mathbf{P}_1^* + \phi_2 \mathbf{P}_2^* - \phi_1 \phi_2 \left[\mathbf{P}_1^* + \mathbf{P}_2^* - 2\zeta (\mathbf{P}_1^* \mathbf{P}_2^*)^{\frac{1}{2}} \right] \tag{3.23}$$

$$\mathbf{T}^* = \frac{\mathbf{P}^*}{\frac{\phi_1 \mathbf{P}_1^*}{\mathbf{T}_1^*} + \frac{(1-\phi_1)\mathbf{P}_2^*}{\mathbf{T}_2^*}} \tag{3.24}$$

$$\rho^* = \frac{1}{\frac{\mathbf{m}_1}{\rho_1^*} + \frac{\mathbf{m}_2}{\rho_2^*}} \tag{3.25}$$

$$\mathbf{r} = \frac{1}{\frac{\phi_1}{\mathbf{r}_1} + \frac{\phi_2}{\mathbf{r}_2}} \tag{3.26}$$

where the subscripts 1 and 2 denote the properties for components 1 and 2, respectively, ϕ is the volume fraction of the component in the mixture, m is the weight fraction of the component in the mixture, and ζ is the binary interaction parameter. The binary interaction parameter corrects for the deviation of the mixture characteristic pressure from the geometric mean. Its value typically ranges from 0.80 to 1.2, which is $\pm$ 20% from the geometric mean.

Because the Sanchez-Lacombe model is based on lattice-fluid theory, its predictions are limited to polymers that are noncrystalline, not cross-linked or only slightly crosslinked, and above their glass transition temperature or melting temperature [49]. Panayiotou and Sanchez [46] developed a modified Sanchez-

Lacombe model that accounts for the presence of crosslinks in the polymer. The model assumes that the contributions to the Gibbs free energy are additive, including a term for the lattice fluid and a term for the elastic contributions due to crosslinks. A similar approach may be applied to crystalline polymers if it is assumed that the crystallites act similar to crosslinks in limiting the swelling and sorption of polymers in the presence of solvent. An approach to modeling the activity of a solvent in the presence of amorphous and crystalline polymer regions has been developed by Michaels and Hausslein [53]. Michaels and Hausslein used this model with the Flory-Huggins equation of state to describe the sorption of para-xylene into semicrystalline polyethylene. The Michaels-Hausslein approach for semicrystalline polymers has also been applied with free volume models for modeling semicrystalline polyethylene and polypropylene with various solvents [37]. The Michaels-Hausslein equation may also be applied to the Sanchez-Lacombe equation of state. This will be further discussed in Section C.1.2.

3.2.1.1 Calculation of Phase Equilibrium

Equations of state can be used to calculate the composition of two phases in equilibrium. The criteria for equilibrium are

$$T^I = T^{II} \tag{3.27}$$

$$P^I = P^{II} \tag{3.28}$$

$$\mu_i^I = \mu_i^{II} \quad (for\ all\ i) \tag{3.29}$$

where the superscripts I and II represent the phases of the mixture and μ_i is the chemical potential of component *i*. In this discussion, the superscript I signifies the fluid phase and superscript II signifies the polymer phase. In a binary mixture of small molecules (component 1) and a high molecular weight polymer (component 2), the chemical potential of component 1 is

$$\mu_1 = \left.\frac{\partial G}{\partial N_1}\right|_{T,P,N_2} \tag{3.30}$$

According to the Sanchez-Lacombe EOS, the chemical potential of component 1 in the polymer is

$$\frac{\mu_1^{II}}{kT} = \ln\phi_1 + (1-\frac{r_1}{r_2})\phi_2 + \tilde{\rho} r_1 X_1 \phi_2^{\,2} + \left[-\frac{\tilde{\rho}}{\tilde{T}_1} + \frac{\tilde{P}_1}{\tilde{T}_1 \tilde{\rho}} + \frac{(1-\tilde{\rho})\ln(1-\tilde{\rho})}{\tilde{\rho}} + \frac{\ln\tilde{\rho}}{r_1} \right] r_1 \tag{3.31}$$

The parameter X_1 is given by

$$X_1 = \frac{v_1^*}{RT}\left(P_1^* + P_2^* - 2\zeta(P_1^* P_2^*)^{1/2}\right) \tag{3.32}$$

The chemical potential of the pure component 1 (ϕ_1=1) is

$$\frac{\mu_1^{I}}{kT} = \left[-\frac{\tilde{\rho}_1}{\tilde{T}_1} + \frac{\tilde{P}_1}{\tilde{T}_1 \tilde{\rho}_1} + \frac{(1-\tilde{\rho}_1)\ln(1-\tilde{\rho}_1)}{\tilde{\rho}_1} + \frac{\ln\tilde{\rho}_1}{r_1} \right] r_1 \tag{3.33}$$

The solution of Equation 3.29 for the polymer and CO_2 allows calculation of the polymer sorption and swelling in the presence of CO_2 and determination of the solubility of the polymer in CO_2. Because most polymers are insoluble in CO_2, calculation of the polymer sorption and swelling is simplified by elimination of Equation 3.29 for the polymer. The chemical potential of pure CO_2 is equated with

the chemical potential of CO_2 in the mixture. The parameter ϕ_1 is obtained by solving the resulting equation. A computer program for solution of the two-component system is detailed in Appendix C.3. The mass fraction of CO_2, ω_1, in the polymer is

$$\omega_1 = \frac{\phi_1}{\phi_1 + \phi_2\left(\frac{\rho_2^*}{\rho_1^*}\right)} \tag{3.34}$$

and the fractional increase in weight based on the original weight of polymer (ΔM) is given by

$$\Delta M = \omega_1 / (1 - \omega_1) \tag{3.35}$$

The degree swelling of the polymer is

$$\frac{V}{V_o} = \frac{\rho_2}{\omega_2 \rho} \tag{3.36}$$

The prediction of the Sanchez-Lacombe model for the sorption of CO_2 into polystyrene is shown in Figure 3.7. The fit of the model to the experimental data was very good with the use of a binary interaction parameter. The interaction parameter increased almost linearly with the temperature. This dependency with temperature suggests that the S-L model is limited in its description of the phase equilibria for this system. Possibly, different mixing rules or characteristic parameters might be used to improve the model's prediction. Nevertheless, the model was capable of providing a good correlation of the data.

For multi-component systems, the partitioning of solutes between polymer and supercritical fluid phases is an important phenomenon. The partition coefficient,

K_c, is defined as the ratio of the concentration of solute in the polymer phase to that in the fluid phase. Calculation of K_c requires solution of Equation 3.29 for all the components. Again, the equations may be simplified if the polymer can be assumed insoluble in the fluid phase. Solution of the equations yields the mass fraction of each component in the two phases. K_c is then calculated according to

$$K_c = \frac{C_i^{II}}{C_i^{I}} = \frac{\omega_i^{II} \tilde{\rho}^{II} \rho^{*II}}{\omega_i^{I} \tilde{\rho}^{I} \rho^{*I}} \tag{3.37}$$

The chemical potential equations for multi-component systems and a computer program for solution of the multi-component equations are described in Sections 5.2, C.1.3, and C.3.4.

The partition coefficient modeling of solute/CO_2/PDMS systems [29] is shown in Figure 3.14. A modified Sanchez-Lacombe model was used to account for the presence of crosslinks in the polymer. Binary interaction parameters for solute-CO_2 and PDMS-CO_2 pairs were determined from two component VLE curves and polymer swelling data, respectively. The interaction parameter for the solute-PDMS pair was determined by fitting the partition coefficient data. The model provided a qualitative as well as quantitative fit to the data.

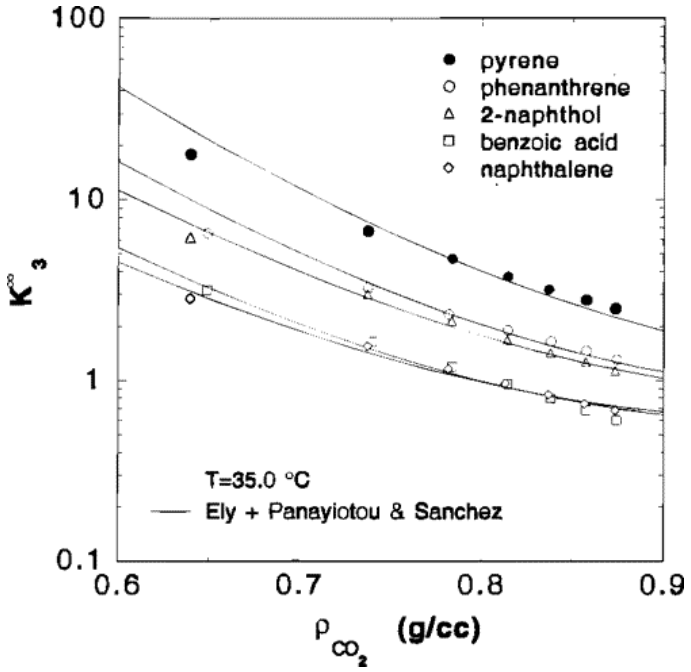

Figure 3.14 Infinite dilution partition coefficients for various solutes between $scCO_2$ and cross-linked PDMS phases at 35 °C. Lines represent calculation with modified Sanchez-Lacombe model. Reprinted from Condo et al [29]

3.3 Phase Equilibrium of Poly(vinylidene fluoride) (PVDF) with CO_2

The interaction between poly(vinylidene fluoride) and carbon dioxide has been studied by several groups [6, 8, 54-57]. The sorption [8, 54-56] and swelling [8, 57] of PVDF in the presence of carbon dioxide and the solubility of PVDF in CO_2 [6] has been investigated. This previous work was focused on elucidating the effect of CO_2 on PVDF chemical processing applications and the potential of CO_2 to "tune" the properties of PVDF for processing.

The solubility of PVDF of varying molecular weights in supercritical carbon dioxide has been studied by Dinoia and coworkers [6]. The weight-average molecular weight of the PVDF samples ranged from 181,000 g/mol to 329,000

g/mol. The solubility of 5 wt% solutions is shown in Figure 3.15. Very high pressures, greater than 1500 bar (21,000 psi), were necessary to solubilize PVDF over the range of temperatures studied. There was not a significant effect of molecular weight on the solubility. Based on these results, the PVDF formed by polymerization of vinylidene fluoride in CO_2 should be insoluble at the mild conditions at which the polymerizations were run (<350 bar, 65-80 °C).

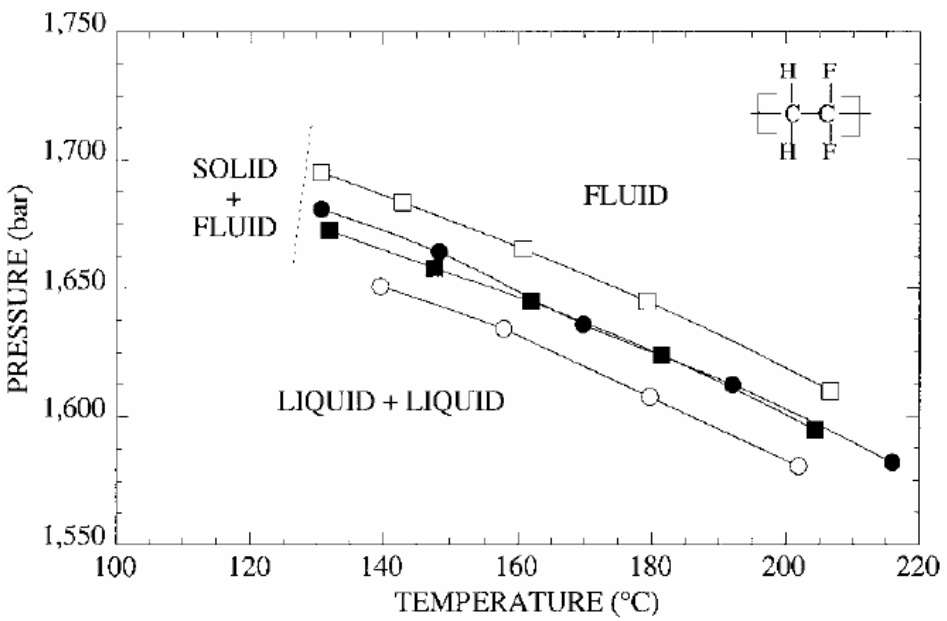

Figure 3.15 Molecular weight effect on the solubility of PVDF in CO_2: PVDF (181,000 g/mol; ○), PVDF (269,000 g/mol; ●), PVDF (275,000 g/mol; ■), PVDF (329,000 g/mol; □) [6]

Carbon dioxide is believed to have a specific interaction with PVDF that impacts the solubility of PVDF in CO_2. The solubility of PVDF and fluorinated copolymers in CO_2 has been investigated [6, 58] to elucidate this interaction. The solubilities of poly(vinylidene fluoride-co-22 mol% hexafluoropropylene) (VF2-co-HFP) and poly(tetrafluroroethylene-co-19 mol% hexafluoropropylene) (TFE-co-HFP)

in CO_2 were compared. The VF2-co-HFP polymer was soluble at much milder conditions. This was attributed, in part, to the polar interactions that existed between CO_2 and VF2-co-HFP that were lacking with nonpolar TFE-co-HFP. Additionally, the dipole of VF2 forms a complex with the quadrupole of CO_2, which is enhanced at lower temperatures. This was concluded based on a comparison of the solubility of VF2-co-HFP in CO_2 and CHF3. Carbon dioxide was a slightly better solvent than fluoromethane. It was expected that because fluoromethane was a more polar solvent, it would interact more favorably with the polar, VF2 repeat units in the polymer. However, CO_2 exhibited a specific interaction with the fluorine atoms, to enhance the solubility.

Briscoe and coworkers [8] measured the sorption and swelling of a CO_2/PVDF system at 42 and 80 °C at pressures up to 30 MPa. The sorption of CO_2 into PVDF was measured using the vibrating beam technique described in Section 3.1.3. The swelling of PVDF in the presence of CO_2 was measured using an ultrasonic transducer submerged in a mercury bath (Figure 3.16). By this method, a bath of mercury, whose properties are essentially unchanged at the conditions of the experiments, is placed on top of a cylindrical polymer sample. An ultrasonic transducer is submerged in the bath at a fixed position in the high-pressure vessel. As the polymer expands or contracts, the path length of the ultrasonic wave is shortened or lengthened. Thus, the linear displacement of the polymer may be obtained.

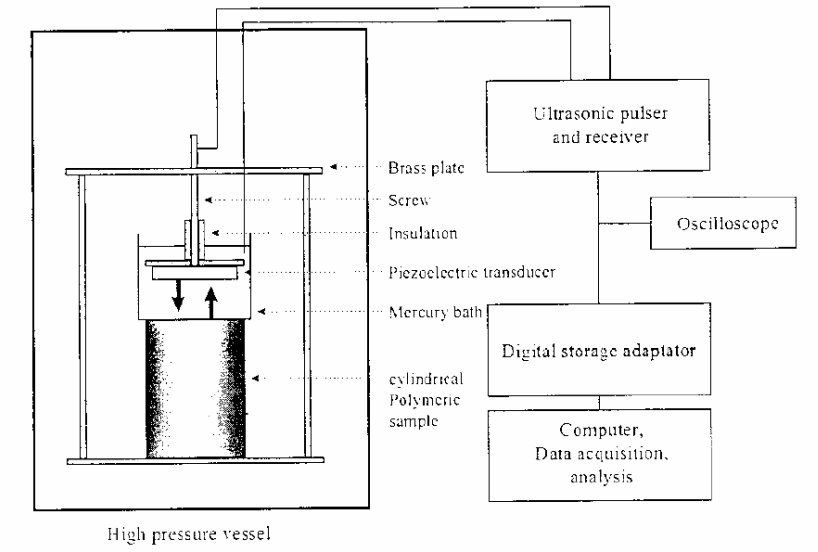

Figure 3.16 Schematic of polymer swelling apparatus [8]

The results for the sorption and swelling of PVDF are shown in Figures 3.6 and 3.17, respectively. Both the sorption and swelling increased with increasing pressure. Although the polymer swells very little (max 1.2%), the polymer sorbs significant amounts of CO_2 (up to 20%) over the range of conditions studied. A prediction of the sorption by the Sanchez-Lacombe model is also shown in Figure 3.6. The model produced only a qualitative fit to the data. The quantitative agreement of the model with the data was poor. There was a systematic deviation of the model from the data. The ability of the Sanchez-Lacombe equation of state to model the phase equilibrium in a PVDF-CO_2 system will be discussed in detail in Section 4.2 and Appendix C.

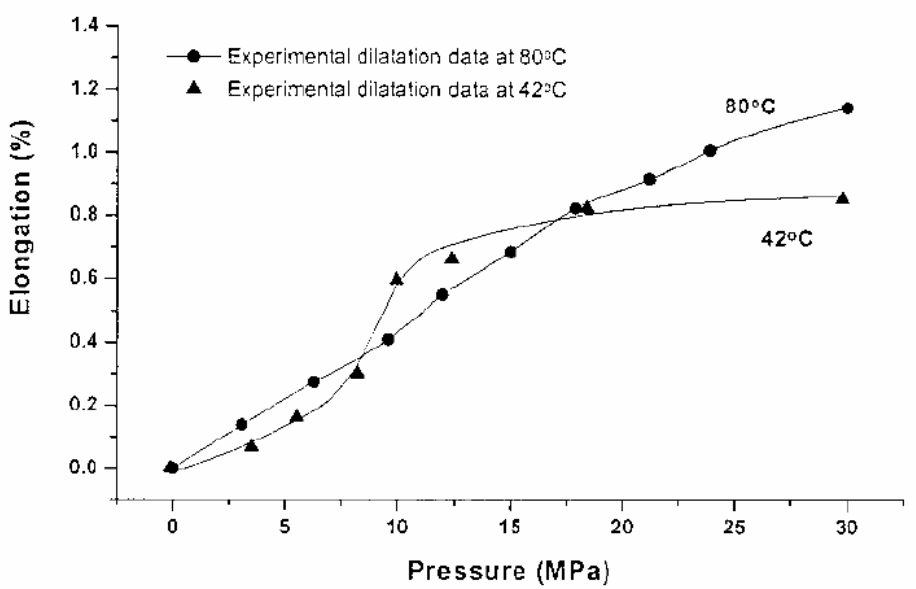

Figure 3.17 Swelling of PVDF in the presence of CO_2 at 42 °C and 80 °C [8]

Briscoe and coworkers [8] calculated diffusion coefficients for CO_2 into PVDF based on their sorption data. At 80 °C, the diffusion coefficient for CO_2 at 5 MPa was calculated to be 0.2 x 10^{-3} cm^2/s. Flaconneche et al [54] used a permeation cell to obtain a diffusion coefficient of 0.98 x 10^{-7} cm^2/s at 4 MPa and 70 °C. The large difference in these reported diffusion coefficients probably is due to a difference in the methods used and the condition of the polymer samples. In both studies, the diffusion coefficient increased with the pressure and increasing concentration of CO_2 in the polymer. This was due to plasticization of the polymer in the presence of CO_2. As the concentration of CO_2 increased, the free volume in the polymer increased to enhance the diffusion of additional CO_2 into the polymer phase.

3.4 Phase Equilibrium of Vinylidene Fluoride Monomer with CO_2

There have been no reports in the literature about the phase equilibrium between vinylidene fluoride monomer and carbon dioxide. However, the complete miscibility of VF2 with CO_2 was verified at conditions of interest to this work [59]. It was also observed at the start of the telomerization of VF2 in CO_2 that the reactions were homogeneous [60]. Thus, the notion of a homogeneous system at the start of polymerization is supported.

The presence of monomer may enhance the solubility of PVDF in the reaction mixture and increase the interaction between CO_2, monomer, and PVDF. It has been shown [61] that by adding ethyl and butyl methacrylate to a system of the corresponding homopolymer and CO_2, the solubility of the homopolymer is enhanced. The monomer provides favorable interactions with the polymer. Also, the monomer increases the solvent density, which magnifies the strength of polymer-cosolvent interactions. The difference in the free-volume of the polymer and solvent is decreased and enhances the solubility. It has been reported that PVDF should precipitate from $scCO_2$ when the chain length reaches about 10 monomer units [60]. However, if we account for the effect of monomer on the polymer solubility, the polymer may be soluble at greater molecular weights before precipitating from solution.

3.5 References

1. DeSimone, J.M., *Practical Approaches to Green Solvents.* Science, 2002. **297**: p. 799-803.

2. Cooper, A.I., *Polymer synthesis and processing using supercritical carbon dioxide.* Journal of Materials Chemistry, 2000. **10**(2): p. 207-234.

3. Kendall, J.L., Canelas, D.A., Young, J.L., and DeSimone, J.M., *Polymerizations in supercritical carbon dioxide.* Chemical Reviews, 1999. **99**(2): p. 543-563.

4. Schubert, K.V., Lusvardi, K.M., and Kaler, E.W., *Polymerization in nonaqueous microemulsions.* Colloid and Polymer Science, 1996. **274**: p. 875-883.

5. Henon, F.E., Camaiti, M., Burke, A.L.C., Carbonell, R.G., DeSimone, J.M., and Piacenti, R., *Supercritical CO_2 as a solvent for polymeric stone protective materials.* Journal of Supercritical Fluids, 1999. **15**(2): p. 173-179.

6. Dinoia, T.P., Conway, S.E., Lim, J.S., and McHugh, M.A., *Solubility of vinylidene fluoride polymers in supercritical CO_2 and halogenated solvents.* Journal of Polymer Science: Part B: Polymer Physics, 2000. **38**(21): p. 2832-2840.

7. O'Neill, M.L., Cao, Q., Fang, M., Johnston, K.P., Wilkinson, S.P., Smith, C.D., Kerschner, J.L., and Jureller, S.H., *Solubility of homopolymers and copolymers in carbon dioxide.* Industrial and Engineering Chemistry Research, 1998. **37**(8): p. 3067-3079.

8. Briscoe, B.J., Lorge, O., Wajs, A., and Dang, P., *Carbon dioxide-poly(vinylidene fluoride) interactions at high pressure.* Journal of Polymer Science: Part B: Polymer Physics, 1998. **36**(13): p. 2435-2447.

9. Koga, T., Seo, Y.-S., Zhang, Y., Shin, K., Kusano, K., Nishikawa, K., Rafailovich, M.H., Sokolov, J.C., Chu, B., Peiffer, D., Occhiogrosso, R., and Satija, S.K., *Density-fluctuation-induced swelling of polymer thin films in carbon dioxide.* Physical Review Letters, 2002. **89**(12): p. 125506/1-125506/4.

10. Shenoy, S., Woerdeman, D., Sebra, R., Garach-Domech, A., and Wynne, K.J., *Quantifying polymer swelling employing a linear variable differential transformer: CO_2 effects on SBS triblock copolymer.* Macromolecular Rapid Communications, 2002. **23**(18): p. 1130-1133.

11. Chang, S.-H., Park, S.-C., and Shim, J.-J., *Phase equilibria of supercritical fluid-polymer systems.* Journal of Supercritical Fluids, 1998. **13**: p. 113-119.

12. Fleming, G.K. and Koros, W.J., *Carbon dioxide conditioning effects on sorption and volume dilation behavior for bisphenol A-polycarbonate.* Macromolecules, 1990. **23**(5): p. 1353-1360.

13. Fleming, G.K. and Koros, W.J., *Dilation of polymers by sorption of carbon dioxide at elevated pressures: Silicone rubber and unconditioned polycarbonate.* Macromolecules, 1986. **19**: p. 2285-2291.

14. Gross, S.M., Givens, R.D., Jikei, M., Royer, J.R., Khan, S., and DeSimone, J.M., *Synthesis and swelling of poly(bisphenol A carbonate) using supercritical CO_2.* Macromolecules, 1998. **31**(25): p. 9090-9092.

15. Shim, J.-J. and Johnston, K.P., *Adjustable solute distribution between polymers and supercritical fluids.* AIChE Journal, 1989. **35**(7): p. 1097-1106.

16. Vincent, M.F., Kazarian, S.G., West, B.L., Berkner, J.A., Bright, F.V., Liotta, C.L., and Eckert, C.A., *Cosolvent effects of modified supercritical carbon dioxide on cross-linked poly(dimethylsiloxane).* Journal of Physical Chemistry B, 1998. **102**(12): p. 2176-2186.

17. Wissinger, R.G. and Paulaitis, M.E., *Swelling and sorption in polymer-CO_2 mixtures at elevated pressures.* Journal of Polymer Science: Part B: Polymer Physics, 1987. **25**: p. 2497-2510.

18. Zhang, Y., Gangwani, K.K., and Lemert, R.M., *Sorption and swelling of block copolymers in the presence of supercritical fluid carbon dioxide.* Journal of Supercritical Fluids, 1997. **11**: p. 115-134.

19. Wang, W.-C.V., Kramer, E.J., and Sachse, W.H., *Effects of high-pressure CO_2 on the glass transition temperature and mechanical properties of polystyrene.* Journal of Polymer Science: Polymer Physics, 1982. **20**(8): p. 1371-1384.

20. Aubert, J.H., *Solubility of carbon dioxide in polymers by the quartz crystal microbalance technique.* Journal of Supercritical Fluids, 1998. **11**(3): p. 163-172.

21. Miura, K.-i., Otake, K., Kurosawa, S., Sako, T., Sugeta, T., Nakane, T., Sato, M., Tsuji, T., Hiaki, T., and Hongo, M., *Solubility and adsorption of high pressure carbon dioxide to poly(styrene).* Fluid Phase Equilibria, 1998. **144**: p. 181-189.

22. Schnitzler, J.v. and Eggers, R., *Mass transfer in polymers in a supercritical CO_2-atmosphere.* Journal of Supercritical Fluids, 1999. **16**(1): p. 81-92.

23. Handa, Y.P., Zhang, Z., and Wong, B., *Solubility, diffusivity, and retrograde vitrification in PMMA-CO_2, and development of sub-micron cellular structures.* Cellular Polymers, 2001. **20**(1): p. 1-16.

24. Lucklum, R., Behling, C., Hauptmann, P., Cernosek, R.W., and Martin, S.J. *Error analysis of quartz crystal resonator applications*. in *Transducers '97: 1997 International Conference on Solid-State Sensors and Actuators*. 1997. Chicago: Institute of Electrical and Electronic Engineers.

25. Sato, Y., Takikawa, T., Takishima, S., and Masuoka, H., *Solubilities and diffusion coefficients of carbon dioxide in poly(vinyl acetate) and polystyrene.* Journal of Supercritical Fluids, 2001. **19**(2): p. 187-198.

26. Condo, P.D., Sanchez, I.C., Panyiotou, C.G., and Johnston, K.P., *Glass-transition behavior including retrograde virification of polymers with compressed fluid diluents.* Macromolecules, 1992. **25**(23): p. 6119-6127.

27. Condo, P.D. and Johnston, K.P., *Retrograde vitrification of polymers with compressed fluid diluents: experimental confirmation.* Macromolecules, 1992. **25**(24): p. 6730-6732.

28. Kazarian, S.G., Vincent, M.F., Bright, F.V., Liotta, C.L., and Eckert, C.A., *Specific intermolecular interaction of carbon dioxide with polymers.* Journal of the American Chemical Society, 1996. **118**(7): p. 1729-1736.

29. Condo, P.D., Sumpter, S.R., Lee, M.L., and Johnston, K.P., *Partition coefficients and polymer-solute interaction parameters by inverse supercritical fluid chromatography.* Industrial and Engineering Chemistry Research, 1996. **35**(4): p. 1115-1123.

30. Kazarian, S.G., Vincent, M.F., West, B.L., and Eckert, C.A., *Partitioning of solutes and cosolvents between supercritical CO_2 and polymer phases.* Journal of Supercritical Fluids, 1998. **13**: p. 107-112.

31. Chunyue, J., Qinmin, P., and Zuren, P., *The solubility of styrene from polystyrene in supercritical CO_2.* Chinese Journal of Chemical Engineering, 1998. **6**(3): p. 239-247.

32. Wu, J., Pan, Q., and Rempel, G.L., *High-pressure phase equilibria for a styrene/CO_2/polystyrene ternary system.* Journal of Applied Polymer Science, 2002. **85**(9): p. 1938-1944.

33. Johnston, K.P., Peck, D.G., and Kim, S., *Modeling supercritical mixtures: How predictive is it?* Industrial and Engineering Chemistry Research, 1989. **28**(8): p. 1115-1125.

34. Peng, D.-Y. and Robinson, D.B., *A new two-constant equation of state.* Industrial and Engineering Chemistry Fundamentals, 1976. **15**(1): p. 59-64.

35. McHugh, M. and Krukonis, V., *Supercritical Fluid Extraction - Principles and Practice*. 1986, Boston: Butterworths.

36. Lambert, S.M., Song, Y., and Prausnitz, J.M., *Equations of state for polymer systems*, in *Equations of State for Fluids and Fluid Mixtures*, J.V. Sengers, R.F. Kayser, C.J. Peters, and H.J. WhiteJr, Editors. 2000, Elsevier Science: Amsterdam. p. 523-588.

37. Kontogeorgis, G.M., *Thermodynamics of polymer solutions*, in *Handbook of Surface and Colloid Chemistry*, K.S. Birdi, Editor. 2003, CRC Press: New York. p. 683-747.

38. Kirby, C.F. and McHugh, M.A., *Phase behavior of polymers in supercritical fluid solvents.* Chemical Reviews, 1999. **99**(2): p. 565-602.

39. Muller, E.A. and Gubbins, K.E., *Molecular-based equations of state for associating fluids: A review of SAFT and related approaches.* Industrial and Engineering Chemistry Research, 2001. **40**(10): p. 2193-2211.

40. Koak, N., Visser, R.M., and de Loos, T.W., *High-pressure phase behavior of the systems polyethylene + ethylene and polybutene + 1-butene.* Fluid Phase Equilibria, 1999. **158-160**: p. 835-846.

41. Garg, A., Gulari, E., and Manke, C.W., *Thermodynamics of polymer melts swollen with supercritical gases.* Macromolecules, 1994. **27**(20): p. 5643-5653.

42. Sanchez, I.C. and Lacombe, R.H., *Statistical thermodynamics of polymer solutions.* Macromolecules, 1978. **11**(6): p. 1145-1156.

43. Sanchez, I.C. and Lacombe, R.H., *An elementary molecular theory of classical fluids. Pure fluids.* Journal of Physical Chemistry, 1976. **80**(21): p. 2352-2362.

44. Lacombe, R.H. and Sanchez, I.C., *Statistical thermodynamics of fluid mixtures.* Journal of Physical Chemistry, 1976. **80**(23): p. 2568-2580.

45. Sanchez, I.C. and Lacombe, R.H., *An elementary equation of state for polymer liquids.* Journal of Polymer Science. Polymer Letters Edition, 1977. **15**: p. 71-75.

46. Panayiotou, C. and Sanchez, I.C., *Swelling of network structures.* Polymer, 1992. **33**: p. 5090-5093.

47. Hariharan, R., Freeman, B.D., Carbonell, R.G., and Sarti, G.C., *Equation of state predictions of sorption isotherms in polymeric materials.* Journal of Applied Polymer Science, 1993. **50**: p. 1781-1795.

48. Pope, D.S., Sanchez, I.C., Koros, W.J., and Fleming, G.K., *Statistical thermodynamic interpretation of sorption/dilation behavior of gases in silicone rubber.* Macromolecules, 1991. **24**(8): p. 1779-1783.

49. Kiszka, M.B., Meilchen, M.A., and McHugh, M.A., *Modeling high pressure gas-polymer mixtures using the Sanchez-Lacombe equation of state.* Journal of Applied Polymer Science, 1988. **36**: p. 583-597.

50. Kilpatrick, P.K. and Chang, S.-H., *Saturated phase equilibria and parameter estimation of pure fluids with two lattice-gas models.* Fluid Phase Equilibria, 1986. **30**: p. 49-56.

51. Gan, P.P. and Paul, D.R., *Blends of glycidyl methacrylate/methyl metehacrylate copolymers with poly(vinylidene fluoride).* Journal of Polymer Science: Part B: Polymer Physics, 1995. **33**: p. 1693-1703.

52. Rodgers, P.A., *Pressure-volume-temperature relationships for poly(vinylidene fluoride) and polyamide-11.* Journal of Applied Polymer Science, 1993. **50**: p. 2075-2083.

53. Michaels, A.S. and Hausslein, R.W., *Elastic factors controlling sorption and transport properties of polyethylene.* Journal of Polymer Science: Part C, 1965. **10**: p. 61-86.

54. Flaconneche, B., Martin, J., and Klopffer, M.H., *Permeability, diffusion and solubility of gases in polyethylene, polyamide 11, and poly(vinylidene fluoride).* Oil & Gas Science and Technology - Revue de L Institut Francais du Petrole, 2001. **56**(3): p. 261-278.

55. Benali, A., Benjelloun-Dabaghi, Z., Flaconneche, B., Klopffer, M.H., and Martin, J., *Simulation of temperature and pressure influence on transport coefficients of CO_2 in PVDF.* Oil & Gas Science and Technology - Revue de L Institut Francais du Petrole, 2001. **56**(3): p. 305-312.

56. Shieh, Y.-T., Su, J.-H., Manivannan, G., Lee, P.H.C., Sawan, S.P., and Spall, W.D., *Interaction of supercritical carbon dioxide with polymers. I. Crystalline polymers.* Journal of Applied Polymer Science, 1996. **59**(4): p. 695-705.

57. Shenoy, S.L., Fujiwara, T., and Wynne, K.J., *Quantifying plasticization and melting behavior of poly(vinylidene fluoride) in supercritical CO_2 utilizing a*

linear variable differential transformer. Macromolecules, 2003. **36**(9): p. 3380-3385.

58. Mertdogan, C.A., DiNoia, T.P., and McHugh, M.A., *Impact of backbone architecture on the solubility of fluorocopolymers in supercritical CO_2 and halogenated supercritical solvents: Comparison of poly(vinylidene fluoride-co-22 mol % hexafluoropropylene) and poly(tetrafluoroethylene-co-19 mol % hexafluoropropylene).* Macromolecules, 1997. **30**(24): p. 7511-7515.

59. Charpentier, P.A., DeSimone, J.M., and Roberts, G.W., *Continuous precipitation polymerization of vinylidene fluoride in supercritical carbon dioxide: Modeling the rate of polymerization.* Industrial and Engineering Chemistry Research, 2000. **39**(12): p. 4588-4596.

60. Combes, J.R., Guan, Z., and DeSimone, J.M., *Homogeneous free-radical polymerizations in carbon dioxide. 3. Telomerization of 1,1-difluoroethylene in supercritical carbon dioxide.* Macromolecules, 1994. **27**(3): p. 865-867.

61. Byun, H.S. and McHugh, M.A., *Impact of "free" monomer concentration on the phase behavior of supercritical carbon dioxide-polymer mixtures.* Industrial and Engineering Chemistry Research, 2000. **39**(12): p. 4658-4662.

Chapter 4

Sorption of carbon dioxide into semi-crystalline poly(vinylidene fluoride): experiments and modeling

The sorption of carbon dioxide into poly(vinylidene fluoride) has been studied by various groups [1-4] to determine the extent to which CO_2 modifies the properties of PVDF and the tunability of the properties with system conditions. It was found that the sorption varies with the temperature and pressure of the carbon dioxide. The Sanchez-Lacombe model was used to correlate data obtained at 42 °C and 80 °C, but with only qualitative agreement. In this study, experiments and modeling for the phase equilibrium between PVDF and CO_2 are reported. The polymer sorption and swelling in the presence of CO_2 has been measured over a range of temperatures and pressures using newly developed methods. A comparison between the results and literature data is discussed. The experimental sorption data is correlated with the Sanchez-Lacombe (S-L) equation of state and found to be in good agreement. A modified S-L model that accounts for the presence of crystallites was used to correlate the literature sorption data in an attempt to explain the difference in that data and the current data. The results of the two-component phase equilibria provide a foundation for the multi-component phase equilibria, as will be discussed in Chapter 5.

4.1 Experimental Studies

4.1.1 Polymer Swelling

The degree to which a polymer swells in CO_2 can greatly affect the transport of small molecules in the polymer and the overall properties of the polymer. The swelling of PVDF in CO_2 was measured in order to quantify the degree to which the overall morphology of the polymer was affected by CO_2 at various conditions.

4.1.1.1 Experimental

4.1.1.1.1 Materials

Three poly(vinylidene fluoride) (PVDF) samples were used. These included two commercial pellet samples (Solef 1010, Solvay) and a sample of PVDF powder (Sample #5, see Appendix B) synthesized in CO_2. The PVDF synthesized in CO_2 and one of the Solef 1010 samples were melt pressed using a Carver Model C laboratory press. A square mold with a 38 mm dimension and 3 mm thick was used to form discs. The polymers were placed in the melt press for 30 minutes at 220-225 °C, removed from the press, and then allowed to air cool. The melt pressed samples were cut into rectangular bars with average dimensions of 5 mm x 10 mm x 3 mm. Coleman grade CO_2 (99.99% purity) was purchased from National Welders and used as received.

4.1.1.1.2 Apparatus and Methods

A linear variable differential transformer (LVDT) swelling apparatus located at Virginia Commonwealth University was used to measure the swelling of PVDF in the

presence of CO_2. The group of Professor Kenneth Wynne has used this system to measure the swelling of several polymers in the presence of CO_2 [5, 6]. This technique has advantages over other swelling techniques because it is sensitive enough to detect very small changes in the swelling. Additionally, polymer swelling can be measured in the solid state below the melting point of the polymer. Schematics of the overall apparatus and the inside of the sample chamber are shown in Figures 4.1 and 4.2, respectively. The apparatus consists of a sample chamber and pressure generation section. The temperature ($\pm$ 0.3 °C) in the sample chamber was controlled using a heating jacket. The pressure ($\pm$ 1.5 bar) of CO_2 in the system was controlled using a Thar pump (Model PCA 50). The system temperature and pressure and the LVDT voltage is recorded using Labview software.

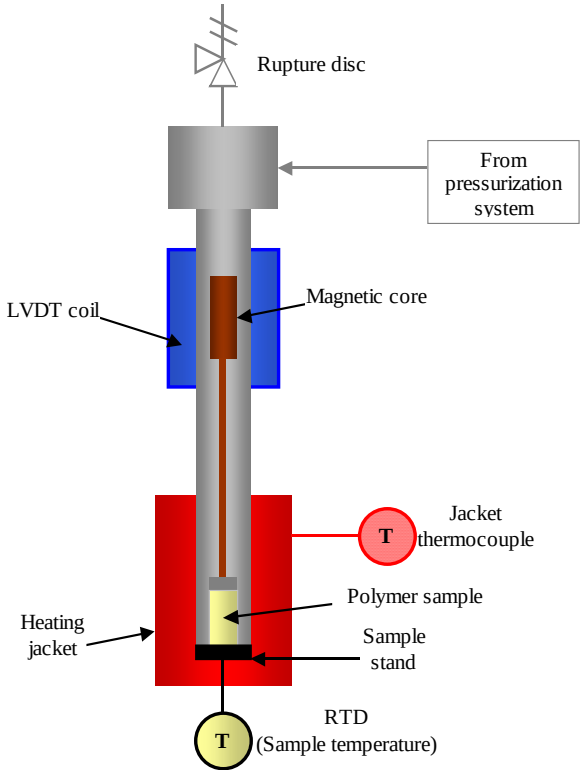

Figure 4.1 LVDT Apparatus for measuring swelling of polymers in carbon dioxide

Within the sample chamber, the polymer is located on a sample stand (Figure 4.2). A magnet attached to a follower rod and hex nut is placed on top of the polymer and the change in height of the polymer is measured with the LVDT. The hex nut is used to evenly distribute the mass of the magnet and follower rod on the polymer sample.

The major components of the LVDT are a solid magnetic core and a transformer consisting of three coils. The coils in the hollow cylindrical shaft of the transformer consist of a primary coil evenly spaced between two secondary coils. When the magnetic core slides past the coils, it affects a certain number of coil windings to generate a unique voltage. This voltage corresponds with the relative

displacement of the magnetic core. The LVDT may be calibrated by using an accurate micrometer and recording the change in voltage with the displacement of the micrometer.

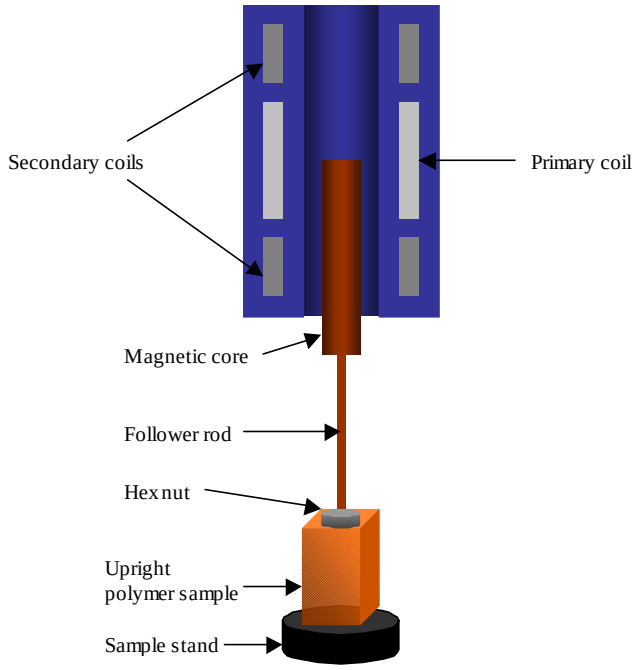

Figure 4.2 Schematic of inside of sample chamber in swelling apparatus

To begin an experiment, the polymer and magnet with follower rod are placed inside the sample chamber. The system is purged and leak checked using nitrogen. The system is then heated to the desired temperature. The LVDT reading at this point corresponds with the zero point for the measurement of the swelling. CO_2 is then added to the sample chamber and Labview records the change in LVDT readings. The swelling is reported as the percent elongation of the polymer, $(L_t - L_o)/L_o \times 100\%$, where L_o is the zero point, initial length of the polymer sample and L_t is the sample length at time t. The error in the percent elongation was $\pm$ 0.2%.

4.1.1.2 Results and Discussion

The results of swelling the melt pressed commercial sample in the presence of CO_2 at 75 °C are shown in Figure 4.3. As the pressure is increased, the swelling in the polymer increases. At pressures greater than 250 bar, the polymer swelling does not significantly increase with further increases in pressure. The data shown in Figure 4.3 were taken by increasing the pressure in increments and then decreasing the pressure in increments. The data were consistent at increasing and decreasing pressure. This suggests that the polymer was free of strain during the swelling process such that no hysteresis was observed in the polymer swelling.

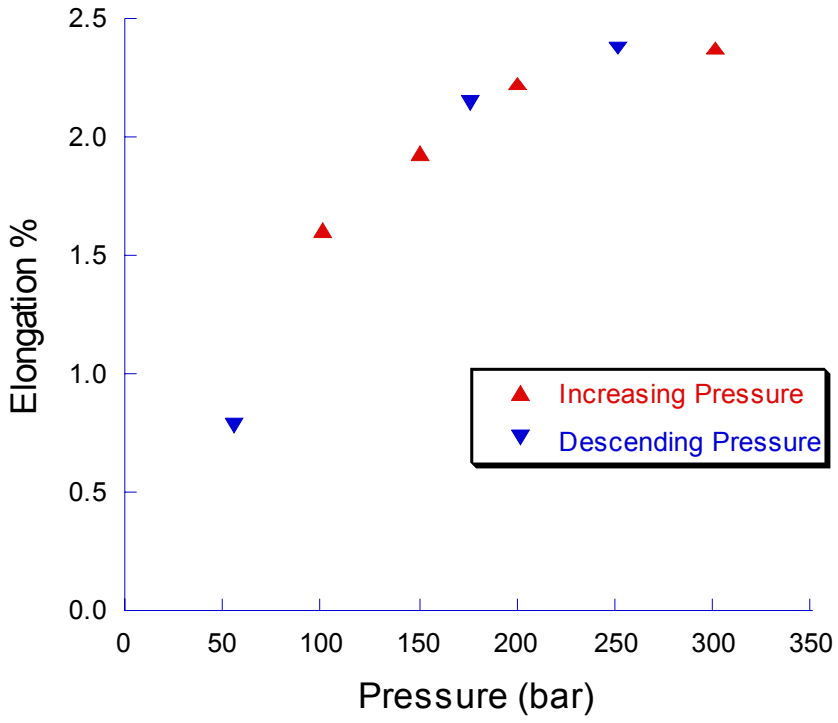

Figure 4.3 Swelling of melt pressed PVDF (Solef 1010) in the presence of CO_2 at 75 °C at increasing and decreasing pressure

The swelling of all the PVDF samples in CO_2 at 75°C is shown in Figure 4.4. In all cases, the swelling begins to level off at pressures greater than 250 bar. Also, as the crystallinity in the polymer samples (see Table 4.1) increases, the swelling decreases. Based on the well-known theory of Flory [7] and others [8], the crystallites act as impenetrable barriers to sorption of CO_2. As the crystallinity increases, a smaller volume of the polymer is available to swell with CO_2, such that the swelling is reduced in the polymer of greater crystallinity.

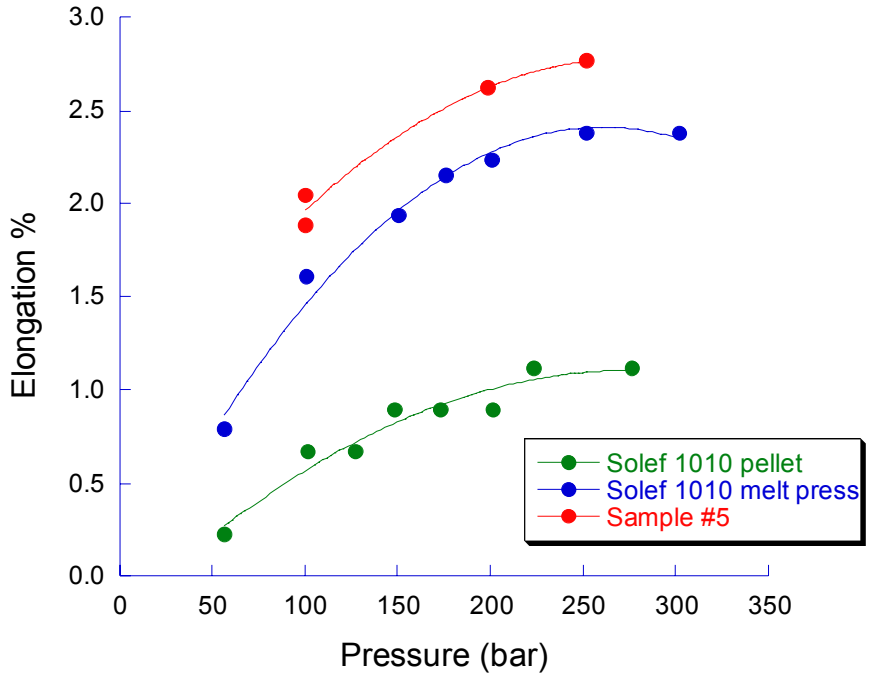

Figure 4.4 Swelling of PVDF in the presence of CO_2 at 75 °C

Table 4.1
DSC analysis of PVDF samples swollen with CO_2

Sample	X % * Before swelling	X % * After swelling
Sample #5	60	63
Solef 1010 melt pressed	47	67
Solef 1010 pellet	64	64

* Based on heat of fusion of 100% crystalline PVDF = 104.6 J/g [9]

Considering the swelling at 75 °C and 150 bar, a linear relationship was observed between the swelling of PVDF in CO_2 and its crystallinity (Figure 4.5). However, this linear relationship might not hold true at lower crystallinities. If the line were extrapolated to zero crystallinity, the elongation would be 8.1%. An adjustable interaction parameter of 0.993 would be necessary for the Sanchez-Lacombe model to predict this elongation. This interaction parameter is not consistent with the interaction parameter (1.017) obtained from sorption experiments (Section 4.2.2). Using the interaction parameter from the sorption experiments, the swelling of amorphous PVDF would be 10.5% at 75 °C and 150 bar. Interaction parameters less than one suggest a specific interaction between the components. The extrapolated, amorphous PVDF swelling predicts such a case, but the sorption experiments do not confirm such an interaction. Additionally, the thermal history may impact the size of the crystallites and therefore the volume of polymer available for swelling. Thus, the extrapolated elongation value may not be consistent with experiments due to variations in the sample thermal history.

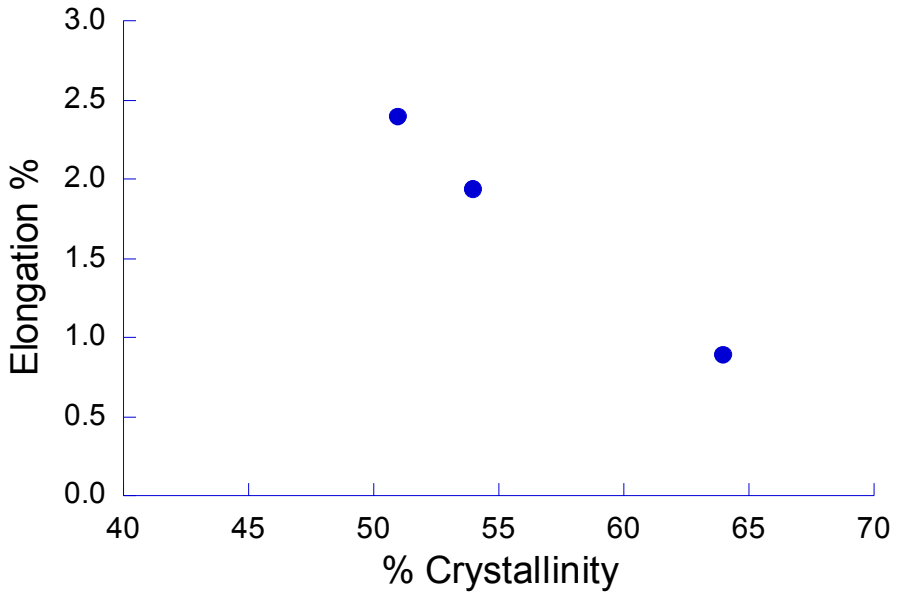

Figure 4.5 Correlation between the pre-swelling % crystallinity and elongation of PVDF in the presence of CO_2 at 75 °C and 150 bar. Data at lowest % crystallinity taken from another source [6, 10]

4.1.2 Polymer Sorption

The sorption of carbon dioxide into poly(vinylidene fluoride) was measured from 42 to 80 °C over a range of pressures up to 250 bar using a magnetic suspension balance. The swelling reported in the previous section was used in the calculation of the mass sorption. The results were compared to data from the literature and found to deviate at high pressures. The sorption of carbon dioxide into polystyrene was measured at 50 °C using the magnetic suspension balance and compared to results obtained another technique to validate the use of the magnetic suspension balance for CO_2 sorption measurements.

4.1.2.1 Experimental

4.1.2.1.1 Materials

Poly(vinylidene fluoride) (Solef 1010, $\overline{M}_w$=180,000) pellets were supplied by Solvay. Polystyrene (#844, $\overline{M}_w$=250,000) pellets were purchased from Scientific Polymer Products and used as received. Coleman grade carbon dioxide was purchased from National Welders and used as received.

4.1.2.1.2 Apparatus and Methods

The sorption of carbon dioxide into PVDF and polystyrene was measured using a magnetic suspension balance (Rubotherm, Germany), also referred to as the ISOSORP. The measurement principles of the Rubotherm balance have been previously described in the literature [11, 12]. A schematic of the system used in this work is shown in Figure 4.6. The temperature and pressure of the system was monitored near the bottom of the sample basket using a platinum resistant sensor and pressure transducer, respectively. The polymer sample (up to 4 g) was placed in a mesh or solid basket suspended from the permanent magnet inside the high-pressure vessel. The permanent magnet was decoupled from an electromagnet suspended from a microbalance at ambient conditions. The precision of the microbalance was reported to be 0.01 mg.

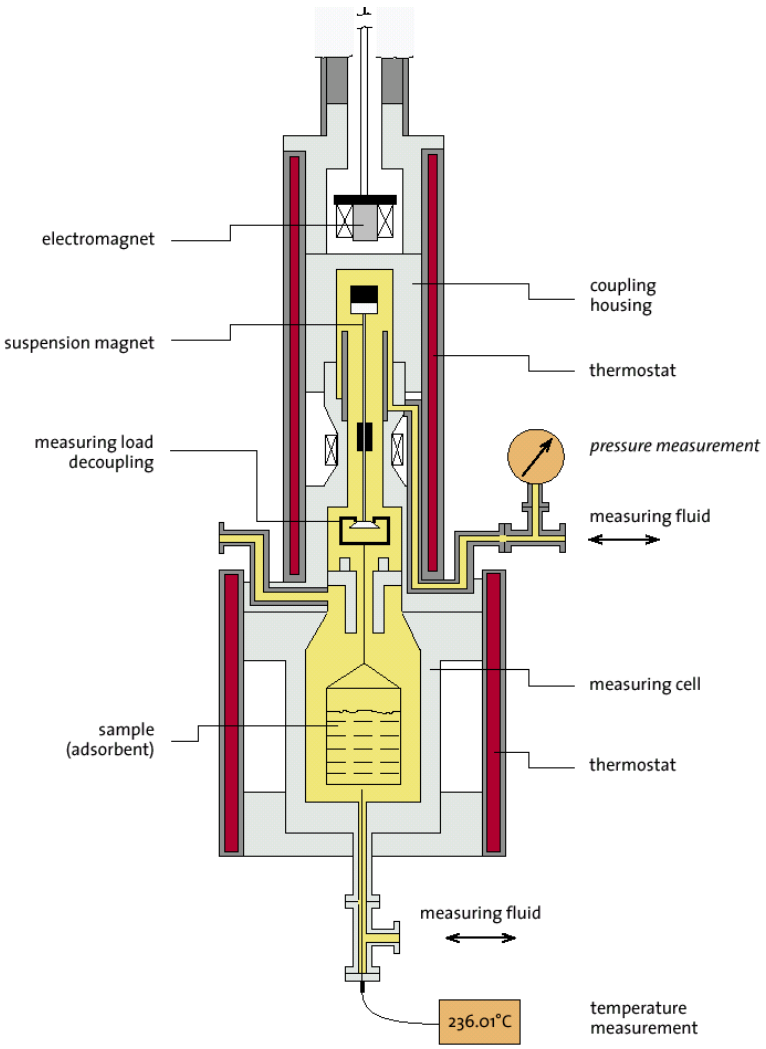

Figure 4.6 Schematic of ISOSORP magnetic suspension balance for polymer sorption measurements

The system was first evacuated using a vacuum pump and was allowed to reach thermal equilibrium. This process took anywhere from two to six hours, depending on the temperature. The balance recorded the mass of the degassed polymer sample and suspension coupling before the addition of carbon dioxide. Carbon dioxide was added to a given pressure and the system was allowed to reach

thermodynamic equilibrium. Equilibrium was defined as the point at which the measured mass did not change more than 0.1 mg in five successive measurements. Equilibrium times ranged from 2 to 24 hours, depending on the conditions. Additional CO_2 was added in increments and the corresponding equilibrium weight of the polymer sample was recorded at each pressure interval. For some experiments, the pressure was then decreased at intervals and the equilibrium sorption with depressurization was recorded.

The weight gain of the polymer sample due to sorption of CO_2, M_{CO_2}, was calculated according to:

$$M_{CO_2} = \Delta m + (V_S + V_{PVDF})\rho_{CO_2} \tag{4.1}$$

$$V_{PVDF} = \Delta S \times V_o \tag{4.2}$$

where Δm is the measured change in mass of the sample from the initial mass under vacuum, V_s is the volume of the sample basket and suspension coupling, V_o is the volume of the polymer sample in the absence of CO_2, ΔS is the degree of swelling of the polymer sample at the system conditions, and ρ_{CO_2} is the density of the fluid at the system conditions. The density of the fluid was calculated based on the measured mass of a titanium sinker of calibrated volume at the system conditions. The degree of swelling was determined based on data presented in Sections 4.1.1.2 and A.2.3.1 for 75 and 80°C and data available in the literature for this polymer [1] at 42°C. The maximum swelling at the temperatures and pressures of the experiments

was less than 1%. This resulted in a very small correction for the swelling in the sorption calculations less than 1%.

4.1.2.2 Results and Discussion

Relatively few groups [11-13] have used the ISOSORP magnetic suspension balance to measure polymer sorption in the presence of CO_2. In order to validate the operability of the instrument and to demonstrate the use of the ISOSORP for CO_2 experiments, the sorption of CO_2 into polystyrene was measured and compared to literature data. Wissinger and Paulaitis [14] measured the sorption of CO_2 into polystyrene using a quartz spring technique. Their polymer was melt-pressed into 0.15 mm thick films and conditioned by heating above the glass transition temperature of the polymer before being sorbed with CO_2. Polymer pellets obtained from the same source and description (Scientific Polymer Products #844) as Wissinger and Paulaitis were used to measure the sorption with the ISOSORP. The results of measuring the sorption by the two different techniques are shown in Figure 4.7. The results are in excellent agreement. These results demonstrate the utility of the magnetic suspension balance for measuring polymer sorption in the presence of supercritical carbon dioxide.

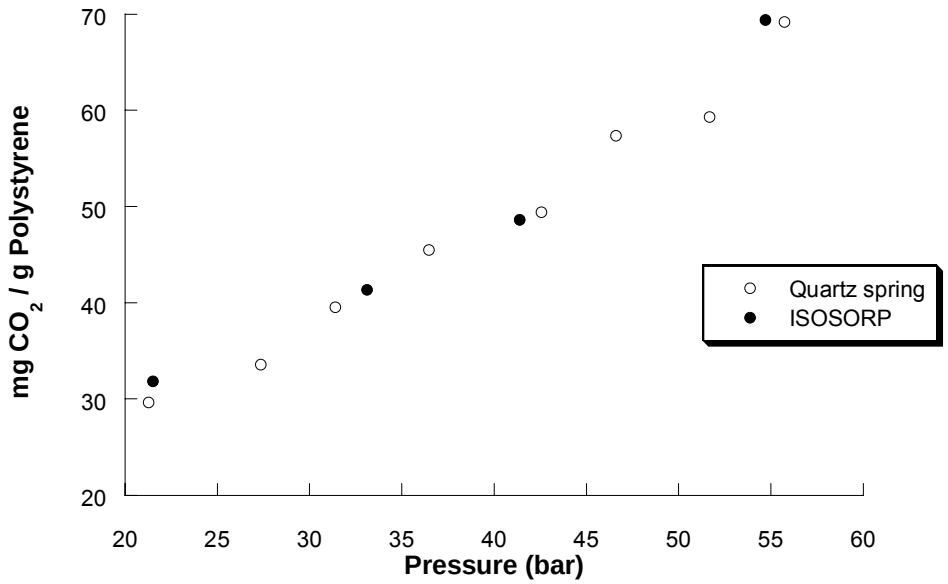

Figure 4.7 Sorption of CO_2 into polystyrene at 50 °C using a quartz spring and magnetic suspension balance (ISOSORP)

The sorption of CO_2 into PVDF was measured at 42, 60, 75, and 80 °C over a range of pressures up to 250 bar. The results at 42, 60 and 80 °C are shown in Figure 4.8. A full detail of the results is summarized in Section A.1.3.1. In general, the sorption increased with increasing pressure and decreasing temperature. The quantity of CO_2 sorbed correlated well with the density of CO_2. Upon replotting the data as a function of the CO_2 density, the data lie on a single curve with no observable temperature effect (Figure 4.9). This is consistent with the increasing solvating power of CO_2 with increasing density. A favorable interaction exists between the polymer and CO_2 such that as the density increases, increasing amounts of CO_2 sorb into the polymer phase. As shown in Figure 4.8, the sorption increases linearly at conditions in which carbon dioxide is a gas. With further increases in the pressure, the rate of increase in the sorption is less. This

corresponds with a reduction in the rate of increase of the chemical potential of CO_2 with pressure. The sorption at 42 °C is greater than the sorption at 80°C over the whole range of pressures studied. This is in contrast to data previously reported [1] (Figure 3.6). In that work, the sorption at 80 °C was greater than the sorption at 42 °C at pressures greater than 200 bar. The authors attributed that behavior to a greater impact of polymer chain mobility at 80 °C. This is unlike the results in the present study in which the increase in sorption correlates with the CO_2 density and its chemical potential over the entire pressure range. Additionally, the data obtained in the present study were higher than the literature data at low pressures and level off at a significantly lower degree of sorption than the literature data (Figures 4.10 and 4.11). The initial linear increase of the sorption data in the present study with pressure is consistent with Henry's law, which states that at low pressures the concentration of gas is independent of the pressure. It is unclear why there is a discrepancy between the data obtained in this study and that reported in the literature. However, one factor may be due to differences in the crystallinity of the polymers used. Briscoe and coworkers [1] report a crystallinity of 53% for the polymer used in their sorption experiments, whereas the polymer used in this research was 64% crystalline. This could explain why the sorption in the literature data is greater than the sorption in the present study at higher pressures. Additionally, the thermal history and the role of the crystalline regions on the sorption in the amorphous phase may have an effect. This will be further discussed in Section C.1.2.

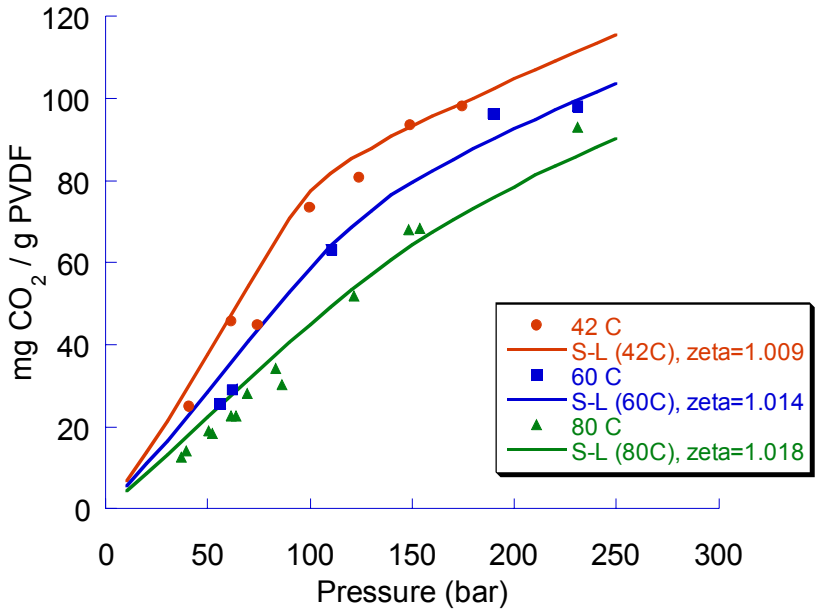

Figure 4.8 Sorption of CO_2 into PVDF at 42 °C (●), 60 °C (■), and 80 °C (▲) as a function of pressure. Lines represent fit using Sanchez-Lacombe equation of state with a single adjustable parameter (zeta)

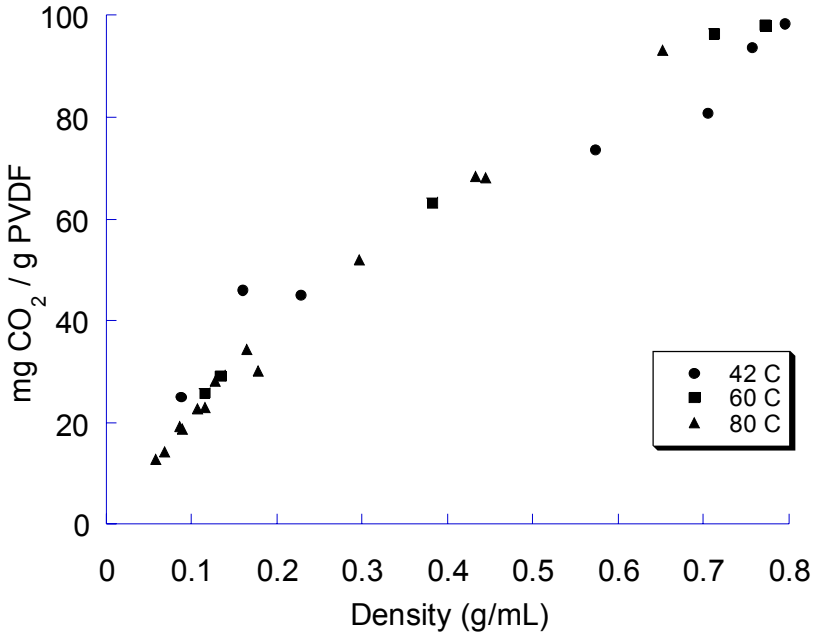

Figure 4.9 Sorption of CO_2 into PVDF at 42 °C (●), 60 °C (■), and 80 °C (▲) as a function of density

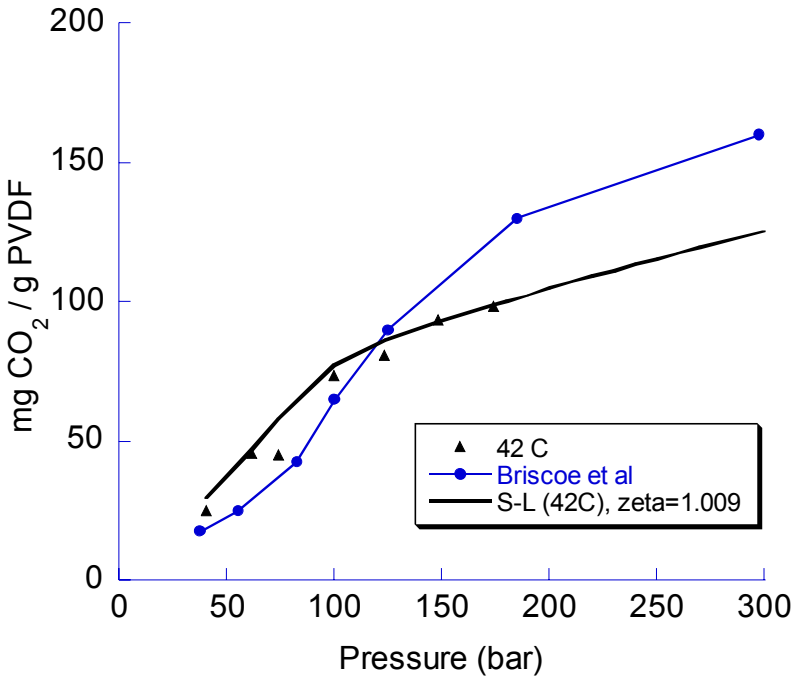

Figure 4.10 Comparison between data from the literature [1] and the present study with the Sanchez-Lacombe model for the sorption of CO_2 into PVDF at 42 °C

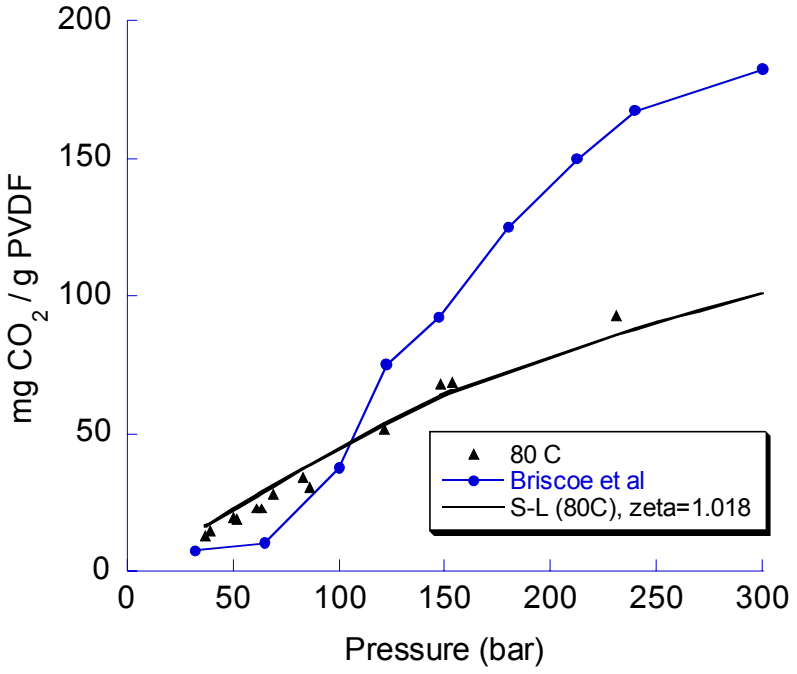

Figure 4.11 Comparison of data from the literature [1] and the present study with the Sanchez-Lacombe model for the sorption of CO_2 into PVDF at 80 °C

4.2 Thermodynamic Modeling with Sanchez-Lacombe EOS

The Sanchez-Lacombe (S-L) equation of state was used to correlate the phase equilibria for PVDF-CO_2. Pure component parameters were taken from the literature or determined by fitting experimental data. The two component phenomena were calculated based on sorption solely in the amorphous regions of the polymer. The S-L model predicts the phase equilibria qualitatively and quantitatively. The model results provide a better understanding of the phase equilibrium and form the basis for modeling the three-component system.

4.2.1 Pure Component Parameters

Characteristic parameters that describe the properties of pure fluids are needed to calculate binary and multi-component phase equilibria. The determination of pure component parameters for PVDF and CO_2 are described in the following sections.

4.2.1.1 Carbon Dioxide

The characteristic parameters for pure components may be determined from a variety of experimental data. The parameters to describe small molecules are commonly determined by fitting the parameters to vapor pressure data. Numerous sources for CO_2 characteristic parameters are available in the literature. Kiszka et al [15] suggest that the pure component parameters be selected based on the temperatures and pressures at which sorption isotherms are calculated. Kiszka et al

report that the S-L model is unable to accurately predict the properties over a very large range of temperatures and pressures. Thus, pure component parameters that are determined at temperatures and pressures in the range of interest for sorption calculations should provide the best correlation and prediction of the sorption data. Several sets of characteristic parameters were analyzed to identify appropriate parameters for CO_2-PVDF. A summary of the parameters considered and the type of data used to determine the parameters are shown in Table 3.4 and reproduced in Table 4.2.

Table 4.2
Sanchez-Lacombe EOS characteristic parameters for carbon dioxide

Parameter Set	P* (bar)	T* (K)	ρ* (g/ml)	r	Data Source	Reference
1	5737	309	1.504	6.54	IUPAC ΔH_v & ρ data @ subcritical and supercritical conditions	[16]
2	4643	328	1.426	5.25	PVT data @ 0-150°C, 0-300 MPa	[17]
3	4126	316	1.369	5.11	VLE data @ -53.89°C, 0.5716 MPa	[18]
4	6510	283	1.62	7.6	ΔH_v & VLE data @ normal b.p., 0.1 MPa	[19]
5	5670	305	1510	6.6	Molar volume @ 40-60°C, 10-60 MPa	[15]
6	7101	280	1.6177	8.4	VLE data @ -56.6-31.1°C, 0.51-7.4 MPa	[20]

The density of CO_2 at 80 °C was calculated using each set of parameters and compared to values for the density reported in the NIST database [21]. The sum of squared errors (SSE) was calculated for each parameter set according to

$$SSE = \sum_{i=1}^{n} \left(x_i^{data} - x_i^{calc} \right)^2 \tag{4.3}$$

where x_i^{data} is a given property, in this case the density, determined from experiments or given by the NIST database, x_i^{calc} is the property calculated with the S-L model, and n is the number of data points. The critical properties of CO_2 were calculated using Equations 3.20 through 3.22. The results are summarized in Table 4.3. It was found that parameters that reasonably predict the critical properties of CO_2 do not necessarily provide an accurate prediction of the density of CO_2. For example, parameter set 3 accurately predicted the critical temperature of CO_2, but had a high value for SSE. The density correlation for this parameter set is shown in Figure 4.12. The model prediction was fairly good at low pressures and near the critical point (P_c = 73.8 bar). However, as the pressure was increased, the deviation of the model from the data increased.

The different sets of CO_2 parameters were used in the two-component S-L model and compared to sorption data for PVDF at 80 °C from the literature (Figure 3.6). Parameter sets 2 & 3 provided the smallest SSE and an interaction parameter closest to one. Thus, a good prediction of the single component properties is not necessarily an indicator of a good prediction of the two component or multi-component properties. Parameter set 3 was chosen for subsequent calculations

because it provided a reasonable prediction of the sorption data with an interaction parameter close to one and it had a good representation of the critical properties of CO_2. Additionally, parameter set 3 has been used previously for modeling CO_2-PVDF [1].

Table 4.3
Results of Modeling the CO_2 density @ 80 °C and the critical properties* with the Sanchez-Lacombe model

Parameter set	SSE for Density ($x10^3$)	Prediction for T_c (K)	Prediction for P_c (bar)	Prediction for ρ_c (g/mL)
1	1.7	319.4	91.7	0.423
2	1.1	317.9	94.4	0.433
3	26.2	303.8	86.3	0.420
4	41.4	304.8	88.0	0.431
5	37.4	316.1	89.7	0.423
6	31.9	309.5	85.6	0.415

* Actual critical properties of CO_2 are T_c = 304.3 K, P_c = 73.8 bar, and ρ_c = 0.471 g/mL [22]

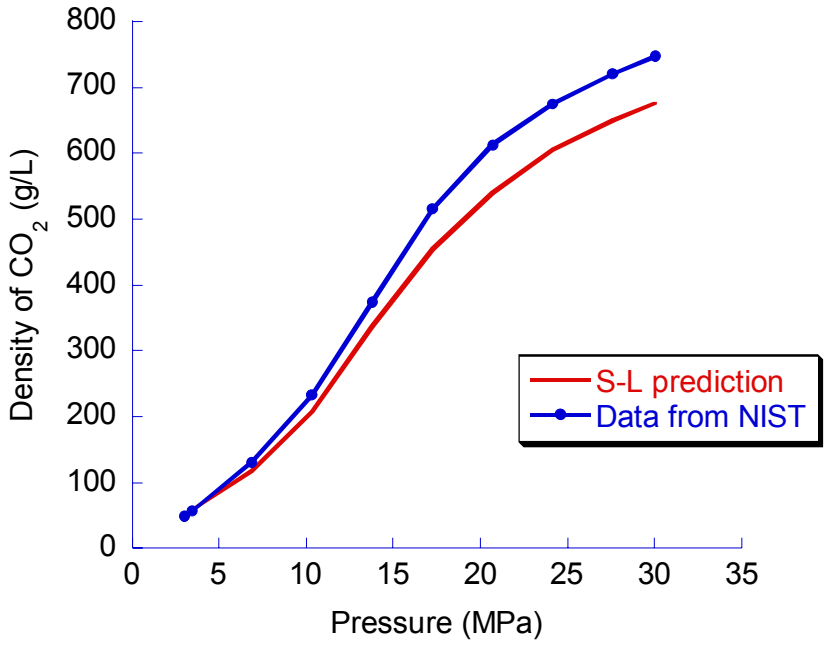

Figure 4.12 Comparison of Sanchez-Lacombe model prediction of CO_2 density at 80 °C, using parameter set 3, to data taken from NIST database

4.2.1.2 Poly(vinylidene fluoride)

Several sets of characteristic parameters for PVDF have been reported in the literature (see Table 3.4). Characteristic parameters for the commercial sample used in this research were determined from PVT data measured at the University of Naples (Appendix B.4). The characteristic parameters were determined based on a non-linear least squares fit to the S-L EOS for polymers ($r \to \infty$)

$$\tilde{\rho}^2 + \tilde{P} + \tilde{T}\left[\ln(1-\tilde{\rho}) + \tilde{\rho}\right] = 0 \tag{4.4}$$

The characteristic parameters for Solvay's Solef 1010 commercial PVDF are summarized in Table 4.4.

Table 4.4
Sanchez-Lacombe EOS characteristic parameters for Solef 1010 PVDF

P* (bar)	T* (K)	ρ* (g/mL)	Mw (g/mol)
4348	714.6	1.860	150,000

4.2.2 Correlation of Model with Sorption Data

The Sanchez-Lacombe equation of state was used to predict the sorption of CO_2 into PVDF at 42, 60, and 80 °C (Figure 4.8). The sorption was modeled based on sorption exclusively in the amorphous phase. The quantity of CO_2 mass sorption per mass of polymer was calculated according to

$$\frac{mg\ \ CO_2}{g\ \ PVDF} = \frac{\omega_1}{1 + X\left(\frac{1-\omega_1}{1-X}\right)} \cdot 1000 \tag{4.5}$$

where ω_1 is the weight fraction of CO_2 in the amorphous phase and X is the weight percent crystallinity of the polymer. Using binary interaction parameters of 1.009 at 42 °C, 1.014 at 60 °C, and 1.018 at 80 °C, which minimize the SSE, the model predicts the present sorption data very well. The Sanchez-Lacombe model is mostly predictive, as indicated by the interaction parameters being close to one. The deviation of the model from the geometric mean is very small (less than 2%). Additionally, it was possible to correlate the interaction parameter with the temperature. This is illustrated in Figure 4.13. Because of the limited data at 75 °C, the interaction parameter at 75 °C was not determined from a fit to this data. Instead, the correlation established in Figure 4.13 was used to determine the interaction parameter. The model fit using the interpolated interaction parameter is shown in Figure 4.14. The model provided a reasonable fit to the data. The results in Figure 4.13 may be used to determine the interaction parameter at temperatures between 42 and 80 °C.

The model sorption was calculated using a single set of characteristic parameters for PVDF (Table 4.4). The parameters were determined from a least-squares fit to PVT data for the polymer (Appendix B). There were previously reported parameters for PVDF [1] in the temperature range 42 to 80 °C that changed with the temperature of the system (Table 3.4). However, the parameters used in this work are applicable over a temperature range of 25 to 180 °C.

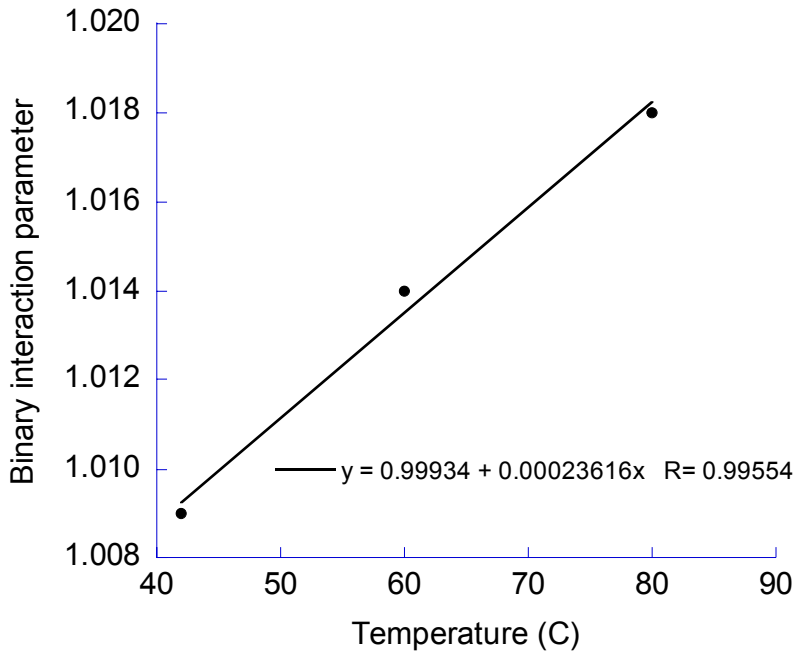

Figure 4.13 Correlation between the binary interaction parameter, ζ_{23}, for CO_2-PVDF and the temperature

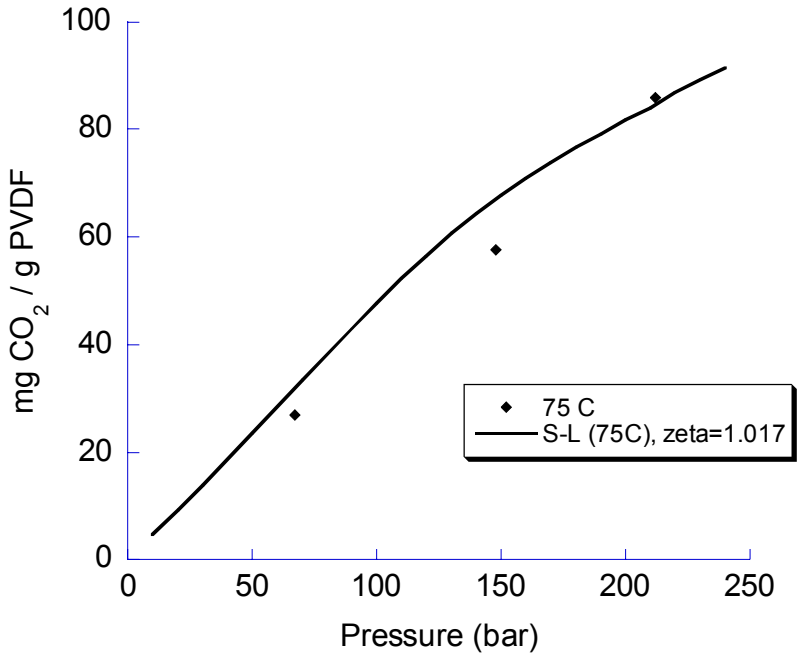

Figure 4.14 Sorption of CO_2 into PVDF at 75 °C as a function of pressure. Line represents fit using Sanchez-Lacombe equation of state with a single adjustable parameter (zeta)

An attempt was made to model the sorption reported in the literature [23]. The S-L model was unable to provide a reasonable fit to the data. In order to explain the inadequacy of the S-L model for describing the data reported in the literature, a “crystalline correction” was applied to the S-L model to account for the possible influence of the crystalline regions on the sorption (Section C.1.2). This approach was unable to describe

As discussed in Section 4.1.2.2, the data reported in the literature did not exhibit the same qualitative and quantitative trends as the present data. Additionally, attempts to model this data with the S-L model did not produce satisfactory results [23]. The influence of the crystalline regions on the sorption in the amorphous phase was investigated using a “crystalline correction” to the model (Section C.1.2). However, this approach also could not fully describe the literature data. That approach as well as other attempts to model the data reported in the literature are described in Appendix C.

4.3 Conclusions

The sorption of carbon dioxide into poly(vinylidene fluoride) and the swelling of poly(vinylidene fluoride) in the presence of carbon dioxide was measured between 42 and 80 °C over a range of pressures. A novel LVDT technique allowed measurements of the swelling as low as 10 microns. A magnetic suspension balance was used to measure the mass sorption of carbon dioxide in the polymer. As the pressure in the system increased, the swelling and sorption increased. The

Sanchez-Lacombe equation of state was used to predict the sorption into PVDF and found to be in good agreement with the data. The binary interaction parameters were very close to one, indicating that the model was mostly predictive in describing the sorption characteristics.

4.4 References

1. Briscoe, B.J., Lorge, O., Wajs, A., and Dang, P., *Carbon dioxide-poly(vinylidene fluoride) interactions at high pressure.* Journal of Polymer Science: Part B: Polymer Physics, 1998. **36**(13): p. 2435-2447.

2. Flaconneche, B., Martin, J., and Klopffer, M.H., *Permeability, diffusion and solubility of gases in polyethylene, polyamide 11, and poly(vinylidene fluoride).* Oil & Gas Science and Technology - Revue de L Institut Francais du Petrole, 2001. **56**(3): p. 261-278.

3. Benali, A., Benjelloun-Dabaghi, Z., Flaconneche, B., Klopffer, M.H., and Martin, J., *Simulation of temperature and pressure influence on transport coefficients of CO_2 in PVDF.* Oil & Gas Science and Technology - Revue de L Institut Francais du Petrole, 2001. **56**(3): p. 305-312.

4. Shieh, Y.-T., Su, J.-H., Manivannan, G., Lee, P.H.C., Sawan, S.P., and Spall, W.D., *Interaction of supercritical carbon dioxide with polymers. I. Crystalline polymers.* Journal of Applied Polymer Science, 1996. **59**(4): p. 695-705.

5. Shenoy, S., Woerdeman, D., Sebra, R., Garach-Domech, A., and Wynne, K.J., *Quantifying polymer swelling employing a linear variable differential transformer: CO_2 effects on SBS triblock copolymer.* Macromolecular Rapid Communications, 2002. **23**(18): p. 1130-1133.

6. Shenoy, S.L., Fujiwara, T., and Wynne, K.J., *Quantifying plasticization and melting behavior of poly(vinylidene fluoride) in supercritical CO_2 utilizing a linear variable differential transformer.* Macromolecules, 2003. **36**(9): p. 3380-3385.

7. Flory, P.J., *Principles of Polymer Chemistry*. 1953, Ithaca, NY: Cornell University Press.

8. Michaels, A.S. and Hausslein, R.W., *Elastic factors controlling sorption and transport properties of polyethylene.* Journal of Polymer Science: Part C, 1965. **10**: p. 61-86.

9. Nakagawa, K. and Ishida, Y., *Annealing effects in poly(vinylidene fluoride) as revealed by specific volume measurements, differential scanning calorimetry, and electron microscopy.* Journal of Polymer Science: Polymer Physics Edition, 1973. **11**: p. 2153-2171.

10. Shenoy, S., Personal Communication, 2003.

11. Handa, Y.P., Zhang, Z., and Wong, B., *Solubility, diffusivity, and retrograde vitrification in PMMA-CO_2, and development of sub-micron cellular structures.* Cellular Polymers, 2001. **20**(1): p. 1-16.

12. Sato, Y., Takikawa, T., Takishima, S., and Masuoka, H., *Solubilities and diffusion coefficients of carbon dioxide in poly(vinyl acetate) and polystyrene.* Journal of Supercritical Fluids, 2001. **19**(2): p. 187-198.

13. Schnitzler, J.v. and Eggers, R., *Mass transfer in polymers in a supercritical CO_2-atmosphere.* Journal of Supercritical Fluids, 1999. **16**(1): p. 81-92.

14. Wissinger, R.G. and Paulaitis, M.E., *Swelling and sorption in polymer-CO_2 mixtures at elevated pressures.* Journal of Polymer Science: Part B: Polymer Physics, 1987. **25**: p. 2497-2510.

15. Kiszka, M.B., Meilchen, M.A., and McHugh, M.A., *Modeling high pressure gas-polymer mixtures using the Sanchez-Lacombe equation of state.* Journal of Applied Polymer Science, 1988. **36**: p. 583-597.

16. Panayiotou, C. and Sanchez, I.C., *Swelling of network structures.* Polymer, 1992. **33**: p. 5090-5093.

17. Garg, A., Gulari, E., and Manke, C.W., *Thermodynamics of polymer melts swollen with supercritical gases.* Macromolecules, 1994. **27**(20): p. 5643-5653.

18. Hariharan, R., Freeman, B.D., Carbonell, R.G., and Sarti, G.C., *Equation of state predictions of sorption isotherms in polymeric materials.* Journal of Applied Polymer Science, 1993. **50**: p. 1781-1795.

19. Pope, D.S., Sanchez, I.C., Koros, W.J., and Fleming, G.K., *Statistical thermodynamic interpretation of sorption/dilation behavior of gases in silicone rubber.* Macromolecules, 1991. **24**(8): p. 1779-1783.

20. Kilpatrick, P.K. and Chang, S.-H., *Saturated phase equilibria and parameter estimation of pure fluids with two lattice-gas models.* Fluid Phase Equilibria, 1986. **30**: p. 49-56.

21. Lemmon, E.W., McLinden, M.O., and Friend, D.G., *Thermophysical properties of fluid systems*, in *NIST Chemistry WebBook, NIST Standard Reference Database Number 69*, P.J. Linstrom and W.G. Mallard, Editors. 2003, National Institute of Standards and Technology: Gaithersburg, MD.

22. Reid, R.C., Prausnitz, J.M., and Sherwood, T.K., *The properties of gases and liquids*. 3rd ed. 1977, New York: McGraw-Hill.

23. Kennedy, K.A., DeSimone, J.M., and Roberts, G.W., *A Commentary of "Carbon dioxide-poly(vinylidene fluoride) interactions at high pressure".* Journal of Polymer Science: Part B: Polymer Physics, 2002. **40**: p. 602-604.

Chapter 5

Partitioning of vinylidene fluoride between supercritical carbon dioxide and poly(vinylidene fluoride) phases: experiments and modeling

Herein, we report experiments and modeling for the phase equilibrium between PVDF, CO_2, and vinylidene fluoride (VF2) monomer. The mass sorption and partition coefficients have been measured by two different techniques. The first technique is based on measurements of the fluid phase composition, referred to as fluid phase measurements. The second technique is based on measurements of the polymer mass, referred to as polymer phase measurements. A model based on the Sanchez-Lacombe equation of state has been developed for the three-component system. A comparison is made between the model and the experimental data. The implications of the three component phase equilibria on the polymerization process are discussed.

5.1 Experimental Studies

5.1.1 Partitioning based on Fluid Phase Measurements

The partitioning of vinylidene fluoride monomer between PVDF and a supercritical fluid phase was measured using a technique based on fluid phase measurements. At equilibrium, the concentration of monomer in the fluid phase was measured and the amount of monomer sorbed into the polymer phase was calculated based on a mass balance. This approach was effective for monitoring the

overall impact of the experimental conditions on the partition coefficient for vinylidene fluoride between the two phases.

5.1.1.1 Experimental

5.1.1.1.1 Materials

Poly(vinylidene fluoride) (Solef 1010, $\overline{M}_w$=180,000) powder and vinylidene fluoride monomer were supplied by Solvay. Coleman grade CO_2 (99.99% purity) was purchased from National Welders and used as received.

5.1.1.1.2 Apparatus and Methods

A schematic of the apparatus used in these studies is shown in Figure 5.1. The major components include 1) the polymer sample holder (F, HIP model MS-12) in which the polymer sample is located during the experiment, 2) an HPLC valve (H, Valco model E90) to sample the fluid phase, 3) a gas chromatograph (G, SRI model 8610C) to analyze samples from the HPLC valve, and 4) a circulating pump (C, Micropump model 1805) to circulate the fluid through the polymer sample and reduce the time to equilibrium. The pressure was monitored using a pressure transducer (Druck model PTX 621). The entire system was enclosed in a microprocessor-controlled oven (VWR model 1330FM), which controlled the temperature within 0.4 °C of the temperature set point. The total volume of the system was 25 mL.

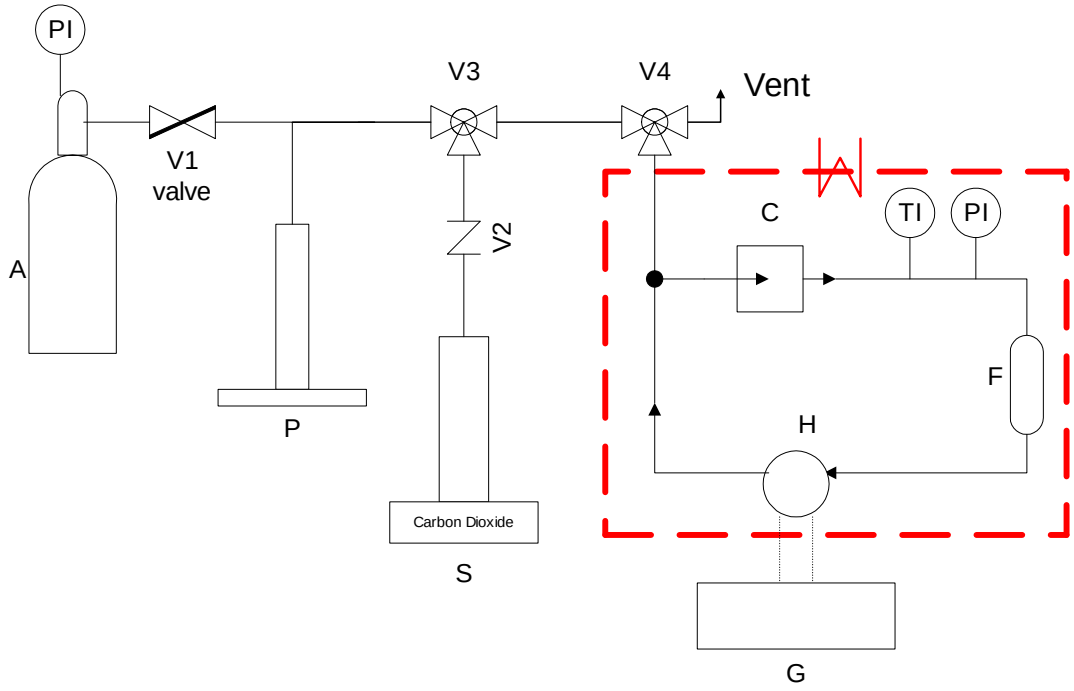

Figure 5.1 Schematic of Partition Coefficient Apparatus: A – Vinylidene fluoride cylinder, C – circulating pump, F – polymer sample holder, G – gas chromatograph, H – HPLC valve, P – HIP pressure generator, S – ISCO syringe pump, TI – temperature indicator, PI – pressure indicator

To begin an experiment, the polymer was weighed before being added to the polymer cylinder. Glass wool and frits were used to retain the polymer in the sample holder. The system was sealed and then purged and checked for leaks using nitrogen. The system was heated and allowed to reach thermal equilibrium before adding VF2 and CO_2 of known weight to the system. The weights of VF2 and CO_2 were calculated based on the volume of the system and components and equations of state for each of the fluids. Valve V4 was then closed and the fluid was circulated at 49 mL/min. Once the system reached equilibrium (usually after four hours), 0.5 μL samples were taken from the fluid phase using the HPLC valve and fed to a gas chromatograph for analysis. The average of three to five samples were taken to

calculate the partition coefficient. Details of the experimental and calculation procedure are given in Appendix A.

5.1.1.2 Results and Discussion

Calculation of the partition coefficients required information about the concentration of the monomer in the fluid phase. A calibration curve (Figure 5.2) was constructed based on known amounts of VF2 and CO_2 in the absence of polymer and the ratio of the component area counts from a gas chromatograph (GC). A thermal conductivity detector (TCD) was used with a silica gel packed column at 55°C in the gas chromatograph. A sample chromatogram for a mixture of VF2 and CO_2 is shown in Figure 5.3.

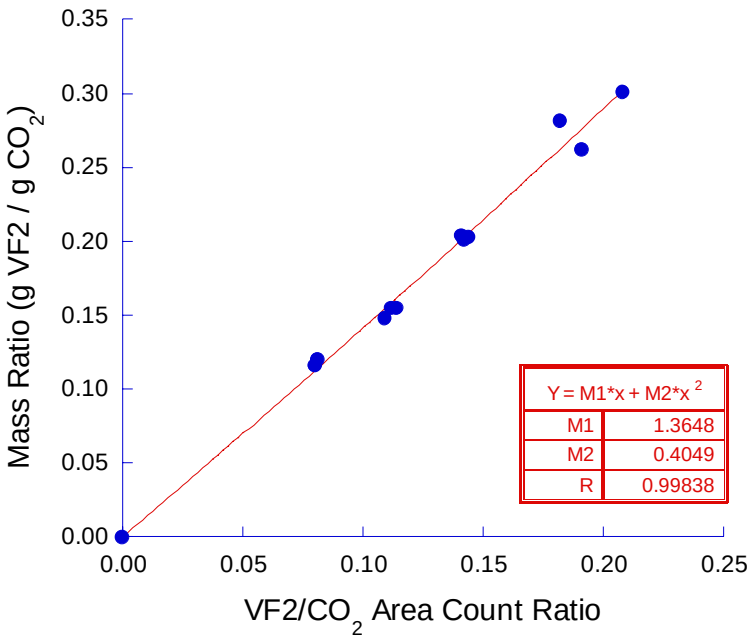

Figure 5.2 Calibration curve for varying amounts of vinylidene fluoride and carbon dioxide at 75 °C and ~276 bar using a gas chromatograph

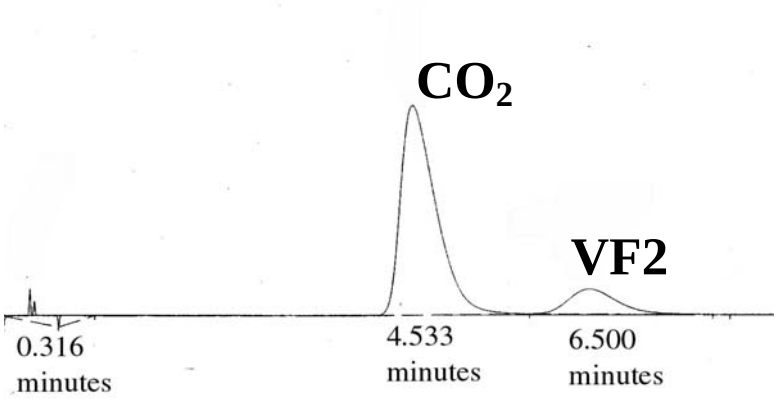

Figure 5.3 Typical chromatogram for VF2 and CO_2. T = 55 °C using a TCD detector and silica gel packed column

The concentration-based partition coefficient, K_c, was calculated according to

$$K_c = \frac{[VF2]^{PVDF}}{[VF2]^{CO_2}} \tag{5.1}$$

which is the ratio of the concentration of vinylidene fluoride in the polymer phase to that in the fluid phase. The concentration of monomer in the fluid phase was determined from the GC analysis. The difference between the amount of VF2 in the fluid phase at equilibrium and the amount of VF2 initially fed to the system should be the amount of VF2 that has partitioned into the polymer phase. The amount of CO_2 that partitioned into the polymer phase was assumed to be very small and not significantly affect the amount of CO_2 that remained in the fluid phase. Therefore, the amount of vinylidene fluoride in the fluid phase was simply the mass ratio (determined from the calibration curve) multiplied by the mass of carbon dioxide fed into the system.

A calculation of the mass of VF2 in the polymer phase as a function of pressure at 75 °C is shown in Figure 5.4. As the total pressure was increased, the amount of VF2 in the polymer phase was found to decrease. At pressures greater than 240 bar, negative values of VF2 in the polymer were obtained. This suggests that more VF2 was in the fluid phase at equilibrium than was initially present. This apparent increase of the monomer in the fluid phase may be partially due to solubilization of low molecular weight polymer at the conditions of the experiments. A thin coating of polymer was observed on the walls of the system after the experiments. This suggests that some polymer was solubilized by CO_2 and, upon depressurization, deposited on the tubing walls. Thus, the ratio of VF2 to CO2 sampled by the HPLC valve was impacted by the presence of solubilized polymer in the fluid phase.

Figure 5.4 illustrates the effect of assuming varying degrees of CO_2 sorption into the polymer on the amount of VF2 in the polymer phase. The maximum level of CO_2 sorption was considered to be 20 wt%, based on the maximum degree of sorption observed in the CO_2-PVDF sorption experiments. The calculated amounts of VF2 were not greatly impacted by whether or not CO_2 sorbed into the polymer phase. Therefore, the CO_2 sorption was neglected in subsequent calculations of the partition coefficient. Additionally, the maximum swelling of the PVDF pellets in the presence of CO_2 was about 1% (Section 4.1.1.2). It was assumed that the swelling would not have a significant impact on the partition coefficient. Therefore, the swelling of the polymer was neglected in the partition coefficient calculations.

The negative values for the amount of VF2 in the polymer phase at elevated pressures suggest that this technique does not provide quantitative results. In cases where negative values were calculated, the partition coefficient was set to zero. Despite the lack of quantitative measure, the qualitative trends were considered useful.

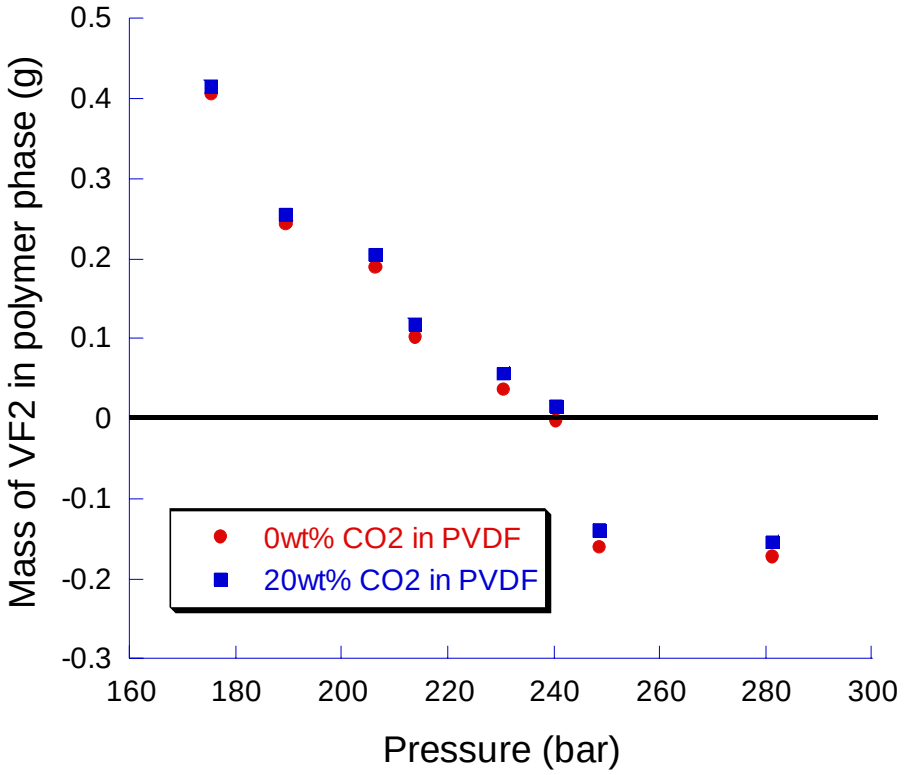

Figure 5.4 Mass of VF2 in the polymer phase at equilibrium, based on area count ratios from a gas chromatograph, at 75 °C as a function of pressure. System initially consists of 5 wt% PVDF and 15 wt% VF2 in CO_2. Legend indicates assumption of degree of CO_2 sorption into polymer

The effect of temperature and pressure on the partition coefficient is illustrated in Figure 5.5. As the pressure was increased or the temperature decreased, the partition coefficient decreased. This suggests that at increasing fluid densities, the monomer was preferentially retained in the fluid phase. There are two

possible reasons for this phenomenon. First, as the density of CO_2 increases, its solvating power increases. Thus, the interaction between the monomer and CO_2 may be enhanced at increased fluid density such that the monomer prefers the fluid phase. However, based on two-component experiments, as the density increases, the sorption of CO_2 into the polymer phase also increases. So, the sorption of carbon dioxide into the polymer phase may inhibit the sorption of monomer.

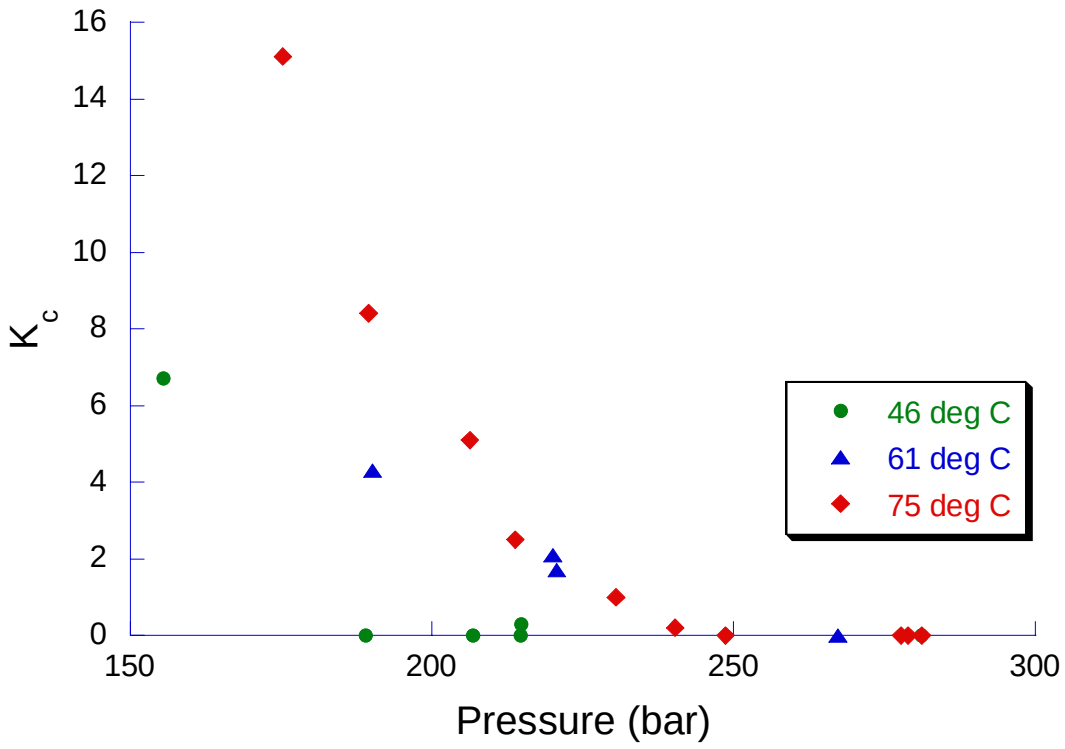

Figure 5.5 Partition coefficients of vinylidene fluoride between PVDF and CO_2 phases as a function of temperature and pressure as determined from fluid-based partitioning measurement. System initially consists of 5 wt% PVDF and 15 wt% VF2 in CO_2

The calculation of the partition coefficient was very sensitive to the area count ratio for VF2 and CO_2 measured by the gas chromatograph. The data presented in

Figure 5.5 were based on the average of three to five samples taken by the gas chromatograph. For any particular experiment, the variation in the area count ratio between samples may equal ± 0.0007. Although this variation seems small, the variation is magnified once it is translated into a mass ratio (Figure 5.2) and then a partition coefficient. This is further illustrated in Figure 5.6. In this case, K_c was allowed to have negative values if the GC analysis determined there was a negative value for the mass of VF2 in the fluid phase at equilibrium (Figure 5.4). Based on the variation in the area count ratio, the variation in the K_c values could be quite large.

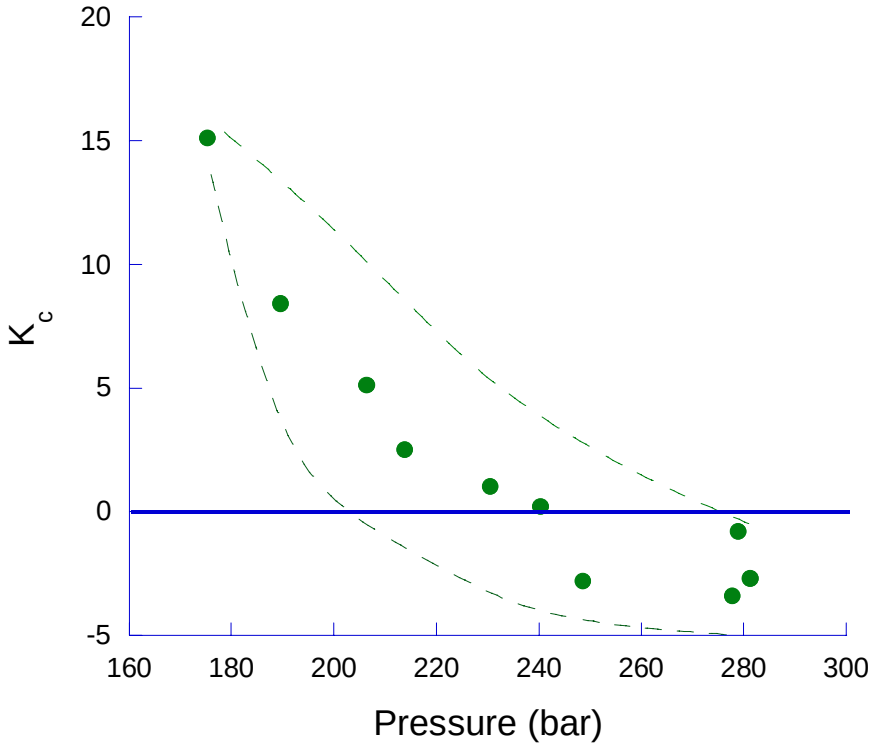

Figure 5.6 Partition coefficients of vinylidene fluoride between PVDF and CO_2 phases at 75 °C as a function of pressure as determined from fluid-based partitioning measurement. Dotted lines represent error in calculation based on deviation of three to five samples taken with gas chromatograph. System initially consists of 5 wt% PVDF and 15 wt% VF2 in CO_2

Additionally, it was mentioned previously that the results from these fluid-based partitioning measurements provide a qualitative, but not a quantitative measure of the partition coefficient. In the next section, the partition coefficients are calculated based on measurements from a magnetic suspension balance that weighs the polymer during the experiments. This technique provides an accurate, quantitative measure of the partition coefficients. These polymer-based partitioning measurements will provide additional information for understanding the observed partitioning behavior.

5.1.2 Partitioning based on Polymer Phase Measurements

A technique based on measuring the change in weight of a polymer sample was used to measure the partitioning of vinylidene fluoride between PVDF and the supercritical fluid phase. The relative amounts of vinylidene fluoride and carbon dioxide that sorbed into the polymer phase were calculated using the Sanchez-Lacombe equation of state after correlating the model with the data. This approach allowed a better understanding of partitioning of the monomer between the two phases.

5.1.2.1 Experimental

5.1.2.1.1 Materials

Poly(vinylidene fluoride) (Solef 1010, $\overline{M}_w$=180,000) pellets (cylinders with an average diameter and length of 35 mm) were supplied by Solvay and used as received. Vinylidene fluoride (VF2) was purchased from Aldrich and used as

received. Coleman grade carbon dioxide was purchased from National Welders and used as received.

5.1.2.1.2 Apparatus and Methods

The sorption of carbon dioxide and vinylidene fluoride into PVDF was measured using a magnetic suspension balance (Rubotherm, Germany), also referred to as the ISOSORP. The measurement principles of the magnetic suspension balance have been previously described in the literature [1, 2]. A schematic of the system used in this work is shown in Figure 5.7. The temperature and pressure of the system were monitored near the bottom of the sample basket using a platinum resistance sensor and pressure transducer, respectively. Known weights of vinylidene fluoride and carbon dioxide were added in the tubing outside of the balance. The polymer sample (~3 grams) was placed in a mesh basket suspended from the permanent magnet inside the high-pressure vessel. The permanent magnet was decoupled from an electromagnet suspended from a microbalance at ambient conditions. The precision of the microbalance was reported to be 0.01 mg.

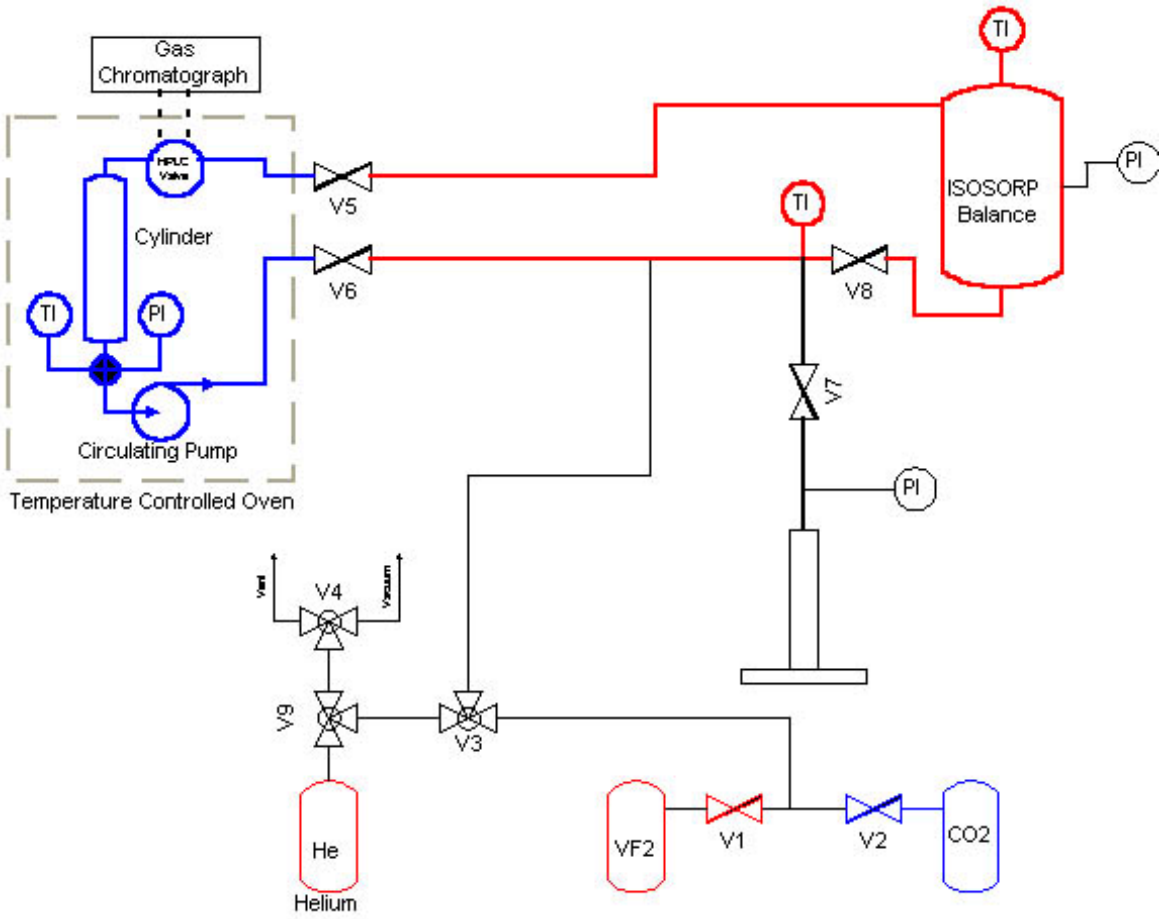

Figure 5.7 Schematic of sorption apparatus

The balance was first evacuated using a vacuum pump and the system was allowed to reach thermal equilibrium. This process took anywhere from two to six hours, depending on the temperature set point. The balance recorded the mass of the degassed polymer sample and suspension coupling before the addition of carbon dioxide and monomer. Valves V5 and V8 were then opened to expose the polymer to a mixture of carbon dioxide and vinylidene fluoride. A magnetic gear pump (Micropump model 1805) was used to circulate the fluid at 17 mL/min. The temperature was controlled by a heating jacket surrounding the measuring cell of the

balance. This maintained a constant temperature around the polymer. The tubing lines around the circulation loop were wrapped with insulation to minimize heat loss. However, the temperature in the tubing outside the measuring cell was at a lower temperature. The system was allowed to reach thermodynamic equilibrium. Equilibrium was defined as the point at which the measured mass did not change more than 0.1 mg (for an average sorption of 250 mg) in five successive measurements. Equilibrium times ranged from 12 to 24 hours, depending on the conditions. The pump was stopped momentarily to record the equilibrium mass of the polymer. The pressure in the system was adjusted using a pressure generator (HIP model 87-6-5).

The weight gain of the polymer sample due to sorption of CO_2 and VF2, M_{abs}, was calculated according to:

$$M_{abs} = \Delta m + (V_S + V_{PVDF})\rho^f \tag{5.1}$$

$$V_{PVDF} = \Delta S \times V_o \tag{5.2}$$

where Δm is the measured change in mass of the sample from the initial weight under vacuum, V_s is the volume of the sample basket and suspension coupling, V_o is the volume of the polymer sample in the absence of CO_2 and VF2, ΔS is the degree of swelling of the polymer sample at the system conditions, and ρ^f is the density of the fluid at the system conditions. The density of the fluid was calculated based on the measured mass of a titanium sinker of calibrated volume at the system conditions. The degree of swelling was assumed to be negligible based on the swelling results in Chapter 4. Therefore ΔS was set equal to one.

5.1.2.2 Results and Discussion

The sorption of mixtures of VF2 and CO_2 into PVDF was measured at 60 and 75 °C. Comparisons between the sorption of pure CO_2 and mixtures of VF2 and CO_2 at 60 °C and 75 °C are shown in Figures 5.8 and 5.9, respectively. At the lowest pressures, the total amount of sorption was similar for the mixture and for the pure CO_2. In fact, at both temperatures the sorption from the mixture was less than from pure CO_2, at pressures below about 100 bar. At higher pressures, the total sorption was higher for the VF2/CO_2 mixtures, at both temperatures. The presence of the monomer increased the density of the fluid to improve the interaction between the polymer and the fluid and increased the sorption. The total sorption was also greater at the lower temperature, which corresponds with an increased density of the fluid.

A slight increase in sorption with monomer concentration was observed (Figure 5.9). However, the values were within the experimental error of the measurement (± 5 mg/ g PVDF).

In the next section, the Sanchez-Lacombe model is fit to the data and the effect of pressure and concentration is further explored with the model.

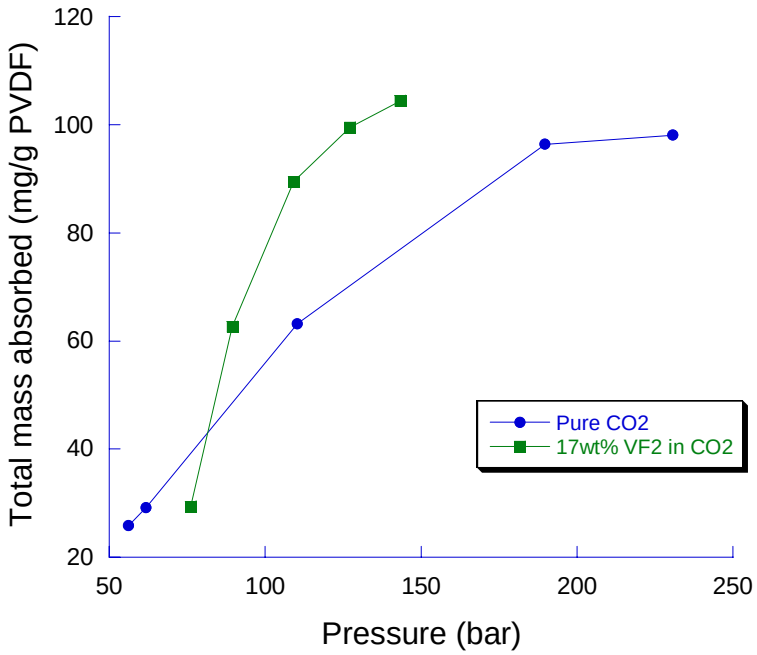

Figure 5.8 Sorption of CO_2 and a mixture of CO_2 and VF2 into PVDF at 60 °C as a function of pressure and the composition of VF2 in the system

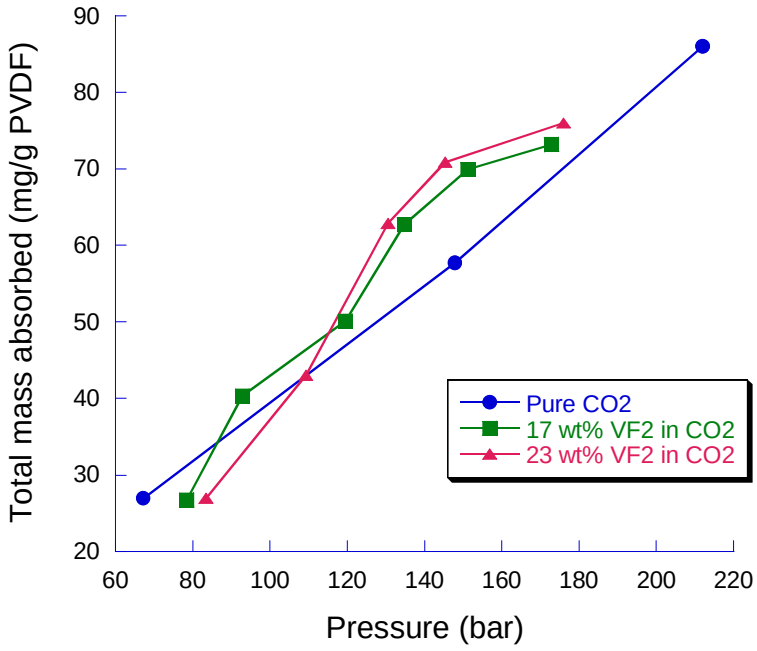

Figure 5.9 Sorption of CO_2 and a mixture of CO_2 and VF2 into PVDF at 75 °C as a function of pressure and the composition of VF2 in the system

5.2 Thermodynamic Modeling with Sanchez-Lacombe EOS

The Sanchez-Lacombe (S-L) equation of state was used to describe the phase equilibria for a three-component system of VF2, CO_2, and PVDF. This required extension of the model equations presented in Chapter 3. The chemical potential equation for component 1 in the three-component mixture is

$$\frac{\mu_1^{II}}{kT} = \ln\phi_1 + (1-\frac{r_1}{r}) + \frac{\tilde{\rho} r_1 \chi}{RT} + \left[-\frac{\tilde{\rho}}{\tilde{T}_1} + \frac{\tilde{P}_1}{\tilde{T}_1 \tilde{\rho}} + \frac{(1-\tilde{\rho})\ln(1-\tilde{\rho})}{\tilde{\rho}} + \frac{\ln\tilde{\rho}}{r_1} \right] r_1 \qquad (5.3)$$

where

$$\chi = \sum \phi_j \chi_{ij} - \sum \phi_j \phi_k \chi_{jk} = \phi_2\chi_{12} + \phi_3\chi_{13} - \left(\phi_1\phi_2\chi_{12} + \phi_1\phi_3\chi_{13} + \phi_2\phi_3\chi_{23}\right) \qquad (5.4)$$

and

$$\chi_{ij} = \varepsilon_i^* + \varepsilon_j^* - \varepsilon_{ij}^* \qquad (5.5)$$

$$\varepsilon_{ij}^* = \zeta_{ij}\sqrt{\varepsilon_i^* \varepsilon_j^*} \qquad (5.6)$$

For a two-component system, Equation 5.3 simplifies to Equation 3.31. The amount of polymer in the CO_2-rich, fluid phase was assumed to be negligible so that only chemical potential equations (Equation 3.29) for CO_2 and VF2 needed to be solved. The model allowed the polymer phase composition at equilibrium to be calculated, given either the equilibrium composition of the fluid phase or the initial amounts of the three components. If the initial amounts were specified, then mass balances for VF2 and CO_2 were required in addition to the chemical potential equations (Equation 3.29). The mass balance on component *i*, where *i* is either VF2 or CO_2, is given by

$$(1-\psi)\omega_i^{II} + \psi\omega_i^{I} - \omega_i^{feed} = 0 \qquad (5.7)$$

where ω_i is the weight fraction and ψ is the weight fraction of the initial feed that remains in the fluid phase at equilibrium. The superscripts represent the polymer phase (II), fluid phase (I), and the feed. Analysis with the three-component model provided a better understanding of the phase equilibrium, as will be discussed in the following discussions.

5.2.1 Estimation of Model Parameters

Characteristic parameters for VF2 were determined by fitting data obtained from the ISCO SF solver to the Sanchez-Lacombe model using a non-linear least squares fit. The characteristic parameters are summarized in Table 5.1. The characteristic parameters for CO_2 and PVDF were taken from parameter set 3 in Table 4.3 and Table 4.4, respectively.

Table 5.1
Sanchez-Lacombe EOS characteristic parameters for vinylidene fluoride

P* (bar)	T* (K)	ρ* (g/mL)	r
1234	431	1.02058	2.16

The binary interaction parameters for VF2-CO_2 and CO_2-PVDF were determined from measurements of the fluid density and the polymer sorption, respectively. Table 5.2 summarizes the binary interaction parameters for CO_2-PVDF determined in Section 4.2.2 based on data for the sorption of carbon dioxide into PVDF at various temperatures.

Table 5.2
Binary interaction parameters for CO_2-PVDF, ζ_{23}

Temperature (°C)	ζ_{23}
42	1.009
60	1.014
75	1.017*
80	1.018

* determined from interpolation of the temperature effect on ζ_{23}

The binary interaction parameters for VF2-CO_2 were determined from measures of the fluid density of mixtures of VF2 and CO_2. The magnetic suspension balance was used to measure the density of a mixture of 10.3 wt% VF2 in CO_2 over a range of temperatures and pressures. The results are shown in Figure 5.10. The Sanchez-Lacombe model was fit to the data to determine the interaction parameter at each temperature (Table 5.3).

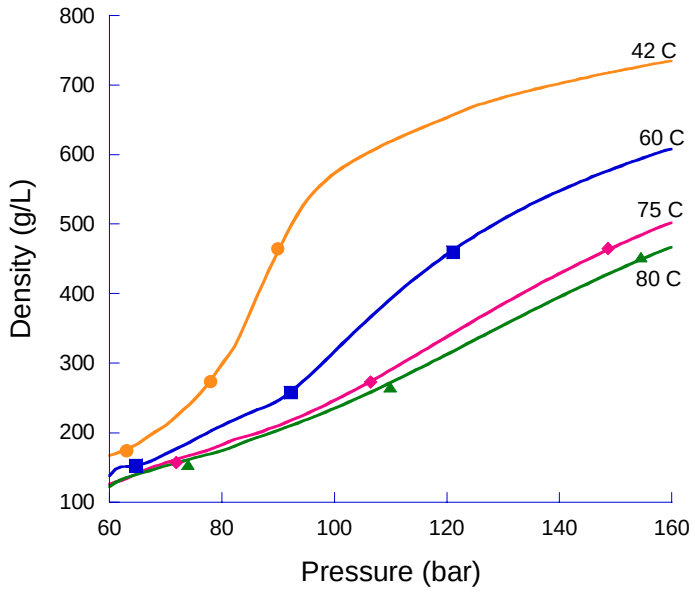

Figure 5.10 Density of a 10.3 wt% VF2 in CO_2 mixture, as measured with a magnetic suspension balance. Lines represent model prediction using the Sanchez-Lacombe equation of state

Table 5.3
Binary interaction parameters for VF2-CO_2*, ζ_{12}

Temperature (°C)	ζ_{12}
42	1.081
60	1.040
75	1.009
80	0.988

* 10.3 wt% VF2 in CO_2

The effect of the monomer concentration on the interaction parameter was studied at 42 °C. The interaction parameter determined for the 10.3 wt% VF2 mixture (1.081) was used to model the density of a mixture of 19.9 wt% VF2. The result is shown in Figure 5.11 (black line). Despite the good correlation of the model with the data at the lower monomer concentration (Figure 5.10), the same interaction parameter did not provide as good a fit at the higher monomer concentration. Therefore, the interaction parameter that minimized the sum of squared errors (SSE) between the model and the higher monomer concentration data, 1.063, was determined. This is represented by the blue line in Figure 5.11. The model fit was not greatly improved over the results using the original interaction parameter. For subsequent calculations, the effect of the concentration on the interaction parameter was neglected. This assumption introduced some error into the model's quantitative results.

The interaction parameters summarized in Tables 5.2 and 5.3 were used in the three-component model and the binary interaction parameter for VF2-PVDF was determined from a fit of the model to the current three-component sorption data.

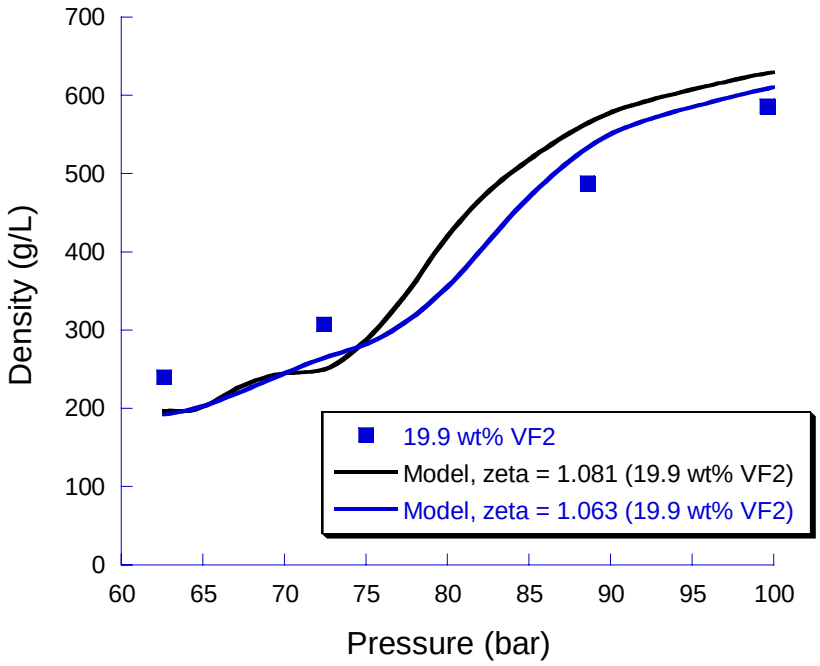

Figure 5.11 Density of mixtures of VF2 in CO_2 at 42 °C, as measured with a magnetic suspension balance. Lines represent model prediction using the Sanchez-Lacombe equation of state

5.2.2 Correlation of Model with Partitioning Data

The Sanchez-Lacombe equation of state was used to predict the sorption of a mixture of 17 wt% VF2 in CO_2 into PVDF at 60 and 75 °C. The initial composition of the mixture was specified in the model. The model results and the experimental data from this work are shown in Figures 5.12 and 5.13. The interaction parameters for VF2-CO_2 and CO_2-PVDF reported in the previous section were used in the model. The interaction parameter for VF2-PVDF, ζ_{13}, was used as a fitting parameter to minimize the SSE between the model and the data. The values of ζ_{13} that minimized the SSE were 0.94 and 0.85 at 60 and 75 °C, respectively. The model agreed qualitatively with the data, although it overpredicted the sorption at low

pressures and underpredicted the sorption at higher pressures. However, the sorption was of the same order in the model and the data. The interaction parameters determined based on the experimental data provide a basis for describing the qualitative nature of the phase equilibria.

Using the interaction parameters determined for VF2-CO_2-PVDF at 60 and 75 °C, additional system properties were calculated. Figures 5.14 and 5.15 show the calculated relative amounts of VF2 and CO_2 sorbed into the polymer. At low pressures, approximately equal amounts of VF2 and CO_2 are predicted to sorb into the polymer, at both temperatures, and the amount sorbed increases with pressure. At higher pressures, the equilibrium CO_2 sorption is greater than the VF2 sorption, and the amount of either component sorbed does not increase very much with increasing pressure. Additionally, the difference in the sorption of monomer versus CO_2 in the polymer phase at higher pressures is magnified at the higher temperature.

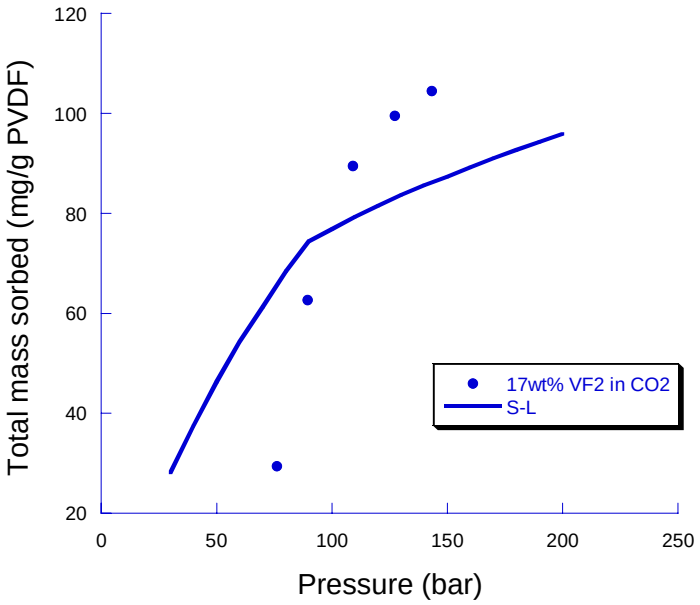

Figure 5.12 Experimental data and model prediction for the sorption of CO_2 and VF2 into PVDF at 60 °C as a function of pressure. System consists of 14.3g VF2, 70.1g CO_2, and 3.8g PVDF. Line represents fit using Sanchez-Lacombe equation of state. ζ_{12} = 1.040, ζ_{13} = 0.94, ζ_{23} =1.014

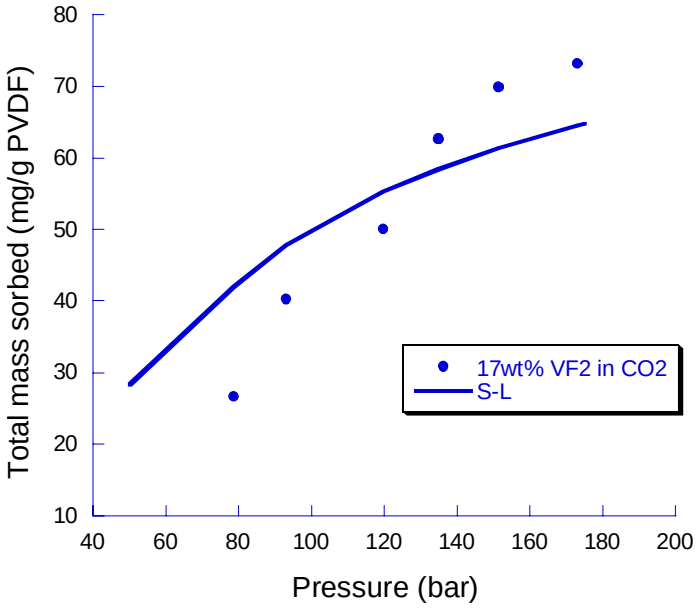

Figure 5.13 Experimental data and model prediction for the sorption of CO_2 and VF2 into PVDF at 75 °C as a function of pressure. System consists of 14.4g VF2, 69.9g CO_2, and 3.3g PVDF. Line represents fit using Sanchez-Lacombe equation of state. ζ_{12} = 1.009, ζ_{13} = 0.85, ζ_{23} =1.017

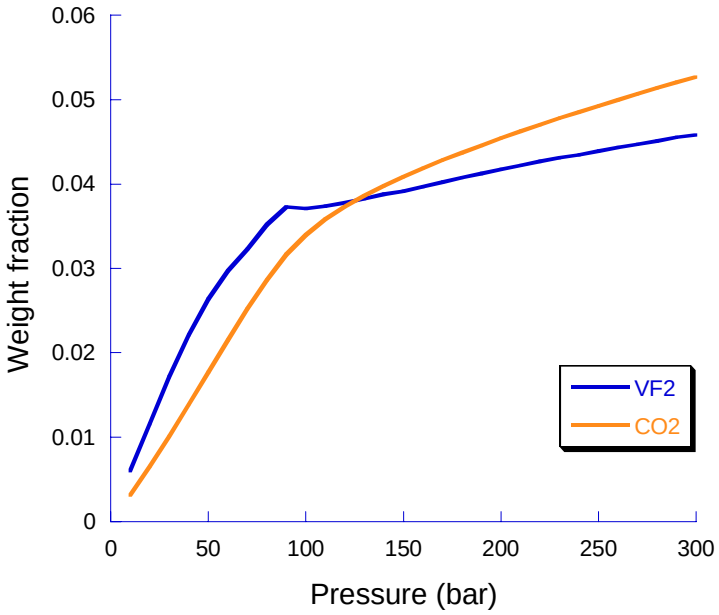

Figure 5.14 Sanchez-Lacombe model prediction of weight fractions of VF2 and CO_2 in PVDF at 60 °C as a function of pressure. System consists of 16.21 wt% VF2, 79.49 wt% CO_2, and 4.3 wt% PVDF. ζ_{12} = 1.009, ζ_{13} = 0.85, ζ_{23} =1.017

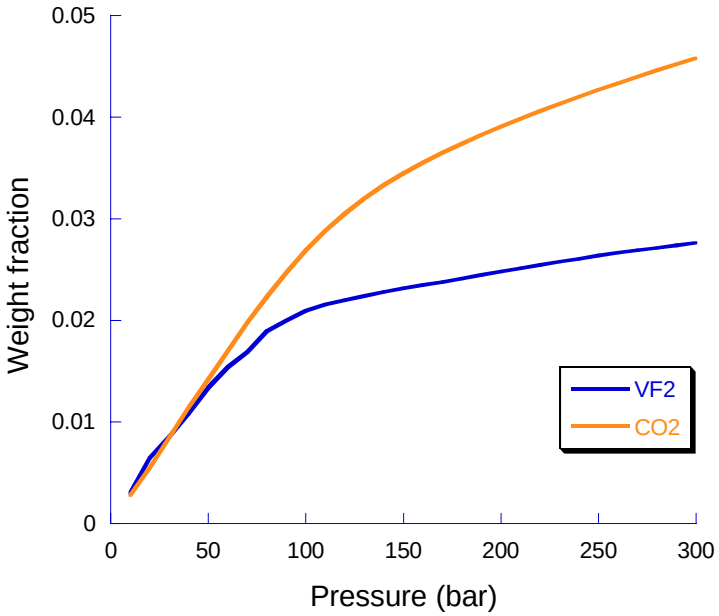

Figure 5.15 Sanchez-Lacombe model prediction of weight fractions of VF2 and CO_2 in PVDF at 75°C as a function of pressure. System consists of 16.44 wt% VF2, 79.81 wt% CO_2, and 3.75 wt% PVDF. ζ_{12} = 1.009, ζ_{13} = 0.85, ζ_{23} =1.017

The effect of the monomer concentration on the sorption of CO_2 in the polymer phase at 75 °C is illustrated in Figure 5.16. As the amount of VF2 in the system increases, the sorption of CO_2 into the polymer phase decreases. The increasing concentration of monomer in the system reduces the chemical potential of CO_2 and its ability to sorb into the polymer phase, and vice versa.

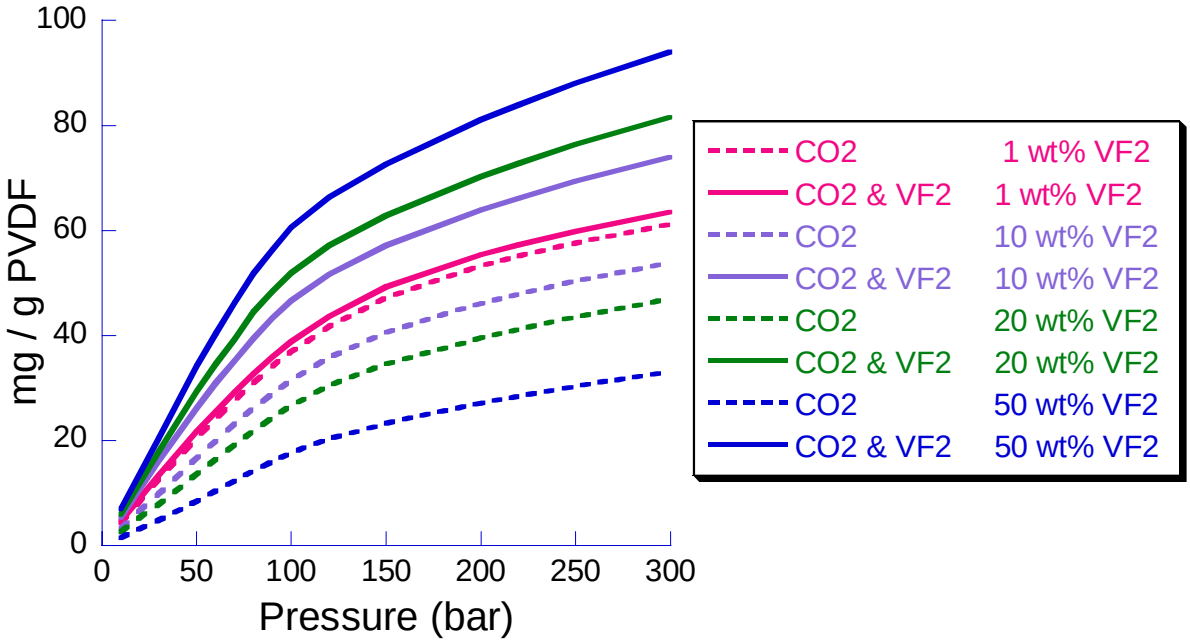

Figure 5.16 Sanchez-Lacombe model prediction of the CO_2 sorption and overall sorption of VF2 and CO_2 into PVDF at 75 °C as a function of pressure and initial weight fraction of VF2 in the system. ζ_{12} = 1.009, ζ_{13} = 0.85, ζ_{23} =1.017

Finally, the partition coefficient for VF2 between the CO_2-rich, fluid phase and the polymer phase was calculated using the model. The qualitative trend in the data with pressure was consistent with the results reported in the fluid-based partition coefficient measurements in Section 5.1.1.2. As shown in Figure 5.17, the partition coefficient was found to decrease with an increase in the pressure and approach a

constant value at higher pressures. As illustrated in Figures 5.14 and 5.15, the amount of VF2 in the polymer increased at a slower rate than the amount of CO_2 in the polymer as the pressure increased. The result is that the partition coefficient decreased with increasing pressure because of the slower rate of increase of VF2 in the polymer phase.

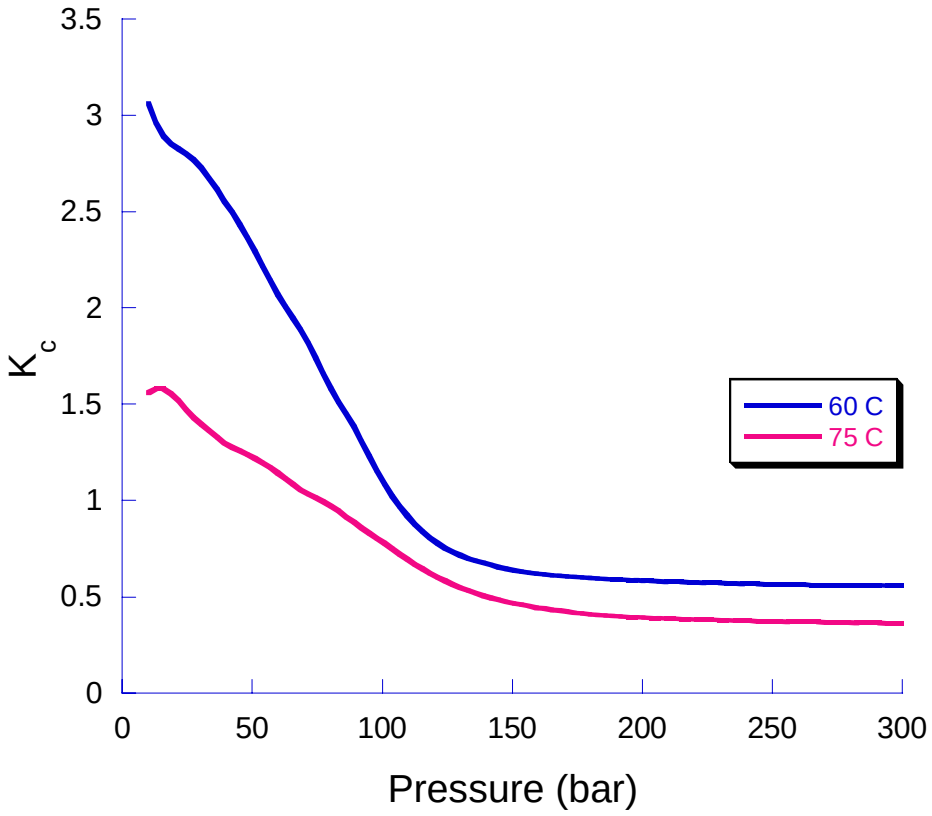

Figure 5.17 Sanchez-Lacombe model prediction of the partition coefficient for VF2 between PVDF and CO_2 phases as a function of temperature and pressure. System consists of 16 wt% VF2, 80 wt% CO_2, and 4 wt% PVDF. The temperature dependent interaction parameters reported in Figures 5.11 and 5.12 were used in the model prediction. Model results are tabulated in Section C.2.2

5.3 Effect of Partitioning on Heterogeneous Polymerizations

The results of the phase equilibria experiments and modeling provide a means in which to explain some of the unique properties of PVDF produced by synthesis in CO_2. Saraf and coworkers [3-5] studied the impact of the polymerization conditions in CO_2 on the molecular weight distribution of the polymer. They found that at monomer concentrations above ~ 1.9 M, the polymer exhibited an increasingly bimodal molecular weight distribution. As shown in Figure 5.16, as the monomer concentration increased, the amount of VF2 in the polymer phase increased. Additionally, the relative amount of VF2 to CO_2 increased in the polymer phase. A monomer feed concentration of 1.9 M in the polymerization would correspond to ~17 wt% VF2 in the system. Figure 5.16 shows that, at low values of the wt% VF2, mostly CO_2 sorbs into the polymer. As the amount of monomer in the fluid increases, the sorption of CO_2 diminishes until the sorption of VF2 in the polymer phase dominates. Around 20 wt% VF2, the sorption of VF2 into the polymer phase begins to dominate over the sorption of CO_2 in the polymer phase. Thus, at conditions in which a bimodal molecular weight distribution was produced, significant amounts of VF2 and CO_2 were sorbed in the polymer phase.

The three-component results indicate that the presence of VF2 enhances the total sorption in the polymer phase. A similar effect may be true for the swelling of the polymer in the presence of VF2 and CO_2. As discussed in Chapter 4, the swelling of highly crystalline PVDF in the presence of CO_2 was very small (less than 1%). However, in the presence of CO_2 and VF2 at high concentrations, the polymer plasticization may be increased to enhance diffusion of the sorbed monomer to the

radical chain ends. The polymerization then proceeds to very high molecular weights within the polymer particles. In fact, it was possible to model the polymerization kinetics to assume a certain distribution of polymer chains propagate in the polymer particles to create the observed bimodal molecular weight distribution [6].

5.4 Conclusions

The partitioning of vinylidene fluoride monomer between PVDF and a CO_2-rich, fluid phase was measured by two different techniques. One technique was based on measurements of the fluid phase composition (fluid-based) with a gas chromatograph. The other technique was based on measurements of the polymer mass (polymer-based) with a magnetic suspension balance. The fluid-based technique was used to establish a qualitative measure of the effect of temperature and pressure on the partition coefficient. It was found that the partition coefficient decreased with an increase in pressure and a decrease in temperature.

The sorption of carbon dioxide and vinylidene fluoride into poly(vinylidene fluoride) was measured at 75 °C and different monomer concentrations using a magnetic suspension balance. The overall sorption into the polymer increased with the concentration of monomer in the system. The results were modeled using the Sanchez-Lacombe equation of state. The model results were in good agreement with the data. The model agreed qualitatively with the fluid-based measurements of the partition coefficient. The model was used to calculate the relative amounts of VF2 and CO_2 that sorbed into the polymer phase. Based on the model, the amount

of CO_2 sorption was greater than the amount of VF2 sorption. However, the model predicted that as the amount of monomer in the system increased the sorption of CO_2 in the polymer would decrease. Finally, the results of this research suggest that the bimodal molecular weight distribution of PVDF synthesized in CO_2 could be due, in part, to the sorption of VF2 into the polymer phase and the plasticization of the polymer to facilitate propagation of the polymer chains to high molecular weights within the polymer particles.

5.5 References

1. Handa, Y.P., Zhang, Z., and Wong, B., *Solubility, diffusivity, and retrograde vitrification in PMMA-CO_2, and development of sub-micron cellular structures.* Cellular Polymers, 2001. **20**(1): p. 1-16.

2. Sato, Y., Takikawa, T., Takishima, S., and Masuoka, H., *Solubilities and diffusion coefficients of carbon dioxide in poly(vinyl acetate) and polystyrene.* Journal of Supercritical Fluids, 2001. **19**(2): p. 187-198.

3. Saraf, M.K., Wojcinski, L.M., Kennedy, K.A., Gerard, S., Charpentier, P.A., DeSimone, J.M., and Roberts, G.W., *Continuous precipitation polymerization of vinylidene fluoride in supercritical carbon dioxide: Molecular weight distribution.* Macromolecular Symposia, 2002. **182**(1): p. 119-129.

4. Saraf, M.K., *Polymerization of vinylidene fluoride in supercritical carbon dioxide: Molecular weight distribution*. Masters Thesis, Department of Chemical Engineering, North Carolina State University, 2001.

5. Saraf, M.K., Gerard, S., Wojcinski.II, L.M., Charpentier, P.A., DeSimone, J.M., and Roberts, G.W., *Continuous precipitation polymerization of vinylidene fluoride in supercritical carbon dioxide: formation of polymers with bimodal molecular weight distributions.* Macromolecules, 2002. **35**(21): p. 7976-7985.

6. Saraf, M.K., Personal communication, 2002.

Chapter 6

Conclusions

6.1 Conclusions

The research in this dissertation has focused on characterizing the phase equilibria associated with polymerizing vinylidene fluoride (VF2) in supercritical carbon dioxide. Poly(vinylidene fluoride) is the second largest produced fluoropolymer after poly(tetrafluoroethylene). Its current form of production uses surfactants that are potentially hazardous to the environment and generates large amounts of wastewater. The precipitation polymerization of VF2 in CO_2 has generated properties similar to the polymer that is produced commercially. However, the polymer produced in $scCO_2$ exhibits a bimodal molecular weight distribution that is not characteristic of conventional polymerization techniques. This bimodality may be due, in part, to the phase equilibria in the system. Techniques have been developed in this work for measuring the sorption and swelling of polymers in the presence of supercritical fluids. Models based on the Sanchez-Lacombe equation of state have also been developed for describing the phase equilibria.

The sorption and swelling of poly(vinylidene fluoride) (PVDF) in the presence of CO_2 was measured. The polymer did not significantly swell in CO_2, probably due largely to the highly crystalline nature of the polymer. However, the polymer sorbed up to 10 wt % CO_2 at the conditions of the experiments. The sorption of mixtures of

VF2 monomer and CO_2 into the polymer also was investigated. As the concentration of monomer increased, the overall sorption increased. The partitioning of VF2 between the polymer and supercritical fluid phases was measured as a function of temperature and pressure. The Sanchez-Lacombe model provided a reasonable fit to the data and established binary interaction parameters for the system. Based on the model results, as the monomer concentration in the fluid phase increased, the sorption of monomer was found to increase, while the sorption of CO_2 decreased. Also, the sorption of VF2 and CO_2 increased with the pressure.

There were three main questions which this dissertation attempted to address: 1) What effect do the polymerization conditions have on the phase equilibria in CO_2, 2) Can these phase equilibria be predicted using equation of state models, and 3) What are the implications of these phase equilibria on the locus of polymerization, polymerization kinetics, and polymer properties in heterogeneous polymerizations in $scCO_2$. The effect of temperature, pressure, and monomer concentration on the sorption of monomer and CO_2 into the polymer phase were measured. The Sanchez-Lacombe model worked well for describing the phase equilibria of VF2-CO_2-PVDF. Based on the phase equilibria experiments and modeling, it was concluded that the bimodal character of the PVDF synthesized in CO_2 might be due, in part, due to the partitioning of the monomer in the polymer phase and plasticization of the polymer which permitted the polymerization to proceed to higher molecular weights in the polymer particles.

The techniques developed in this work for measuring the phase equilibria of polymer-supercritical fluid systems have application beyond the system studied in this work. The sorption and swelling of the polymer in the presence of supercritical fluids has importance for heterogeneous polymerizations, such as solid state, precipitation, and dispersion polymerizations, design of membranes for separation of supercritical fluids, polymer processing to modify the polymer properties with supercritical fluids, and polymer purification processes, just to name a few. Additionally, development of a model for describing the phase equilibria may be useful for identifying optimal conditions for operation of these polymer-supercritical fluid systems.

6.2 Recommendations

The magnetic suspension balance described in this work is a powerful technique for measuring mass sorption and diffusion coefficients into solid samples. Several recommendations are made for expanding the utility of this technique for phase equilibria measurements. Two-component measurements with the balance were very quantitative. The system can be easily adapted to a variety of polymer-CO_2 systems. However, there was uncertainty in the quantitative measure of the partitioning of monomer between the polymer-rich and CO_2-rich phases in the three-component experiments. The fluid-phase based measurements of the partition coefficients provided only qualitative measures of the partitioning. The polymer-phase based measurements with the magnetic suspension balance provided a quantitative measure of the total sorption in the polymer phase, but could not directly

quantify the relative amounts of VF2 and CO_2 in the polymer phase. The major limitation was maintaining a uniform temperature throughout the circulation loop. The magnetic suspension balance is very sensitive to the presence of magnetic materials close to the instrument and heating materials that were non-magnetic were not readily available. A water bath would provide a better means for heating the entire circulation loop, including the jacketed portion of the magnetic suspension balance. This would require a major re-configuration of the balance, but would improve the temperature control to make it possible to perform a mass balance on the system and solve for the relative amounts of VF2 and CO_2 that partition into the polymer phase. Also, diffusion coefficients for the monomer and CO_2 from the fluid mixture into the polymer phase may be quantified. Finally, the system could be equipped with a "non-invasive" analytical technique, such as FTIR, to use as a secondary measure of the monomer concentration in the fluid phase. This is an improvement over the gas chromatographic technique in which samples were taken from the fluid phase for analysis.

Studies of the phase equilibria associated with copolymerizations in CO_2 would be very valuable, and could be carried out using the techniques and models developed in this work. The preferential sorption of one of the monomers in the polymer phase could effectively change the reactivity ratios at the reaction site and impact the polymer properties produced. It was demonstrated in this work that changing the temperature, pressure, or monomer concentration could effectively tune the phase equilibria and thus, may have an impact on tuning the properties of

the copolymer synthesized in CO_2. The phase equilibria model could be used to identify conditions at which to optimize the partitioning effect in the reaction. One such copolymer that would be interesting to study is that of vinylidene fluoride and hexafluoropropylene. This industrially important copolymer could be readily studied, given that the interaction of VF2 with CO_2 and its polymer has already been established in this work.

Appendix A

Experimental details

This section details the experimental procedures for the apparatuses used in this dissertation in enough detail to operate the equipment. Additionally, all data are summarized in this section.

A.1 Rubotherm Magnetic Suspension Balance (ISOSORP)

A schematic of the experimental setup for the ISOSORP is shown in Figure A.1. The major components include the ISOSORP balance in which the polymer sample is weighed during the experiment, a cylinder of calibrated volume located within a temperature controlled oven, an HPLC valve to take samples for analysis in a gas chromatograph, a circulating pump to circulate the fluid pass the polymer sample, and a pressure generator to adjust the volume and pressure of the system. A heating jacket surrounding the balance controls temperature within the balance. Temperature in the oven is controlled by a microprocessor. Rope heaters wrapped around the tubing control temperature in the lines between the oven and balance. The volumes between the valves are summarized in Table A.1.

The magnetic suspension and weight measurement may be controlled with the MessPro software or can be operated from the control unit similar to what is shown in Figure A.2. The suspension control unit consists of a main power switch, a dial to control the suspension coupling, and another dial on the rear of the unit to check the voltages in the system. The dial on the front of the unit can be set to “off”,

zero point (ZP), measuring point 1 (MP1), or measuring point 2 (MP2). In zero point, the polymer sample is resting on a landing such that the balance only measures the weight of the suspension coupling. In measuring point 1, the balance lifts the basket containing the polymer sample. In measuring point 2, the balance lifts the sample basket and a titanium sinker.

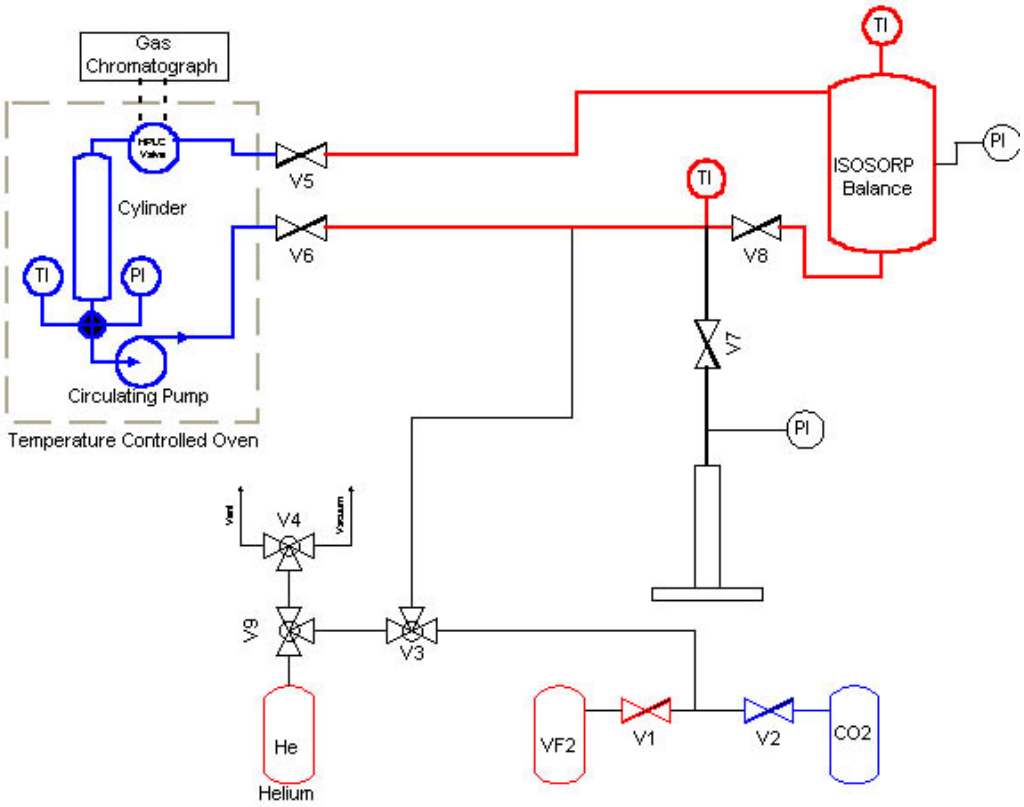

Figure A.1 Schematic of Phase Equilibrium Apparatus

Table A.1
Volume of tubing in phase equilibrium apparatus

Section	Volume (mL)
Between V5 & V6, inside oven (does not include HPLC valve)	30.1
Between V5 & V8, including measuring cell	97.3
Between V6 & V8, V3 & V7 closed	1.4
Between V7 and zero volume of pressure generator	12.4
Pressure generator	60

Figure A.2 Illustration of suspension control and balance indicator units

A.1.1 Operating Procedure

When the suspension coupling is already aligned and deposit screws are in place, the following procedure may be followed for conducting sorption experiments.

1) The polymer sample is added to the sample basket. If the mesh basket is used, extra non-magnetic weight, such as several stainless steel discs, are needed to have the required weight. Typically, one gram of sample is sufficient in the solid metal basket and three grams of sample are sufficient in the mesh basket with five stainless steel discs. The weight in the basket is sufficient if the balance indicator is stable at the zero point and measuring point 1.
2) Insert an o-ring and then seal the measuring cell by securing the bolts on the flange in a star pattern to 90 ft-lb torque. The star pattern requires tightening of the bolts in the following order: 1,4,2,5,3,6, and repeat. Viton o-rings will

only seal a CO_2 atmosphere for ~3 days before total failure. EPR o-rings are limited to CO_2 pressures less than 1500 psi (gas phase). However, CO_2 will extracts oils from EPR, which may contaminate the polymer sample. Buna-N o-rings will hold pressure for at least 7 days. The polymeric o-rings can only be used once before discarding.

3) Feed ultra high-pressure helium to the measuring cell to leak test the system. Verify that the bolts do not protrude outside the diameter of the measuring cell. This is so that the heating jacket will slide on with ease.
4) Disconnect helium connection and install heating jacket around measuring cell.
5) Connect gas delivery system to measuring cell.
6) Activate heating in jacket and turn on vacuum pump.
7) After system has reached temperature equilibrium and has had sufficient time under vacuum, software may be initiated (turn off the vacuum pump). The "interval time" is the time between measuring points. The "settle time" is the time that a sample is allowed to settle in each state of the suspension coupling before the value is recorded.
8) For single component sorption experiments, gas is fed to the measuring cell and the system is allowed to reach equilibrium before adding additional gas and allowing the system to equilibrate again. Equilibrium is reached when MP1 does not change within $\pm$ 0.1 mg in five successive measurements.

9) For two component sorption experiments, the first gas (in this work, VF2) is fed into the section between valves V5 and V6 inside the oven to a given temperature and pressure. The mass is determined based on the density and the known volume between valves V5 and V6. The second gas (in this work, CO_2) is added between valves V6 and V8 using the pressure generator to add a sufficient mass of CO_2. Valves V6, V5 and V8, in that order, are opened to allow the fluid mixture to flow into the ISOSORP. The circulation pump is started. Once the system reaches equilibrium, the pump is stopped momentarily to record the mass. The pressure is adjusted using the pressure generator.

For cases where the temperature is uniform throughout the circulation loop, it is possible to perform a mass balance on the system and experimentally determine the masses of VF2, M_{VF2}, and CO_2, M_{CO_2}, that partition into the polymer phase.

$$M_{abs} = M_{CO_2} + M_{VF2} \tag{A.1}$$

$$M_i^{feed} = M_i + M_i^f \quad for\ i=CO_2, VF2 \tag{A.2}$$

where M_i^{feed} is the starting mass of each species in the system and M_i^f is the mass of each species in the fluid phase at equilibrium. Given the density of the mixture at the temperature and pressure of the system, the composition of the fluid phase is determined from the Sanchez-Lacombe equation of state. The masses of VF2 and CO_2 in the fluid phase are then

$$M_i^f = \rho^f V^f x_i \text{ for } i=CO_2, VF2 \quad \text{(A.3)}$$

where x_i is the weight fraction of the component.

A.1.1.1 Initialization of Suspension Coupling

The following steps are necessary when the suspension magnet is not inserted in the balance or if the system becomes unstable and the coupling needs to be reinitialized. Before beginning, the balance indicator should be turned off or indicate "L".

1) Check bubble level on rear of Sartorius balance and adjust legs on balance accordingly.
2) Verify indication of temperature, pressure, and balance weight. If the balance indicator is not already on, it can only be turned on when suspension control is in "zero point" position (Step 6). Once the balance indicator is turned on, the balance needs 24 hours to warm up before taking sorption measurements.
3) Turn on main power switch with the suspension control switch in the "off" position. Check the voltages with the signal selection switch on rear of display rack according to Table A.2. If U_a indicates –1.4 V, then sensor electronics are no longer operational and should be replaced. If U_r indicates a value around 13.7 V, turn the power off momentarily to reinitialize the system. After voltages are checked, the switch should be turned back to U_a.

Table A.2*
Voltages for magnetic suspension balance

Signal	Correct Value of Voltage
+ 15V	+15V ± 0.5V
- 15V	- 15V ± 0.5V
U_s	~ 0.0 V
U_a	~ 8.8 V
U_{ag}	ca. 0 V
U_r	~ - 0.3 V
U_m	0 V
U_{KSH}	0 V
U_{KSR}	0 V

*Adapted from page 11 of manual

4) Insert the suspension magnet and screw the deposit screw until you find the minimum voltage of U_a (~5.0 V). Then screw it in further until U_a is ~0.5 V greater than the minimum voltage.
5) Turn off the main power switch momentarily, and then switch suspension to "zero point".
6) Turn on the balance indicator if it is not already turned on.
7) Attach the titanium sinker to the hook.
    - If light indicating zero point goes out after adding weight, U_R may be ~13.7V (instead of ~ -0.3 V). If so, momentarily turn off main power switch to reinitialize.
8) Tare the balance indicator.
9) Switch between "zero point" and "measuring point 1" three or four times so the sensor gets aligned initially. Verify visually that the measuring load is properly raised.

10) Switch to “measuring point 1” (MP1). The weight should be indicated on the balance indicator. (The weight of the titanium sinker is ~22g) The balance indicator should settle after a few moments. If it does not, check troubleshooting actions.
11) Switch back to “zero point” (ZP).
12) Screw the adapter into the coupling housing until it is fixed at the bottom of the housing.
13) If the second deposit screw is not already in the adapter, install the deposit screw and verify that the titanium sinker remains on the deposit screw when in “measuring point 1” and is lifted when in “measuring point 2”. A weight should be added to the hook before changing from ZP to MP1 and MP2. The weight should be non-magnetic. The solid metal basket has sufficient weight for this use.
14) Verify that the zero point and measuring point are stable (check troubleshooting actions).
15) The system is now ready for conducting sorption experiments (Section A.1.1).

A.1.1.2 Troubleshooting

- Upper deposit screw is TOO HIGH if
    - Balance indicates “L” after attempting to measure weight.
    - Zero point and/or measuring is not stable after 30 seconds.

    - Balance attempts to raise measuring load in MP1, but after a short time lowers it onto the deposit screw. Balance then indicates a zero-point value.
- Upper deposit screw is TOO LOW if
    - Suspension magnet overloads and balance indicates “H” or unreasonably high value such as “88.77g”.
- If the balance indicates load is too high, set knob to “zero point”. Slightly tug on sample basket or hook and watch if the balance resets itself. If not, momentarily cut off the power switch, watching that basket does not fall. Tug on basket/hook again and balance should reset itself.
- If system is sealed and balance indicates load is too high, by “H” or 79.999g, turn off main power and suspension control. Switch cables for ground “_|_” and Um. Turn back on main power. Balance should now indicate “L”. Momentarily turn on suspension control to “zero point”. Turn off main power and switch cables back. *This fix should not be done regularly; otherwise integrity of balance will be compromised.*
- If balance indicates “L”, set knob to “zero point” and momentarily turn off main power switch.

A.1.2 Error Analysis

Rubotherm reports the precision of the ISOSORP to be 0.01 mg. The balance displayed the mass at this precision. However, the accuracy of the measurements at equilibrium was 0.1 mg. The accuracy of the temperature probe

was not reported. Using a temperature-controlled oil bath, it was possible to control the temperature in the measuring cell within ±0.2°C. The pressure transducer had a reproducibility of 0.1%. The pressure reading had to be adjusted for temperature. The pressure adjustment was determined from “blank” experiments in which the mass of an empty basket was monitored at a set temperature over a range of pressures. Using the titanium sinker, the density was recorded at the different pressures. The NIST database was used to determine the pressure of CO_2 that corresponded with the measured density and pressure of the system. A plot of the pressure given by the transducer and that determined from the NIST database was plotted. The correlation at 80°C is shown in Figure A.3. The pressure from the density and the pressure transducer followed a perfectly linear relationship. A similar relationship was obtained at 42, 60 and 75°C. A summary of the pressure corrections based on the linear relationships is shown in Table A.3.

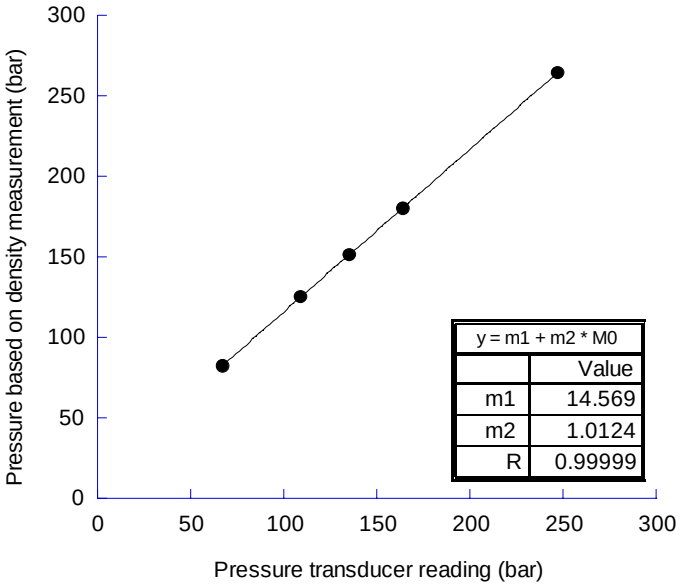

Figure A.3 Correlation between pressure from transducer and pressure given by NIST database based on density measurement with magnetic suspension balance at 80°C

Table A.3
Temperature adjusted correction for pressure transducer

Temperature (°C)	m1	m2
42	5.2188	1.0106
60	12.336	0.9785
75	13.277	1.0067
80	14.569	1.0124

Note: Actual pressure in bar = m1 + (m2)×(Pressure transducer reading in bar)

The weight gain of the polymer in the presence of CO_2 is calculated from the following equation (Equation 4.1):

$$M_{CO_2} = \Delta m + (V_S + V_{PVDF})\rho_{CO_2}$$

Calculation of the weight gain requires accurate determination of each parameter in the equation. The change in mass is reported with an accuracy of ±0.1 mg. The volume of the polymer is measured by swelling experiments in which the accuracy is of the order of 10^{-6} cm^3 (Section A.2.2). The density of the fluid phase is calculated from the weight of a titanium sinker of calibrated volume. Finally, the volume of the sample basket and suspension coupling can be accurately determined from blank experiments in the ISOSORP. Plots of MP1 and the zero point versus the density are plotted. The difference in the slopes of the lines is the volume of the suspension coupling and sample basket. The volumes of the mesh baskets and solid basket used in the experiments are reported in Table A.4.

Finally, based on the error associated with the parameters involved in the calculation of the mass, the limitations in the temperature and pressure measurement, and the repeatability of the measurements, the error in the reported mass sorption is ± 5 mg sorbed/ g polymer.

Table A.4
Volume of suspension coupling and sample basket, V_s, for different basket configurations

Basket type	Volume (cm^3)
Mesh*	1.3414
Mesh* (after 5/18/03)	1.4657
Solid metal	1.5572

*Includes five SS discs for added weight

A.1.3 Experimental Data

A.1.3.1 PVDF-CO_2

Table A.5
Sorption of CO_2 into PVDF at 42 °C

Data Set	Pressure (bar)	ρ_{CO2} (g/mL)	mg CO_2 / g PVDF
1*	30.5	0.061	19.0
	56.8	0.142	31.1
	126.1	0.727	81.8
	181.7	0.817	86.1
	222.0	0.857	92.1
	156.9	0.273	84.5
	59.1	0.152	30.0
	29.8	0.061	18.4
2*	28.3	0.056	18.1
	34.8	0.088	25.9
	56.1	0.165	36.7
3	74.2	0.228	45.0
	123.6	0.705	80.8
4	40.4	0.088	25.0
	61.3	0.16	45.9
	99.8	0.573	73.6
	148.7	0.757	93.7
	174.4	0.795	98.3

*Did not have good temperature control

Table A.6
Sorption of CO_2 into PVDF at 60 °C

Data Set	Pressure (bar)	ρ_{CO2} (g/mL)	mg CO_2 / g PVDF
1	61.8	0.134	29.2*
2	56.1	0.115	25.8*
	110.3	0.382	63.2*
	189.7	0.712	96.4*
	230.7	0.772	98.1*

*Does not account for swelling of the polymer

Table A.7
Sorption of CO_2 into PVDF at 75 °C

Data Set	Pressure (bar)	ρ_{CO2} (g/mL)	mg CO_2 / g PVDF
1	67.2	0.132	26.9
	147.9	0.454	57.7
	212.0	0.649	86.0

Table A.8
Sorption of CO_2 into PVDF at 80 °C

Data Set	Pressure (bar)	ρ_{CO2} (g/mL)	mg CO_2 / g PVDF
1*	50.5	0.086	19.2
	148.2	0.445	68.0
2*	39.2	0.068	14.3
	63.6	0.115	22.8
	86.0	0.319	30.2
3	36.8	0.058	12.7
	51.9	0.089	18.5
	61.2	0.107	22.7
	69.2	0.128	28.2
	83.2	0.165	34.3
	121.2	0.296	51.9
	153.7	0.432	68.4
	231.0	0.652	93.1
4	42.0	0.069	13.7
	63.0	0.114	19.5
	110.9	0.26	32.6
	141.2	0.387	51.7
	168.6	0.499	69.5
	190.7	0.567	81.5
	211.2	0.616	89.3
	230.7	0.654	95.5

*Did not have good temperature control

Table A.9
Sorption of CO_2 and VF2 into PVDF at 60 and 75 °C

Temperature (°C)	Data Set	VF2 feed (g)	CO_2 feed (g)	PVDF feed (g)	Pressure (bar)	Total system volume (L)	$[VF2]_{feed}$ (mol/L)	ρ_{fluid} (g/mL)	Total mass sorbed (mg / g PVDF)
60	1	14.3	70.1	3.7960	76.2	0.2012	1.1	0.243	29.3
					89.5	0.1862	1.2	0.304	62.6
					109.2	0.1661	1.3	0.420	89.5
					127.3	0.1511	1.5	0.522	99.5
					143.3	0.1412	1.6	0.586	104.4
75	1	19.8	71.8	3.1304	176.6	0.1412	2.2	0.570	44.7
	2	14.4	69.9	3.2798	78.5	0.2012	1.1	0.213	26.7
					92.9	0.1912	1.2	0.261	40.3
					119.6	0.1712	1.3	0.365	50.1
					134.8	0.1612	1.4	0.428	62.7
					151.2	0.1512	1.5	0.491	69.6
					172.9	0.1412	1.6	0.559	73.2
	3	21.3	71.0	2.5034	83.5	0.2012	1.7	0.235	26.9
					109.3	0.1812	1.8	0.331	43.0
					130.6	0.1662	2.0	0.420	62.9
					145.4	0.1562	2.1	0.478	70.9
					176.0	0.1412	2.4	0.573	76.0

A.2 LVDT Swelling Apparatus

A.2.1 Operating Procedure

The polymer sample is prepared by first melt-pressing the polymer at 220-225°C using a Carver Model C laboratory press. A square mold of 38 mm dimension was used. For these experiments, the polymer was heated in the press for 30 minutes before flowing cooling water through the press plates for one minute to quickly lower the temperature. The mold was removed from the press and allowed to air dry (at least 15 minutes). The sample used for swelling experiments was smooth without any bubbles present. Samples were cut from the mold into rectangular pieces of the approximate dimension shown in Figure A.4.

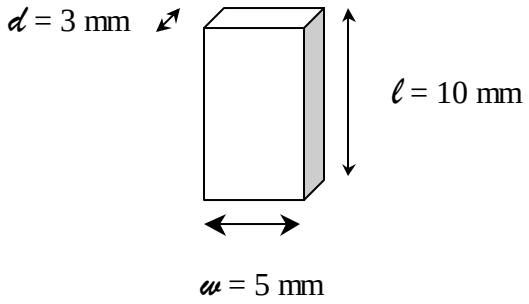

Figure A.4 Approximate dimensions of polymer samples used in swelling experiments

The swelling experiments were conducted in the laboratory of Ken Wynne at Virginia Commonwealth University. A schematic of the LVDT apparatus is shown in Figure A.5. The major components for running experiments include: an LVDT coil, a nonmagnetic steel pipe that was surrounded by the LVDT coil whose position could be adjusted along the y-axis of the pipe, a follower rod with a magnet attached on

the end that affected the voltage in the LVDT coil, a hex nut that is screwed into the bottom of the follower rod and stabilizes the weight of the follower rod on the polymer sample, an HIP microreactor (sample chamber) in which the polymer sample is located, and a heating jacket wrapped around the sample chamber. The LVDT apparatus is connected to a computer. Labview software records the temperature, pressure, and LVDT displacement. A graph illustrates the change in variables with time. The numeric display updates every 10 seconds.

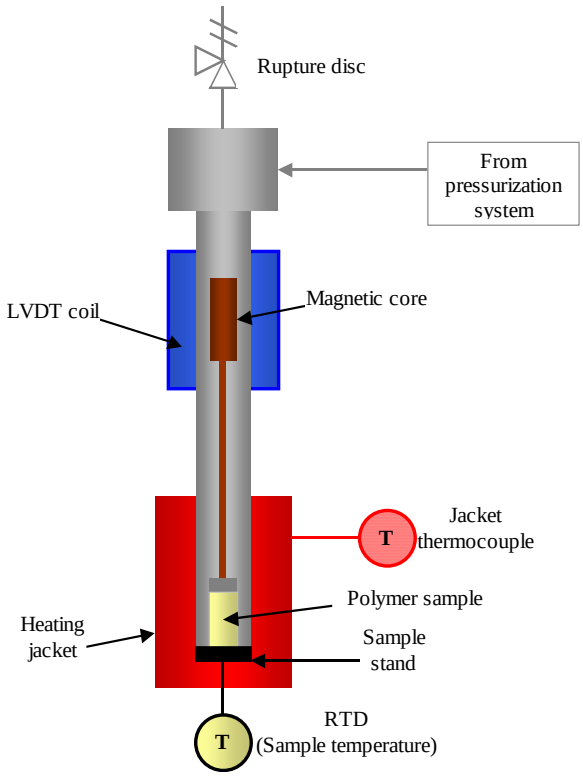

Figure A.5 LVDT Apparatus for measuring swelling of polymers in carbon dioxide

Before beginning swelling experiments, the LVDT apparatus was calibrated using a micrometer. The follower rod was placed on top of the central shaft of the micrometer. The micrometer was screwed into the bottom of the sample chamber.

The micrometer was adjusted between 0.3” and 0.0” and the corresponding displacement, in inches, was displayed in Labview. The change in displacement of the micrometer was plotted versus the displacement output given by Labview. This is plotted in Figure A.6. The slope of the line was used in subsequent swelling experiments to determine the change in dimension of the polymer samples.

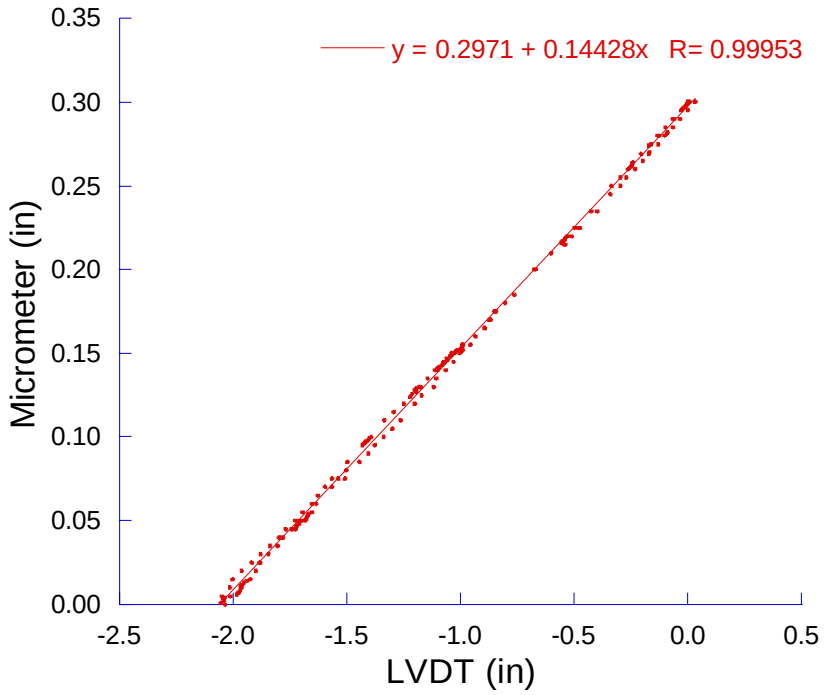

Figure A.6 Calibration curve for LVDT

The procedure for conducting swelling experiments is as follows:

1) The polymer sample dimensions and weight are recorded. The dimensions are measured at several points on the sample.

2) The polymer sample is placed on the sample stand. The follower rod and hex nut are placed on top of the sample. The sample chamber is closed to 50 ft-lb torque.
3) The sample chamber is connected to the steel pipe and tightened to 20 ft-lb torque. Care should be taken to keep the chamber upright so that the sample is not disturbed. It may be necessary to guide the follower rod into the steel pipe to maintain stability.
4) Labview is turned on and the current data file starts recording.
5) The position of the LVDT coil is adjusted until the LVDT readout is close to zero.
6) The system is pressurized with nitrogen to test for leaks and remove any air from the system.
7) The heating jacket is wrapped around the sample chamber. The Omega temperature controller is set to a given temperature before turning on the Variac. The set point on the temperature controller may be set at a temperature greater than the desired system set point because the temperature control is for the jacket only, not the system fluid.
8) The safety shield is placed in front of the apparatus.
9) The system is allowed to equilibrate at the setpoint (as recorded by Labview) before adding CO_2. The LVDT reading just before adding CO_2 is the zero point for the elongation measurement. (The system undergoes some thermal expansion with heating.)

10) The Thar pump is set to constant pressure and CO_2 is added to the apparatus.
11) Once equilibrium is reached, the pressure is increased or decreased using the Thar pump. In general, the Thar pump can control pressures in the supercritical region of CO_2 (>74 bar).
12) At the end of the experiment, heating is ceased and the pressure vented from the apparatus. The polymer sample is removed from the sample chamber and the dimensions and weight are recorded.

A.2.2 Error Analysis

The sensitivity of the LVDT apparatus was calculated based on the results of the swelling experiments. The LVDT was capable of detecting changes in dimension as small as 10 microns. The reported accuracy of the temperature probe was unknown. The pressure transducer (Omega PX-602) was rated at ± 0.4% (± 3 bar). Using the temperature controlled heating jacket, it was possible to maintain the temperature within ± 0.3°C of the system temperature set point. The Thar pump controlled the pressure within ± 1.5 bar of the set point. If a leak was present in the apparatus, the pressure would oscillate between two pressures (< 50 psi difference). The reported pressure of the swelling experiment was reported as the average of the two pressures.

Based on the sensitivity of the swelling technique and the accuracy of the temperature and pressure control, the error in the swelling experiments is 0.2% of the reported elongation.

A.2.3 Experimental Data

A.2.3.1 PVDF-CO_2

Table A.10
PVDF samples used for swelling experiments

Sample #	Description	Initial Wt (g)	Initial Length (cm)	Initial Width (cm)	Initial Thickness (cm)
1	Solef 1010	0.3734	1.270	0.848	0.32
	Melt-pressed		1.264	0.88	0.32
			1.268	0.89	0.318
			1.270	0.89	0.32
			1.268	0.896	
2	Solef 1010	0.2345	1.092	0.416	0.314
	Melt-pressed		1.140	0.412	0.32
				0.412	0.322
				0.408	0.324
				0.398	0.316
3	Solef 1010	0.0501	0.470		0.324
	Pellet				0.28
					0.288
4	CSTR #58	0.2048	1.452	0.72	0.12
			1.464	0.688	0.12
			1.436	0.638	0.12
6	Solef 1010	0.3008	1.242	0.5	0.286
	Melt-pressed		1.230	0.512	0.284
				0.5	0.286
7	Solef 1010		0.410		0.334
	Pellet				0.314
					0.314
8	Solef 1010	0.0487	0.428		0.334
	Pellet				0.304
					0.306

Table A.11
PVDF sample characteristics after swelling in the presence of CO_2

Sample #	Final Wt (g)	Final Length (cm)	Final Width (cm)	Final Thickness (cm)
1	0.3872	1.28	0.61	0.33
2	0.2393	1.1	0.418	0.316
		1.13	0.406	0.314
			0.38	0.326
3		0.472		0.29
				0.278
				0.294
4	0.2105	1.460	0.712	0.122
		1.470	0.68	0.124
		1.458	0.64	0.126
6	0.3134	1.266		
		1.266		
7	0.0530	0.430		0.332
				0.320
				0.310
8				

Table A.12
PVDF swelling results

Sample #	Initial Length, L_o (in)	Temperature (°C)	Pressure (bar)	ΔL (in) x 10^{-3}	Elongation, $\Delta L/L_o$ (%)
1	0.5	80	49.8	2.45	0.49
			101.3	5.84	1.17
			151.0	9.96	1.99
			201.2	11.3	2.25
			251.7	12.0	2.40
			176.3	10.8	2.15
			126.6	10.1	2.02
2	0.4394	75	101.0	7.07	1.61
			151.0	8.51	1.94
			200.9	9.81	2.23
			301.9	10.5	2.38
			251.9	10.5	2.38
			175.9	94.5	2.15
			56.6	34.6	0.79
3	0.185	75	101.0	1.44*	0.78*
4	0.5711	75	100.5	10.8	1.88
			252.0	15.8	2.77
			198.7	15.0	2.62
			100.7	11.7	2.05
6		42			
7	0.1614	75	101.7	1.08	0.67
			148.8	1.44	0.89
			201.4	1.44	0.89
			276.4	1.80	1.12
			223.6	1.80	1.12
			173.1	1.44	0.89
			127.7	1.08	0.67
			56.6	0.361	0.22
8	0.1685	42	101.0	3.18	1.88
			276.8	3.46	2.06
			201.0	3.82	2.27
			48.5	2.81	1.67

* System was stopped before reaching equilibrium

A.3 Partition Coefficient Apparatus

A schematic of the experimental setup for the partition coefficient apparatus is shown in Figure A.7. The major components include the polymer cylinder (F) in which the polymer sample is located during the experiment, an HPLC valve (H) to take samples for analysis in a gas chromatograph (G), and a circulating pump (C) to

circulate the fluid through the polymer sample and speed the time to equilibrium. The entire system is enclosed in an oven whose temperature is controlled by a microprocessor.

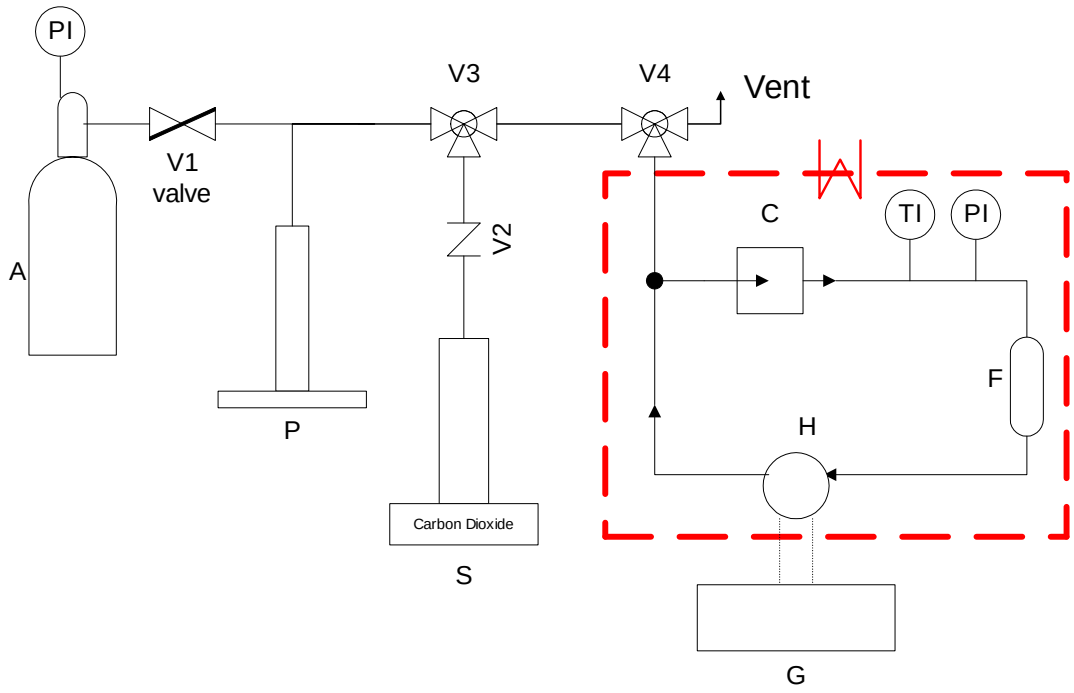

Figure A.7 Schematic of partition coefficient apparatus

The gas chromatograph (GC) is equipped with a gas-sampling valve, in addition to the HPLC valve external to the system. Helium at 40 mL/min is used as a carrier gas. When taking samples, the gas-sampling valve is opened for 0.3 minutes before switching the HPLC valve (0.5 μL) open for 0.2 minutes. The gas sampling valve remains open an additional 0.3 minutes to ensure that the entire sample enters the GC column. The sample is flowed through a 6' silica gel packed column at 55°C and then a thermal conductivity detector (TCD) to determine the ratio of VF2 to CO_2 in the fluid phase. A typical chromatogram is shown in Figure

A.8. The ratio of the area counts of VF2 and CO_2 correspond with the mass ratios of the two species. A calibration curve may be constructed from systems of known amounts of VF2 and CO_2 in the absence of polymer. The calibration curve must be constructed every three to six months or after the GC hasn't been used for an extended period of time. An example of a calibration curve is shown in Figure A.9.

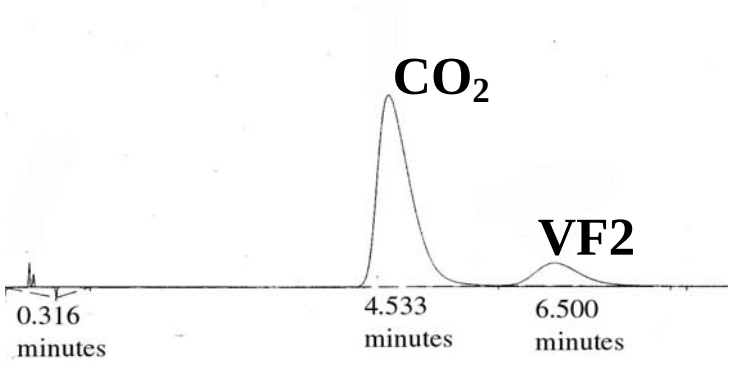

Figure A.8 Typical chromatogram for VF2 and CO_2 fed to a gas chromatograph at 55 °C using a TCD detector and silica gel packed column

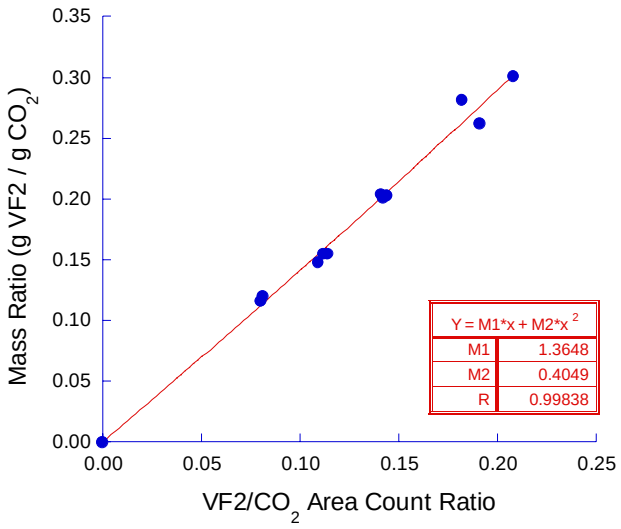

Figure A.9 Calibration curve for varying amounts of vinylidene fluoride and carbon dioxide at 75 °C and ~276 bar using a gas chromatograph

A.3.1 Operating Procedure

The procedure for conducting partition coefficient experiments is as follows:

1) Prepare polymer cylinder for polymer sample by inserting a small amount of glass wool and a frit (0.5μm x ¼"OD) into one end of the cylinder. Add a fitting with 1/8"NPT connector to this end of the cylinder.
2) Add a weighed amount of polymer powder to the opposite end of the polymer cylinder. Add glass wool, a frit, and a fitting with a 1/16" tubing connector to this end.
3) Connect polymer cylinder to system. The system is pressurized with nitrogen or helium to test for leaks and remove any air from the system.
4) With the system open to vent (V3 closed), the system is heated to the desired temperature.
5) Close V4 (vent side). Open valves V1, V3 (VF2 side), and V4 (system side). Vinylidene fluoride is added to the desired conditions based on the known volume of the system (minus the volume of polymer and glass wool), the given temperature and pressure in the system, and the density of VF2 as reported by ISCO SF Solver software. Close V4 (system side) and V3 (VF2 side). Vent tubing between these valves before opening V3 (CO_2 side) to add CO_2.
6) Open V3 (CO_2 side) and add CO_2 to the desired temperature and pressure conditions. Close V3 and V4.
7) Start the circulation pump. Pump should be set to 2877 RPM.

8) After the system reaches equilibrium (usually four hours), samples may be taken by the HPLC valve to the gas chromatograph. The lines running from the HPLC valve in the oven to the GC should be heated before taking a sample. Open control file VF2CO2.con in the GC software. Enter specifics for the particular run in the comments section. Press the spacebar on the keyboard to take a sample. Once the chromatogram is complete, another sample may be taken. The average of three or more samples is taken to calculate the partition coefficient.

A.3.1.1 Calculation of Partition Coefficient

- Gas chromatograph area count ratio at equilibrium (ACR^{equil}) = area count for VF2 ÷ area count for CO_2
    - The equilibrium mass ratio, MR^{equil}, is determined from a calibration curve for the mass ratio versus the area count ratio for known amounts of VF2 and CO_2 in the absence of polymer
- Molecular weight of VF2 (MW_{VF2}) = 64.04
- Volume of polymer (V_{PVDF}) = Mass of polymer (in grams) ÷ Density of polymer (1.78 g/mL)
- Volume of system (V_S) = 25 mL
- Volume of polymer phase (V^P) = V_{PVDF} x 1.25
    - The factor 1.25 accounts for the additional volume of the frits and glass wool
- Volume of fluid phase (V^F) = $V_S - V^P$

- Mass of VF2 in feed, $M_{VF2}^{feed} = \rho_{VF2}(T_1, P_1) \cdot V^F$
  - T_1 and P_1 are at the temperature and pressure after VF2 is added
- Mass of CO2 in feed, $M_{CO_2}^{feed} = \rho_{CO_2}(T_2, P_2) \cdot \left(V^F - \frac{M_{VF2}^{feed}}{\rho_{VF2}(T_2, P_2)} \right)$
  - T_2 and P_2 are at the temperature and pressure after CO_2 is added
- Mass of VF2 in fluid phase, $M_{VF2}^F = MR^{equil} M_{CO_2}^{feed}$
- Mass of VF2 in polymer phase, $M_{VF2}^P = M_{VF2}^{feed} - M_{VF2}^F$
- Concentration of VF2 in polymer phase, $[VF2]^{PVDF} = \frac{\frac{M_{VF2}^P}{MW_{VF2}}}{V_{PVDF}}$
- Concentration of VF2 in fluid phase, $[VF2]^{CO_2} = \frac{\frac{M_{VF2}^F}{MW_{VF2}}}{V_s}$
- Partition coefficient, $K_c = \frac{[VF2]^{PVDF}}{[VF2]^{CO_2}}$

A.3.2 Error Analysis

Calculation of the partition coefficient is largely dependent on the area count ratio measured by the gas chromatograph. The composition of the fluid phase is determined from a calibration curve for known amounts of VF2 and CO_2 and the area counts. As shown in Figure A.9, a good correlation is obtained between the ratio of the masses and the area counts. The data exhibit good repeatability at the lower concentrations, but the data do exhibit some scatter at higher concentrations.

It is well reported that a linear relationship exists between the mass and area count at low concentrations, but begins to deviate at higher concentrations. A polynomial was used to provide a best curve fit the data.

The average of three to five samples was used for the area count ratio (ACR) in the partition coefficient calculations. Based on the averages, the calculated partition coefficients were fairly consistent, as illustrated in Figure A.10. The effect of the initial monomer concentration on the partition coefficient was examined at 66 °C and 207 bar. As shown in Figure A.10, in the range of conditions studied, there was not a significant effect of the monomer concentration on the partition coefficient. However, the error bars demonstrate that the variation between samples measured by the gas chromatograph caused the uncertainty of the partition coefficient to be very large. For example, at the lowest concentration, the average ACR was 0.082. Using the calibration curve in Figure A.9, the mass ratio equaled 0.126. Between samples, the ACR varied from 0.075 to 0.089. Although this is a seemingly small variation (± 0.007), the resulting variation in the mass ratio produces a large variation in the calculated mass of VF2 in the fluid phase (0.2 ± 0.2 g) and finally the partition coefficient. The variation in the ACR for the calibration experiments (in the absence of polymer) is significantly less (± 0.002). It is unclear why the variation increases with the presence of the polymer, but it may be due to regions of imperfect mixing in the system.

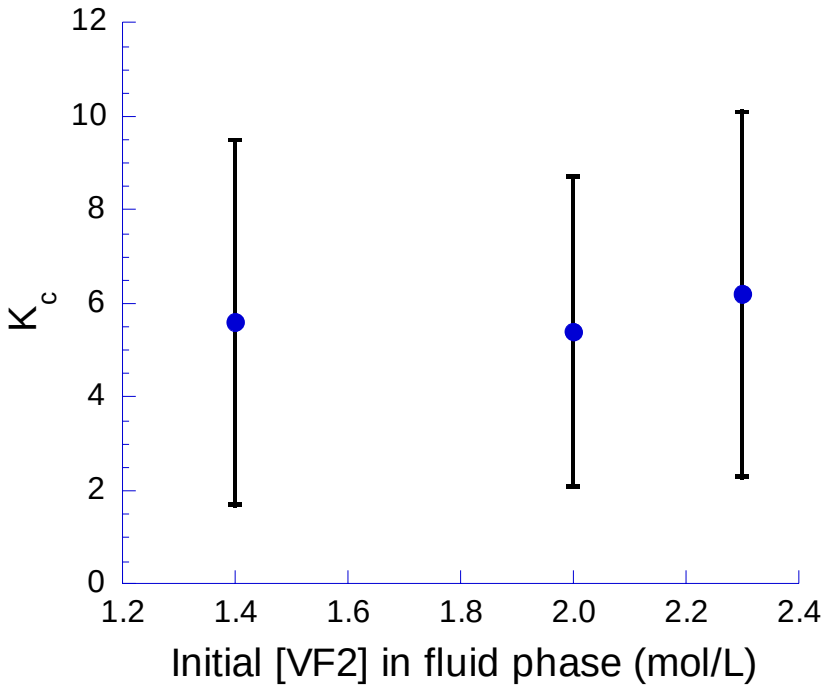

Figure A.10 Effect of initial monomer concentration on the partitioning of VF2 between PVDF and CO_2 phases at 66°C, 207 bar, as determined from fluid-based partitioning measurements

It is not believed that the variation in the ACR between samples is due to a lack of an equilibrium condition. Figure A.11 shows the change in the VF2 area count with time in a system consisting of VF2, CO_2, and PVDF. The system reaches equilibrium around 3.5 hours. In most cases, the partition coefficient experiments were allowed to run overnight, allowing sufficient time for the system to be at equilibrium.

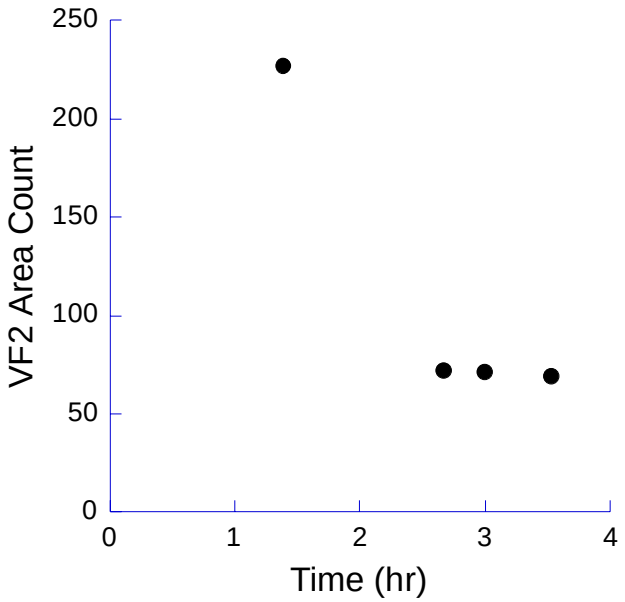

Figure A.11 Plot of change in VF2 area count, as measured by a gas chromatograph, with time for a system of 6.8 grams VF2, 7.6 grams CO_2 and 2.9 grams PVDF

A.3.3 Experimental Data

A.3.3.1 PVDF-CO_2-VF2

Table A.13
Partitioning of VF2 between CO_2 and PVDF phases at 46 °C

Pressure (bar)	VF2 feed (g)	CO_2 feed (g)	PVDF feed (g)	Feed mass ratio in fluid phase	$[VF2]_{feed}$ in fluid phase (mol/L)	Equilibrium mass ratio in fluid phase	$[VF2]_{equil}$ in fluid phase (mol/L)	$[VF2]_{equil}$ in polymer phase (mol/L)	VF2 sorbed in polymer phase (g)	K_c
155.5	2.7	15.1	0.95	0.176	1.7	0.153	1.5	9.9	0.3	6.7
189.1	2.9	16.0	1.02	0.184	1.9	0.193	2.0	0	0	0
206.9	2.9	16.6	1.02	0.175	1.9	0.191	2.0	0	0	0
214.7	3.0	16.7	1.05	0.179	1.9	0.180	1.9	0	0	0
214.8	3.9	14.6	2.82	0.264	2.6	0.258	2.6	0.84	0.9	0.3
281.2	3.2	17.7	1.1	0.179	2.1	0.194	2.2	0	0	0

Note: Mass ratio equals grams of VF2 divided by grams of CO_2

Table A.14
Partitioning of VF2 between CO_2 and PVDF phases at 61 °C

Pressure (bar)	VF2 feed (g)	CO_2 feed (g)	PVDF feed (g)	Feed mass ratio in fluid phase	$[VF2]_{feed}$ in fluid phase (mol/L)	Equilibrium mass ratio in fluid phase	$[VF2]_{equil}$ in fluid phase (mol/L)	$[VF2]_{equil}$ in polymer phase (mol/L)	VF2 sorbed in polymer phase (g)	K_c
190.2	2.6	14.0	0.92	0.184	1.7	0.168	1.5	6.5	0.2	4.3
220.1	2.7	15.2	0.95	0.178	1.7	0.170	1.7	3.5	0.1	2.1
220.7	2.6	15.4	0.91	0.170	1.7	0.163	1.6	2.8	0.1	1.7
267.3	2.7	16.8	0.95	0.161	1.7	0.164	1.8	0	0	0

Note: Mass ratio equals grams of VF2 divided by grams of CO_2

Table A.15
Partitioning of VF2 between CO_2 and PVDF phases at 66 °C

Pressure (bar)	VF2 feed (g)	CO_2 feed (g)	PVDF feed (g)	Feed mass ratio in fluid phase	$[VF2]_{feed}$ in fluid phase (mol/L)	Equilibrium mass ratio in fluid phase	$[VF2]_{equil}$ in fluid phase (mol/L)	$[VF2]_{equil}$ in polymer phase (mol/L)	VF2 sorbed in polymer phase (g)	K_c
204.8	2.1	15.2	0.94	0.141	1.4	0.126	1.2	6.9	0.2	5.6
206.4	3.6	13.6	0.94	0.262	2.3	0.231	2.0	12.5	0.4	6.2
208.9	3.1	14.1	0.94	0.223	2.0	0.200	1.8	9.8	0.3	5.4

Note: Mass ratio equals grams of VF2 divided by grams of CO_2

Table A.16
Partitioning of VF2 between CO_2 and PVDF phases at 75 °C

Pressure (bar)	VF2 feed (g)	CO_2 feed (g)	PVDF feed (g)	Feed mass ratio in fluid phase	$[VF2]_{feed}$ in fluid phase (mol/L)	Equilibrium mass ratio in fluid phase	$[VF2]_{equil}$ in fluid phase (mol/L)	$[VF2]_{equil}$ in polymer phase (mol/L)	VF2 sorbed in polymer phase (g)	K_c
175.3	2.0	11.4	0.72	0.176	1.3	0.140	1.0	15.5	0.4	15.1
189.5	2.0	12.3	0.72	0.161	1.3	0.141	1.1	9.3	0.3	8.4
206.4	2.3	12.8	0.80	0.180	1.5	0.164	1.3	6.8	0.2	5.1
213.8	2.4	13.6	0.85	0.174	1.5	0.166	1.4	3.6	0.1	2.5
230.5	2.5	13.9	0.88	0.182	1.6	0.178	1.6	1.6	0.1	1.0
240.4	2.5	14.1	0.87	0.178	1.6	0.177	1.6	0.4	0.0	0.2
248.6	2.6	14.4	0.90	0.179	1.7	0.188	1.7	0	0	0
281.2	2.7	15.3	0.96	0.178	1.8	0.188	1.9	0	0	0

Note: Mass ratio equals grams of VF2 divided by grams of CO_2

Appendix B

Characterization data

The poly(vinylidene fluoride) (PVDF) obtained from synthesis of vinylidene fluoride in supercritical carbon dioxide [1] was characterized by several techniques. These included BET surface area measurements, DSC analysis, and SEM. The results are summarized in Sections B.1, B.2, and B.3. The polymerization conditions of the polymer samples characterized are summarized in Table B.1. The shaded areas highlight the main variable in the experimental conditions.

Table B.1
Polymerization conditions for polymer samples

Sample #	Polymerization Run # (Run # in Ref 1)	Temperature (°C)	Pressure (psig)	$[I]_{in}$ (mmol/L)	$[M]_{in}$ (mmol/L)	τ (min)	M_w x 10^4	PDI
1	14 (2)	75	4000	2.79	1.46	20.3	5.95	2.1
2	63 (4)	75	4000	2.84	2.79	20.5	14.5	2.6
3	56 (5)	75	4000	3.32	3.53	21.1	44.3	5.6
4	48 (11)	75	4000	2.67	2.75	11.2	10.3	2.4
5	58 (15)	75	4000	2.86	2.90	25.5	44.1	6.6
6	Commercial sample (Solef 1010)							

In order to determine the characteristic parameters for PVDF needed in the Sanchez-Lacombe model, PVT data for the polymer was necessary. Measurements of the specific volume of a commercial sample of PVDF over a range of temperatures and pressures are summarized in Section B.4.

B.1 BET surface area measurements

BET surface area measurements were conducted using a Flow Sorb II 2300 instrument. The polymer surface area was characterized to determine if a correlation existed between the polymerization conditions and the particle characteristics. As shown in Table B.2, no correlation was identified using this technique. The increase in surface area did not correlate with the increase in monomer concentration or residence time. Additionally, as shown for Sample #2, the surface area was not consistent between measurements. This was due to the limited polymer sample available for the measurements. Therefore, this technique was not reliable for characterizing the surface area of these polymer samples.

Table B.2
Surface area measurements

Sample #	BET (m^2/g)	
	Run 1	Run 2
1	9.8	
2	2.9	24.6
3	7.3	
4	26.6	
6	13.5	

B.2 DSC measurements

The crystallinity of the polymer samples was measured using differential scanning calorimetry (DSC). The DSCs was taken using the following temperature program. Starting at 25 °C, the temperature was ramped from 25 °C to 210 °C at 10 °C/min. The temperature was held at 210 °C for 5 minutes. The temperature was

then cooled from 210 °C down to 50 °C at 10 °C/min. The temperature was held at 50 °C for 5 minutes before being ramped up to 210 °C at 10 °C/min. The temperature was held at 210 °C for 5 minutes before cooling the system from 210 °C to 25 °C at 20 °C/min. The temperature program ended after holding at 25 °C for 3 minutes. The results of the DSC measurements are summarized in Table B.3. The melting enthalpy and temperature after the first and second heating of the polymer were measured and the crystallinity calculated in each case. The crystallinity was calculated as the measured enthalpy divided by the heat of fusion for 100% crystalline PVDF multiplied by 100%. The heat of fusion for 100% crystalline PVDF is 104.6 J/g [2].

Table B.3
DSC measurements

	1st Heat			*2nd Heat*		
	Melting Enthalpy (J/g)	Melting Temperature (°C)	% Crystallinity	Melting Enthalpy (J/g)	Melting Temperature (°C)	% Crystallinity
1	91.6	146.6 164.3 171.2	87.6%	79.5	165.2 171.2	76%
2	75.5	149.4 170.8	72.2%	69.9	171.1	66.8%
3	88.4	150.6 170.6	84.5%	77.9	169.7	74.5%
4	43.2	148.5 165.5 170.9	41.3%	73.3	168.0 171.5	70.1%
5*	69.8	151.8 171.9	66.7%	70.2	170.3	67.1%
6a (pellets)	57.3	177.5	54.8%	67.4	176.4	64.4%
6b (powder)	64.0	173.8	61.2%	66.8	173.6	63.9%

*Temperature program was 25/250/50/250 instead of 25/210/50/210/25

Observing the PVDF samples synthesized in CO_2 (Samples 1-5) and comparing the 1st and 2nd heats, we observe in all cases a melting peak at ~150°C in the first heat that does not appear in the second heat. This temperature is usually associated with β crystals, which are less stable than α crystals (melting around 170°C). Upon cooling and reheating of the samples, the polymer was able to rearrange into the more stable α crystals.

A double peak was observed in samples 1 and 4. This double peak may be associated with metastable crystallites that melt at the lower of the two temperatures. The samples with double peaks were obtained at either a low residence time or a low monomer concentration. Also, the molecular weight was lowest in samples 1 and 4. It has been reported that increases in molecular weight can decrease the rate of crystallization [3]. Conceivably, upon recrystallization of the low molecular weight samples, the crystallation rate was sufficiently faster than the other samples such that imperfect crystals were formed.

B.3 SEM results

Scanning electron microscopy (SEM) was used to characterize the polymer particle size and shape after synthesis in carbon dioxide. Pictures of the polymer particles for samples 1 through 4 are shown in Figures B.1 to B.4, respectively. In each case, the polymer particles are irregularly shaped. As the weight-averaged molecular weight of the polymer increased, the agglomeration of the particles increased until the particle size was indistinguishable. Additionally, at low molecular

weights, the polymer exhibits an open, fluffy structure that becomes more compacted at higher molecular weights.

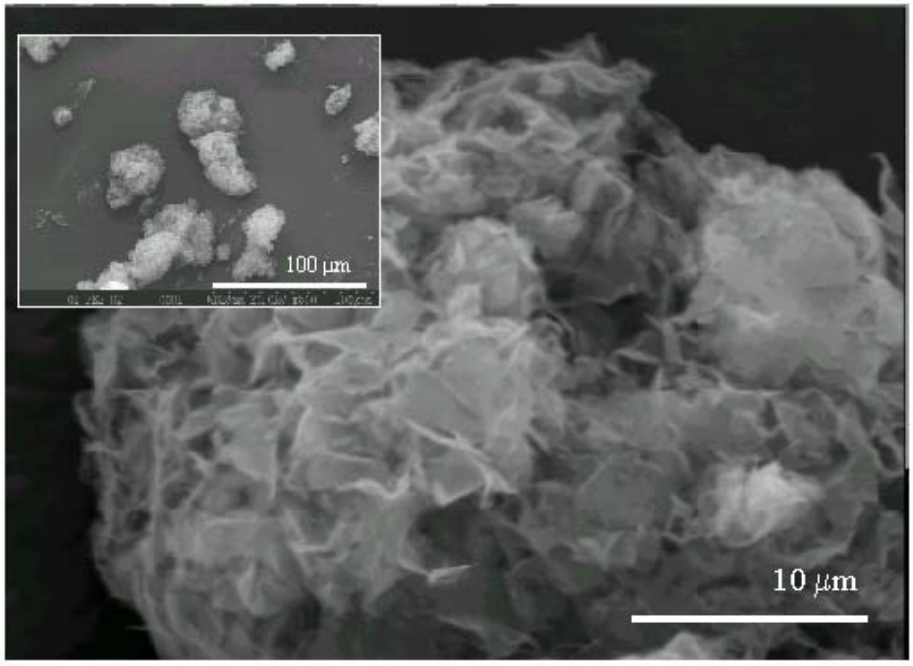

Figure B.1 Scanning electron micrograph of polymer particles synthesized in carbon dioxide, $[M]_{in}$ = 1.5 mol/L, $M_w = 5.95 \times 10^4$ g/mol. Inset is lower magnification micrograph

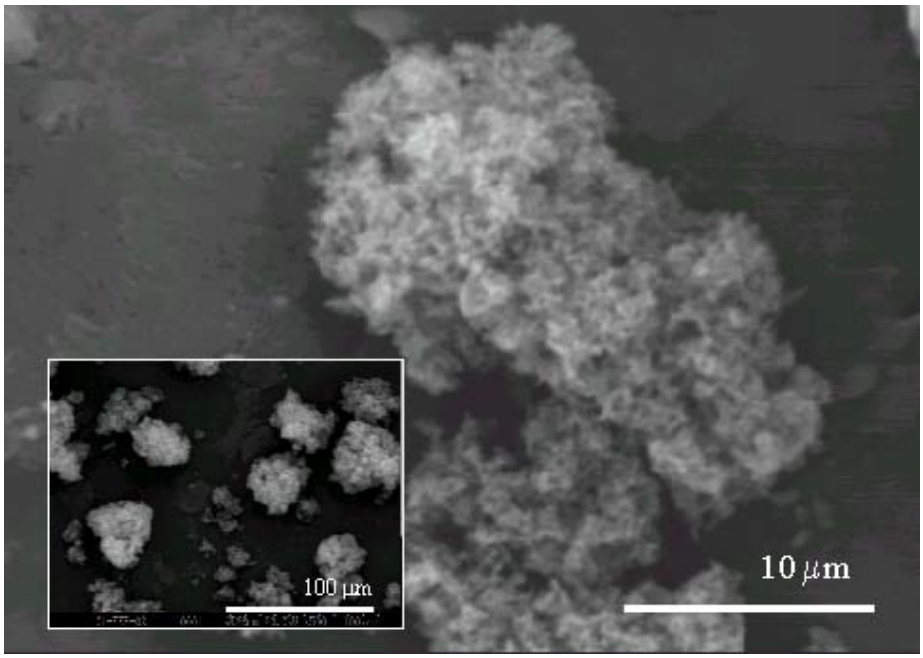

Figure B.2 Scanning electron micrograph of polymer particles synthesized in carbon dioxide, $[M]_{in}$ = 2.8 mol/L, M_w = 14.5x10^4 g/mol. Inset is lower magnification micrograph

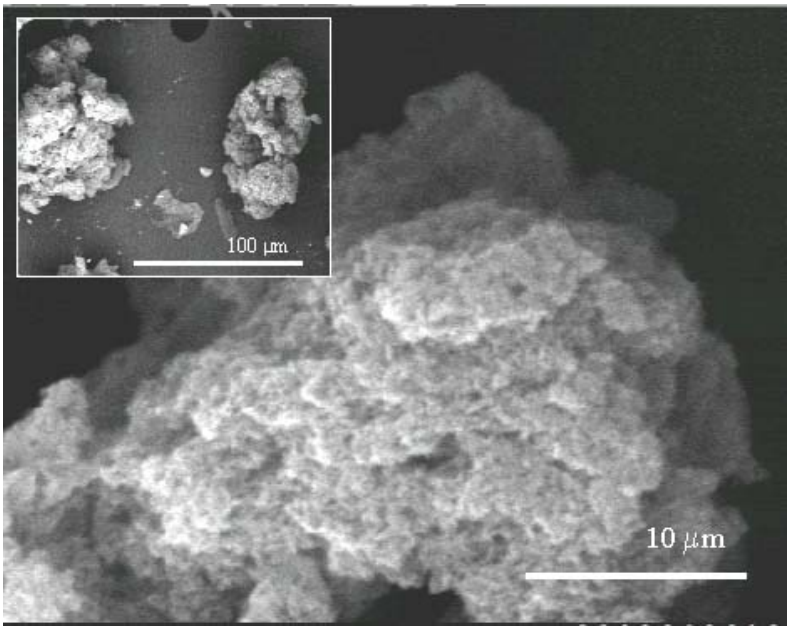

Figure B.3 Scanning electron micrograph of polymer particles synthesized in carbon dioxide, $[M]_{in}$ = 3.5 mol/L, M_w = 44.3x10^4 g/mol. Inset is lower magnification micrograph

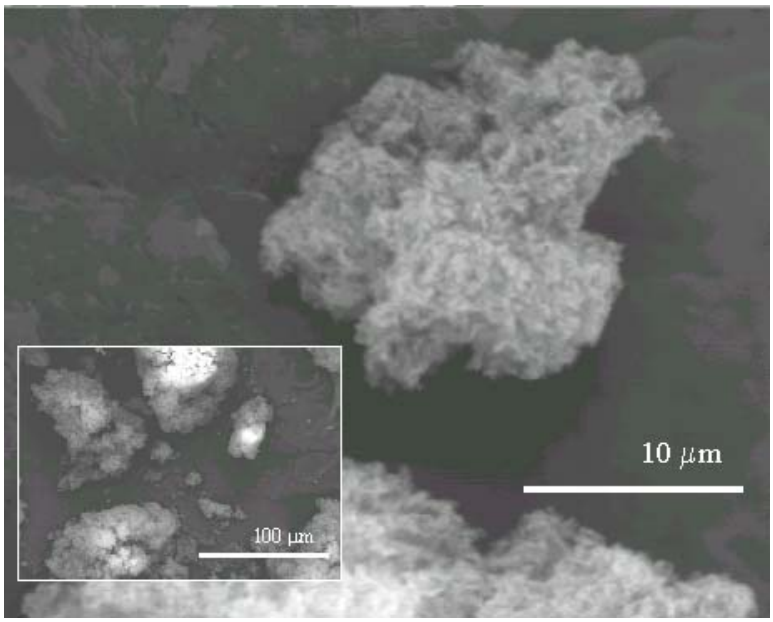

Figure B.4 Scanning electron micrograph of polymer particles synthesized in carbon dioxide, $[M]_{in}$ = 2.8 mol/L, M_w = 10.3x10^4 g/mol. Inset is lower magnification micrograph

Finally, a powder sample of the commercial polymer used in the phase equilibrium experiments was characterized by SEM. This is shown in Figure B.5. The particles are spherical with an even distribution of large (110 μm) and small (30-70 μm) particle sizes. Based on the observed particle shape of the commercial polymer and the polymer synthesized in CO_2, it is expected that the polymer synthesized in CO_2 would more readily sorb CO_2 and monomer due to its open, layered structure.

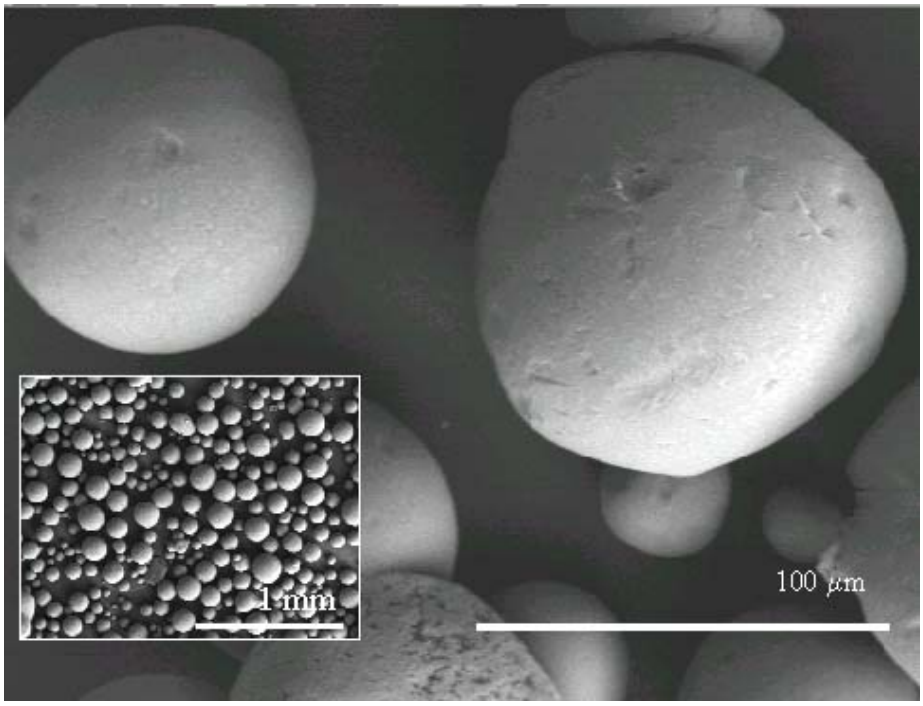

Figure B.5 Scanning electron micrograph of commercial PVDF powder (Solef 1010)

B.4 PVT results

The specific volume of Solef 1010 pellets was measured over a range of temperatures and pressures using a PVT apparatus located at the University of Naples. The data was used to determine the characteristic parameters of PVDF for use in the Sanchez-Lacombe equation of state. The data are plotted as the change in the specific volume versus the pressure at various temperatures (Figure B.6). The data are tabulated in Tables B.4 to B.6. The specific volume of Solef 1010 at atmospheric conditions is 0.562 cm^3/g.

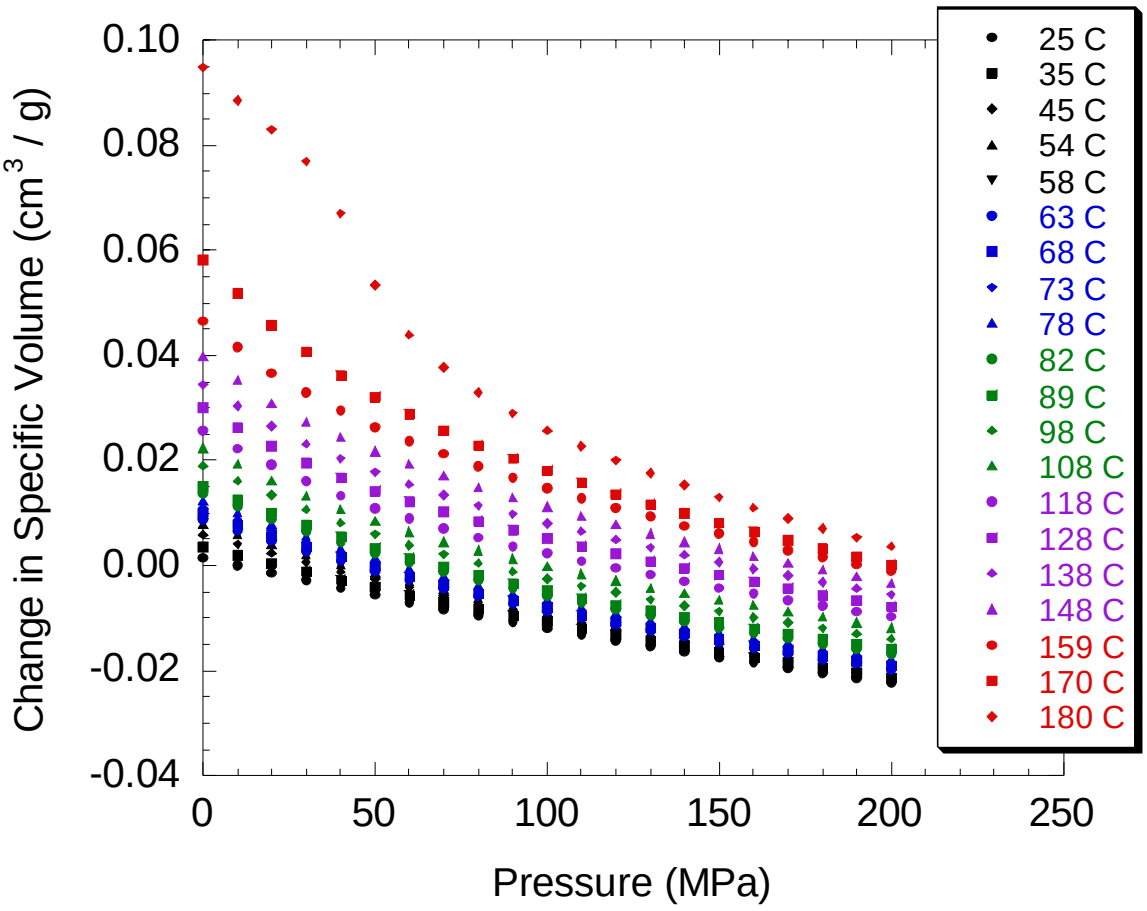

Figure B.6 Pressure-volume-temperature (PVT) data for PVDF (Solef 1010) reported as a change in the specific volume from atmospheric conditions (0.562 cm^3/g)

Table B.4
PVT data for Solef 1010 at 25, 35, 45, 54, and 58 °C
reported as the change in specific volume (cm^3/g)

Pressure (MPa)	25°C	35°C	45°C	54°C	58°C
0	0.00146	0.003519	0.005861	0.007907	0.008007
10	3.31E-05	0.001962	0.004088	0.005962	0.005951
20	-0.00137	0.000465	0.002333	0.004044	0.00395
30	-0.00272	-0.00108	0.00061	0.00217	0.00198
40	-0.00421	-0.00263	-0.00113	0.000344	0.000117
50	-0.00554	-0.00407	-0.00263	-0.00141	-0.0016
60	-0.00694	-0.00555	-0.00417	-0.0031	-0.00323
70	-0.00823	-0.00695	-0.00571	-0.00462	-0.00487
80	-0.00945	-0.00824	-0.00697	-0.00617	-0.00629
90	-0.01073	-0.00948	-0.00835	-0.00758	-0.00777
100	-0.01189	-0.01067	-0.00974	-0.00897	-0.00914
110	-0.01303	-0.01193	-0.01088	-0.01027	-0.01029
120	-0.0142	-0.01308	-0.01215	-0.01152	-0.01159
130	-0.01526	-0.01418	-0.01327	-0.01278	-0.01286
140	-0.01631	-0.01527	-0.01441	-0.01387	-0.01395
150	-0.0174	-0.01635	-0.01549	-0.01513	-0.01504
160	-0.01837	-0.01751	-0.01656	-0.01625	-0.01611
170	-0.01945	-0.01845	-0.01763	-0.01736	-0.01714
180	-0.0204	-0.01946	-0.0187	-0.01848	-0.0182
190	-0.02133	-0.02038	-0.01986	-0.01965	-0.01925
200	-0.02218	-0.02136	-0.02092	-0.02065	-0.02021

Table B.5
PVT data for Solef 1010 at 63, 68, 73, 78, 82, 89, and 98 °C
reported as the change in specific volume (cm^3/g)

Pressure (MPa)	63°C	68°C	73°C	78°C	82°C	89°C	98°C
0	0.008686	0.01007	0.010971	0.01239	0.013753	0.015034	0.018988
10	0.006649	0.007844	0.00876	0.010019	0.011253	0.012487	0.016068
20	0.004732	0.005688	0.00659	0.007827	0.008835	0.010049	0.013363
30	0.002715	0.003611	0.004426	0.005599	0.006481	0.007689	0.010678
40	0.000842	0.001635	0.002497	0.003416	0.004344	0.00547	0.008151
50	-0.00102	-0.00023	0.000654	0.001438	0.002408	0.003418	0.005936
60	-0.00269	-0.00205	-0.00125	-0.00044	0.000521	0.001573	0.003849
70	-0.00434	-0.00355	-0.00288	-0.00207	-0.00118	-0.00019	0.00214
80	-0.0058	-0.00517	-0.00443	-0.00372	-0.00276	-0.0019	0.000455
90	-0.00717	-0.00669	-0.00586	-0.00515	-0.00434	-0.00335	-0.00112
100	-0.00861	-0.00796	-0.00722	-0.00652	-0.00575	-0.00473	-0.00254
110	-0.00998	-0.00931	-0.00869	-0.00782	-0.00705	-0.00612	-0.00391
120	-0.01123	-0.0106	-0.00985	-0.00905	-0.00825	-0.0074	-0.00505
130	-0.01238	-0.01179	-0.01115	-0.01033	-0.00948	-0.00853	-0.00644
140	-0.01349	-0.01297	-0.01224	-0.01148	-0.01061	-0.00977	-0.00761
150	-0.01454	-0.01398	-0.01338	-0.01257	-0.01178	-0.01084	-0.00872
160	-0.01577	-0.01508	-0.01432	-0.01372	-0.01285	-0.01188	-0.00988
170	-0.01672	-0.01608	-0.01536	-0.01465	-0.01378	-0.01295	-0.01081
180	-0.0178	-0.01723	-0.0164	-0.0156	-0.01482	-0.01389	-0.01189
190	-0.01864	-0.01817	-0.01734	-0.01658	-0.01582	-0.0149	-0.01293
200	-0.01973	-0.019	-0.01826	-0.01759	-0.01674	-0.01575	-0.01393

Table B.6
PVT data for Solef 1010 at 108, 118, 128, 138, 148, 159, 170, and 180 °C
reported as the change in specific volume (cm^3/g)

Pressure (MPa)	108°C	118°C	128°C	138°C	148°C	159°C	170°C	180°C
0	0.022486	0.025815	0.030155	0.034552	0.039773	0.046626	0.058224	0.094894
10	0.019244	0.022368	0.026389	0.030501	0.035317	0.041624	0.051797	0.088611
20	0.016098	0.01913	0.022793	0.026613	0.031005	0.036749	0.045761	0.08308
30	0.013306	0.01605	0.019522	0.023209	0.027509	0.032947	0.040764	0.076904
40	0.010731	0.013311	0.016706	0.020374	0.024473	0.029549	0.036266	0.066986
50	0.008409	0.010905	0.014323	0.017759	0.021788	0.026465	0.032272	0.053485
60	0.00636	0.008912	0.012165	0.015478	0.019257	0.023717	0.02889	0.043966
70	0.004454	0.007054	0.010292	0.013413	0.017042	0.02129	0.025713	0.037816
80	0.002921	0.005352	0.008474	0.011447	0.014905	0.018888	0.023049	0.033042
90	0.001256	0.003672	0.006733	0.009762	0.012984	0.016718	0.020425	0.029038
100	-0.00025	0.002313	0.005175	0.008022	0.011205	0.014765	0.018064	0.02575
110	-0.00156	0.00093	0.003727	0.006497	0.009414	0.012825	0.015811	0.022824
120	-0.00281	-0.00046	0.002217	0.004914	0.007867	0.010985	0.013621	0.020062
130	-0.00421	-0.00168	0.000887	0.003428	0.006124	0.009338	0.011714	0.017554
140	-0.00532	-0.00293	-0.00042	0.00204	0.004537	0.007574	0.00991	0.015354
150	-0.00658	-0.00421	-0.0018	0.000641	0.003205	0.006052	0.008079	0.012999
160	-0.00754	-0.00529	-0.00309	-0.00061	0.001812	0.004454	0.00641	0.010971
170	-0.00873	-0.00655	-0.0042	-0.00186	0.00051	0.002905	0.004829	0.008997
180	-0.00974	-0.00759	-0.00556	-0.00322	-0.00083	0.001575	0.00325	0.007086
190	-0.01079	-0.00866	-0.0066	-0.00435	-0.00214	0.000227	0.001716	0.005327
200	-0.01182	-0.00968	-0.00779	-0.00545	-0.0033	-0.00106	0.000279	0.003667

B.5 References

1. Saraf, M.K., *Polymerization of vinylidene fluoride in supercritical carbon dioxide: Molecular weight distribution*. Masters Thesis, Department of Chemical Engineering, North Carolina State University, 2001.

2. Nakagawa, K. and Ishida, Y., *Annealing effects in poly(vinylidene fluoride) as revealed by specific volume measurements, differential scanning calorimetry, and electron microscopy.* Journal of Polymer Science: Polymer Physics Edition, 1973. **11**: p. 2153-2171.

3. Wunderlich, B., *Macromolecular Physics*. Vol. 2. 1976, New York: Academic Press.

Appendix C

Modeling results

This section summarizes the various modeling approaches used in this work and supplemental modeling calculations not covered in the major results of this dissertation.

C.1 Modeling approaches with Sanchez-Lacombe Equation of State

During the early stages of the modeling work, the Sanchez-Lacombe (S-L) equation of state was compared to data reported by Briscoe et al [1] for the sorption of carbon dioxide into poly(vinylidene fluoride) (PVDF). There was a systematic deviation between the Sanchez-Lacombe model and the experimental data [2]. This is illustrated in Figure C.1. The model over predicted the sorption at low pressures and under predicted the sorption at high pressures. Several approaches were attempted in order to improve the model correlation to the data. These included 1) using different characteristic parameters for CO_2 and PVDF, 2) "fitting" the PVDF characteristic parameters to the sorption data, 3) adding a second adjustable parameter to the closed-packed volume, v*, of the mixture of CO_2 and PVDF, 4) using different mixing rules for v*, 5) combining equations of state to describe the fluid phase thermodynamics with the S-L equation of state to describe the polymer phase, and 6) modifying the S-L model to account for the presence of crystallites. A discussion of the results of using different CO_2 parameters is discussed in Section 4.2.1.1. It was found that using PVDF parameters other than what was reported by

Briscoe et al resulted in convergence of the model at lower pressures and it was unnecessary to use an adjustable interaction parameter (ζ=1). This was attributed to the fact that the other parameters were obtained from PVT data covering a broad range of conditions, whereas Briscoe et al determined their parameters from singular values of the density, isothermal compressibility, and thermal expansion coefficient for PVDF at atmospheric pressure. However, despite the improvement in the convergence of the model with these different parameters, the model correlation with the data was not greatly improved. Similarly, several of the other modeling approaches did not greatly improve the model correlation with the data. These included “fitting “ the PVDF parameters to the sorption data, using an additional adjustable interaction parameter, and using different mixing rules for v*. Combining the Sanchez-Lacombe equation of state with other equations of state did have an impact on the model correlation with the data and will be discussed in the following section. Modifying the S-L model to account for the presence of crystallites worked well at 42 °C, but could not adequately describe the system at 80 °C. Those results are detailed in Section C.1.2.

The final modeling approach involved consideration of ternary and multi-component systems. The Sanchez-Lacombe model was used to predict the sorption of mixtures into the polymer phase and partition coefficients for the monomer between the polymer and supercritical phases. This work was discussed in Chapter 5.

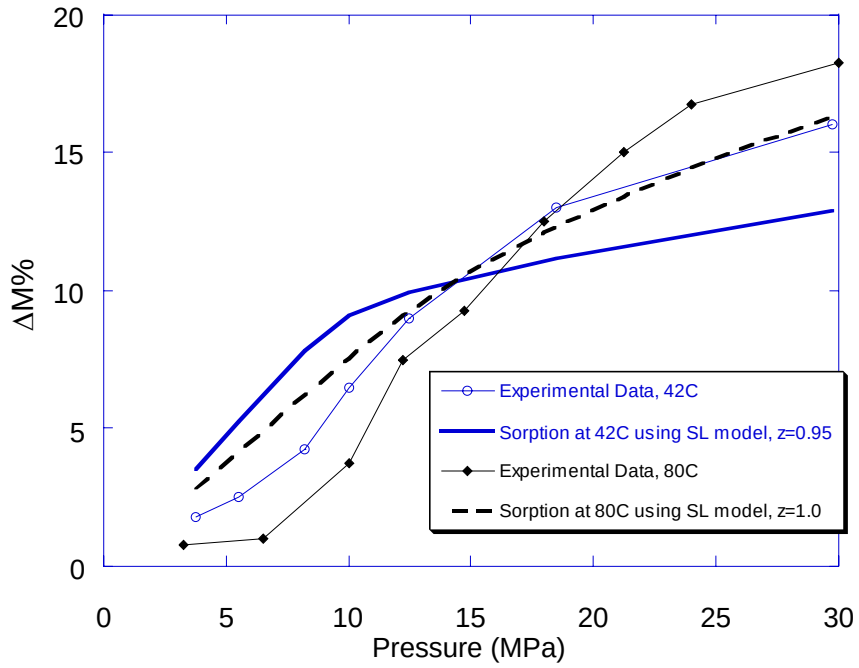

Figure C.1 Comparison of Sanchez-Lacombe model prediction to sorption data reported in the literature [1] for the sorption of carbon dioxide into poly(vinylidene fluoride)

C.1.1 Combined Equations of State

The Sanchez-Lacombe model has been shown to work very well with modeling polymer thermodynamics. However, it is not always a good predictor of the thermodynamics of small molecules. For this reason, models that describe the thermodynamics of small molecule systems were combined with the S-L model to describe the polymer phase thermodynamics. The models selected for the fluid phase were the Peng-Robinson [3] and Wagner [4] equations of state. The Peng-Robinson equation of state is very successful at describing the thermodynamics of small molecule systems and is commonly used to describe supercritical fluid

systems [5]. The Wagner equation of state was developed specifically for modeling carbon dioxide properties.

The Peng-Robinson (P-R) equation of state is given by [3],

$$P = \frac{RT}{v - b} - \frac{a(T)}{v(v + b) + b(v - b)} \tag{C.1}$$

where P is the pressure, R is the gas constant, T is the temperature, v is the molar volume, a is a measure of the intermolecular attraction force, and b is related to the size of the hard sphere molecules. Equation C.1 may be rewritten as

$$Z^3 - (1 - B)Z^2 + (A - 3B^2 - 2B)Z - (AB - B^2 - B^3) = 0 \tag{C.2}$$

where

$$A = \frac{aP}{R^2T^2} \tag{C.3}$$

$$B = \frac{bP}{RT} \tag{C.4}$$

$$Z = \frac{Pv}{RT} \tag{C.5}$$

Solution of the equation of state requires information about the pure component critical properties and acentric factor, and an equation that describes the fugacity of the fluid [3]. The properties of CO_2 are summarized in Table C.1.

Table C.1
Properties of carbon dioxide used in the Peng-Robinson equation of state

Tc (K)	Pc (bar)	ω
304.15	73.8	0.22394

The Wagner equation of state is given by [4],

$$Z = 1 + \sum_{i=1}^{9} a_i \delta^{r_i} \tau^{t_i} = \frac{P}{\rho_n RT} \tag{C.6}$$

where a_i, r_i, and t_i are coefficients tabulated in the literature [4], $\delta = \rho / \rho_c$, $\tau = T_c / T$, $\rho_n = \rho / M$, and M is the molar mass of CO_2. The virial equation for Equation C.6 is

$$Z = 1 + B(T)\rho_n + C(T)\rho_n^2 \tag{C.7}$$

The fugacity of the fluid is solved from the virial equation.

In order to combine the Sanchez-Lacombe equation of state with either the Peng-Robinson or Wagner equation of state, it is necessary to choose a reference pressure. The reference pressure P^o is arbitrary, but must be consistent in both EOS. The reference pressure used in this work was 20 MPa. The chemical potential of pure CO_2 is calculated using either the Wagner or P-R EOS according to

$$\mu_{CO2}^{fluid}(T, P) = \ln f(T, P) - \ln f(T, P^o) \tag{C.8}$$

The chemical potential of CO_2 in the polymer phase is calculated using the Sanchez-Lacombe EOS according to

$$\mu_{CO2}^{polymer}(T, P) = \mu'_{CO2}(T, P) - \mu_{CO2}(T, P^o) \tag{C.9}$$

where μ' is the chemical potential before the adjustment for the reference pressure.

The results of using the combined equation of state approach with the literature data is shown in Figures C.2 and C.3. The results using the different equations were very similar, particularly the combined Wagner-S-L and S-L models. Additionally, the same interaction parameter optimized the fit for each set of equations. It was found that the SSE could be reduced slightly if a different

reference pressure was used. However, the standard S-L model provided the best fit to the data. Thus, using an equation of state that was considered very accurate for describing the fluid phase equilibrium did not improve the model fit over that obtained with the standard S-L model.

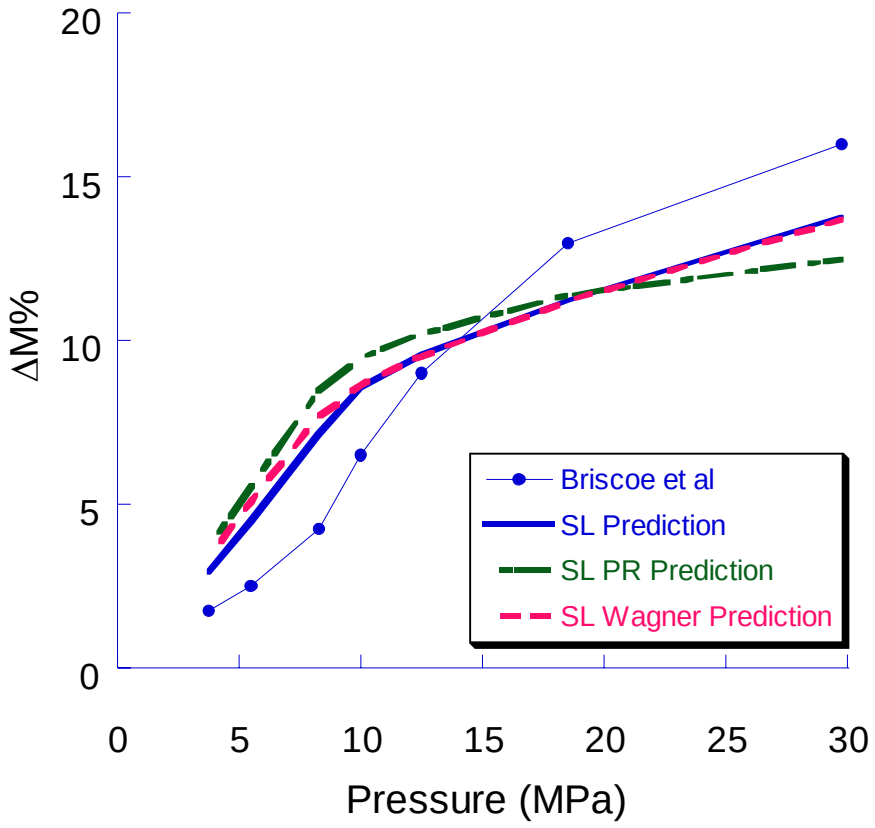

Figure C.2 Model prediction for the sorption of CO_2 into PVDF at 42 °C using the Sanchez-Lacombe equation of state to describe the polymer phase and the Sanchez-Lacombe (—), Peng-Robinson (– —), and Wagner (- -) equations of state to describe the fluid phase. $\zeta = 1.01$. Data taken from the literature [1]

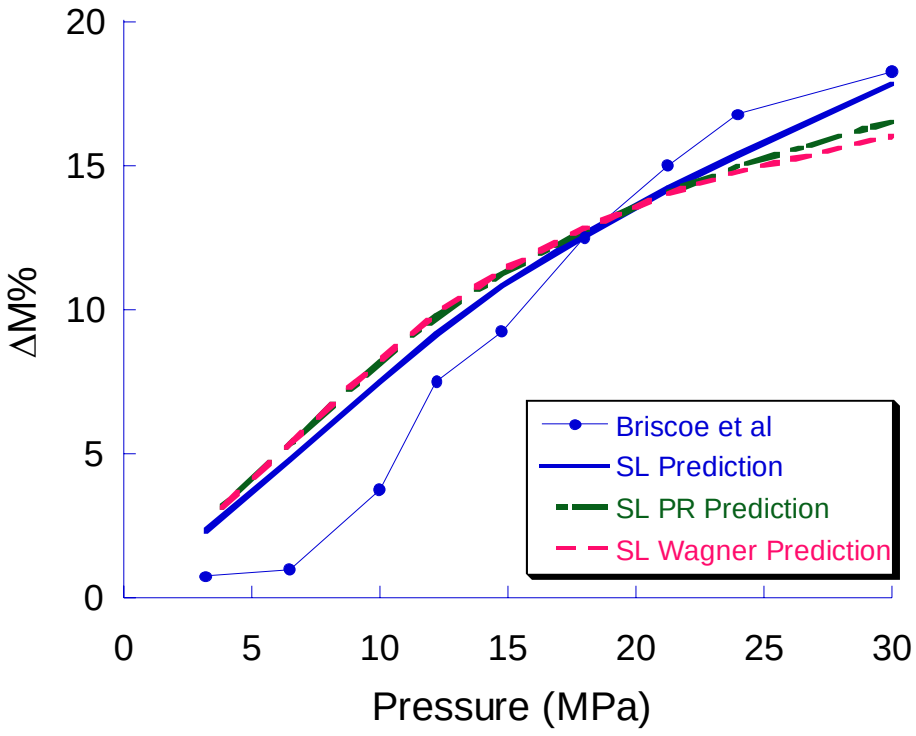

Figure C.3 Model prediction for the sorption of CO_2 into PVDF at 80 °C using the Sanchez-Lacombe equation of state to describe the polymer phase and the Sanchez-Lacombe (—), Peng-Robinson (– —), and Wagner (- -) equations of state to describe the fluid phase. $\zeta = 1.09$. Data taken from the literature [1]

C.1.2 "Crystalline Correction" Modified Sanchez-Lacombe EOS

The Sanchez-Lacombe model is limited to describing polymer melts and amorphous polymers. In the previous discussions in Chapters 3 & 4, the sorption was calculated based on sorption solely in the amorphous phase of the polymer. The model provided a good fit to the experimental data measured in this work. However, the model exhibited a systematic deviation from data previously reported in the literature [2]. One of the reasons proposed for the deviation between the model and the data was due to the possible influence of the crystalline regions on the sorption in the amorphous phase. In the present discussion, the Sanchez-

Lacombe model is modified to account for the presence of crystallites in the polymer. The crystallites act to restrict the sorption of CO_2 in the amorphous regions. The S-L model is modified to account for the presence of crystallites using an approach developed by Michaels and Hausslein for semi-crystalline polymers. Based on that work, it is assumed that sorption occurs only in the amorphous phase. Also, the amorphous phase consists of elastically effective and ineffective chains. The elastically ineffective chains behave similar to the lattice chains in the Sanchez-Lacombe model. These chains may be totally amorphous, may loop through the crystalline phase, or the chains may terminate in the amorphous phase. The elastically effective chains traverse the amorphous phase and are terminated in crystalline regions. The elastically effective chains are limited in their sorption capacity because they are restricted between crystalline regions. This generates tension in the chains and increased activity of the solvent.

The Gibbs free energy for the polymer is given by

$$\mathbf{G} = \mathbf{G}^{\mathbf{LF}} + \mathbf{G}^{\mathbf{EL}} \tag{C.10}$$

where G^{LF} is the Gibbs free energy described by the Sanchez-Lacombe model and G^{EL} is the energy due to the elastically effective chains. The chemical potential equation for a solvent (component 1) in the polymer is then

$$\mu_1 = \mu_1^{\mathbf{LF}} + \mu_1^{\mathbf{EL}} \tag{C.11}$$

where μ^{EL} is given by

$$\mu_1^{\mathbf{EL}} = \mathbf{RT}\ln\gamma_{\mathbf{e}} \tag{C.12}$$

The enhanced activity coefficient, γ_e, is defined as

$$\ln \gamma_e = \frac{\frac{\Delta H_p V_s}{R V_p}\left[\frac{1}{T} - \frac{1}{T_m'}\right]}{(3/2 f v_2) - 1} \qquad \text{(C.13)}$$

where ΔH_P is the molar heat of fusion of the polymer, V_s is the molar volume of the solvent, V_P is molar volume of the polymer, R is the gas constant, T is the temperature, T_m' is the melting point of the crystallites in the presence of solvent when μ_1^{EL} = 0, v_2 is the volume fraction of amorphous polymer with sorbed solvent (1 - ϕ_1), and f is the fraction of non-crystalline polymer that is elastically effective. The T_m' parameter may be calculated according to the melting point depression equation,

$$\frac{1}{T_m'} - \frac{1}{T_m^o} = \left(\frac{R}{\Delta H_p}\right)\left(\frac{V_p}{V_s}\right)\left[1 - v_2 - \chi(1 - v_2)^2\right] \qquad \text{(C.14)}$$

$$\chi = \frac{P_1^* + P_2^* - 2\zeta(P_1^* P_2^*)^{\frac{1}{2}}}{RT} \qquad \text{(C.15)}$$

where T_m^o is the normal melting point of the polymer. The chemical potential of component 1 in a solvent-swollen, semi-crystalline polymer is then

$$\mu_1^{II} = \mu_1^{LF} + \frac{\frac{\Delta H_p V_s}{R V_p}\left[\frac{1}{T} - \frac{1}{T_m'}\right]}{(3/2 f v_2) - 1} \qquad \text{(C.16)}$$

where μ_1^{LF} is given by Equation 3.31. Equation 3.33 gives the chemical potential of pure solvent. The sorption of carbon dioxide into PVDF is calculated as before,

except Equation C.16 is substituted into Equation 3.29 for the chemical potential in the polymer phase.

The crystalline correction approach was applied to the S-L model to determine if a certain value of f would predict the sorption behavior of the literature data. The characteristic parameters for PVDF determined in this work were used in the current model. At 42 °C, the interaction parameter (1.009) determined from the data presented in this research was used in the model. The f value was varied to optimize the fit to the data. Figure C.4 illustrates the effect of f, the amount of elastically effective chains, on the sorption at 42 °C. At f equal to 0.000001 ($f \cong 0$), the model approximates the standard S-L model (Figure C.5). At an f value of 0.11, the model fit is optimized. Using the modified S-L model at 42 °C, it was possible to improve the model fit at lower pressures, but the sorption at higher pressures was underestimated. A similar approach was applied to the 80 °C data using the interaction parameter (1.018) determined from the data in this work (Figure C.6). Despite varying the f value, the model prediction did not shift greatly from the standard S-L model. Thus, the f value was fixed at 0.11, the value determined at 42 °C and the interaction parameter was adjusted to optimize the model fit. This is illustrated in Figure C.7. The interaction parameter was increased from the previous investigation in order to optimize the fit. However, despite the improved qualitative agreement, the model could not adequately provide a quantitative description of the sorption over the full pressure range.

In this approach, the f value was used as a fitting parameter. However, it is possible to measure f independently. The sorption of CO_2 into completely amorphous polymer would be measured to get μ_1^{LF} and then the enhanced activity in the semi-crystalline polymer could be calculated from Equations C.11 through C.13 to determine f experimentally. Michaels and Hausslein measured the sorption of para-xylene in polyethylene of different thermal histories. They found that the thermal history had a strong impact on the f value. The elastically effective fraction, f, increased from 0.25 to 0.35 with the rate at which the polymer was cooled from the melt and approached unity for highly oriented, cold-drawn samples.

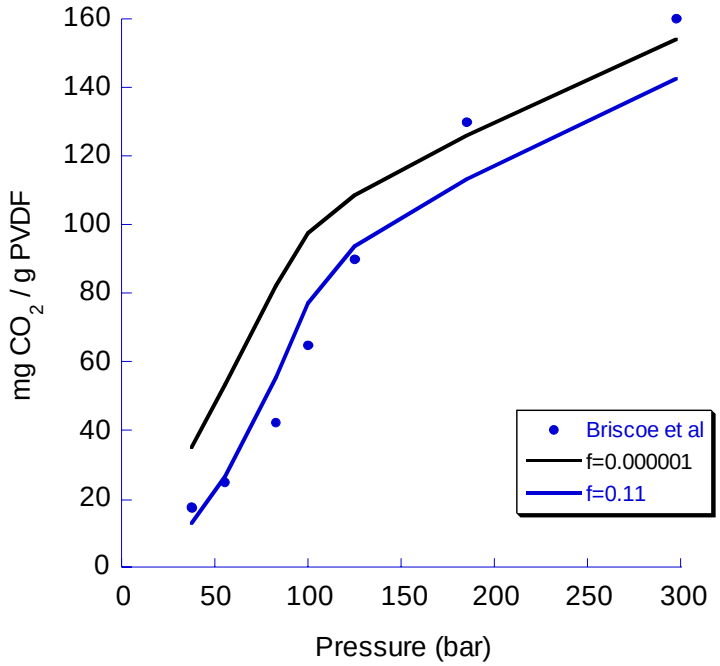

Figure C.4 Model prediction of the sorption of CO_2 into PVDF at 42 ^{o}C for varying f values using a modified Sanchez-Lacombe equation of state. Experimental data were taken from the literature [1]. ζ = 1.009

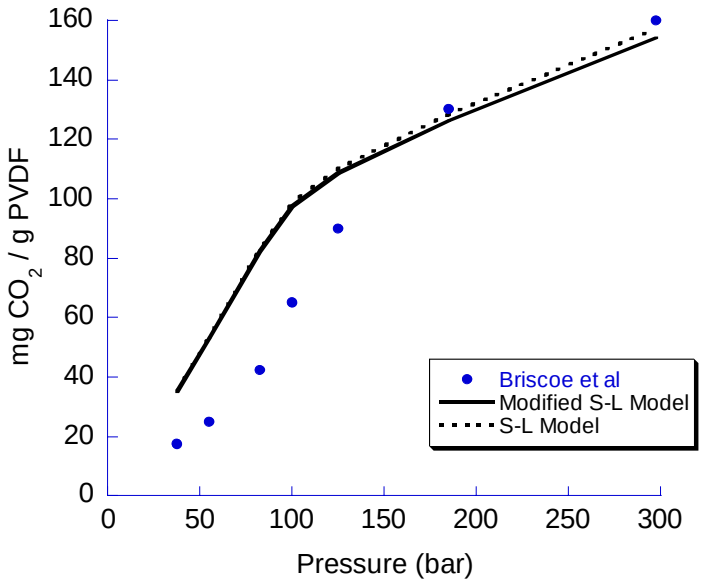

Figure C.5 Comparison of the Sanchez-Lacombe and modified Sanchez-Lacombe (f=0.000001) model prediction for the sorption of CO_2 into PVDF at 42 °C. Experimental data were taken from the literature [1]. ζ = 1.009

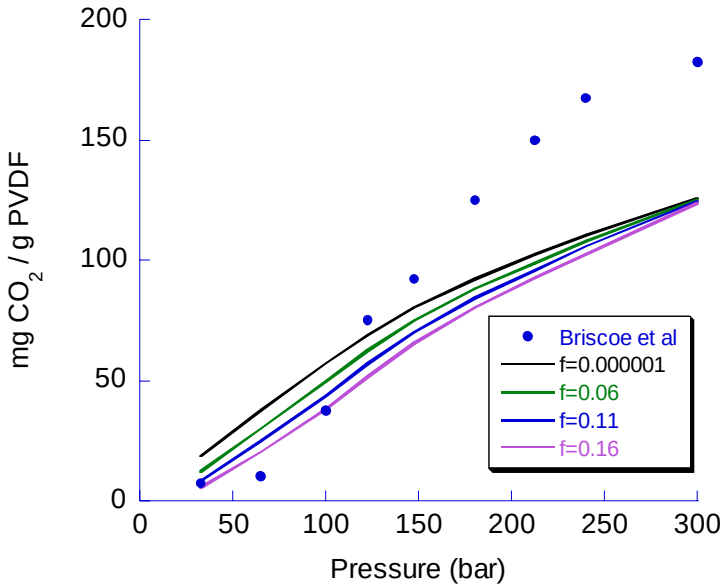

Figure C.6 Model prediction of the sorption of CO_2 into PVDF at 80 ^{o}C for varying f values using a modified Sanchez-Lacombe equation of state. Experimental data were taken from the literature [1]. ζ = 1.018

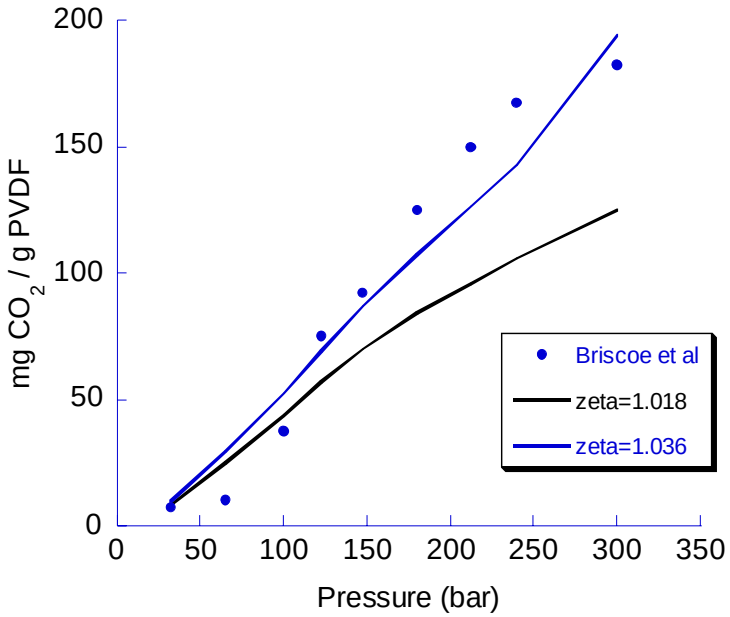

Figure C.7 Model prediction of the sorption of CO_2 into PVDF at 80 ^{o}C for varying interaction parameters using a modified Sanchez-Lacombe equation of state. Experimental data were taken from the literature [1]. f = 0.11

C.2 Supplemental Modeling Results

C.2.1 PVDF Solubility

The solubility of poly(vinylidene fluoride) in carbon dioxide, vinylidene fluoride, and mixtures of vinylidene fluoride and carbon dioxide at 75 °C was modeled using the Sanchez-Lacombe EOS. The pressure at which PVDF became insoluble in a given solution, the cloud point pressure, was designated as the pressure at which further increases in the pressure caused the model to no longer converge or when the weight fraction of fluid in the polymer phase reached a maximum. The results are summarized in Table C.2.

Table C.2
Cloud point pressures for PVDF in various solutions at 75 °C

Solvent	PVDF Mw (g/mol)	ζ	Cloud point Pressure (MPa)
CO_2	150,000	1.0	195
CO_2	20,000	1.0	194
VF2	150,000	0.88	178
VF2	20,000	0.88	178
CO_2-VF2	150,000	1.009	121
CO_2-VF2	20,000	1.009	121

The cloud point for PVDF with a molecular weight of 150,000 g/mol in CO_2 at 75°C was determined to be 195 MPa. This value is consistent with the expected value for the cloud point based on literature data [6] (see Figure 3.2) extrapolated to 75°C. The molecular weight was decreased to 20,000 g/mol to study the effect of molecular weight on the cloud point pressure. This molecular weight was of the same order as the unimodal polymer formed by polymerization in CO_2. The cloud point pressure decreased to 194 MPa at this lower molecular weight. The reduction in the cloud point pressure was not significant.

The cloud point pressure for PVDF in the presence of vinylidene fluoride was calculated. A binary interaction parameter of 0.88 was chosen based on values determined in Chapter 5. An enhancement in the solubility was observed. For the low molecular weight polymer, the pressure dropped from 194 MPa to 178 when carbon dioxide was replaced with vinylidene fluoride. The monomer had a more

favorable interaction with the polymer such that lower pressures were required to solubilize the polymer in the monomer.

The three-component model was used to determine the cloud point of PVDF in a mixture of carbon dioxide and vinylidene fluoride. The binary interaction parameters used to calculate the cloud point pressures in vinylidene fluoride and carbon dioxide were used in the three-component model. An interaction parameter equal to 1.009 was used for the CO_2-VF2 interaction based on values determined in Chapter 5. The three-component mixture was assumed to have a polymer phase in equilibrium with a fluid phase that consisted of 17 wt% VF2 in CO_2. In a mixture of VF2 and CO_2, the solubility was greatly enhanced over the solubility in the presence of either VF2 or CO_2. VF2 enhances the solvating ability of CO_2 by increasing the density of the fluid and providing favorable interactions with the polymer. However, the solubility was still much greater than the conditions at which polymerizations were conducted. A molecular weight as low as 200 g/mol and a composition of VF2 in the fluid phase as high as 70 wt% VF2 in CO_2 was considered in the model. The solubility was never less than ~100 MPa – significantly greater than the conditions of the polymerizations.

C.2.2 Partition Coefficient Results

Results were presented in Chapter 5 (Figure 5.16) for the model prediction of the partition coefficient for VF2 between PVDF and CO2 phases. Those results are summarized in Table C.3.

Table C.3
Summary of model results for partition coefficient of VF2 between PVDF and CO_2 phases at 60 °C and 75 °C

	K_c	
Pressure (bar)	@ 60 °C	@ 75 °C
10	3.1	1.6
20	2.8	1.6
30	2.8	1.4
40	2.6	1.2
50	2.3	1.3
60	2.0	1.2
70	1.9	1.0
80	1.6	1.0
90	1.4	0.9
100	1.0	0.8
110	0.86	0.68
120	0.76	0.60
130	0.70	0.54
140	0.66	0.49
150	0.63	0.46
160	0.62	0.44
170	0.60	0.42
180	0.60	0.41
190	0.59	0.40
200	0.58	0.39
210	0.58	0.39
220	0.57	0.38
230	0.57	0.38
240	0.56	0.37
250	0.56	0.37
260	0.56	0.37
270	0.56	0.37
280	0.56	0.37
290	0.56	0.36
300	0.56	0.36

C.3 MathCad Programs

MathCad was used to solve the system of equations in the two-component and three-component model. Following are the main functions used in the MathCad programs.

C.3.1 Sanchez-Lacombe Equation of State for Binary Mixtures

This section uses the Sanchez-Lacombe equation of state to evaluate the sorption of penetrants in a polymer phase. The program is set up for a two-component system of carbon dioxide and PVDF. The algorithm used by Wissinger [7] is used for the calculations. The units for this section are Kelvin for temperature, MPa for pressure, g/L for density, and MPa*L/mol/K for the gas constant.

Characteristic parameters for **CO_2**

$T1star := 316$

$P1star := 412.6$

$\rho 1star := 1369$

$M1 := 44.01$

$r1 := 5.11$

Characteristic parameters for **PVDF** (determined from PVT data for Solef 1010)

$T2star := 714.6$

$P2star := 434.8$

$\rho 2star := 1860$

$M2 := 150000$

Gas Constant

$R := 8314 \cdot 10^{-6}$

$$r2 := \frac{P2star \cdot M2}{R \cdot T2star \cdot \rho 2star}$$

Function ρr_SL calculates the reduced density of a mixture given the pressure (MPa), Temperature (K), weight fraction of CO_2 dissolved in the polymer phase, and the binary interaction parameter.

$$\rho r\_SL(P, T, m1, \zeta) := \left| \begin{array}{l} \phi 1 \leftarrow \dfrac{\left(\dfrac{m1}{\rho 1star}\right)}{\left[\dfrac{(1-m1)}{\rho 2star} + \dfrac{m1}{\rho 1star}\right]} \\ Pstar \leftarrow \phi 1 \cdot P1star + (1-\phi 1) \cdot P2star - \phi 1 \cdot (1-\phi 1) \cdot \left(P1star + P2star - 2 \cdot \zeta \cdot \sqrt{P1star \cdot P2star}\right) \\ Tstar \leftarrow \dfrac{Pstar}{\left[\dfrac{\phi 1 \cdot P1star}{T1star} + \dfrac{(1-\phi 1) \cdot P2star}{T2star}\right]} \\ r \leftarrow \dfrac{1}{\dfrac{\phi 1}{r1} + \dfrac{(1-\phi 1)}{r2}} \\ Treduced \leftarrow \dfrac{T}{Tstar} \\ Preduced \leftarrow \dfrac{P}{Pstar} \\ \rho r\_guess \leftarrow 0.9 \\ root\left[\rho r\_guess^{\,2} + Preduced + Treduced \cdot \left[\ln(1-\rho r\_guess) + \rho r\_guess \cdot \left(1 - \dfrac{1}{r}\right)\right], \rho r\_guess\right] \end{array} \right.$$

Function μ1_SL determines the chemical potential of the penetrant carbon dioxide given the pressure (MPa), temperature (K), weight fraction of CO_2 dissolved in the polymer phase, and the binary interaction parameter.

$$\mu 1\_SL(P, T, m1, \zeta) := \left| \begin{array}{l} \phi 1 \leftarrow \dfrac{\left(\dfrac{m1}{\rho 1star}\right)}{\left[\dfrac{(1-m1)}{\rho 2star} + \dfrac{m1}{\rho 1star}\right]} \\ \chi \leftarrow \dfrac{P1star + P2star - 2\cdot\zeta\cdot\sqrt{P1star\cdot P2star}}{R\cdot T} \\ P1reduced \leftarrow \dfrac{P}{P1star} \\ T1reduced \leftarrow \dfrac{T}{T1star} \\ \rho star \leftarrow \dfrac{1}{\dfrac{m1}{\rho 1star} + \dfrac{(1-m1)}{\rho 2star}} \\ \rho reduced \leftarrow \rho r\_SL(P, T, m1, \zeta) \\ C \leftarrow \left[\dfrac{-\rho reduced}{T1reduced} + \dfrac{P1reduced}{T1reduced\cdot\rho reduced} + (1-\rho reduced)\cdot\dfrac{\ln(1-\rho reduced)}{\rho reduced} + \dfrac{\ln(\rho reduced)}{r1}\right] \\ \ln(\phi 1) + 1 - \phi 1 + \rho reduced\cdot\dfrac{M1}{\rho 1star}\cdot\chi\cdot(1-\phi 1)^2 + C\cdot r1 \end{array} \right.$$

Function w1_SL determines the solubility of CO_2 in a polymer reported as a weight fraction. Inputs to the function are the pressure (MPa), temperature (K), and the binary interaction parameter.

$$w1\_SL(P, T, \zeta) := \left| \begin{array}{l} m1\_guess \leftarrow 0.1 \quad \text{if} \quad P \geq 10 \\ m1\_guess \leftarrow 0.03 \quad \text{otherwise} \\ \mu pure \leftarrow \mu 1\_SL(P, T, 1, 1) \\ root(\mu pure - \mu 1\_SL(P, T, m1\_guess, \zeta), m1\_guess) \end{array} \right.$$

Table "Data" is an array of values for pressure. Function "P" defines the array for pressure.

$$\text{Data} := \begin{bmatrix} 1.00 \\ 2.00 \\ 3.00 \\ 5.00 \\ 7.00 \\ 9.00 \end{bmatrix}$$

$P := \text{Data}^{\langle 0 \rangle}$

Function Sorption determines the degree of sorption of CO_2 in the polymer. Inputs to the function are the pressure (MPa) as an array of pressures, temperature (K), and the binary interaction parameter. The output is a matrix, w, in which the first column is the pressure, the second column is ΔM%, accounting for the amorphous phase of the polymer, the third column is the weight fraction of carbon dioxide, and the fourth column is ΔM%, accounting for the entire polymer.

$$\begin{aligned}
&\text{Sorption}(p, t, \text{zeta}) := \\
&\quad j \leftarrow 0 \\
&\quad \text{for } i \in 0..\text{rows}(p) - 1 \\
&\quad\quad w_{j,0} \leftarrow p_i \\
&\quad\quad w_{j,1} \leftarrow \left(\frac{1}{1 - \text{w1_SL}\left(p_i, t, \text{zeta}\right)} - 1 \right) \cdot 100 \\
&\quad\quad w_{j,2} \leftarrow \text{w1_SL}\left(p_i, t, \text{zeta}\right) \\
&\quad\quad w_{j,3} \leftarrow \frac{w_{j,2}}{1 + 0.64 \cdot \frac{\left(1 - w_{j,2}\right)}{(1 - 0.64)}} \cdot 100 \\
&\quad\quad j \leftarrow j + 1 \\
&\quad w
\end{aligned}$$

C.3.2 Combined Equation of State

This section uses the Sanchez-Lacombe equation of state to describe the polymer phase combined with either the Peng-Robinson or Wagner equations of state to describe the fluid phase. The equations of state are combined to evaluate

the sorption of penetrants in the polymer phase. The program is set up for a two-component system of carbon dioxide and PVDF. The units for this section are Kelvin for temperature, MPa for pressure, g/L for density, and MPa*L/mol/K for the gas constant. The functions ρr_SL, μ1_SL, P, and Sorption and the definitions for the characteristic parameters from the previous section are used in the combined equation of state.

Function μ1prime_SL evaluates the chemical potential of the penetrant carbon dioxide given the pressure (MPa), temperature (K), weight fraction of CO_2 dissolved in the polymer phase, and the binary interaction parameter. The reference pressure is 20 MPa.

$$\mu 1prime\_SL(P, T, m1, \zeta) := \mu 1\_SL(P, T, m1, \zeta) - \mu 1\_SL(20, T, 1, \zeta)$$

Function w1_SL determines the solubility of CO_2 in a polymer reported as a weight fraction. Inputs to the function are the pressure (MPa), temperature (K), and the binary interaction parameter. The first function for w1_SL is used with the Peng-Robinson equation of state and the second function is used with the Wagner equation of state. The functions μ_PR and μ_wagner and their associated sub-functions and parameters are defined in the next sections.

$$w1\_SL(P, T, \zeta) := \begin{| l} m1\_guess \leftarrow 0.1 \text{ if } P \geq 10 \\ m1\_guess \leftarrow 0.03 \text{ otherwise} \\ \mu pure \leftarrow \mu\_PR(P, T) \\ root(\mu pure - \mu 1prime\_SL(P, T, m1\_guess, \zeta), m1\_guess) \end{| l}$$

$$w1\_SL(P,T,\zeta) := \begin{vmatrix} m1\_guess \leftarrow 0.1 \text{ if } P \geq 10 \\ m1\_guess \leftarrow 0.03 \text{ otherwise} \\ \mu pure \leftarrow \mu\_wagner(P, T - 273.15) \\ root(\mu pure - \mu 1prime\_SL(P,T,m1\_guess,\zeta), m1\_guess) \end{vmatrix}$$

C.3.2.1 Peng-Robinson Equation of State

This section uses the Peng-Robinson equation of state to evaluate the properties of supercritical carbon dioxide. The units for this section are Kelvin for temperature, bar for pressure, g/L for density, and bar*L/mol/K for the gas constant.

Gas Constant

$R := 8314 \cdot 10^{-5}$

Characteristic parameters for **CO_2**

$Tc1 := 304.15$

$Pc1 := 73.8$

$\omega 1 := 0.2239$

$M1 := 44.01$

$$b1 := 0.07780\frac{R \cdot Tc1}{Pc1}$$

$$\kappa 1 := 0.37464 + 1.54226\omega 1 - 0.26992\omega 1^2$$

$$a1\_Tc := 0.45724\frac{R^2 \cdot Tc1^2}{Pc1}$$

$a1\_Tc = 3.962$

$b1 = 0.027$

$\kappa 1 = 0.706$

Function Z_PR determines the compressibility factor of CO_2 given the pressure (MPa) and Temperature (K).

$$Z\_PR(P,T) := \left| \begin{array}{l} P \leftarrow P \cdot 10 \\ \alpha 1 \leftarrow \left[1 + \kappa 1 \cdot \left(1 - \sqrt{\frac{T}{Tc1}}\right)\right]^2 \\ a1 \leftarrow a1\_Tc \cdot \alpha 1 \\ A \leftarrow \frac{a1 \cdot P}{R^2 \cdot T^2} \\ B \leftarrow \frac{b1 \cdot P}{R \cdot T} \\ Z \leftarrow 1 \\ \text{root}\left[Z^3 - (1 - B) \cdot Z^2 + \left(A - 3 \cdot B^2 - 2 \cdot B\right) \cdot Z - \left(A \cdot B - B^2 - B^3\right), Z\right] \end{array} \right.$$

Function lnf_PR evaluates the fugacity of CO_2 given the pressure (MPa) and temperature (K).

$$lnf\_PR(P,T) := \left| \begin{array}{l} P \leftarrow P \cdot 10 \\ \alpha 1 \leftarrow \left[1 + \kappa 1 \cdot \left(1 - \sqrt{\frac{T}{Tc1}}\right)\right]^2 \\ a1 \leftarrow a1\_Tc \cdot \alpha 1 \\ A \leftarrow \frac{a1 \cdot P}{R^2 \cdot T^2} \\ B \leftarrow \frac{b1 \cdot P}{R \cdot T} \\ Z \leftarrow Z\_PR\left(\frac{P}{10}, T\right) \\ (Z - 1) - \ln(Z - B) - \frac{A}{2 \cdot \sqrt{2} \cdot B} \cdot \ln\left[\frac{Z + \left(1 + \sqrt{2}\right) \cdot B}{Z + \left(1 - \sqrt{2}\right) \cdot B}\right] + \ln\left(\frac{P}{10}\right) \end{array} \right.$$

Function μ_PR evaluates the chemical potential with input values of pressure (MPa) and temperature (K). The reference pressure is 20 MPa.

$$\mu\_PR(P,T) := lnf\_PR(P,T) - lnf\_PR(20,T)$$

C.3.2.2 Wagner Equation of State

This section uses the Wagner equation of state to evaluate the properties of supercritical carbon dioxide. This equation of state was designed specifically for modeling the properties of carbon dioxide and considered highly accurate. The units for this section are Kelvin for temperature, bar for pressure, g/L for density, and cm^3*MPa/mol/K for the gas constant.

Constants for Wagner EOS

$Tc := 304.136$

$\rho c := 0.4676$

$M := 44.0098$

$R := 8.31451$

$$t := \begin{bmatrix} -1 \\ 2 \\ 5 \\ 5.5 \\ 2 \\ 4 \\ 8.5 \\ 9.5 \\ 10 \end{bmatrix} \quad r := \begin{bmatrix} 1 \\ 1 \\ 1 \\ 1 \\ 2 \\ 2 \\ 3 \\ 3 \\ 3 \end{bmatrix} \quad a := \begin{bmatrix} 0.9815871410^{-1} \\ -0.1332950510^{1} \\ 0.7609609710^{-1} \\ -0.9056789510^{-1} \\ 0.71016170 \\ -0.18302968 \\ -0.7886429310^{1} \\ 0.2356222710^{2} \\ -0.1564924910^{2} \end{bmatrix}$$

Function P_wagner calculates the pressure (MPa) of CO_2 with input values of density (g/cm^3) and temperature (°C).

$$P\_wagner(\rho, T) := \left| \begin{array}{l} T \leftarrow T + 273.15 \\ \delta \leftarrow \dfrac{\rho}{\rho c} \\ \tau \leftarrow \dfrac{Tc}{T} \\ Z \leftarrow 1 + \displaystyle\sum_{i=0}^{8} a_i \cdot \delta^{r_i} \cdot \tau^{t_i} \\ \dfrac{Z \cdot \rho \cdot R \cdot T}{M} \end{array} \right.$$

Function ρ_wagner calculates the density (g/cm^3) given the pressure (MPa) and temperature (°C). An initial guess for the density, ρguess, is made to the function.

$$\rho guess := 0.01$$
$$\rho\_wagner(P, T) := root(P - P\_wagner(\rho guess, T), \rho guess)$$

Function lnf evaluates the natural logarithm of fugacity with input values of pressure (MPa) and temperature (°C).

$$lnf(P, T) := \left| \begin{array}{l} \rho \leftarrow \rho\_wagner(P, T) \\ T \leftarrow T + 273.15 \\ \tau \leftarrow \dfrac{Tc}{T} \\ Z \leftarrow \dfrac{P \cdot M}{\rho \cdot R \cdot T} \\ \delta \leftarrow \dfrac{\rho}{\rho c} \\ \displaystyle\sum_{i=0}^{8} \frac{a_i \cdot \delta^{r_i} \cdot \tau^{t_i}}{r_i} + (Z - 1) - \ln(Z) + \ln(P) \end{array} \right.$$

Function μ_wagner evaluates the chemical potential with input values of pressure (MPa) and temperature (°C). The reference pressure is 20 MPa.

$\mu\_wagner(P,T) := lnf(P,T) - lnf(20,T)$

C.3.3 "Crystalline Correction" Modified Sanchez-Lacombe EOS in Binary Mixtures

This section uses the Sanchez-Lacombe equation of state to evaluate the sorption of penetrants in a polymer phase. The equation of state is modified to include an extra term to account for the additional activity of the solute in a crystalline polymer. The program is set up for a two-component system of carbon dioxide and PVDF. The algorithm used by Wissinger [7] is used for the calculations. The units for this section are Kelvin for temperature, MPa for pressure, g/L for density, and MPa*L/mol/K for the gas constant.

Characteristic parameters for **CO_2**

$T1star := 316$
$P1star := 412.6$
$\rho 1star := 1369$
$M1 := 44.01$
$r1 := 5.11$

Characteristic parameters for **PVDF** (determined from PVT data for Solef 1010)

$T2star := 714.6$
$P2star := 434.8$
$\rho 2star := 1860$
$M2 := 150000$

Gas Constant

$R := 8314 \cdot 10^{-6}$

$$r2 := \frac{P2star \cdot M2}{R \cdot T2star \cdot \rho 2star}$$

Function Ccrys is the ratio of the molar heat of fusion (1505 cal/mol) to the gas constant (1.987 cal/mol/K) multiplied by the molar volume of the polymer (36.8 cm^3/mol).

$$Ccrys := \frac{1505}{1.987 \cdot 36.8}$$

Function ρr_SL calculates the reduced density of a mixture given the pressure (MPa), Temperature (K), weight fraction of CO_2 dissolved in the polymer phase, and the binary interaction parameter.

$$\rho r\_SL(P, T, m1, \zeta) := \left| \begin{array}{l} \phi 1 \leftarrow \dfrac{\left(\dfrac{m1}{\rho 1star}\right)}{\left[\dfrac{(1-m1)}{\rho 2star} + \dfrac{m1}{\rho 1star}\right]} \\ Pstar \leftarrow \phi 1 \cdot P1star + (1-\phi 1) \cdot P2star - \phi 1 \cdot (1-\phi 1) \cdot \left(P1star + P2star - 2 \cdot \zeta \cdot \sqrt{P1star \cdot P2star}\right) \\ Tstar \leftarrow \dfrac{Pstar}{\left[\dfrac{\phi 1 \cdot P1star}{T1star} + \dfrac{(1-\phi 1) \cdot P2star}{T2star}\right]} \\ r \leftarrow \dfrac{1}{\dfrac{\phi 1}{r1} + \dfrac{(1-\phi 1)}{r2}} \\ Treduced \leftarrow \dfrac{T}{Tstar} \\ Preduced \leftarrow \dfrac{P}{Pstar} \\ \rho r\_guess \leftarrow 0.9 \\ root\left[\rho r\_guess^{\,2} + Preduced + Treduced \cdot \left[\ln(1-\rho r\_guess) + \rho r\_guess \cdot \left(1 - \dfrac{1}{r}\right)\right], \rho r\_guess\right] \end{array} \right.$$

Function μpure evaluates the chemical potential of pure carbon dioxide given the pressure (Pa) and temperature (K) of CO_2.

$$\mu pure(P,T) := \left| \begin{array}{l} P1reduced \leftarrow \dfrac{P}{P1star} \\ T1reduced \leftarrow \dfrac{T}{T1star} \\ \rho reduced \leftarrow \rho r\_SL(P,T,1,1,M2) \\ C \leftarrow \left[\dfrac{-\rho reduced}{T1reduced} + \dfrac{P1reduced}{T1reduced \cdot \rho reduced} + (1-\rho reduced) \cdot \dfrac{\ln(1-\rho reduced)}{\rho reduced} + \dfrac{\ln(\rho reduced)}{r1} \right] \\ C \cdot r1 \end{array} \right.$$

Function μ1_SL determines the chemical potential of the penetrant carbon dioxide given the pressure (MPa), temperature (K), weight fraction of CO_2 dissolved in the polymer phase, the binary interaction parameter, and the weight fraction of amorphous phase that is elastically effective (f). The expression Tm_term represents $1/Tm'$, where Tm' is the melting point of the polymer in the presence of solvent..

$$\mu 1\_SL(P,T,m1,\zeta,f) := \left|\begin{array}{l} \phi 1 \leftarrow \dfrac{\left(\dfrac{m1}{\rho 1star}\right)}{\left[\dfrac{(1-m1)}{\rho 2star}+\dfrac{m1}{\rho 1star}\right]} \\ \chi \leftarrow \dfrac{P1star+P2star-2\cdot\zeta\cdot\sqrt{P1star\cdot P2star}}{R\cdot T} \\ P1reduced \leftarrow \dfrac{P}{P1star} \\ T1reduced \leftarrow \dfrac{T}{T1star} \\ \rho star \leftarrow \dfrac{1}{\dfrac{m1}{\rho 1star}+\dfrac{(1-m1)}{\rho 2star}} \\ \rho reduced \leftarrow \rho r\_SL(P,T,m1,\zeta,M2) \\ Tm\_term \leftarrow \dfrac{1}{447.15}+\dfrac{\rho r\_SL(P,T,1,1,M2)\cdot\rho 1star}{Ccrys\cdot 1000\cdot M1}\cdot\left[\phi 1-\chi\cdot(\phi 1)^2\right] \\ C \leftarrow \left[\dfrac{-\rho reduced}{T1reduced}+\dfrac{P1reduced}{T1reduced\cdot\rho reduced}+(1-\rho reduced)\cdot\dfrac{\ln(1-\rho reduced)}{\rho reduced}+\dfrac{\ln(\rho reduced)}{r1}\right] \\ \ln(\phi 1)+1-\phi 1+\rho reduced\cdot\dfrac{M1}{\rho 1star}\cdot\chi\cdot(1-\phi 1)^2+C\cdot r1+\dfrac{\dfrac{Ccrys\cdot 1000\cdot M1}{(\rho r\_SL(P,T,1,1,M2))\cdot\rho 1star}\cdot\left(\dfrac{1}{T}-Tm\_term\right)}{\left[\dfrac{3}{2\cdot f\cdot(1-\phi 1)}\right]-1} \end{array}\right.$$

Function w1_SL determines the solubility of CO_2 in a polymer reported as a weight fraction. Inputs to the function are the pressure (MPa), temperature (K), the binary interaction parameter, and the fraction of amorphous polymer that is elastically effective.

$$w1\_SL(P,T,\zeta,f) := \left|\begin{array}{l} m1\_guess \leftarrow 0.1 \quad \text{if} \quad P \geq 10 \\ m1\_guess \leftarrow 0.03 \quad \text{otherwise} \\ root(\mu pure(P,T)-\mu 1\_SL(P,T,m1\_guess,\zeta,f),m1\_guess) \end{array}\right.$$

Table "Data" is an array of values for pressure. Function "P" defines the array for pressure.

$$\text{Data} := \begin{bmatrix} 1.00 \\ 2.00 \\ 3.00 \\ 5.00 \\ 7.00 \\ 9.00 \end{bmatrix}$$

$P := \text{Data}^{\langle 0 \rangle}$

Function Sorption determines the degree of sorption of CO_2 in the polymer. Inputs to the function are the pressure (MPa) as an array of pressures, temperature (K), the binary interaction parameter, and the fraction of amorphous polymer that is elastically effective. The output is a matrix, w, in which the first column is the pressure, the second column is ΔM%, accounting for the amorphous phase of the polymer, the third column is the weight fraction of carbon dioxide, and the fourth column is ΔM%, accounting for the entire polymer.

$$\begin{aligned}
&\text{Sorption}(p, t, \text{zeta}, f) := \left| \begin{array}{l} j \leftarrow 0 \\ \text{for } i \in 0..\text{rows}(p) - 1 \\ \quad \left| \begin{array}{l} w_{j,0} \leftarrow p_i \\ w_{j,1} \leftarrow \left(\dfrac{1}{1 - \text{w1_SL}\left(p_i, t, \text{zeta}, f\right)} - 1 \right) \cdot 100 \\ w_{j,2} \leftarrow \text{w1_SL}\left(p_i, t, \text{zeta}, f\right) \\ w_{j,3} \leftarrow \left(\dfrac{1}{1 - \text{w1_SL}\left(p_i, t, \text{zeta}, f\right) \cdot .47} - 1 \right) \cdot 100 \\ j \leftarrow j + 1 \end{array} \right. \\ w \end{array} \right.
\end{aligned}$$

C.3.4 Sanchez-Lacombe Equation of State for Ternary Mixtures

This section uses the Sanchez-Lacombe equation of state to evaluate the partitioning of species between the fluid phase and polymer phase. The program is

set up for a three-component system of vinylidene fluoride, carbon dioxide, and PVDF. The Levenberg-Marquardt algorithm is used to solve the equations for this three-component system. The units for this section are Kelvin for temperature, MPa for pressure, g/L for density, J/mol for the interaction energy (ε^*), cm^3/mol for the molar volume, and MPa*L/mol/K (R1) and J/mol/K (R2) for the gas constant.

The overall program is broken into several files to easily manage the program. The files include “3 SL EOS constants,” “3 SL EOS fluid phase,” “3 SL EOS polymer phase,” “3 SL EOS LevenbergMarquardt,” and “3 SL EOS LevenbergMarquardt FLASH”. The difference between the last two files is whether the calculations are based on a set equilibrium fluid phase composition or a set feed composition, respectively. These files calculate the composition of the fluid phase and polymer phase at equilibrium and the partition coefficient. The file “3 SL EOS constants” contains all the characteristic parameters and binary interaction parameters used in the program. The file “3 SL EOS fluid phase” calculates the reduced density of the fluid phase and the chemical potentials of VF2 and CO_2 in the fluid phase. The file “3 SL EOS polymer phase” calculates the reduced density of the fluid phase and the chemical potentials of VF2 and CO_2 in the polymer phase.

C.3.4.1 File – 3 SL EOS constants

Characteristic parameters for **VF2 (1)**

$P1star := 123.4$

$T1star := 431$

$\varepsilon 1star := R2 \cdot T1star$

$\rho 1star := 1020.58$

$M1 := 64.04$

$v1star := \frac{\varepsilon 1star}{P1star}$

$\varepsilon 1star = 3.583 \cdot 10^{3}$

$r1 := \frac{P1star \cdot M1}{R1 \cdot T1star \cdot \rho 1star}$

$v1star = 29.038$

$r1 = 2.161$

Characteristic parameters for **CO_2 (2)**

$P2star := 412.6$

$T2star := 316$

$\varepsilon 2star := R2 \cdot T2star$

$\rho 2star := 1369$

$v2star := \frac{\varepsilon 2star}{P2star}$

$r2 := 5.11$

$M2 := 44.01$

$\varepsilon 2star = 2.627 \cdot 10^{3}$

$v2star = 6.367$

Characteristic parameters for **PVDF (3)**

$T3star := 714.6$

$\varepsilon 3star := R2 \cdot T3star$

$P3star := 434.8$

$v3star := \frac{\varepsilon 3star}{P3star}$

$\rho 3star := 1860$

$M3 := 150000$

$r3 := \frac{P3star \cdot M3}{R1 \cdot T3star \cdot \rho 3star}$

$\varepsilon 3star = 5.941 \cdot 10^{3}$

$v3star = 13.664$

$r3 = 5.902 \cdot 10^{3}$

Gas Constant

$R1 := 8314 \cdot 10^{-6}$ $R2 := 8.314$

Interaction parameters

$\zeta_{12} := 1.009$ $\zeta_{13} := 1.13$ $\zeta_{23} := 1$

The interaction parameters vary with the temperature of the system.

C.3.4.2 File – 3 SL EOS fluid phase

This file references the constants file for input of all the constants and parameters (characteristic and interaction) for the model.

 Reference:C:\Documents and Settings\user\My Documents\Modeling\3 SL EOS constants.mcd

Function ρr_fluid determines the reduced density of a mixture given the pressure (MPa), Temperature (K), weight fraction of VF2 dissolved in the fluid phase, and binary interaction parameter.

$$
\begin{aligned}
\rho r\_fluid\left(P, T, m1, \zeta_{12}\right) := \;& \phi 1 \leftarrow \frac{\left(\frac{m1}{\rho 1star}\right)}{\left[\frac{(1-m1)}{\rho 2star} + \frac{m1}{\rho 1star}\right]} \\
& v12star \leftarrow \left(\frac{\sqrt[3]{v1star} + \sqrt[3]{v2star}}{2}\right)^3 \\
& \varepsilon 12star \leftarrow \zeta_{12} \cdot \sqrt{\varepsilon 1star \cdot \varepsilon 2star} \\
& vstar \leftarrow \phi 1^2 \cdot v1star + (1-\phi 1)^2 \cdot v2star + 2 \cdot \phi 1 \cdot (1-\phi 1) \cdot v12star \\
& \varepsilon star \leftarrow \phi 1 \cdot \varepsilon 1star + (1-\phi 1) \cdot \varepsilon 2star - \phi 1 \cdot (1-\phi 1) \cdot (\varepsilon 1star + \varepsilon 2star - 2 \cdot \varepsilon 12star) \\
& r \leftarrow \frac{1}{\frac{\phi 1}{r1} + \frac{(1-\phi 1)}{r2}} \\
& Treduced \leftarrow \frac{T \cdot R2}{\varepsilon star} \\
& Preduced \leftarrow \frac{P \cdot vstar}{\varepsilon star} \\
& \rho r\_guess \leftarrow 0.9 \\
& root\left[\rho r\_guess^2 + Preduced + Treduced \cdot \left[\ln(1-\rho r\_guess) + \rho r\_guess \cdot \left(1 - \frac{1}{r}\right)\right], \rho r\_guess\right]
\end{aligned}
$$

Function μ1_fluid evaluates the chemical potential of vinylidene fluoride given the pressure (MPa), temperature (K), weight fraction of VF2 dissolved in the fluid phase, and binary interaction parameter.

$$\mu 1\_fluid\left(P, T, m1, \zeta_{12}\right) := \left|\begin{array}{l} \phi 1 \leftarrow \dfrac{\left(\dfrac{m1}{\rho 1star}\right)}{\left[\dfrac{(1-m1)}{\rho 2star}+\dfrac{m1}{\rho 1star}\right]} \\ v12star \leftarrow \left(\dfrac{\sqrt[3]{v1star}+\sqrt[3]{v2star}}{2}\right)^3 \\ \varepsilon 12star \leftarrow \zeta_{12}\cdot\sqrt{\varepsilon 1star\cdot\varepsilon 2star} \\ vstar \leftarrow \phi 1^2\cdot v1star + (1-\phi 1)^2\cdot v2star + 2\cdot\phi 1\cdot(1-\phi 1)\cdot v12star \\ interact\_term \leftarrow (\varepsilon 1star + \varepsilon 2star - 2\cdot\varepsilon 12star)\cdot(1-\phi 1)^2 \\ P1reduced \leftarrow \dfrac{P}{P1star} \\ T1reduced \leftarrow \dfrac{T}{T1star} \\ \rho reduced \leftarrow \rho r\_fluid\left(P, T, m1, \zeta_{12}\right) \\ C \leftarrow \left[\dfrac{-\rho reduced}{T1reduced}+\dfrac{P1reduced}{T1reduced\cdot\rho reduced}+(1-\rho reduced)\cdot\dfrac{\ln(1-\rho reduced)}{\rho reduced}+\dfrac{\ln(\rho reduced)}{r1}\right] \\ \ln(\phi 1)+(1-\phi 1)\cdot\left(1-\dfrac{r1}{r2}\right)+\dfrac{\rho reduced\cdot r1\cdot interact\_term}{R2\cdot T}+C\cdot r1 \end{array}\right.$$

Function $\mu 2$_fluid evaluates the chemical potential of carbon dioxide given the pressure (MPa), temperature (K), weight fraction of VF2 dissolved in the fluid phase, and binary interaction parameter.

$$\mu 2\_fluid(P, T, m1, \zeta_{12}) := \left| \begin{array}{l} \phi 2 \leftarrow \dfrac{\left(\dfrac{1-m1}{\rho 2star}\right)}{\left[\dfrac{(1-m1)}{\rho 2star} + \dfrac{m1}{\rho 1star}\right]} \\ v12star \leftarrow \left(\dfrac{\sqrt[3]{v1star} + \sqrt[3]{v2star}}{2}\right)^3 \\ \varepsilon 12star \leftarrow \zeta_{12} \cdot \sqrt{\varepsilon 1star \cdot \varepsilon 2star} \\ vstar \leftarrow \phi 2^2 \cdot v2star + (1-\phi 2)^2 \cdot v1star + 2 \cdot \phi 2 \cdot (1-\phi 2) \cdot v12star \\ interact\_term \leftarrow (\varepsilon 1star + \varepsilon 2star - 2 \cdot \varepsilon 12star) \cdot (1-\phi 2)^2 \\ P2reduced \leftarrow \dfrac{P}{P2star} \\ T2reduced \leftarrow \dfrac{T}{T2star} \\ \rho reduced \leftarrow \rho r\_fluid(P, T, m1, \zeta_{12}) \\ C \leftarrow \left[\dfrac{-\rho reduced}{T2reduced} + \dfrac{P2reduced}{T2reduced \cdot \rho reduced} + (1-\rho reduced) \cdot \dfrac{\ln(1-\rho reduced)}{\rho reduced} + \dfrac{\ln(\rho reduced)}{r2}\right] \\ \ln(\phi 2) + (1-\phi 2) \cdot \left(1 - \dfrac{r2}{r1}\right) + \dfrac{\rho reduced \cdot r2 \cdot interact\_term}{R2 \cdot T} + C \cdot r2 \end{array} \right.$$

Function ρ_mixture calculates the density of the fluid mixture given the pressure (MPa), temperature (K), weight fraction of VF2 in the fluid phase, and the interaction parameter.

$$\rho\_mixture(P, T, m1, \zeta_{12}) := \left| \begin{array}{l} \rho star \leftarrow \dfrac{1}{\dfrac{m1}{\rho 1star} + \dfrac{(1-m1)}{\rho 2star}} \\ \rho r\_fluid(P, T, m1, \zeta_{12}) \cdot \rho star \end{array} \right.$$

C.3.4.3 File – 3 SL EOS polymer phase

This file references the constants file for input of all the constants and parameters (characteristic and interaction) for the model.

Reference:C:\Documents and Settings\user\My Documents\Modeling\3 SL EOS constants.mcd

Function ρr_polymer determines the reduced density of a mixture given the pressure (MPa), Temperature (K), weight fraction of VF2 dissolved in the polymer phase (m1), weight fraction of CO_2 dissolved in the polymer phase (m2), and the binary interaction parameters.

$$\rho r_polymer\left(P, T, m1, m2, \zeta_{12}, \zeta_{13}, \zeta_{23}\right) := \left|\begin{array}{l}
\phi1 \leftarrow \dfrac{\left(\dfrac{m1}{\rho1star}\right)}{\dfrac{m2}{\rho2star}+\dfrac{m1}{\rho1star}+\dfrac{(1-m1-m2)}{\rho3star}} \\
\phi2 \leftarrow \dfrac{\left(\dfrac{m2}{\rho2star}\right)}{\dfrac{m2}{\rho2star}+\dfrac{m1}{\rho1star}+\dfrac{(1-m1-m2)}{\rho3star}} \\
\phi3 \leftarrow 1-\phi1-\phi2 \\
v12star \leftarrow \left(\dfrac{\sqrt[3]{v1star}+\sqrt[3]{v2star}}{2}\right)^3 \\
v13star \leftarrow \left(\dfrac{\sqrt[3]{v1star}+\sqrt[3]{v3star}}{2}\right)^3 \\
v23star \leftarrow \left(\dfrac{\sqrt[3]{v2star}+\sqrt[3]{v3star}}{2}\right)^3 \\
\varepsilon12star \leftarrow \zeta_{12}\cdot\sqrt{\varepsilon1star\cdot\varepsilon2star} \\
\varepsilon13star \leftarrow \zeta_{13}\cdot\sqrt{\varepsilon1star\cdot\varepsilon3star} \\
\varepsilon23star \leftarrow \zeta_{23}\cdot\sqrt{\varepsilon2star\cdot\varepsilon3star} \\
\chi_{12} \leftarrow \varepsilon1star+\varepsilon2star-2\cdot\varepsilon12star \\
\chi_{13} \leftarrow \varepsilon1star+\varepsilon3star-2\cdot\varepsilon13star \\
\chi_{23} \leftarrow \varepsilon2star+\varepsilon3star-2\cdot\varepsilon23star \\
mix_vstar \leftarrow 2\cdot\phi1\cdot\phi2\cdot v12star+2\cdot\phi1\cdot\phi3\cdot v13star+2\cdot\phi2\cdot\phi3\cdot v23star \\
vstar \leftarrow \phi1^2\cdot v1star+\phi2^2\cdot v2star+\phi3^2\cdot v3star+mix_vstar \\
mix_\varepsilon star \leftarrow \phi1\cdot\phi2\cdot\chi_{12}+\phi1\cdot\phi3\cdot\chi_{13}+\phi2\cdot\phi3\cdot\chi_{23} \\
\varepsilon star \leftarrow \phi1\cdot\varepsilon1star+\phi2\cdot\varepsilon2star+\phi3\cdot\varepsilon3star-mix_\varepsilon star \\
Tstar \leftarrow \dfrac{\varepsilon star}{R2} \\
r \leftarrow \dfrac{1}{\dfrac{\phi1}{r1}+\dfrac{\phi2}{r2}+\dfrac{\phi3}{r3}} \\
Treduced \leftarrow \dfrac{T}{Tstar} \\
Preduced \leftarrow \dfrac{P}{\left(\dfrac{\varepsilon star}{vstar}\right)} \\
\rho r_guess \leftarrow 0.9 \\
root\left[\rho r_guess^2+Preduced+Treduced\cdot\left[\ln(1-\rho r_guess)+\rho r_guess\cdot\left(1-\dfrac{1}{r}\right)\right], \rho r_guess\right]
\end{array}\right.$$

Function μ1_polymer evaluates the chemical potential of vinylidene fluoride given the pressure (MPa), temperature (K), weight fraction of VF2 dissolved in the polymer phase (m1), weight fraction of CO_2 dissolved in the polymer phase (m2), and the binary interaction parameters.

$$\mu1_polymer\left(P, T, m1, m2, \zeta_{12}, \zeta_{13}, \zeta_{23}\right) := \left|\begin{array}{l}
\phi1 \leftarrow \dfrac{\left(\dfrac{m1}{\rho1star}\right)}{\dfrac{m2}{\rho2star}+\dfrac{m1}{\rho1star}+\dfrac{(1-m1-m2)}{\rho3star}} \\
\phi2 \leftarrow \dfrac{\left(\dfrac{m2}{\rho2star}\right)}{\dfrac{m2}{\rho2star}+\dfrac{m1}{\rho1star}+\dfrac{(1-m1-m2)}{\rho3star}} \\
\phi3 \leftarrow 1-\phi1-\phi2 \\
r \leftarrow \dfrac{1}{\dfrac{\phi1}{r1}+\dfrac{\phi2}{r2}+\dfrac{\phi3}{r3}} \\
\varepsilon12star \leftarrow \zeta_{12}\cdot\sqrt{\varepsilon1star\cdot\varepsilon2star} \\
\varepsilon13star \leftarrow \zeta_{13}\cdot\sqrt{\varepsilon1star\cdot\varepsilon3star} \\
\varepsilon23star \leftarrow \zeta_{23}\cdot\sqrt{\varepsilon2star\cdot\varepsilon3star} \\
\chi_{12} \leftarrow \varepsilon1star+\varepsilon2star-2\cdot\varepsilon12star \\
\chi_{13} \leftarrow \varepsilon1star+\varepsilon3star-2\cdot\varepsilon13star \\
\chi_{23} \leftarrow \varepsilon2star+\varepsilon3star-2\cdot\varepsilon23star \\
interact_term \leftarrow \phi2\cdot\chi_{12}+\phi3\cdot\chi_{13}-\left(\phi1\cdot\phi2\cdot\chi_{12}+\phi1\cdot\phi3\cdot\chi_{13}+\phi2\cdot\phi3\cdot\chi_{23}\right) \\
P1reduced \leftarrow \dfrac{P}{P1star} \\
T1reduced \leftarrow \dfrac{T}{T1star} \\
\rho reduced \leftarrow \rho r_polymer\left(P, T, m1, m2, \zeta_{12}, \zeta_{13}, \zeta_{23}\right) \\
C \leftarrow \left[\dfrac{-\rho reduced}{T1reduced}+\dfrac{P1reduced}{T1reduced\cdot\rho reduced}+(1-\rho reduced)\cdot\dfrac{\ln(1-\rho reduced)}{\rho reduced}+\dfrac{\ln(\rho reduced)}{r1}\right] \\
\ln(\phi1)+1-\dfrac{r1}{r}+\dfrac{\rho reduced\cdot r1\cdot interact_term}{R2\cdot T}+C\cdot r1
\end{array}\right.$$

Function μ2_polymer evaluates the chemical potential of carbon dioxide given the pressure (MPa), temperature (K), weight fraction of VF2 dissolved in the polymer

phase (m1), weight fraction of CO_2 dissolved in the polymer phase (m2), and the binary interaction parameters.

$$\mu 2_polymer\left(P, T, m1, m2, \zeta_{12}, \zeta_{13}, \zeta_{23}\right) := \left|\begin{array}{l}
\phi 1 \leftarrow \dfrac{\left(\dfrac{m1}{\rho 1star}\right)}{\dfrac{m2}{\rho 2star}+\dfrac{m1}{\rho 1star}+\dfrac{(1-m1-m2)}{\rho 3star}} \\
\phi 2 \leftarrow \dfrac{\left(\dfrac{m2}{\rho 2star}\right)}{\dfrac{m2}{\rho 2star}+\dfrac{m1}{\rho 1star}+\dfrac{(1-m1-m2)}{\rho 3star}} \\
\phi 3 \leftarrow 1-\phi 1-\phi 2 \\
r \leftarrow \dfrac{1}{\dfrac{\phi 1}{r1}+\dfrac{\phi 2}{r2}+\dfrac{\phi 3}{r3}} \\
\varepsilon 12star \leftarrow \zeta_{12}\cdot\sqrt{\varepsilon 1star\cdot\varepsilon 2star} \\
\varepsilon 13star \leftarrow \zeta_{13}\cdot\sqrt{\varepsilon 1star\cdot\varepsilon 3star} \\
\varepsilon 23star \leftarrow \zeta_{23}\cdot\sqrt{\varepsilon 2star\cdot\varepsilon 3star} \\
\chi_{12} \leftarrow \varepsilon 1star+\varepsilon 2star-2\cdot\varepsilon 12star \\
\chi_{13} \leftarrow \varepsilon 1star+\varepsilon 3star-2\cdot\varepsilon 13star \\
\chi_{23} \leftarrow \varepsilon 2star+\varepsilon 3star-2\cdot\varepsilon 23star \\
interact_term \leftarrow \phi 1\cdot\chi_{12}+\phi 3\cdot\chi_{23}-\left(\phi 1\cdot\phi 2\cdot\chi_{12}+\phi 1\cdot\phi 3\cdot\chi_{13}+\phi 2\cdot\phi 3\cdot\chi_{23}\right) \\
P2reduced \leftarrow \dfrac{P}{P2star} \\
T2reduced \leftarrow \dfrac{T}{T2star} \\
\rho reduced \leftarrow \rho r_polymer\left(P, T, m1, m2, \zeta_{12}, \zeta_{13}, \zeta_{23}\right) \\
C \leftarrow \left[\dfrac{-\rho reduced}{T2reduced}+\dfrac{P2reduced}{T2reduced\cdot\rho reduced}+(1-\rho reduced)\cdot\dfrac{\ln(1-\rho reduced)}{\rho reduced}+\dfrac{\ln(\rho reduced)}{r2}\right] \\
\ln(\phi 2)+1-\dfrac{r2}{r}+\dfrac{\rho reduced\cdot r2\cdot interact_term}{R2\cdot T}+C\cdot r2
\end{array}\right.$$

Function ρstar_p determines the characteristic density of the mixture, given the weight fraction of VF2 and CO_2 in the polymer phase.

$$\rho star\_p(m1, m2) := \frac{1}{\dfrac{m1}{\rho 1star}+\dfrac{m2}{\rho 2star}+\dfrac{(1-m1-m2)}{\rho 3star}}$$

C.3.4.4 File – 3 SL EOS LevenbergMarquardt

This file references the previous three files for the constants, parameters, and chemical potential equations.

Reference:C:\Documents and Settings\user\My Documents\Modeling\3 SL EOS constants.mcd

Reference:C:\Documents and Settings\user\My Documents\Modeling\3 SL EOS fluid phase.mcd

Reference:C:\Documents and Settings\user\My Documents\Modeling\3 SL EOS polymer phase.mcd

Guess values are input for the unknown composition of the polymer phase

$m1p := 0.01 \qquad m2p := 0.001$

The solve block for the Levenberg-Marquardt algorithm is set up to equate the chemical potential equations and solve for the polymer phase composition, given the fluid phase composition at equilibrium.

Given

$\mu 1\_polymer\left(P, T, m1p, m2p, \zeta_{12}, \zeta_{13}, \zeta_{23}\right) = \mu 1\_fluid\left(P, T, m1f, \zeta_{12}\right)$

$\mu 2\_polymer\left(P, T, m1p, m2p, \zeta_{12}, \zeta_{13}, \zeta_{23}\right) = \mu 2\_fluid\left(P, T, m1f, \zeta_{12}\right)$

$Answer(P, T, m1f) := Minerr(m1p, m2p)$

Functions m1p and m2p solve for the composition of VF2 and CO_2 in the polymer phase, respectively, using the solve block.

$$m1p(P,T,m1f) := Answer(P,T,m1f)_0$$

$$m2p(P,T,m1f) := Answer(P,T,m1f)_1$$

Function Kc_value calculates the partition coefficient of VF2 between the fluid and polymer phases given the pressure (MPa), temperature (K), and the weight fraction of VF2 in the fluid phase.

$$Kc\_value(P,T,m1f) := \frac{m1p(P,T,m1f)}{m1f} \cdot \frac{\rho r\_polymer\left(P,T,m1p(P,T,m1f),m2p(P,T,m1f),\zeta_{12},\zeta_{13},\zeta_{23}\right)\cdot \rho star\_p(m1p(P,T,m1f),m2p(P,T,m1f))}{\rho\_mixture\left(P,T,m1f,\zeta_{12}\right)}$$

Functions ConcVF2_II and ConcVF2_I calculate the concentration of VF2 in the polymer and fluid phases, respectively, given the pressure (MPa), temperature (K), and the weight fraction of VF2 in the fluid phase.

$$ConcVF2\_II(P,T,m1f) := \frac{m1p(P,T,m1f)}{M1} \cdot \left(\rho r\_polymer\left(P,T,m1p(P,T,m1f),m2p(P,T,m1f),\zeta_{12},\zeta_{13},\zeta_{23}\right)\cdot \rho star\_p(m1p(P,T,m1f),m2p(P,T,m1f))\right)$$

$$ConcVF2\_I(P,T,m1f) := \frac{m1f}{M1}\cdot \rho\_mixture\left(P,T,m1f,\zeta_{12}\right)$$

C.3.4.5 File – 3 SL EOS LevenbergMarquardt FLASH

This file references the previous three files for the constants, parameters, and chemical potential equations.

Reference:C:\Documents and Settings\user\My Documents\Modeling\3 SL EOS constants.mcd

Reference:C:\Documents and Settings\user\My Documents\Modeling\3 SL EOS fluid phase.mcd

Reference:C:\Documents and Settings\user\My Documents\Modeling\3 SL EOS polymer phase.mcd

The weight fraction of VF2 and CO_2 in the feed is defined.

$m1i := 0.1636$ $m2i := 0.7988$

Guess values are input for the unknown weight fractions of VF2 (m1p) and CO_2 (m2p) in the polymer phase, the weight fraction of VF2 (m1f) in the fluid phase, and the fraction of the fluid phase that remins in the fluid phase at equilibrium (ψ).

$m1p := 0.001$ $m2p := 0.001$

$\psi := 0.9$ $m1f := 0.1$

The interaction parameters are redefined as A, B, and C to simplify their use in the calculations.

$\zeta_{13} := 0.88$ $\zeta_{23} := 1.012$ $\zeta_{12} := 1.009$

$A := \zeta_{13}$ $B := \zeta_{23}$ $C := \zeta_{12}$

The solve block for the Levenberg-Marquardt algorithm is set up to equate the chemical potential equations, perform a mass balance on the system, and solve for the polymer phase composition, given an initial feed composition.

Given

$$\mu 1\_polymer(P, T, m1p, m2p, C, A, B) = \mu 1\_fluid(P, T, m1f, C)$$

$$\mu 2\_polymer(P, T, m1p, m2p, C, A, B) = \mu 2\_fluid(P, T, m1f, C)$$

$$(1 - \psi) \cdot m1p + \psi \cdot m1f - m1i = 0$$

$$(1 - \psi) \cdot m2p + \psi \cdot (1 - m1f) - m2i = 0$$

$$Answer(P, T, m1i, m2i, A) := Minerr(m1p, m2p, m1f, \psi)$$

Functions m1p, m2p, and m1f solve for the composition of VF2 and CO_2 in the polymer phase and the composition of VF2 in the fluid phase, respectively, using the solve block.

$$m1p(P, T, m1i, m2i, A) := Answer(P, T, m1i, m2i, A)_0$$

$$m2p(P, T, m1i, m2i, A) := Answer(P, T, m1i, m2i, A)_1$$

$$m1f(P, T, m1i, m2i, A) := Answer(P, T, m1i, m2i, A)_2$$

Function Yaxis calculates the mg sorbed per gram polymer, as reported by the sorption experiments.

$$Yaxis(P, A) := \frac{m1p(P, 348.15, m1i, m2i, A) + m2p(P, 348.15, m1i, m2i, A)}{1 - m1p(P, 348.15, m1i, m2i, A) - m2p(P, 348.15, m1i, m2i, A)} \cdot 1000$$

Function Kc_value calculates the partition coefficient of VF2 between the fluid and polymer phases given the pressure (MPa), temperature (K), and the weight fraction of VF2 and CO_2 in the feed.

$$Kc\_value(P,T,m1i,m2i) := \frac{m1p(P,T,m1i,m2i,A)}{m1f(P,T,m1i,m2i,A)} \cdot \frac{\rho r\_polymer\left(P,T,m1p(P,T,m1i,m2i,A),m2p(P,T,m1i,m2i,A),\zeta_{12},\zeta_{13},\zeta_{23}\right)\cdot \rho star\_p(m1p(P,T,m1i,m2i,A),m2p(P,T,m1i,m2i,A))}{\rho\_mixture(P,T,m1f(P,T,m1i,m2i,A),C)}$$

Functions ConcVF2_II and ConcVF2_I calculate the concentration of VF2 in the polymer and fluid phases, respectively, given the pressure (MPa), temperature (K), and the weight fraction of VF2 and CO_2 in the feed.

$$ConcVF2\_II(P,T,m1i,m2i) := \frac{m1p(P,T,m1i,m2i,A)}{M1} \cdot \left(\rho r\_polymer\left(P,T,m1p(P,T,m1i,m2i,A),m2p(P,T,m1i,m2i,A),\zeta_{12},\zeta_{13},\zeta_{23}\right)\cdot \rho star\_p(m1p(P,T,m1i,m2i,A),m2p(P,T,m1i,m2i,A))\right)$$

$$ConcVF2\_I(P,T,m1i,m2i) := \frac{m1f(P,T,m1i,m2i,A)}{M1} \cdot \rho\_mixture(P,T,m1f(P,T,m1i,m2i,A),C)$$

C.4 References

1. Briscoe, B.J., Lorge, O., Wajs, A., and Dang, P., *Carbon dioxide-poly(vinylidene fluoride) interactions at high pressure.* Journal of Polymer Science: Part B: Polymer Physics, 1998. **36**(13): p. 2435-2447.

2. Kennedy, K.A., DeSimone, J.M., and Roberts, G.W., *A Commentary of "Carbon dioxide-poly(vinylidene fluoride) interactions at high pressure".* Journal of Polymer Science: Part B: Polymer Physics, 2002. **40**: p. 602-604.

3. Peng, D.-Y. and Robinson, D.B., *A new two-constant equation of state.* Industrial and Engineering Chemistry Fundamentals, 1976. **15**(1): p. 59-64.

4. Duschek, W., Kleinrahm, R., and Wagner, W., *Measurement and correlation of the (pressure, density, temperature) relation of carbon dioxide.* Journal of Chemical Thermodynamics, 1990. **22**: p. 827-840.

5. McHugh, M. and Krukonis, V., *Supercritical Fluid Extraction - Principles and Practice*. 1986, Boston: Butterworths.

6. Dinoia, T.P., Conway, S.E., Lim, J.S., and McHugh, M.A., *Solubility of vinylidene fluoride polymers in supercritical CO_2 and halogenated solvents.* Journal of Polymer Science: Part B: Polymer Physics, 2000. **38**(21): p. 2832-2840.

7. Wissinger, R.G. and Paulaitis, M.E., *Molecular thermodynamic model for sorption and swelling in glassy polymer-CO_2 systems at elevated pressures.* Industrial and Engineering Chemistry Research, 1991. **30**(5): p. 842-851.